NASA Contractor Report 181917

Application of Laminar Flow Control to Supersonic Transport Configurations

Boeing Commercial Airplane Company
Seattle, WA. 98124-2207

Contract NAS1-15325
July 1990

National Aeronautics and
Space Administration

Langley Research Center
Hampton, Virginia 23665-5225

NASA Contractor Report 181917

Application of Laminar Flow Control to Supersonic Transport Configurations

Boeing Commercial Airplane Company
Seattle, WA. 98124-2207

Contract NAS1-15325
July 1990

National Aeronautics and
Space Administration

Langley Research Center
Hampton, Virginia 23665-5225

FOREWORD

The work reported in this document was performed under contract NAS1-15325 with the Laminar Flow Control Projects Office (LFCPO) of the NASA Langley Research Center. The period of performance was October 1987 through November 1988. The contract was managed by R. D. Wagner, head of LFCPO and D. W. Bartlett and D. Maddalon, technical monitors. The study was conducted in the Aerodynamics Research and Advanced Programs organizations of Boeing Commercial Airplanes. The following were the members of the study team:

A. L. Nagel	Project Manager
P. G. Parikh	Principal Investigator
E. D. Bermingham	Aerodynamics
P. P. Sullivan	Aerodynamics
T. Derbyshire	Configurations
T. Timar	Systems
D. Stensrud	Structures
S. S. Ogg	Performance
K. E. Siedentopf	Weights
G. W. Klees	Propulsion

Several individuals, in addition to those listed above, assisted in the effort. These include: R. A. Rozendaal, L. J. Runyan, E. N. Tinoco, N. J. Yu, D. N. Ball, R. Behbehani, and T. J. Kao. Their assistance is gratefully acknowledged. A special note of appreciation is extended to Joreen Califano for her efforts in speedy typing of the manuscript.

TABLE OF CONTENTS

TABLE OF CONTENTS
(continued)

LIST OF FIGURES

LIST OF TABLES

LIST OF SYMBOLS AND ABBREVIATIONS

Symbol

A_{ref}	Wing reference area
b	Wing span
c	Streamwise chord length
C_D	Drag coefficient
$C_{D,f}$	Skin friction drag coefficient
$C_{D,L}$	Coefficient of drag due to lift
$C_{D,W}$	Wave drag coefficient
C_f	Skin friction coefficient
C_L	Lift coefficient
C_p	Pressure coefficient
C_q	Nondimensional suction coefficient $\rho_o V_o/\rho_\infty U_\infty$
Cq,a.l.	attachment line suction coefficient
M	Mach number
N_{CF}	N-factor for crossflow disturbance growth
N_{TS}	N-factor for Tollmien-Schlichting disturbance growth
dN/ds	Disturbance spatial growth rate
q	Dynamic pressure
Re_1	unit Reynolds number (ft^{-1})
R_{ec}	Chord Reynolds number
R_{ex}	x-Reynolds number
R_{etr}	x-Reynolds number at transition
RLE	Leading edge radius
$Re_{\theta,a.l.}$	Attachment line momentum thickness Reynolds number
RXFLO	Crossflow Reynolds number, $W_{cf,max}*\delta_{cf}/\nu_\infty$
S	Streamwise distance along the wing surface, measured from the attachment line
U_∞	Free stream velocity
V_o	Suction velocity at the surface
V_{app}	Airplane approach velocity
$W_{cf,max}$	Maximum value of crossflow velocity in the 3D boundary layer
t	Local wing thickness
T_W	Wing surface temperature
T_{AW}	Adiabatic wall temperature
X	Streamwise distance along chordline

Greek Letters

α	Angle of attack
α_i	Nondimensional spatial Amplification Rate
λ	Disturbance wave angle
ω	Disturbance frequency
ψ	Wave angle measured from local edge velocity direction
η	Fractional semispan station

μ	Mach angle
Λ	Sweep angle
θ	Boundary layer momentum thickness
ν_∞	Free stream kinematic viscosity
p_o	Air density at wall
ρ_∞	Free stream air density
δ_{cf}	Greatest height in the 3D boundary layer where the crossflow velocity is $0.1*W_{cf,max}$

Abbreviations

ASM	Airplane Seat Mile
BLC	Boundary Layer Control
BLGL	Boundary Layer Grid Generation Program
CF	Cross Flow
CFD	Computational Fluid Dynamics
DOC	Direct Operating Costs
HLFC	Hybrid Laminar Flow Control
HSCT	High Speed Civil Transport
L/D	Lift/Drag ratio
LAM	Laminar
LaRC	Langley Research Center
LFC	Laminar Flow Control
MTOW	Maximum Takeoff (Gross) Weight
NLF	Natural Laminar Flow
NMi	Nautical Miles
OEW	Operational Empty Weight
PAX	Number of passengers
SST	Supersonic Transport
SW	Wing Area
TG	Taylor-Gortler
TOFL	Takeoff Field Length
TS	Tollemien-Schlichting
TSFC	Thrust Specific Fuel Consumption
TURB	Turbulent
T/W	Thrust/weight ratio
W/S	Wing loading
WBL	Wing Buttock line

EXECUTIVE SUMMARY

This report documents the results of a one year study aimed at assessing the feasibility and impact of implementing a laminar flow control (LFC) system on a Supersonic Transport (SST) configuration. The work was performed under contract NAS1-15325 with the Laminar Flow Control Projects Office (LFCPO) of the NASA Langley Research Center.

Several benefits could potentially be realized from the implementation of LFC on a SST configuration. These include improved lift/drag (L/D) ratio, reduced maximum takeoff weight (MTOW), increased range, improved fuel economy and reduced aerodynamic heating. However, many issues need to be addressed with regard to the application of LFC to a SST configuration to determine the extent to which these potential benefits could actually be realized in practice. These issues relate not only to the feasibility of achieving high transition Reynolds number on a complex SST configuration, but also to the associated structural and systems requirements and penalties. The present study was an initial attempt at addressing many of these issues. The primary emphasis was on the aerodynamic modifications needed to achieve a significant run of laminar flow on the wing surface of an SST configuration. However, sufficient emphasis was placed on the determination of associated structural and systems requirements to arrive at a realistic assessment of the net performance benefits of LFC implementation.

The feasibility and impact of LFC implementation were studied with reference to a specific SST configuration, model 733-633, which is a Mach 2.4 double delta wing planform configuration developed at Boeing during the NASA funded SCAR* studies of the 1970's [36]. The geometry definition of this configuration was reasonably well documented and an extensive performance database was available. An updated version (Model 1080-834) of this configuration with geometrically similar wing but with an all composite structure and longer range capability became available during the course of the present study from the concurrent NASA/Boeing HSCT studies [44]. The assessment of the potential performance benefits of LFC implementation was made with reference to this updated configuration.

The present study was organized in the following four tasks:

1. Supersonic Transition Prediction and Laminarization Schemes.

   In this task, existing stability theory calculations as well as wind tunnel and flight experiments on supersonic transition with and without laminar flow control employing suction and wall cooling were sur-

---

* Supersonic Cruise Aircraft Research

veyed. Existing 3D linear and nonlinear inviscid codes at Boeing were utilized to predict the pressure distribution on the SST configuration. Suction requirements for stabilization of the attachment line boundary layer on a highly swept, rounded leading edge were estimated. The wing boundary layer developing under the predicted inviscid pressure distribution was calculated, under the swept tapered wing approximation, using a Boeing 3D boundary layer code. The effects of wall cooling and suction could be modeled in these calculations. The stability of the boundary layer profiles for both Tollmien-Schlichting (TS) and crossflow (CF) modes was then calculated using a Boeing modified version of the Mack code [13]. A transition criterion based on subsonic natural laminar flow flight tests on F-111 [8] and Boeing 757 [10] aircraft was used for prediction of transition in supersonic boundary layers with simultaneous growths of TS and CF modes of instability. Suction requirements for significant laminarization of both subsonic and supersonic leading edge wing regions were determined. Three different hybrid wing laminarization schemes consisting of suction controlled and natural laminar flow combinations, were considered. Two of these were selected for detailed design/benefit evaluation. Issues of the compatibility of the proposed laminarization schemes with the high lift system of the configuration were addressed and preliminary concepts for use of the LFC system as a boundary layer control (BLC) system for high lift performance improvement were proposed.

2. Structural and Systems Concept Development

In this task concepts for structural and systems modifications required to achieve suction laminarization of a baseline turbulent SST configuration were developed. Suction through a perforated titanium skin was assumed in all cases. Possibilities of accommodating required size ducting within the existing structure were explored. Various arrangements for ducting the air to the suction compressors were considered with a view to minimizing the fuel displacement and weight penalties. Availability of-or the feasibility of the development of suction compressors required for the present application was explored with two suppliers. Various means of powering and locating the suction compressors were considered, again with a view to minimizing the TSFC, weight and fuel displacement penalties.

3. Design/Benefit Studies

The net viscous drag reduction for the predicted extent of laminar run for two laminarization schemes was calculated by a strip theory method. The impact on the total cruise drag of the configuration was then calculated. Suction locations, mass flow requirements and pressure distribution over the suction regions were specified for systems

evaluation. Compressor power requirements were estimated and compression ratios selected after evaluating trades between suction air momentum drag penalty and the TSFC and weight penalties. The impacts of aerodynamic (L/D) improvements as well as weight, TSFC, suction air momentum drag and fuel displacement penalties on the overall performance of the sized vehicle were evaluated by means of a Boeing SST performance and sizing program. The net benefits in terms of MTOW, OEW and fuel burn reduction were estimated for the two laminarization schemes.

4. Future Research Requirements

Several research needs were identified during the course of the present study for improvements in existing transition prediction capability, development of nonlinear supersonic wing design capability, validation of laminarization concepts as well as enhancement of net benefits of LFC implementation. These were organized in three general areas: A) Improved Transition Prediction and Wing Design Capability, B) Conceptual Design Studies and C) Wind Tunnel and Flight Experiments.

In the aerodynamics part of the study it was found that increasing Mach number has a stabilizing influence on the TS mode and that mild suction and wall cooling further enhance this stability. However, the influence of these parameters on the cross flow (CF) mode of instability is rather weak. Therefore, the control of CF instability, by careful tailoring of pressure distribution and suction is the key to the achievement of high transition Reynolds numbers on a SST configuration. Significant alteration of the predicted pressure distribution on the (subsonic leading edge) inboard wing was found necessary to achieve a laminar run without excessive suction. Only a slight modification of the predicted pressure distribution was necessary for the (supersonic leading edge) outboard wing. A wing design capability to achieve the specified pressure distribution was not available.

A survey of existing stability calculations and wind tunnel/flight experiments revealed a lack of 3D supersonic boundary layer transition data to formulate reliable transition criteria. Based on the present boundary layer stability calculations and an existing subsonic transition criterion, hybrid laminarization of the outboard wing up to 60 percent chord was considered achievable by a dual region suction scheme. The suction requirements of the subsonic leading edge inboard wing were significantly larger. Hybrid laminarization up to approximately 30 percent chord was considered achievable for the inboard wing with a tailored pressure distribution and suction applied over the first 10 percent chord.

As shown in Fig. 1, a 6 percent reduction in the total cruise drag of the configuration resulted from Scheme 1 where laminarization of the outboard

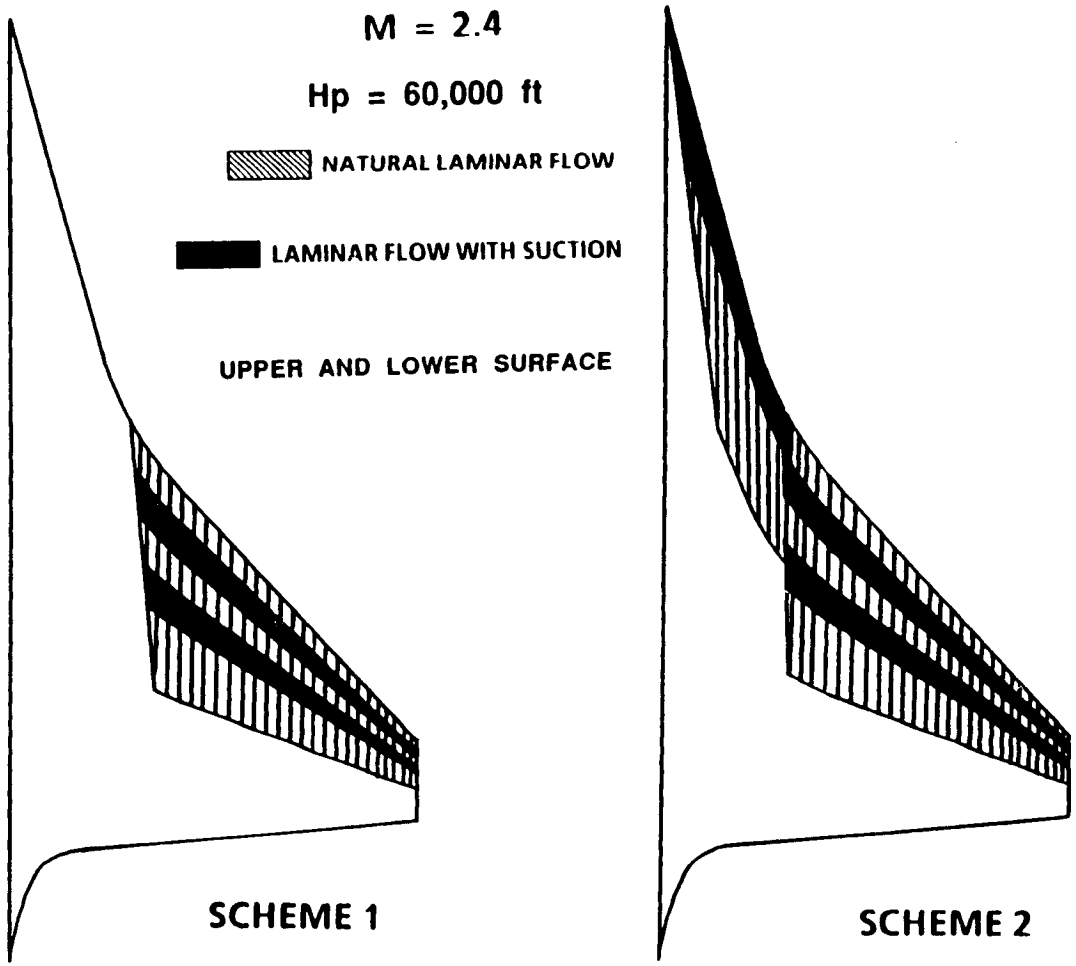

	SCHEME 1	SCHEME 2
TOTAL CRUISE DRAG REDUCTION BENEFIT	6.0%	8.2%
CRUISE L/D (Turbulent Baseline = 9.2)	9.8	10.0

Figure 1 Total Cruise Drag Reduction Benefit of Two Hybrid Laminarization Schemes

wing alone was attempted. Scheme 2, which attempted laminarization of both inboard and outboard areas of the wing resulted in an 8.2 percent reduction in the total cruise drag. Both upper and lower surface laminarization was assumed in the two schemes.

In the structural and systems concept development task, it was found that the ducting required to handle the suction flow rates specified from aerodynamic analysis, could be accommodated within the available space on the SST configuration. A distributed, electric motor driven suction compressor scheme was compared with a central mechanically driven compressor scheme with direct shaft power extraction from the main engines. Although the electric motor driven compressor scheme had a slight advantage in terms of fuel volume displaced, the mechanically driven compressor scheme proved clearly superior in terms of system weight and power extraction penalties. Discharge of the suction air at the free stream velocity, although resulting in no net suction air momentum drag penalty, required excessive compressor and drive system weight as well as power extraction penalties. A trade study determined the condition of sonic discharge for the compressed suction air to be the best compromise. Preliminary structural concepts were developed for integrating the suction ducting with the composite structure in order to minimize the weight and fuel volume displacement penalties. Preliminary leading edge concepts which would enable the use of suction system for boundary layer control and thereby improve the low speed, high lift performance were also developed.

The aerodynamic benefits of reduced skin friction drag due to laminarization were weighed against the penalties of suction system weight, fuel displacement and engine power extraction in the SST performance and sizing program. The results for laminarization scheme 2 are shown in Fig. 2, where the effect of range is also evident. At the 5000 nmi range, the cycled LFC configuration showed 8.5, 6.2 and 12.0 percent reductions in MTOW, OEW and fuel consumption respectively when compared to the baseline turbulent configuration. At the 6500 nmi range, these benefits increased to 12.6, 9.8 and 16.0 percent reductions respectively. A preliminary calculation showed a 25 percent reduction in the fuel heating rate resulting from the implementation of this laminarization scheme.

In conclusion, this initial study of LFC application to an SST configuration indicated the aerodynamic feasibility of achieving significant laminarization of the wing surface.

Preliminary assessment of the systems and structural requirements to achieve this laminarization showed that the aerodynamic benefits of drag reduction outweigh the system weight, volume and power requirement penalties. The potential net performance benefits in terms of reductions in MTOW, OEW and fuel consumption are impressive and improve with increasing mission range.

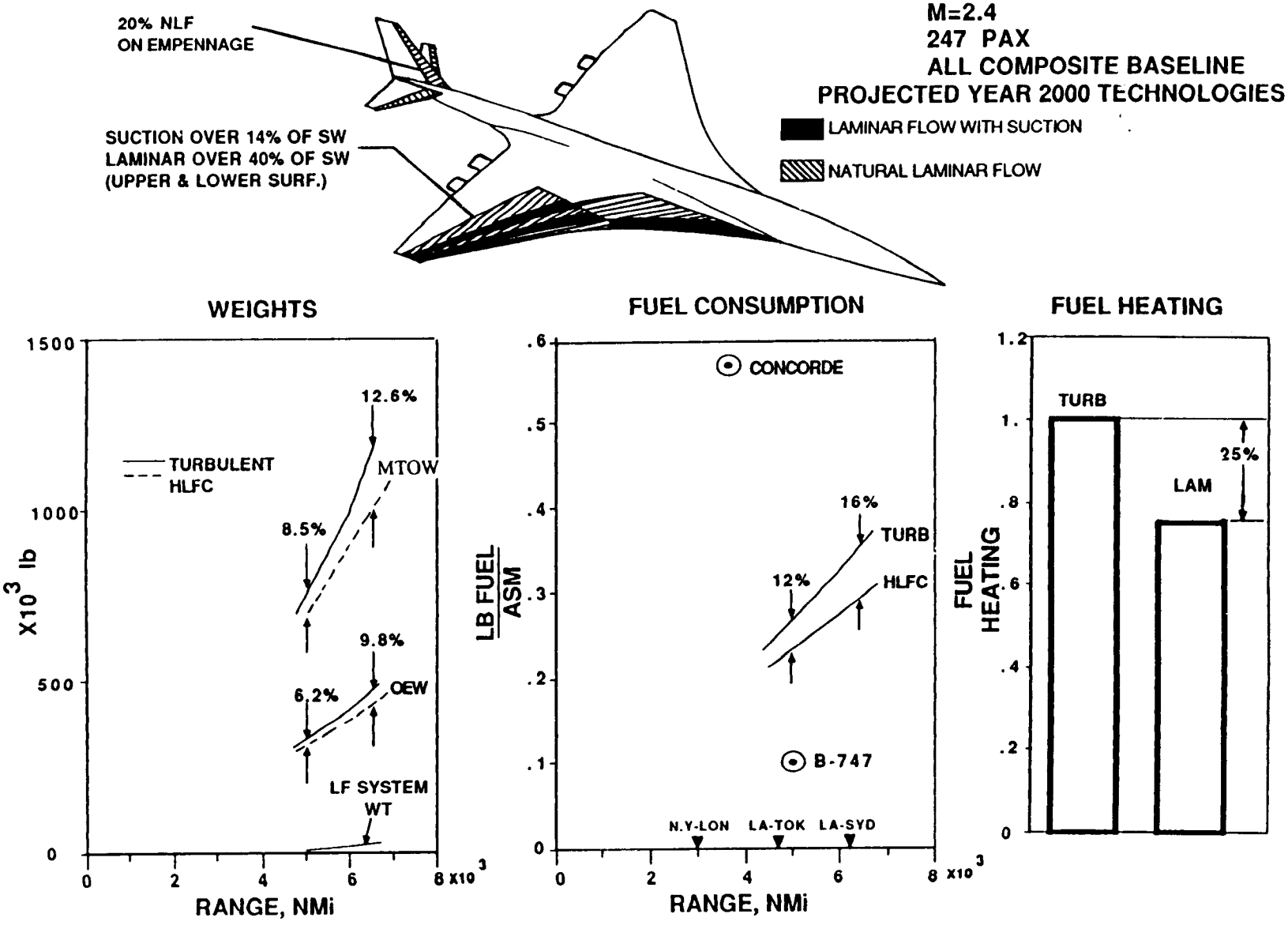

Figure 2 Net Performance Benefits of HLFC (Scheme 2) Implementation

However the present study also pointed to a significant research and development effort in aerodynamics, structures and systems technologies which will be needed to realize these potential benefits in a practical system.

In aerodynamics, 3D nonlinear configuration design capability will need to be developed to achieve wing pressure distributions desirable for laminar flow design. A general 3D boundary layer and stability analysis capability is also needed. Wind tunnel tests will be needed to assess the impact of laminar flow design on the overall aerodynamic performance of the configuration. Flight tests on supersonic aircraft will be needed to develop transition criteria for 3D supersonic boundary layers and to validate laminar flow control concepts. Concepts for integration of the LFC system with the high lift flap system of SST configurations will require considerable development. The potential for use of the LFC suction system as a BLC system for high lift performance improvement needs to be fully explored.

In structures, design concepts for perforated suction surface assemblies and their integration with composite wing skin need to be developed. Work on manufacturing and fabrication technology development in these areas should also be initiated early. Concepts for integration of suction ducts with the structure should be further developed to minimize the impact of system weight and fuel displacement penalties.

In the systems area, much needs to be done in the development of suction air flow control concepts. Concepts and systems for leading edge protection from insect contamination, deicing and anti-icing for both subsonic and supersonic type leading edge geometries need to be developed. The systems compatibility of the LFC suction system with the requirements of the BLC system for high lift needs to be evaluated.

1.0 INTRODUCTION

There are several potential benefits to be gained from an application of laminar flow control technology to supersonic transport aircraft configurations. These include:

1. Impressive increase in range or reduction in maximum takeoff weight (MTOW). Based on a NASA Langley Research Center estimate for an advanced technology Mach 2.7, 250 passenger SST, the MTOW would be reduced by 28 percent if laminar flow over the entire configuration were achieved [1].

2. Reduced sonic boom intensity. The reduction in MTOW leads to a corresponding reduction in sonic boom intensity. If the sonic boom over pressures are reduced below 1 psf level, overland supersonic cruise may become allowable.

3. Reduced community noise during takeoffs. Reduced MTOW reduces takeoff thrust requirements and results in decreased community noise during takeoff.

4. Improved economics. Reduced MTOW and improved fuel efficiency leads to reduced DOC.

5. Reduced aerodynamic heating loads.
   Consequently,
   a. structural temperatures are reduced, increasing material options
   b. fuel heating rate is reduced, enhancing the value of fuel as a heat sink for environmental control systems
   c. for military applications, reduced skin temperature means reduced observables.

However, many issues need to be resolved with regard to the application of laminar flow control to supersonic transport configurations to determine the extent to which these potential benefits could be realized in practice and the associated systems requirements and penalties.

In contrast to the design considerations for subsonic transports, fuel volume requirements are a critical element in the overall sizing considerations of supersonic transport configurations. This is dictated by the desire to minimize the wave drag-due-to-volume and the much larger quantity of fuel required for a given mission range as compared to subsonics. Fuel weight, as a fraction of MTOW for a SST is nearly twice that for a subsonic transport. Consequently, the MTOW of a SST has a much greater sensitivity to any reduction in the drag (i.e., an improvement in L/D). Not only is the quantity of

fuel required to do the mission diminished, there is also a reduction in the structural weight (OEW) because a smaller wing may be allowed to carry the reduced amount of fuel.

Improvements in engine fuel efficiency (TSFC) and reductions in structural weight (OEW) have a similar impact on the vehicle MTOW as shown in the sizing plot of Figure 1.0-1. The airplane OEW is plotted against the MTOW. The upper solid line shows the minimum achievable OEW as a function of MTOW, as dictated by the structural considerations. The lower solid line shows the maximum allowable OEW as a function of MTOW, as determined by the fuel quantity required for the mission. A sized airplane is obtained when the minimum achievable OEW line crosses over the maximum allowable OEW line. The breaks in the two lines represent effects of the need for larger size landing gears or increased number of engines as the MTOW is increased to obtain "closure". The requirements of larger landing gear or additional engines aggravates the closure problem even further and leads to even greater MTOW of the sized airplane. Increase in the required range has a similar impact. The slope of the maximum allowable OEW line is reduced as shown in Figure 1.0-1, leading to large increases in the MTOW of the sized vehicle. Further increases in the range requirement may even lead to situations where the maximum allowable OEW line becomes parallel or divergent with the minimum achievable OEW line and a closed configuration is not found even if the MTOW is allowed to increase indefinitely. Improvements in L/D, TSFC and efficient structural materials have the opposite effect. They allow closure at a lower MTOW or lead to increased range for a fixed MTOW. In this light, improvements in L/D, TSFC and materials technology become particularly important for a long range SST.

Typically, skin friction (viscous) drag accounts for approximately 50 percent of the total drag of a subsonic transport at cruise. For SST configurations that percentage is smaller, because of the presence of wave drag components at supersonic speeds. The drag buildup of two supersonic configurations at a typical cruise condition (C_L = 0.12) is shown in Figure 1.0-2. Configuration 733-633, having a "double delta" planform, has a supersonic leading edge over the outboard portion of the wing, while configuration 733-636, having an "arrow wing" planform, has a subsonic leading edge. The -636 configuration has a lower wave drag as well as a lower total cruise drag as compared to the -633 configuration. The arrow wing planform, while more efficient in supersonic cruise, has poorer low speed performance and generally a larger wing weight. Skin friction drag is about 35 and 42 percent of the total drag for configurations -633 and -636 respectively. The percent skin friction drag for -636 is higher because of two reasons: 1) lower wave drag and 2) larger wing (wetted) area to achieve the same span as -633, the latter element being dictated by low speed performance requirements. The smaller value of viscous drag as a fraction of total drag means that for a given percent reduction in the viscous drag due to laminar

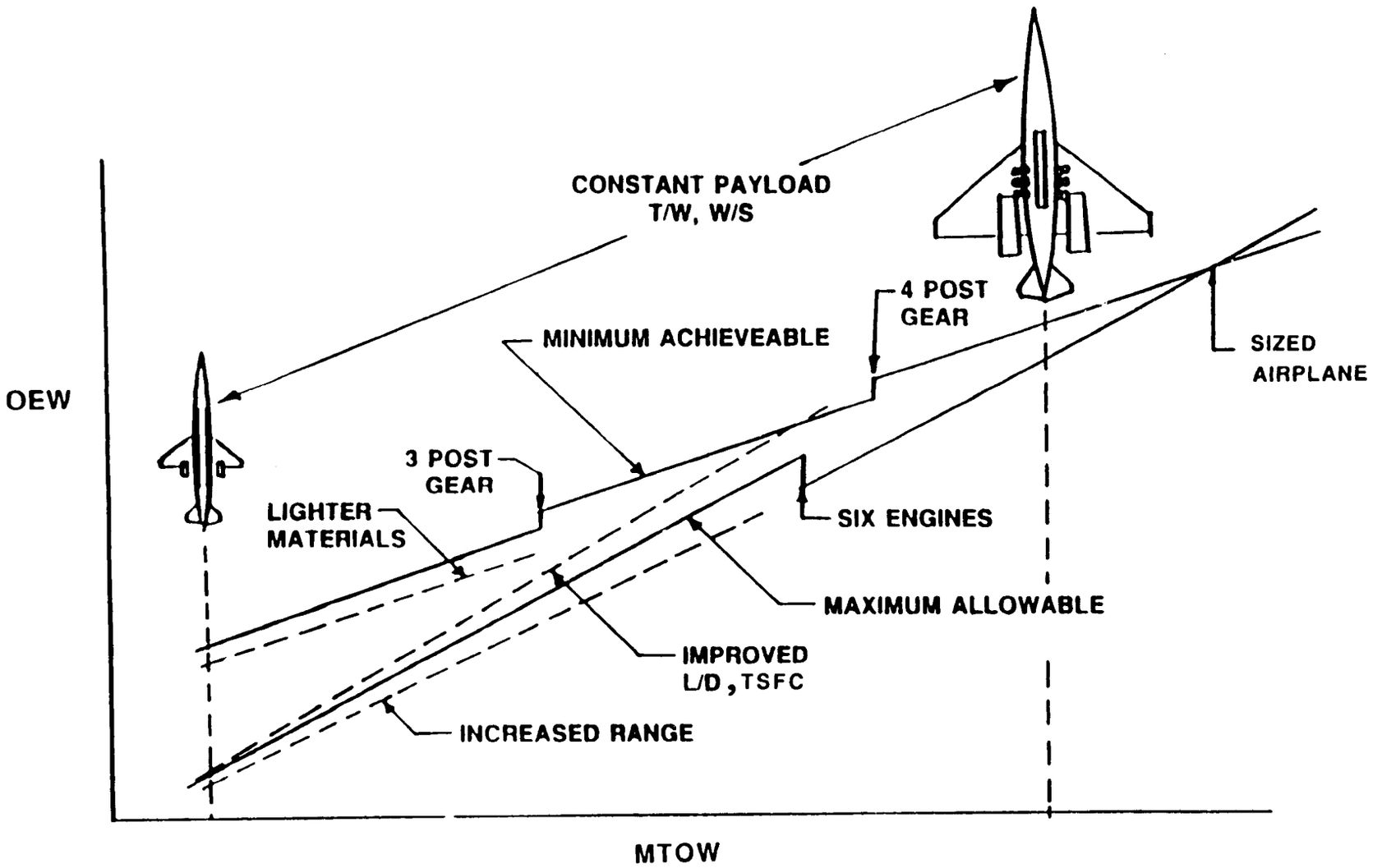

Figure 1.0-1 Airplane Sizing Plot

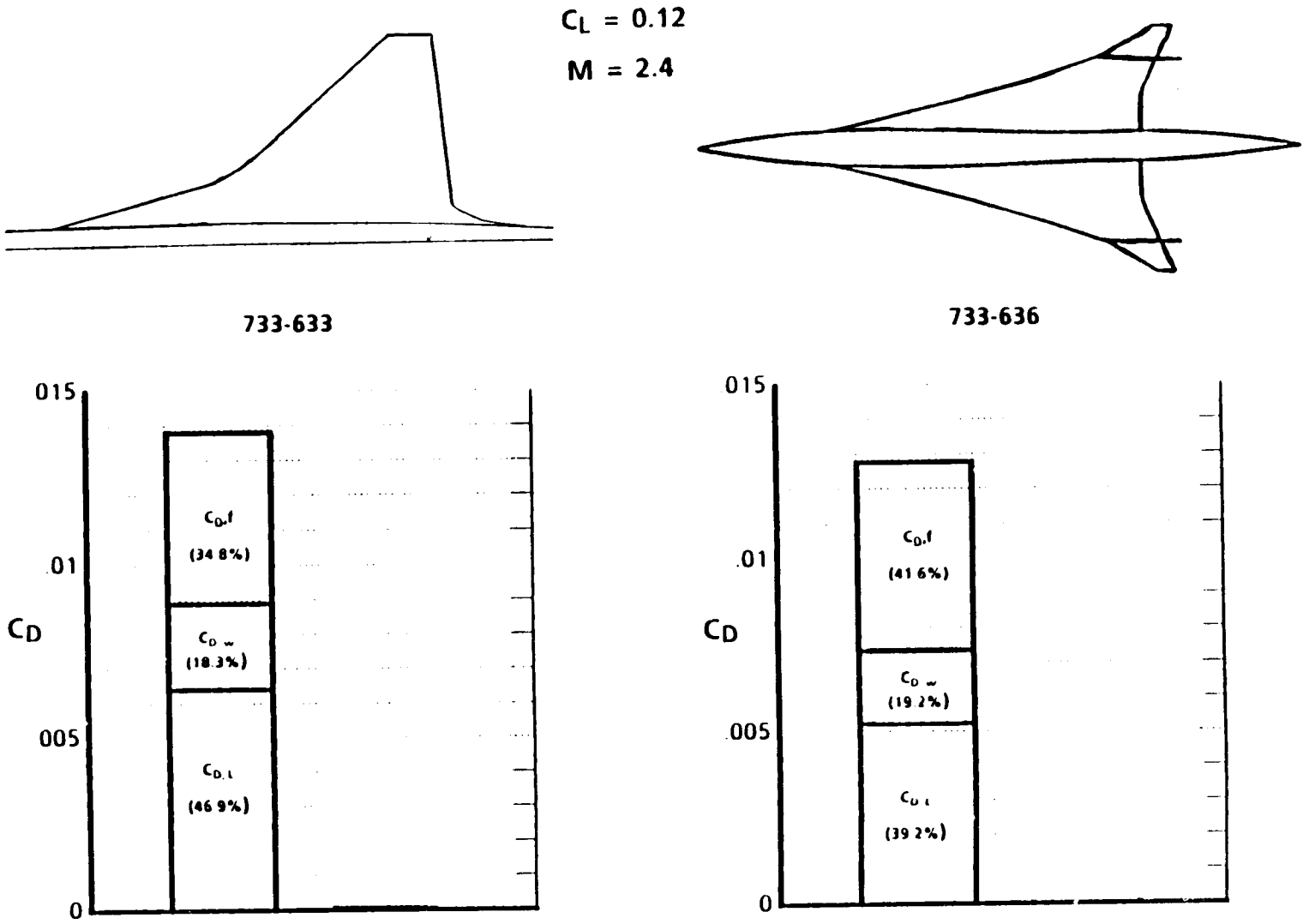

Figure 1.0-2 Cruise Drag Buildup of Two Supersonic Configurations

ization, the percent reduction in the total drag for supersonic transport configurations is somewhat smaller as compared to subsonics.

In evaluating the net benefits of LFC implementation on a supersonic transport configuration, the improvements in L/D due to viscous drag reduction must be weighed against the possible penalties associated with the effect on other drag components, suction system weight, power requirement and fuel volume displacement. The implementation of laminar flow may require a specific type of pressure distribution on the configuration surface which may adversely impact the drag-due-to-lift. The suction system weight adds to the OEW of the configuration and therefore tends to increase the MTOW. Installation of suction ducting in an already fuel volume limited configuration may require thickening of the wing to accommodate the displaced fuel and thereby increase the wave drag-due-to-volume. The power required to drive the suction compressors may be extracted from the main engines, but at an expense of a TSFC penalty. In addition, the compatibility of any LFC scheme with the high lift flap system of the configuration must also be evaluated. Thus, the issues to be addressed in a successful application of laminar flow control to supersonic transport configurations relate not only to achievement of high transition Reynolds Numbers on the configuration surface, but also to how a typical turbulent SST configuration would have to be modified, both aerodynamically and structurally, as well as considerations of the attendant penalties.

1.1 STUDY OBJECTIVES

The present study was an initial attempt at addressing many of these issues with the following specific objectives:

1. Utilize existing analytical tools and transition criteria to predict the extent of laminar flow on supersonic transport configurations with and without laminar flow control.

2. Identify the necessary modifications to an existing SST configuration to achieve significant laminarization on the wing surface and assess the impact of these modifications on viscous and other drag components.

3. Evaluate structural and systems concepts required for the modification of the existing baseline SST configuration to achieve significant laminarization.

4. Assess the overall performance benefits of applying laminar flow control to the baseline turbulent SST configuration.

5. Identify future research requirements, including wind tunnel and flight tests, for improvements in existing transition prediction and

wing design capability, validation of laminarization concepts, evaluation of the impact of laminar flow design on the overall aerodynamic performance and the enhancement of the net benefits of LFC implementation.

1.2 STUDY APPROACH

To meet the above objectives, the study was organized into the following four tasks.

1. **Supersonic Transition Prediction and Laminarization Schemes**
   In this task, existing stability theory calculations as well as wind tunnel and flight experiments on supersonic transition with and without laminar flow control employing suction and wall cooling were surveyed. The specific SST configuration chosen for the present study was Model 733-633, a double delta wing planform configuration developed at Boeing during the NASA funded SCAR* studies of the 1970's [36]. Existing 3D linear and nonlinear inviscid codes at Boeing were utilized to predict the pressure distribution on the baseline SST configuration. The momentum thickness Reynolds number ($Re_{\theta,a.l}$) of the attachment line boundary layer on the highly swept leading edge of the inboard wing was estimated. The attachment line suction requirements to keep $Re_{\theta,a.l.}$ value below a currently accepted threshold to ensure its stability against small free stream disturbances were determined. The wing boundary layer developing under the predicted inviscid pressure distribution was calculated using a Boeing 3D boundary layer code and the swept tapered wing (conical flow) approximation. The effects of wall cooling and suction could be modeled in these calculations. The stability of the boundary layer profiles for both Tollmien-Schlichting (TS) and cross flow (CF) modes was then calculated using a Boeing modified version of the Mack Code. The calculations of 3D boundary layers, stability analyses for TS and CF, and the integration of disturbance growth rates were all carried out within a system of programs known as Unified Stability System (USS). Several modifications to parts of this system of programs were required for specific applications to supersonic boundary layers. A transition criterion based on subsonic natural laminar flow flight tests on F-111 [8] and Boeing 757 [10] aircraft was used for prediction of transition in supersonic boundary layers with simultaneous growth of TS and CF modes of instability. Suction requirements for significant laminarization of both subsonic and supersonic leading edge regions were determined. Three different wing laminarization schemes were considered, of which two were selected for detailed design/benefit

* Supersonic Cruise Aircraft Research

evaluation. Issues of the compatibility of the proposed laminarization schemes with the high lift system of the configuration were addressed.

2. Structural and Systems Concept Development

In this task concepts for structural and systems modifications required to achieve suction laminarization of an all composite baseline turbulent SST configuration were developed. An aerodynamically similar but structurally updated version (Model 1080-834) of Model 733-633 was used as the baseline turbulent configuration. Suction through a perforated titanium skin was assumed in all cases. Possibilities of accommodating required size ducting within the existing structure were explored. Various arrangements for ducting the air to suction compressors were considered with a view to minimizing the fuel volume displacement and weight penalties. Availability of or the feasibility of the development of suction compressors required for the present application was explored with two suppliers. Various means of powering and locating the suction compressors were considered, again with a view to minimizing the TSFC, weight and fuel volume displacement penalties.

3. Design/Benefit Studies

The net viscous drag reduction for the predicted extent of laminar flow for two laminarization schemes was calculated by a strip theory method. The impact on the total drag of the configuration was then calculated. Suction locations and mass flow requirements were specified for systems evaluation. Compressor power requirements were estimated and compression ratios selected after evaluating trades between suction air momentum drag penalty and the TSFC and weight penalties. The impacts of aerodynamic (L/D) improvements as well as weight, TSFC, suction air momentum drag and fuel volume displacement penalties on the overall performance of the sized vehicle were evaluated by means of a Boeing SST performance and sizing program. The net benefits in terms of MTOW, OEW and fuel consumption reduction were estimated for the two laminarization schemes.

4. Future Research Requirements

Several research needs were identified during the course of the present study for improvements in existing transition prediction capability, development of nonlinear supersonic wing design capability, validation of laminarization concepts, assessment of the impact of laminar flow design on the overall aerodynamic performance of the configuration as well as enhancement of the net benefits of LFC implementation. These were organized in three general areas: a) Improved Transition Prediction and Wing Design Capability, b)

Conceptual Design Studies, and c) Wind Tunnel and Flight Experiments.

2.0 SUPERSONIC TRANSITION PREDICTION AND LAMINARIZATION SCHEMES

2.1 TRANSITION PROCESS

The problem of predicting transition from laminar to turbulent flow in the boundary layer on the surface of a body immersed in a fluid stream is a complex one. It is now widely accepted that transition is a result of the instability of the laminar boundary layer. Disturbances present in the external stream or emanating from the body surface are amplified in the laminar boundary layer due to the hydrodynamic instability, leading to increasing amplitudes of fluctuations and an eventual breakdown of the orderly laminar flow into a chaotic turbulent motion. If the initial disturbance levels are large enough, the transition to turbulence can be spontaneous rather than gradual as described above. For situations where the initial disturbance levels are small enough, so that transition occurs as a result of the amplification of disturbances within the boundary layer, the process may be depicted by three stages as shown in Figure 2.1-1.

The first stage in an orderly transition process involves receptivity. In this stage external disturbances are "internalized" into the boundary layer. Not all disturbances (as characterized by their rms level and spectral content) are equally well received by the laminar boundary layer at a given stage in its growth. Some disturbances are internalized more efficiently than others. This stage of the transition process is not well understood and research into receptivity mechanisms is currently in progress [2,3].

The external disturbances, once internalized in the boundary layer are either amplified or suppressed depending upon their characteristics (frequency, wave length, wave angle). There can be rare situations where all disturbances, regardless of their character are suppressed. Eventually, however, as the laminar boundary layer grows, a so-called neutral stability point is reached, beyond which at least some of the internalized disturbances begin to amplify. This is the second stage of the transition process - the linear disturbance growth stage.

In the linear disturbance growth stage, the internalized disturbances, although continually growing in amplitude, remain small (less than 0.5 percent) compared to the mean flow. The growth (and decay) of such small disturbances in the laminar boundary layer can be analyzed by linear methods and an elegant mathematical structure of linear stability theory has been developed over the past several decades following the original work of Tollmien and Schlichting [4]. The aim of the linear stability theory is to predict the growth of the amplitude ratio (A/A_0, where A_0 = initial amplitude at neutral point) in an evolving laminar boundary layer. The amplitude ratio is conventionally represented as

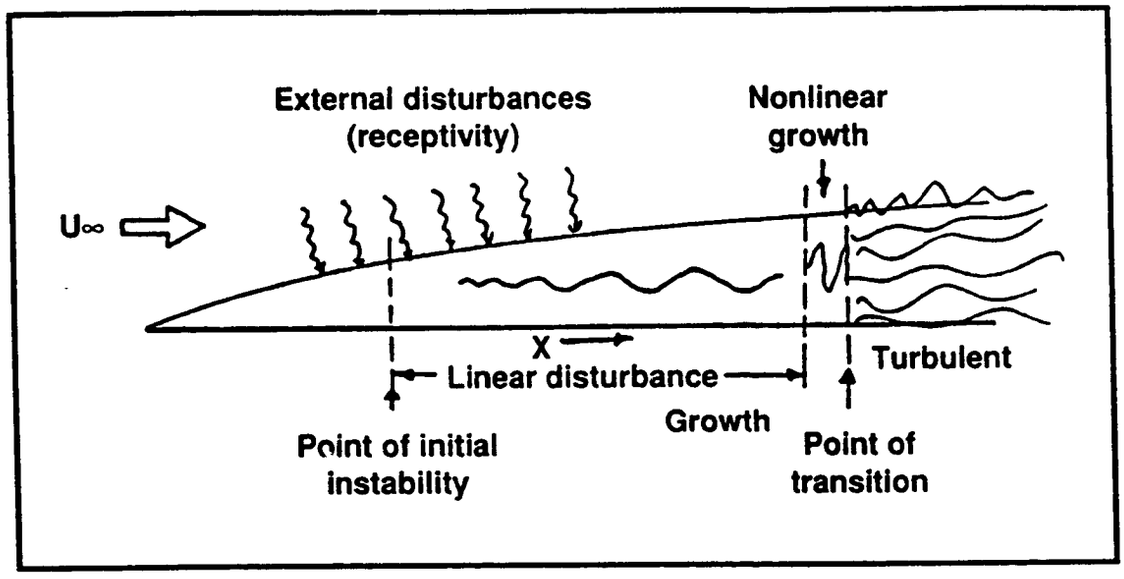

Figure 2.1-1 Transition Process

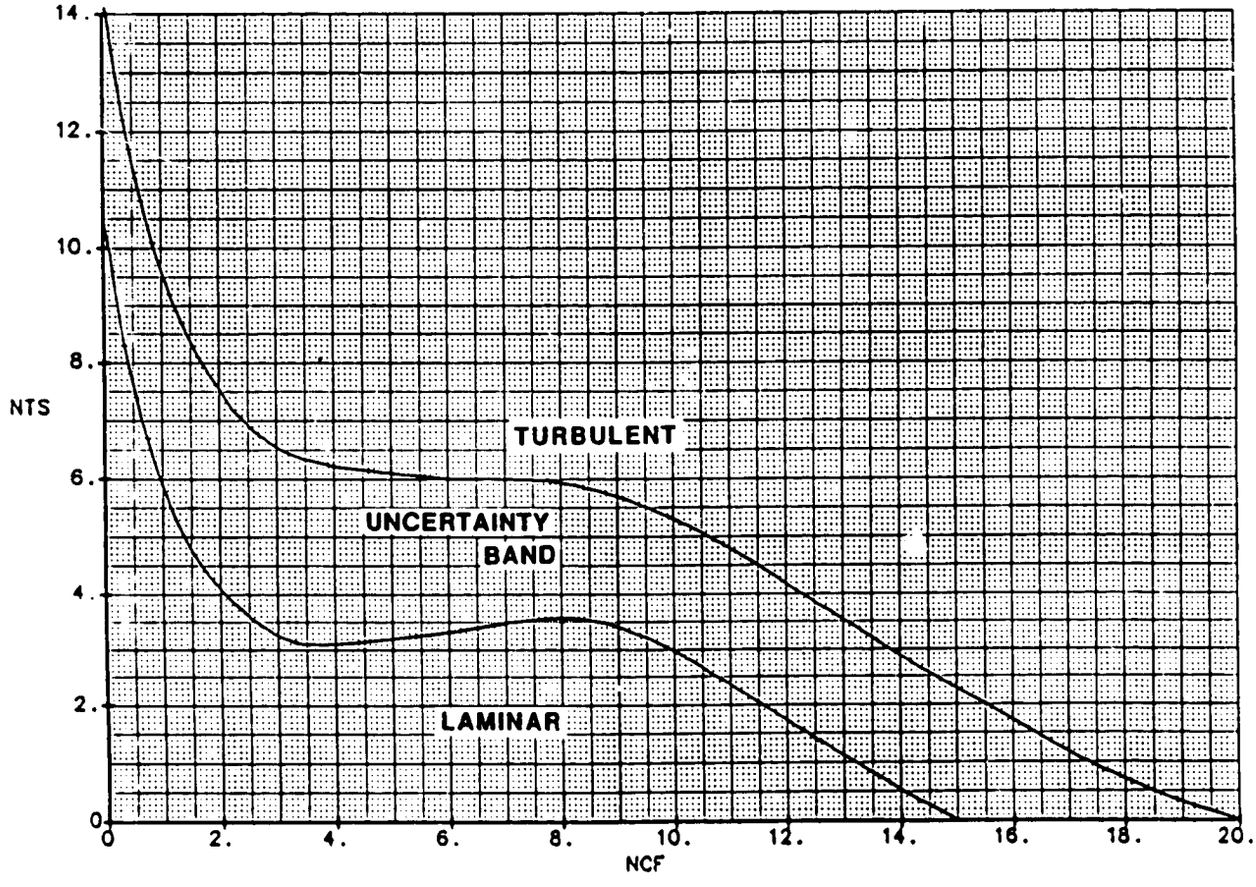

Figure 2.2-1 Transition Data Band (F111/B757 Data)

$$A/A_o = \exp(N)$$

where, the exponent N, also known as the N-factor, is a measure of the linear disturbance growth.

Beyond the linear disturbance growth stage, the disturbance amplitudes in the boundary layer may no longer be regarded as small and the approximations of linear stability theory are no longer valid. Nonlinear interactions between the large amplitude disturbances and mean flow cause a rapid increase in disturbance growth, leading to a breakdown of laminar motion into turbulent "spots". Both skin friction and heat transfer coefficients at the body surface begin to rise rapidly and transition is said to have occurred. This final stage of the transition process - the nonlinear growth stage - is relatively short in its spatial extent in comparison with the linear disturbance growth stage.

2.2 TRANSITION PREDICTION

A relatively simplistic approach has been used with reasonable success to model this complex three stage transition process and to predict the transition location [5]. In this so-called e^N approach, the initial (receptivity) and final (nonlinear growth) stages of the transition process are completely disregarded. The amplitude ratio (A/A_o) is calculated on the basis of linear stability theory and transition is predicted at the point where an empirical value of the amplitude ratio is attained. The amplitude ratio value is conventionally expressed in terms of the N-factor such that $N = \ln (A/A_o)$. The empirical N-factor value at transition is determined from a correlation of linear stability theory calculations with available experimental data.

Much of the discussion up to this point relates to transition in a 2D boundary layer wherein the instability is of the viscous type, also known as the Tollmien-Schlichting (TS) type. In 3D boundary layers two additional types of instability are of concern: The cross flow (CF) instability and Taylor-Gortler (TG) type of instability. The CF type of instability arises in a 3D boundary layer where there exists, within the boundary layer, a significant velocity component (cross flow) normal to the local external (inviscid) flow velocity vector. The profile of cross flow velocity component contains a point of inflection since, by definition, the crossflow velocity component is zero at the wall as well as at the edge of the boundary layer. For this reason, the cross flow (CF) instability is of the inflectional type. This type of situation arises in the boundary layer on a swept wing when a streamwise pressure gradient is present in combination with sweep. The TG type of instability arises in boundary layer flow over a streamwise concave surface.

When more than one type of instability is present in a 3D boundary layer, the interaction between them becomes a significant factor in predicting the transition location. The CF type instability results in a set of stationary or travelling co-rotating, streamwise vortices in the boundary layer with a spacing which is predictable by linear stability theory. The TG instability, on the other hand, results in pairs of stationary, counter-rotating streamwise vortices in the boundary layer. Both CF and TG types of instability distort the mean boundary layer profile and thereby have a destabilizing influence on the TS waves as well. When CF and TG vortices are present simultaneously and the cross flow strength exceeds a certain threshold value, the TG vortices get progressively weaker and disappear [6]. The CF instability then becomes the dominant mechanism for transition.

For most wing boundary layer analyses, streamwise concavities are not encountered until the aft portion of the lower surface, at which point transition will probably already have occurred due to mechanisms other than the TG instability. Therefore, for most transition studies, the interaction between the TS and CF types of instability is of interest. A theoretical treatment of the influence of CF on TS waves was presented by Reed [7], where it was concluded that CF vortices would strongly enhance the growth of TS waves. This means that in the presence of CF vortices, the threshold TS N-factor (as calculated by linear theory not accounting for CF-TS interaction) at transition would be significantly reduced. To determine the impact of this interaction, two series of in-flight transition tests using the F-111 [8] and F-14 [9] variable sweep aircraft have been conducted by NASA. Wing pressure distributions and transition locations were carefully measured in flight as a function of the sweep angle. The N-factors at transition for TS and stationery CF instabilities are calculated from the experimental Cp distributions, sweep angles and wing geometry after an approximate 3D boundary layer analysis. Based on the analysis of F-111 transition data at Boeing, a transition data "band" was constructed on an NTS versus (stationery) NCF plot similar to the one shown in Figure 2.2-1. Such a transition criterion was used for natural laminar flow (NLF) glove design on a Boeing 757 aircraft [10]. Based on the transition data from the B-757 NLF tests, a revised transition data band (Fig. 2.2-1) was derived and is currently being used for a hybrid laminar flow glove design [11] on the same aircraft. This approach has also been used in the present study for transition prediction.

It is possible that in the Boeing-757 NLF tests from which the transition data band of Fig. 2.2-1 was derived, stabilizing influence of convex curvature effects in the wing leading edge region may have resulted in delay of transition to relatively high values of NCF for stationery waves. Inclusion of curvature effects in the calculations of Collier et-al [47] showed a stabilizing influence of convex surface curvature on crossflow waves.

A different approach for arriving at a transition criterion has been used for 3D boundary layers by Bushnell and Malik [12]. In the latter approach, no distinction is made between TS and CF wave growths. Instead, the disturbance growth rate at each point on the wing is computed and maximized over a range of wave angles and wave lengths for several frequencies for the 3D boundary layer profile. These maximum growth rates calculated at various stations are then integrated for each frequency to yield the N-factor as a function of distance along the wing chord. Transition is said to occur when the N-factor reaches a value of 10 for any frequency value.

2.3 SUPERSONIC BOUNDARY LAYER TRANSITION

Although a great deal of theoretical and experimental work has been reported on supersonic boundary layer transition, almost all of it is concerned with the TS instability in 2D boundary layers. There are very few investigations, theoretical or experimental, of transition in supersonic 3D boundary layers having CF or TG types of instability in addition to the TS type.

The most striking feature of the TS instability in supersonic boundary layers is the presence of the so-called higher modes of instability, discovered by Mack [13]. These higher modes of instability, however, do not become significant until the free-stream Mach number exceeds about 3.5.

The most amplified first mode TS disturbances even in a 2D boundary layer become oblique to the flow direction as the Mach number increases above 0.8. At Mach number of 3, the most amplified first mode TS disturbance is inclined as much as 65 degrees to the flow direction in a 2D boundary layer. The first mode TS spatial amplification rate shows a dramatic reduction with increasing Mach number as shown in Figure 2.3-1, reprinted from [14]. Notice that the spatial amplification rate of first mode TS instability decreases from its incompressible ($M_\infty = 0$) value of 6.6×10^{-3} to 3.9×10^{-3} at $M_\infty = 1$ and then down to 2.0×10^{-3} at $M_\infty = 2.4$. The wave orientation angle for maximum amplification is indicated on the first mode curve and is seen to increase up to $M_\infty = 3$. The emergence and rapid increase in the amplification rate of the second mode TS instability beyond M = 3.5 may also be seen in this figure.

Another important effect in supersonic boundary layers is the effect of wall cooling on first mode TS amplification rates and transition location. Viscous dissipation, fluid thermal diffusivity and transformation of kinetic energy into internal energy lead to a non uniform temperature distribution in a high speed boundary layer. For insulated wall condition, the maximum temperature occurs at the wall and this maximum temperature is termed

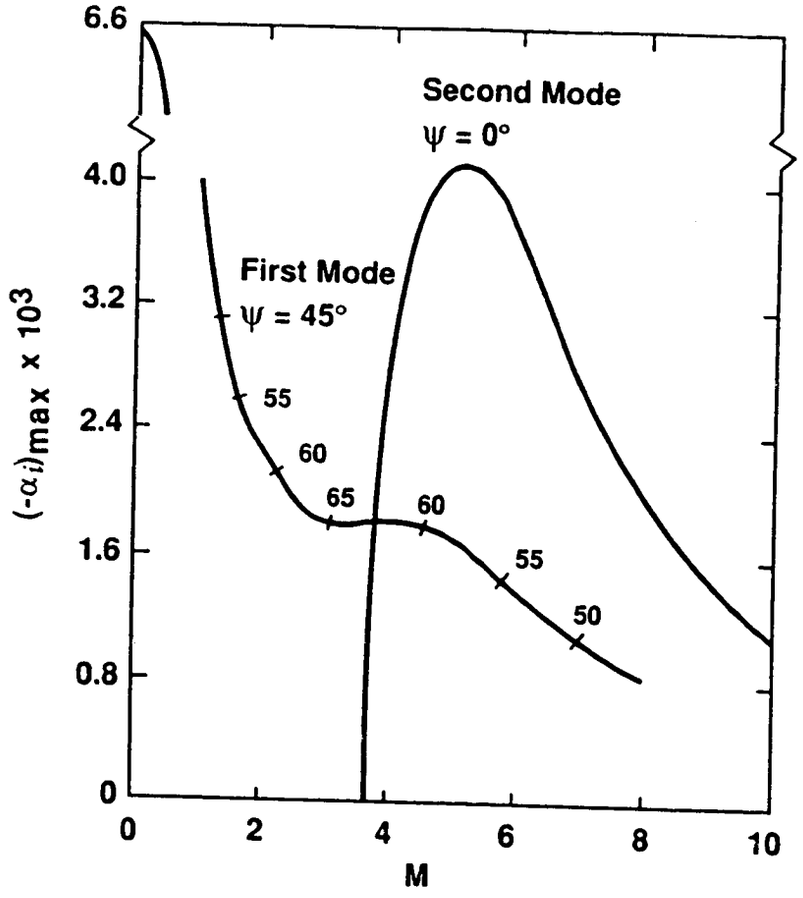

Figure 2.3-1 Effect of Mach Number on Maximum Spatial Amplification Rate at $Re_x=2.25\times10^6$. Adiabatic Flat Plate Mack [14]

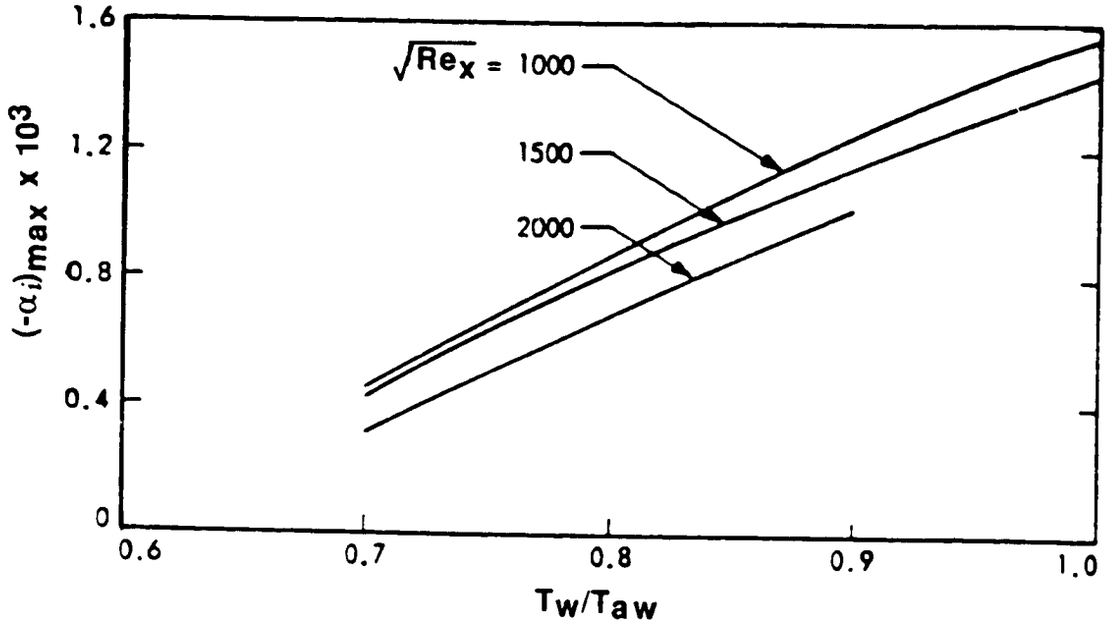

Figure 2.3-2 Effect of Cooling on Maximum Spatial Amplification Rate at M = 3, ψ = 55° and Three Reynolds Numbers. Mack [14]

the adiabatic wall (or recovery) temperature. For air, the adiabatic wall temperature is somewhat lower than the total temperature of the freestream. If the wall temperature is maintained below the adiabatic wall temperature by application of cooling, the maximum spatial amplification rate of first mode TS instability is dramatically reduced below its insulated wall value as shown in Figure 2.3-2. Here Mack's [14] calculated results at M_∞ = 3 and for three flat plate Reynolds Numbers are shown. The maximum spatial amplification rate decreases by a factor of 3 to 4 as the T_w/T_{aw} ratio is reduced from 1.0 to 0.7. While wall cooling has a stabilizing influence on the first mode TS disturbances, the effect on the second mode TS is destabilizing [14,15]. Thus, wall cooling would not be effective in delaying transition for Mach numbers beyond 3.5.

2.4 SUPERSONIC WIND TUNNEL AND FLIGHT NLF EXPERIMENTS

Several wind tunnel and flight tests have been conducted to validate the wall cooling effectiveness in delaying transition for Mach numbers below 3.5. Van Driest, et. al.'s [16,17] wind tunnel results on increase in transition Reynolds Numbers in supersonic boundary layer on a 10 degree cone due to wall cooling are shown in Figure 2.4-1. Notice that the transition Reynolds number increases by a factor of 3 at M = 2.7 as the T_w/T_{aw} ratio is lowered from 1.0 to 0.67. In flight experiments on cones mounted on rockets, Rumsey [18] measured transition Reynolds Number of 33 x 10^6 at M = 3.15 and T_w/T_{aw} = 0.6. In earlier flight tests with a cooled cone mounted on a V2 rocket, Sternberg [19] measured transition Reynolds numbers as high as 90 x 10^6 at M = 2.7. Some of the flight transition data from Rumsey [18] experiments are compared with wind tunnel data correlation of Beckwith [20] in Figure 2.4-2. Notice that the wind tunnel transition Reynolds Numbers are an order of magnitude or more lower than flight data, particularly in the range of Mach numbers between 2 and 4.

The inability to achieve high transition Reynolds Numbers in supersonic wind tunnel experiments has been blamed on the "noise" in supersonic wind tunnels [21,22]. This noise originates in the turbulent boundary layers on the nozzle and test section walls and irradiates the laminar boundary layer on the test article with an intensity sufficient to cause an early transition. In the "quiet" mode of operation, the nozzle and test section wall boundary layers of a supersonic wind tunnel are laminar. In the JPL 20" supersonic tunnel, Kendall observed no transition on a flat plate of a length Reynolds Number 3.3 x 10^6 at M = 4.5 in the quiet mode of operation [15]. The same tunnel at the same Mach number, but with turbulent side wall boundary layers yielded only Re_{tr} = 1 x 10^6 [23]. Thus a vast body of transition data obtained in supersonic wind tunnels is suspect [15,24]. The only supersonic wind tunnel transition data which would possibly yield results comparable to

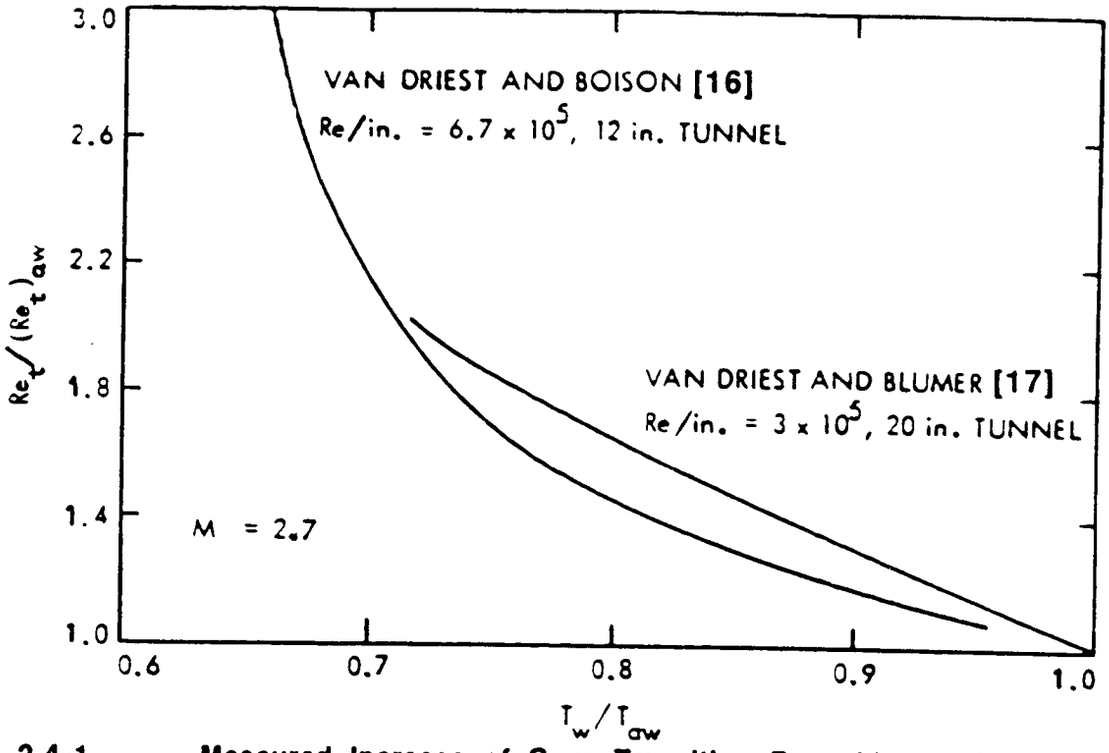

Figure 2.4-1 **Measured Increase of Cone Transition Reynolds Number with Cooling at M =2.7 in Two Different Wind Tunnels. Mack [14]**

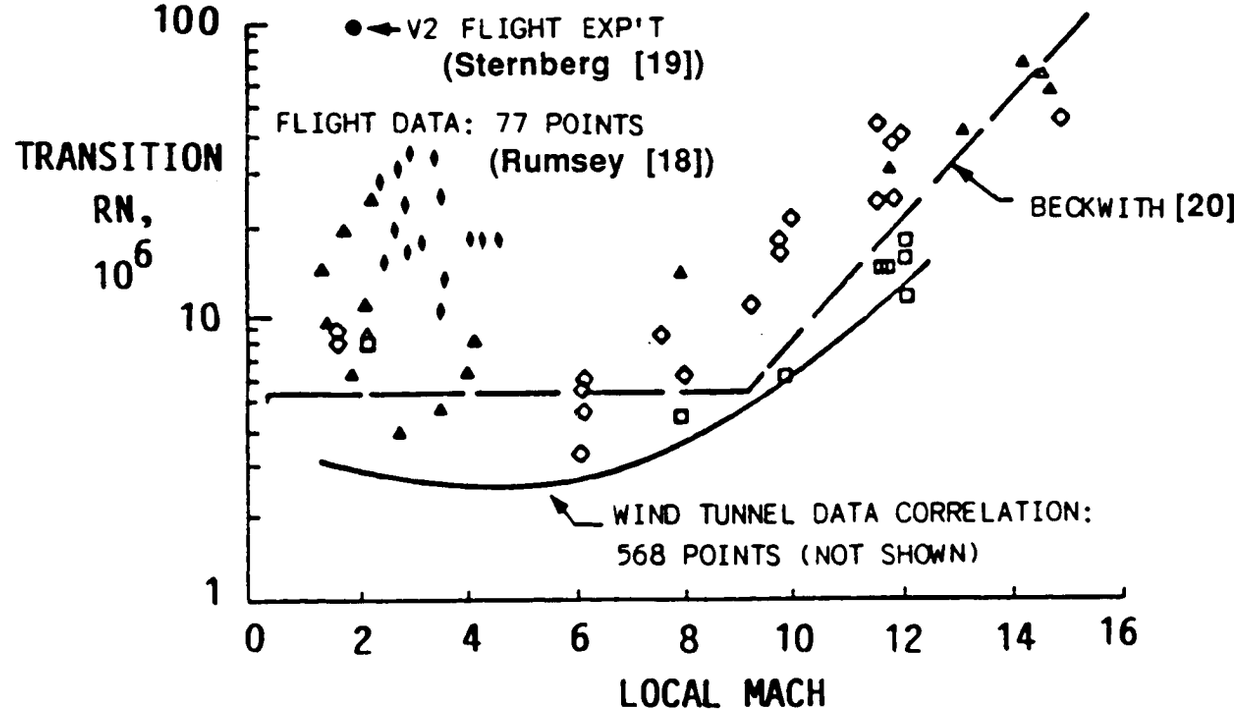

Figure 2.4-2 **Comparison of Wind Tunnel and Flight Transition Data on Cones. Beckwith [20]**

(low freestream turbulence) flight data are the ones obtained in a "quiet" tunnel. At the present time, there is only one such facility: the small scale quiet supersonic pilot tunnel at NASA LaRC [25,26].

Since most of the supersonic transition data in flight have been obtained on cones [18,19,27], there is a need to correlate transition results with flat plate results. Previous tests [31] in "noisy" wind tunnels showed that higher (by a factor of 2 to 3) transition Reynolds Numbers were achievable on cones as compared with a flat plate. Stability theory calculations indicated opposite results. Recent transition tests [26] at M = 3.5 in the NASA LaRC quiet tunnel appear to have resolved this contradiction. Transition tests on a flat plate and a cone in this tunnel have shown that higher transition Reynolds Numbers are indeed achievable on a flat plate. Under "quiet" conditions in the tunnel, a cone-to-flat plate transition Reynolds number ratio of 0.8 was obtained. Stability theory calculations [26] using the COSAL code [28] indicated this ratio to be 0.65 at M = 3.5.

A careful series of supersonic transition flight tests on a 10 degree cone was conducted at NASA Dryden Flight Research facility [27]. The instrumented cone was mounted on the nose of an F-15 aircraft. Transition data were obtained up to a freestream Mach number of 2.0. Although the cone did not have active wall cooling, effect of wall temperature on transition was also investigated during transient heating of the cone at supersonic speeds. Figure 2.4-3 shows transition Reynolds Numbers as a function of the boundary layer edge Mach number at different unit Reynolds Number values for adiabatic wall condition. A threefold increase in the transition Reynolds Number is seen as the Mach number increases from 0.4 to 1.8. The very significant influence of wall temperature on transition location may be seen in Figure 2.4-4. For small departures from adiabatic wall temperature, the transition Reynolds Number is seen to vary as $(T_w/T_{aw})^{-7}$. A comparison of the stability theory predictions of the present study with these transition data will be shown later in Section 2.7.7.

Very few flight tests on supersonic transition in the presence of both TS and CF types of instability have been conducted despite the fact that an early investigation [29] of natural laminar flow on an F-104 fighter wing showed very promising results. Transition measurements were conducted on the wing having a modified biconvex airfoil section with a 3.4 percent thickness-to-chord ratio and a leading edge sweepback angle of 27 degrees. The Mach number range explored was 1.2 to 2.0 at altitudes ranging from 35,000 to 56,000 ft, and unit Reynolds Numbers in the 2 to 4 million per foot range. The modified biconvex section of the wing would result in a streamwise pressure gradient, which, combined with leading edge sweep would generate a boundary layer cross flow component. A laminar run, in the combined presence of TS and CF types of instability, up to a transition Reynolds number of 8 million was observed corresponding to a 35 percent chordwise location of the transition point. A trend of increasing transition

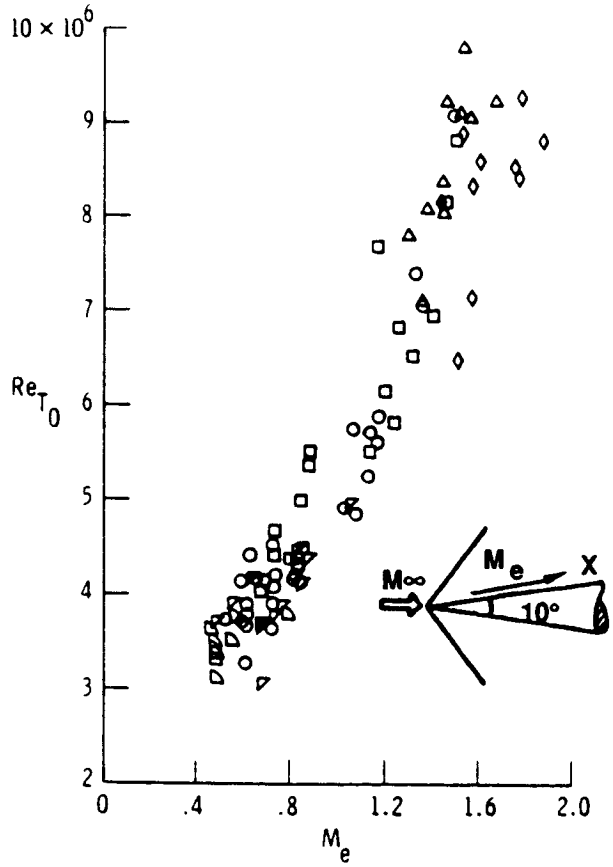

Figure 2.4-3 **Cone Transition Reynolds Number as a Function of Mach Number Fisher and Daugherty [27]**

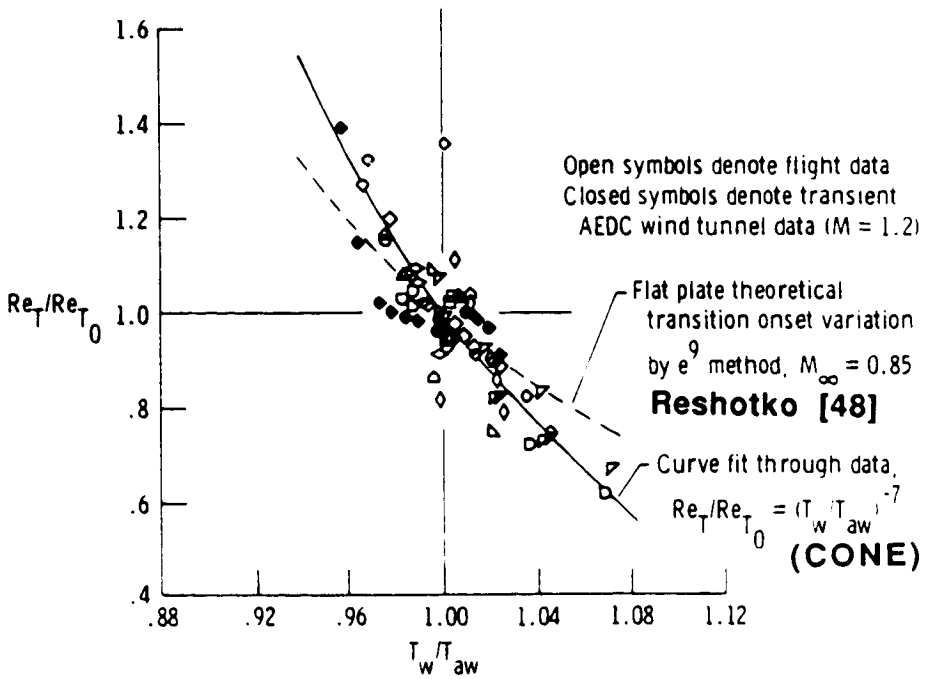

Figure 2.4-4 **Variation in Cone Transition Reynolds Number with Wall Temperature and Comparison with Theoretical and Wind Tunnel Results Fisher and Daugherty [27]**

Reynolds Number with increasing Mach number was observed. Since no airfoil geometry or pressure distribution data were reported, no correlations with stability theory predictions have been performed.

Supersonic transition flight tests were conducted more recently by NASA LaRC and Dryden Flight Research Facility on F-106 and F-15 aircraft [30]. In both cases, transition occurred very close to the attachment line on the wing at flight Mach numbers greater than 1.2 This was believed to have been caused by the initial contamination of the attachment line boundary layer on the rounded leading edge, or strong cross flow development due to high sweep angle (45 and 60 degrees).

2.5 SUPERSONIC WIND TUNNEL LFC EXPERIMENTS

No supersonic flight tests of suction laminarization have been conducted to date. A series of suction laminarization tests was conducted in the AEDC supersonic wind tunnel A in the early 1960's [32,33,34]. Despite the tunnel noise problem discussed earlier, these tests were highly successful in obtaining laminarization up to high Reynolds numbers on flat plate and axisymmetric bodies as well as on unswept to highly swept wing geometries. Given adequate suction, laminarization was maintained even across impinging shocks [32].

On a flat plate suction surface [32], laminarization was achieved up to a Reynolds number of 25.7 million at a suction level of C_Q = 0.0002 in the Mach number range of 2.5 to 3.5. In a subsequent suction experiment [32] on an axisymmetric body with a cylindrical aft portion, laminarization was maintained up to Re_X of 51 million at M = 3, again with a suction level of C_Q = 0.0002. In both the above cases, the maximum achievable laminarization length was limited by the length of the model, i.e., if the model length had been longer, laminar run would have been maintained over even larger Reynolds numbers. For maintaining laminarization across impinging shocks, a local suction level of C_Q = 0.012 was necessary in the impingement region. Slot suction was used in all cases.

Results of suction laminarization tests on a 50 degree swept, tapered wing at Mach numbers from 2.5 to 4.0 were reported in [33]. The wing had a biconvex streamwise section with a thickness to chord ratio of 2.5 percent. Note that this type of airfoil geometry leads to a linearly decreasing pressure from leading to trailing edge. This pressure gradient, combined with the sweep and taper effects gives rise to CF type instability in addition to the TS type. Full chord laminarization was achieved with slot suction up to M = 3.5 and $Re_X = 19.5 \times 10^{-6}$. The suction distribution was quite uniform in the chordwise direction and an average value of C_Q = 0.0002 to 0.0004 was employed depending upon the angle of attack.

Goldsmith [34] conducted suction laminarization tests on a 72 degree infinite swept wing at M = 2 and 2.25. The wing had a rounded, subsonic leading edge and an airfoil section normal to the leading edge which remained subcritical up to freestream Mach number of 2.0. Suction was applied through a series of slots which were cut parallel to the isobars and very closely spaced near the leading edge. The tests were conducted in Tullahoma AEDC Tunnel A. Full chord laminarization was achieved up to chord Reynolds number of 9 million and at Mach numbers of 2.0 and 2.25.

2.6 SUMMARY OF CURRENT KNOWLEDGE OF SUPERSONIC TRANSITION

Summarizing what is known about supersonic transition, increasing Mach number has a stabilizing influence on the first mode TS instability and wall cooling further enhances this stability. Beyond Mach 3.5 second mode TS instability becomes important and wall cooling has a destabilizing influence on this mode. The majority of the transition data obtained in supersonic wind tunnels are affected by the tunnel wall boundary layer noise and are therefore unreliable. Supersonic flight transition experiments on cones under adiabatic and cooled wall conditions have achieved high transition Reynolds numbers consistent with stability theory predictions. Supersonic natural laminar flow (NLF) flight tests on the sharp, supersonic leading edge wing of an F-104 fighter showed some very promising results. In recent supersonic NLF flight tests on F-15 and F-106 aircraft, transition was observed very close to the leading edge because of either attachment line contamination or strong crossflow development at the highly swept rounded leading edge. Supersonic LFC tests conducted in the early sixties in Tullahoma Tunnel A showed excellent prospects for suction laminarization of moderate to high sweep supersonic wings despite the tunnel noise problem and even through impinging shocks.

Very few stability theory calculations of TS and CF instability growths on complex supersonic configurations have been conducted to date. No reliable supersonic flight test data are available with complete documentation of configuration geometry, pressure distributions and measured transition locations to correlate with stability theory calculations and to formulate supersonic transition criteria in the presence of both TS and CF types of instability. Consequently, achievable transition Reynolds numbers on complex SST configurations, either by natural laminar flow or by suction laminarization, were unknown at the time of initiation of the present study. Furthermore, the location and amount of suction required to achieve a desired extent of laminar run based on some adopted transition criterion derived from available transonic flight test data, were also unknown.

2.7 TRANSITION PREDICTION ON A COMPLEX SST CONFIGURATION

Task 1, Supersonic Transition Prediction and Laminarization Schemes, of the present study was a first attempt at determining the existence and extent of laminar flow on a supersonic transport configuration and at determining the aerodynamic modifications and suction requirements to extend the laminar run to high transition Reynolds numbers on the configuration surface.

2.7.1 Baseline SST Configuration

The SST configuration chosen for the aerodynamics part of the present study was Model 733-633, a Mach 2.4 cruise double delta wing planform configuration developed at Boeing during the NASA funded SCAR studies of the 1970's [36]. Figure 2.7.1-1 shows an artist's concept of this SST configuration. The configuration has a large, highly swept inboard strake to accommodate the landing gear and to provide adequate fuel volume capacity. The sweep angle in the strake region is 75 degrees which gives the inboard wing a subsonic leading edge (i.e. Mach number normal to the leading edge is subsonic). The outboard wing has a sharp supersonic leading edge with a sweep angle of 47 degrees. The outboard wing section is wedge-slab-wedge shaped as shown in Figure 2.7.1-2, while the inboard wing has a modified NACA Series 65A section. The fuselage cross-sectional area distribution is selected on the basis of the supersonic area rule to minimize the wave drag due-to-volume, while satisfying minimum area requirements at several specified axial locations. In the mid-chord region, the wing root airfoil section has a thickness comparable to the local fuselage dimension. Therefore a blending of the wing and the fuselage is employed in this region. The blended design helps reduce the zero lift wave drag as well as the viscous drag, because the configuration wetted area is reduced.

The wing camber and twist were designed by use of a linearized lifting surface supersonic design and analysis code [35], accounting for wing/body interference as well as the favorable wing/nacelle interference effects. The engine nacelles are located far aft on the wing lower surface to exploit this favorable interference.

The configuration has an empennage with horizontal and vertical surfaces to meet the stability and control requirements at both cruise and low speed flight conditions. The wing has leading edge high lift devices on both inboard and outboard portions of the wing. The inboard wing leading edge has variable camber flaps while the outboard wing has drooping sharp edge vortex flaps. The wing also has trailing edge flaps with the hinge line at 80 percent chord and spoilers on the upper surface with the hinge line at 70 percent chord.

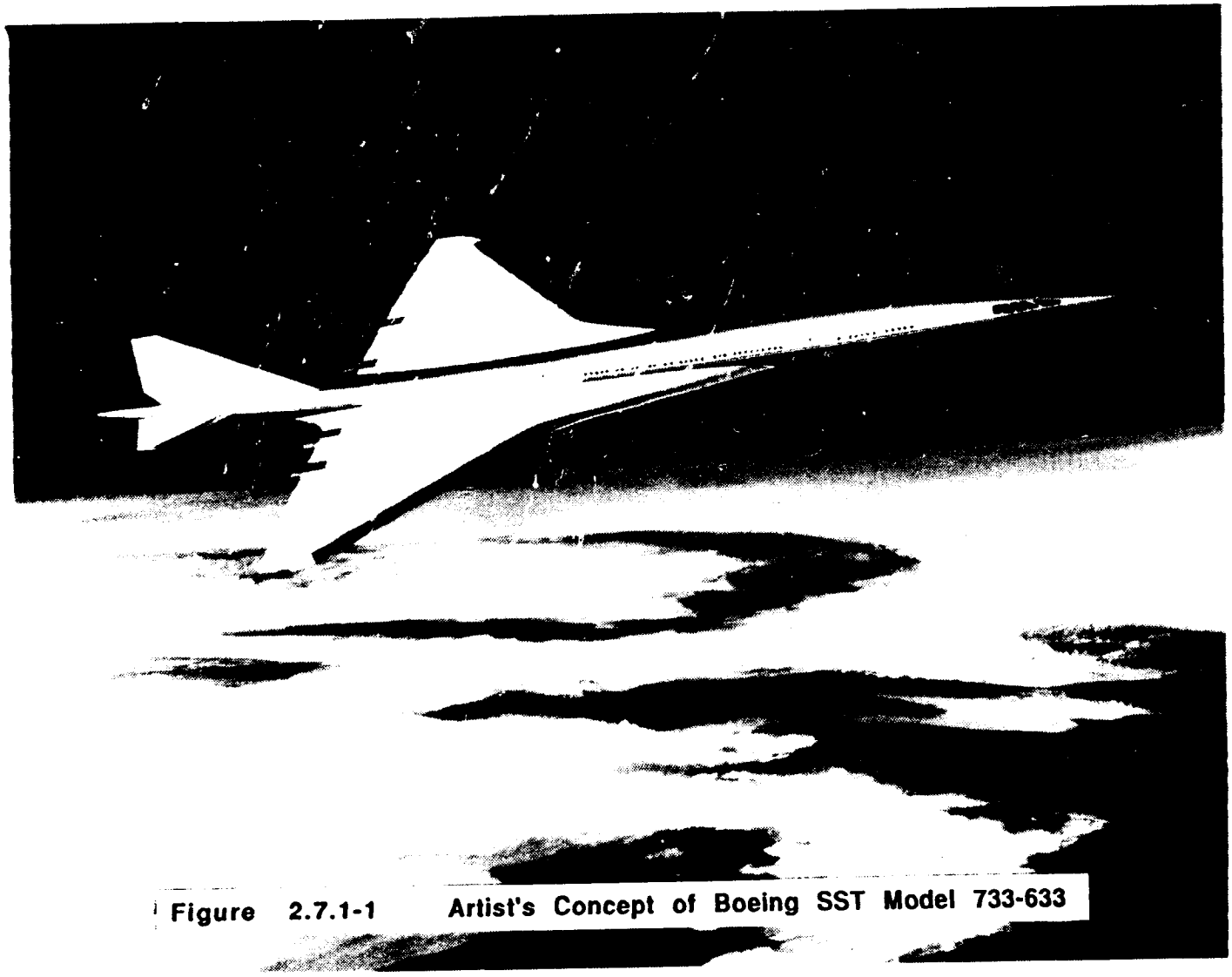

Figure 2.7.1-1 Artist's Concept of Boeing SST Model 733-633

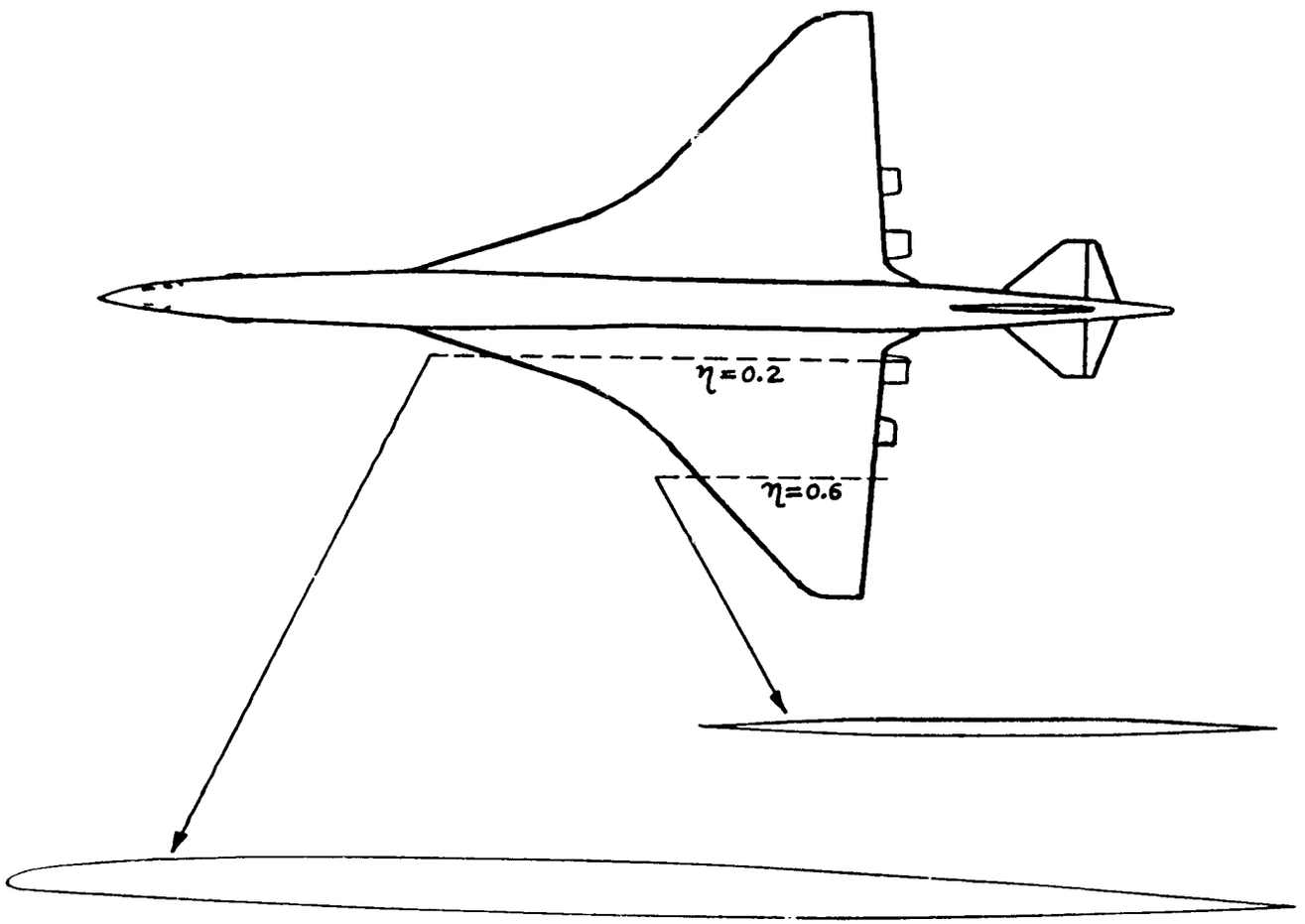

Figure 2.7.1-2 Typical Inboard and Outboard Wing Sections

2.7.2 Aerodynamic Analysis Approach

The steps involved in the aerodynamic analysis leading up to a prediction of transition location on the configuration surface are outlined in Figure 2.7.2-1.

The first step is to compile a precise definition of the configuration geometry. This means that a specification of cartesian (x, y, z) coordinates at a sufficient number of points on the configuration surface is needed so that the coordinates of any other points on the surface can be derived with sufficient accuracy by three dimensional curve-fitting procedures.

The second step is the solution of the inviscid flow field over the configuration surface by use of linear or nonlinear 3D inviscid flow codes. A solution for the pressure (Cp) distribution as well as inviscid surface velocity vectors is obtained as a boundary condition for the 3D boundary layer code.

Next, the 3D boundary layer evolving under the influence of the inviscid flow field on the configuration surface is calculated. Of particular interest are the characteristics of the "attachment line" boundary layer. The attachment line is the surface streamline of the inviscid flow field which separates the flows passing over the upper and lower surfaces of the wing. The boundary layer profiles of two velocity components as well as of temperature and density are obtained at points on the wing surface downstream of the attachment line. For higher accuracy, the viscous/inviscid interaction of the boundary layer and the inviscid flow field should be accounted for by use of the displacement surface concept and cycling of the viscous and inviscid solutions. In the present study this cycling was not carried out, and the boundary layer profiles at various streamwise locations were calculated under the swept, tapered wing (conical flow) approximation.

The stability of the attachment line boundary layer is judged from the momentum thickness Reynolds number (Re_θ) criterion as discussed in Ref. [49]. The latter parameter is dependent on the local redius of curvature, the sweep angle and the gradient of chordwise inviscid velocity component.

A linear stability analysis is then carried out on the computed boundary layer profiles under the assumption of local parallel flow. TS and CF spatial growth rates as well as the group velocity direction are determined for each profile. The term group velocity direction refers to the direction of propagation of the wave packet containing many different amplitudes, wave lengths, frequencies and wave directions characteristic of the disturbance at the analysis station. In most cases, the group velocity direction of a 3D boundary layer profile is close to the local edge velocity direction.

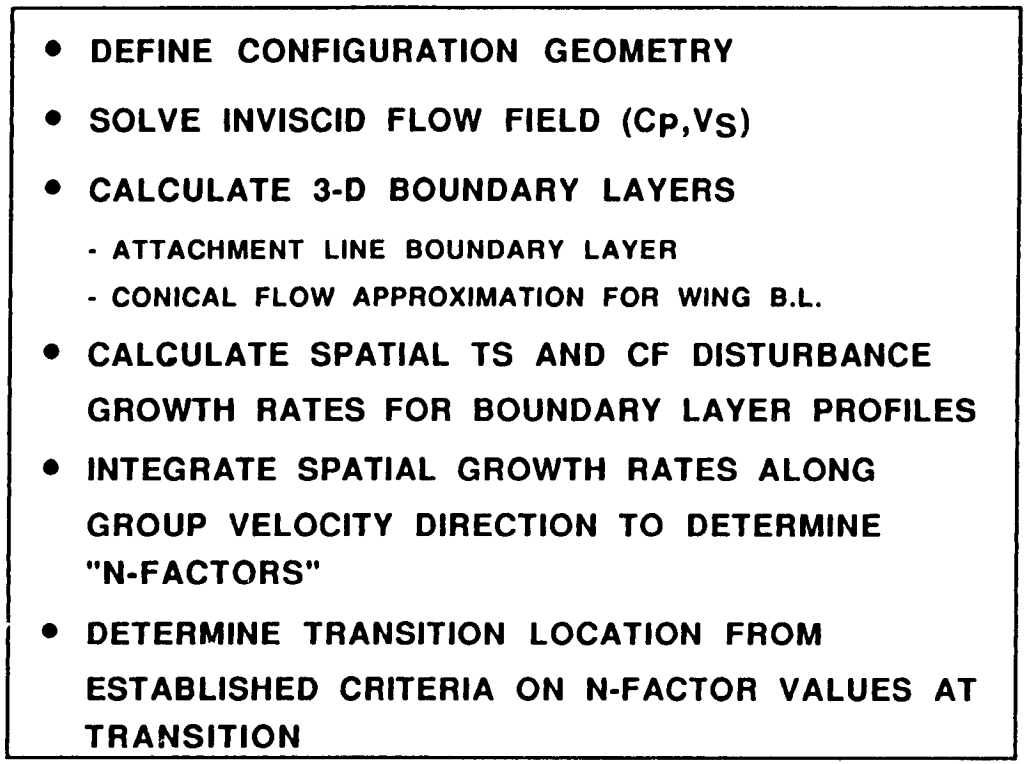

Figure 2.7.2-1 Steps Involved in Aerodynamic Analysis for Transition Prediction

The TS and CF N-factors are then computed by integration of TS and CF spatial growth rates along the group velocity direction. This process yields pairs of values of TS and CF N-factors at various points on the configuration surface.

In the present study for a prediction of transition based on these TS and CF N-factor pairs, a criterion showing a transition line on an N_{TS} versus N_{CF} plot is needed. Such a criterion derived from the NLF tests on F-111 and B-757 aircraft wings [6,8] is shown in Figure 2.2-1. Due to the scatter in the transition data, a "band" separating laminar and turbulent regions is shown rather than a single line.

At the inception of the present study, it was intended to calculate a full 3D laminar boundary layer on the wing surfaces and perform a general stability analysis on the computed profiles as described above. However, due to difficulties in calculating a general 3D boundary layer on the wing (as will be discussed in Section 2.7.4) a simpler quasi-3D boundary layer solution was obtained under the tapered, swept wing approximation. The stability analyses were performed on these approximate 3D boundary layer solutions.

2.7.3 Configuration Geometry Definition

The geometry definition of the 733-633 configuration analyzed in the present study was available separately for wing and body in different forms. The wing definition was available from [36] in the form of an output from the camber design and optimization module of the linearized supersonic flow code A389 [35]. The wing geometry definition is included in Appendix I of this report. The definition consists of a) the planform shape, b) camber distribution and c) thickness distribution.

The planform definition consists of the semispan fraction (2y/b) and corresponding values of the leading edge Z coordinate with respect to the wing reference plane, the leading edge x-coordinate and the chord length.

The wing camber distribution as designed and optimized by the A389 program [33] is tabulated next for various semispan locations and 14 chord fraction values for each semispan station.

Finally, the wing thickness distribution (t/2c) is tabulated in a similar fashion for various semispan stations and 20 different chordwise locations. Note that the chordwise (percent chord) stations where the camber shape is prescribed are different from those where the thickness distribution is prescribed. The percent semispan stations are identical for camber and thickness prescriptions.

A computer program was written to combine these planform, camber and thickness definitions and prepare geometry information in the form of upper and lower surface wing coordinates at various streamwise (rib) cuts.

The body definition was not available in digitized form. This information had to be extracted from the drawings of a wind tunnel model which was built in 1978. Body cross-sections at various streamwise stations were digitized by use of an x-y digitizer. For the (wing/body) blended part of the configuration the wing/body junction was specified at 0.075 semispan to enable separate geometric definitions of wing and body in this region. Body cross-sections at several streamwise stations are shown in Figure 2.7.3-1.

The digital information on wing and body definitions was combined by use of a Boeing geometry software package known as Aero Grid and Paneling System (AGPS) [50]. AGPS contains 3D curve fitting and smoothing routines and prepares configuration geometry in a form acceptable for CFD analysis codes. It also combines the geometry definitions of wing and body to define the wing/body junction.

The original wing definition did not contain sufficient number of points near the leading edge to define the airfoil nose region accurately. Also the nose radius distribution in the original geometry was as shown in Figure 2.7.3-2, i.e., the nose radius dropped to zero (sharp leading edge) at 42.5 percent semispan. On the other hand, the leading edge sweep angle Λ becomes the same as the Mach angle (μ) at 32.5 percent semispan station. Thus in the region between 32.5 and 42.5 percent semispan the leading edge is inclined with respect to the freestream at an angle less than the Mach angle, i.e., it becomes a supersonic leading edge. However, it is still rounded in this region. The first attempt at an inviscid supersonic solution for this configuration was planned to be with an application of a panel method code. It was anticipated that a combination of a rounded nose together with supersonic leading edge in the region of 32.5 to 42.5 percent semispan as discussed above would have resulted in superinclined panels, unacceptable for the panel code. To alleviate this problem, the configuration geometry was revised with a new leading edge radius distribution such that the nose radius dropped to zero at 32.5 percent semispan. In the inboard part of the strake region the radius was prescribed to be constant at 2 inches as shown in Figure 2.7.3-2.

Nacelles and empennage were not included in the geometry definition of the present study because their influence on the wing pressure field was expected to be in regions beyond where wing laminarization was being considered. A photograph of the AGPS definition of the 733-633 wing/body configuration is shown in Figure 2.7.3-3.

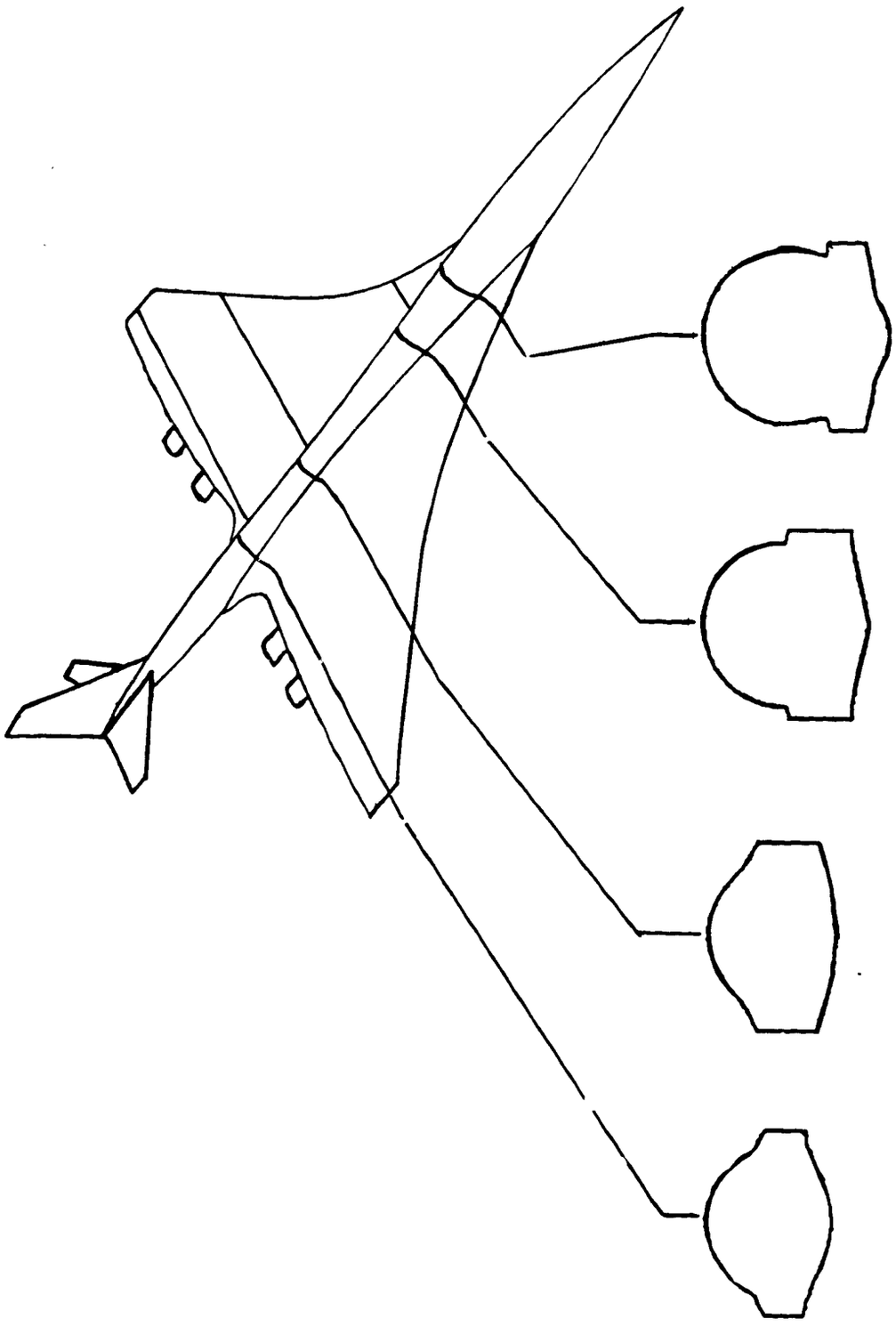

Figure 2.7.3-1 Typical Body Cross Sections

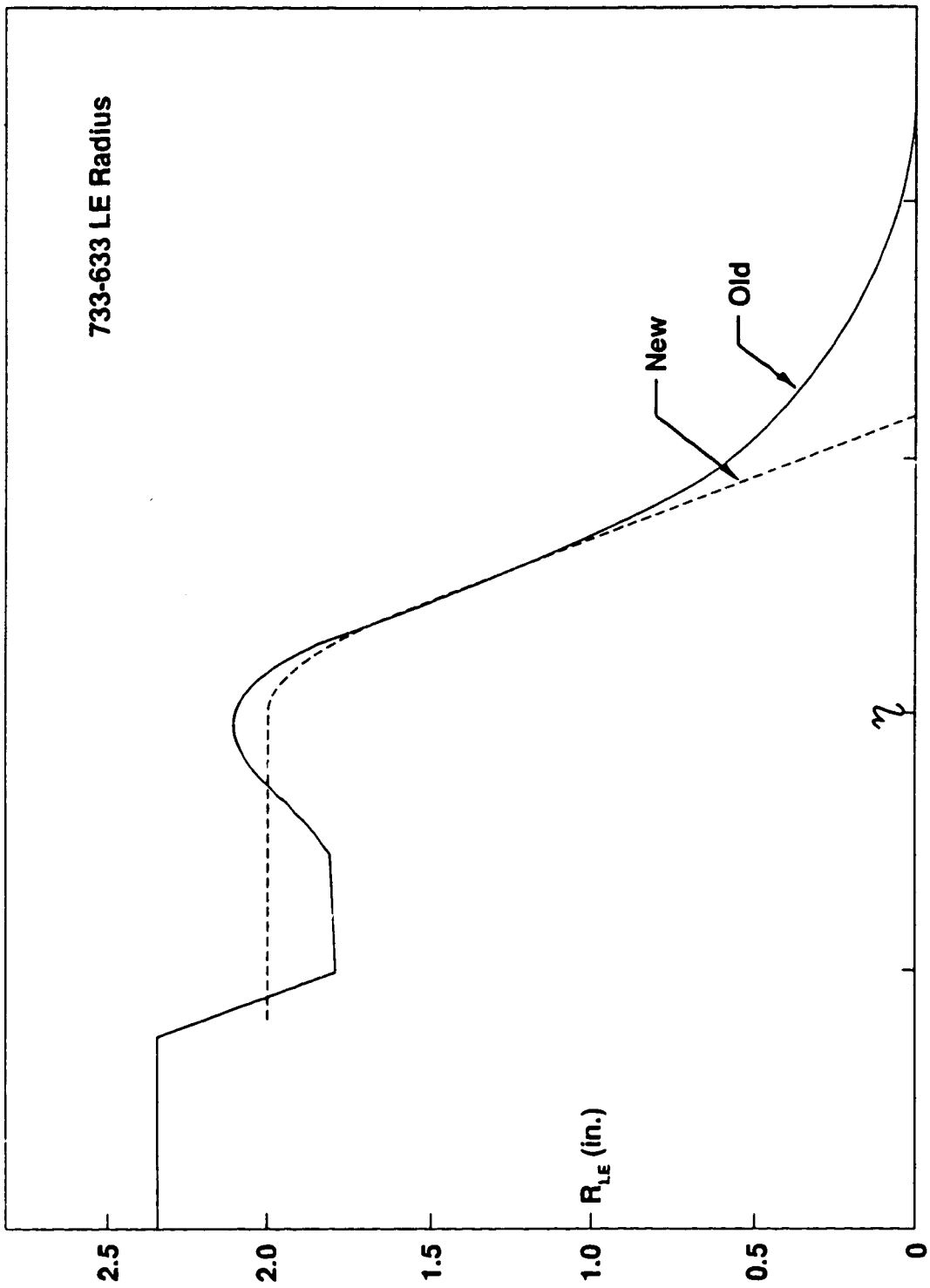

Figure 2.7.3-2 Original and Modified Nose Radius Distributions

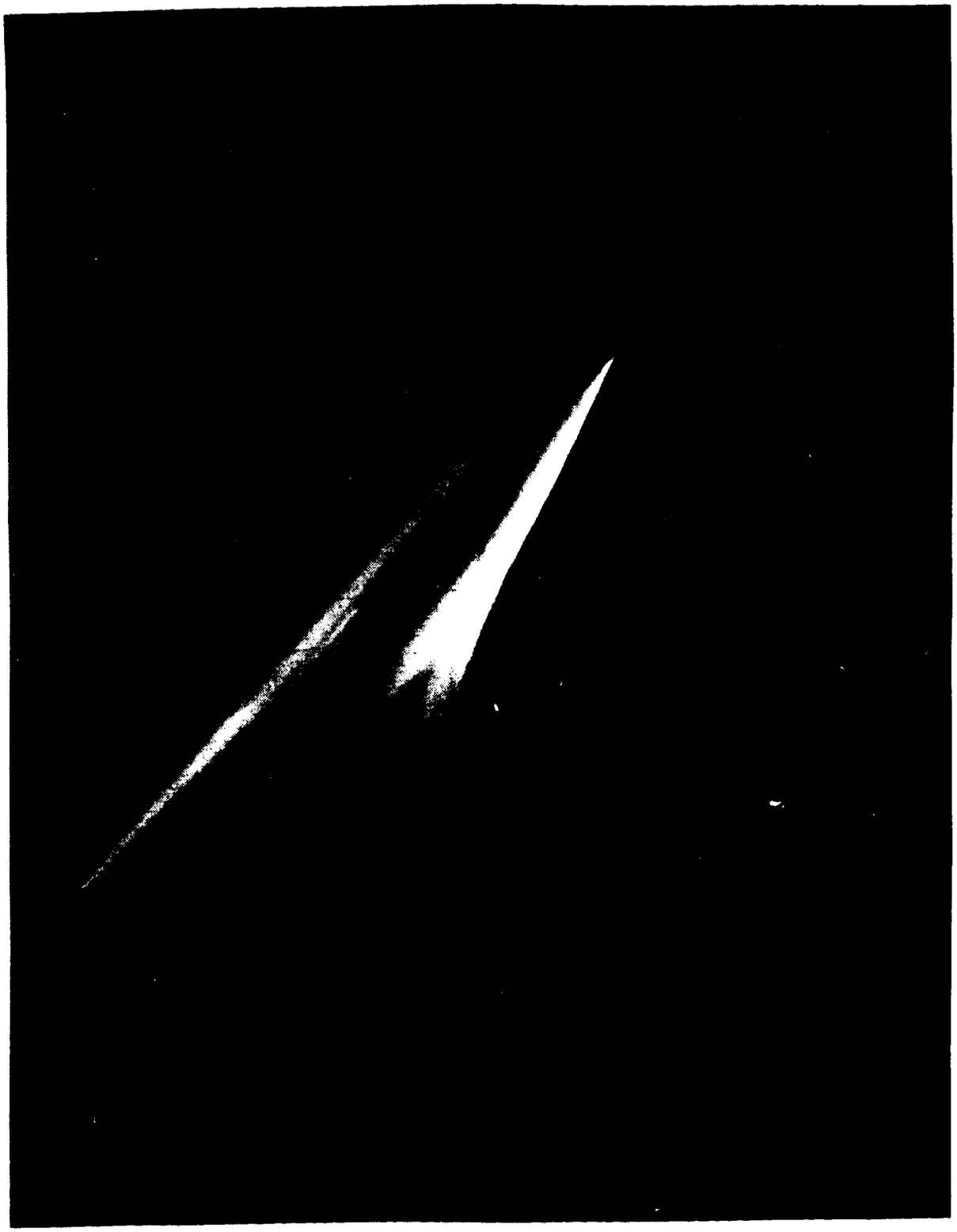

Figure 2.7.3-3 Computer Generated Geometry Definition of 733-633

2.7.4 Inviscid Flow Field Analysis

Two linear (lifting surface and panel) methods and one nonlinear (Euler) method were employed for the inviscid flow field solution on the configuration wing surface. The pressure (Cp) distributions on the wing surface as predicted by the three methods showed good agreement in some regions while exhibiting significant differences in others.

The first method employed the linearized lifting surface supersonic flow code (A389) as described in [35]. In this method, the wing/body interference effects are only approximately modeled and body cross-sections are assumed to be circular. The wing pressure field is split into a thickness part and a camber part and added linearly. Considerable smoothing is applied to the resulting pressure distributions. The results of this method will be discussed along with those of the panel code described next.

Panel codes remove some of the approximations inherent in the lifting surface approach. The boundary conditions are applied at the actual configuration surface rather than at a mean surface. The fuselage is accurately modeled and wing/body interference is more accurately accounted for. The Boeing panel code (A502) is a version of the PANAIR [35] code developed for NASA. It employs a "higher order" panel method with a quadratic distribution of doublets on each panel.

The AGPS software package described earlier is capable of decomposing the surface of the configuration geometry into user specified groups (networks) of discrete panels with coordinates describing each panel. Figure 2.7.4-1 shows the wing/body paneling of the 733-633 configuration. A dense distribution of panels was used near the leading edge to resolve the steep velocity and pressure gradients in this region. The total number of panels on the half configuration was in excess of 3600. The panel code was run with both velocity impermeability (KT = 11) and mass flux impermeability (KT = 1) boundary conditions as discussed in [35]. The two types of boundary conditions did yield somewhat different Cp distributions as will be discussed later when the two panel code solutions are compared with the Euler code results.

A comparison of C_L versus α predictions of A502 panel code (KT = 11) with the linear lifting surface code A389 [35] are shown in Figure 2.7.4-2. The two predictions are close to the wind tunnel results.

A comparison of wing upper surface Cp distribution as predicted by A502 panel code (KT = 11) and A389 code is shown in Figure 2.7.4-3 for $\alpha = 6$ degrees. There is a similarity of gross features in the two predictions. However, detailed distributions are significantly different as shown in Figures 2.7.4-4(a) through 2.7.4-4(g). The panel code Cp predictions display

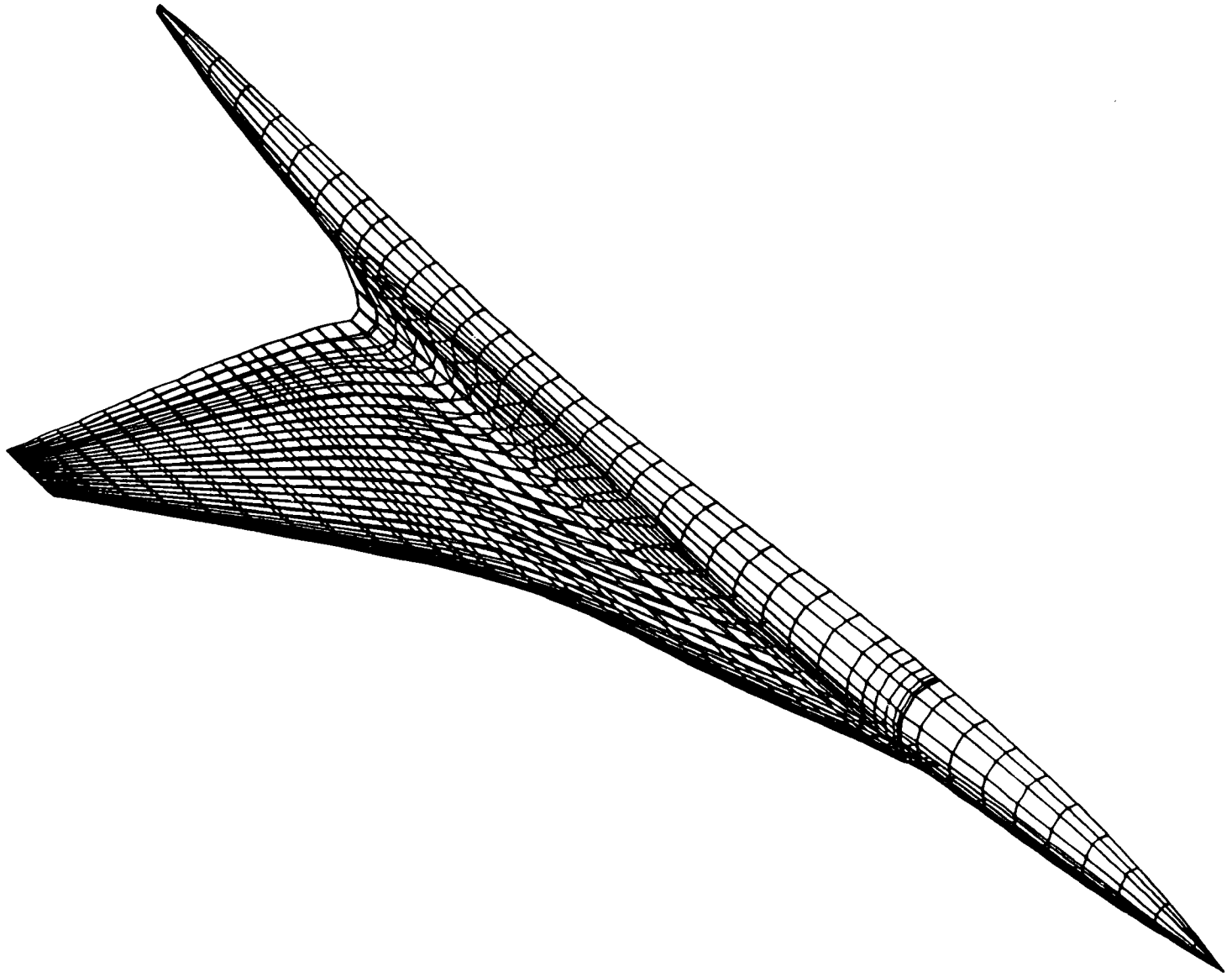

Figure 2.7.4-1 Wing/Body Paneling of 733-633

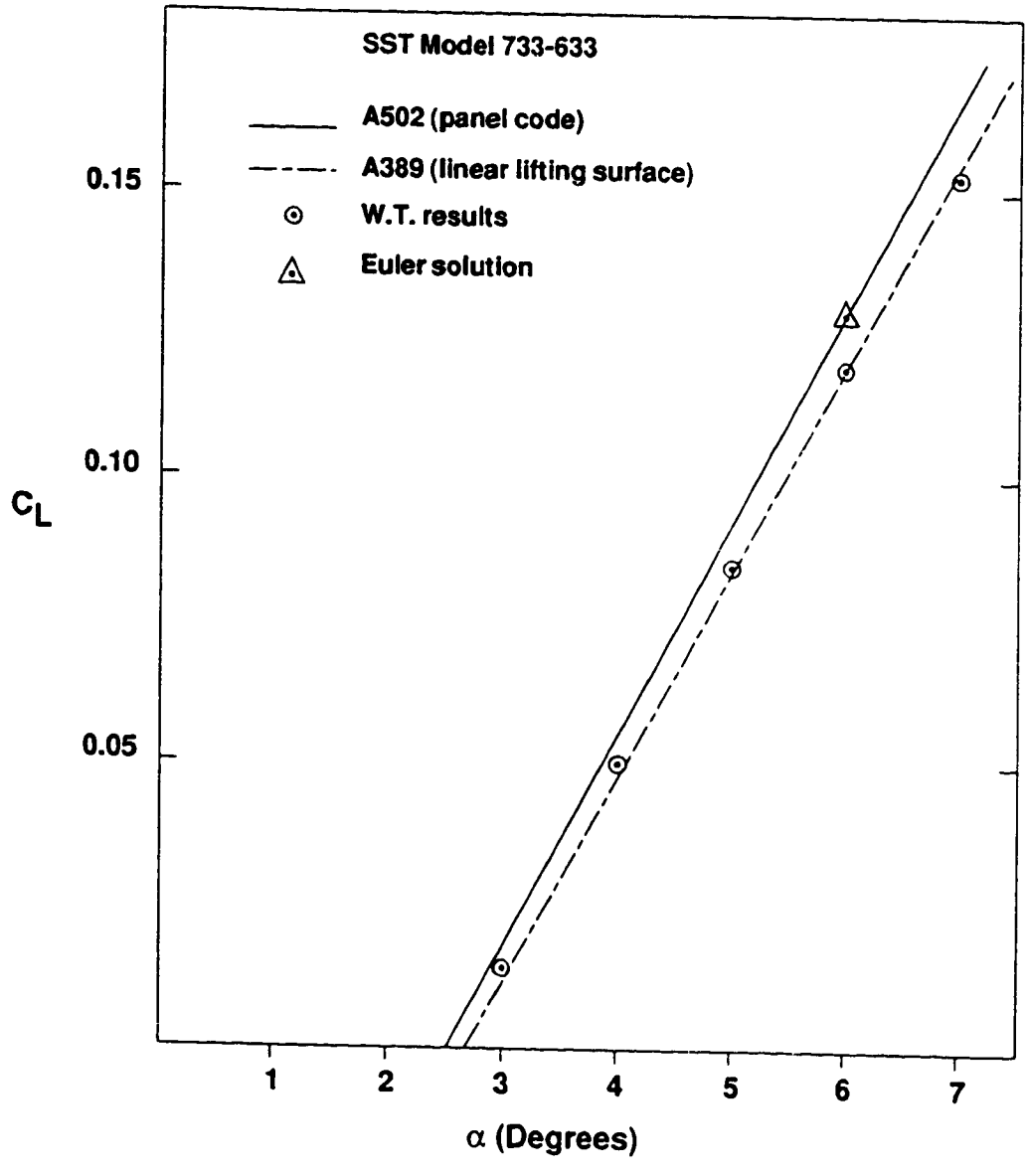

2.7.4-2 Comparison of CL vs a for A502 and A389 Solutions with Wind Tunnel Results

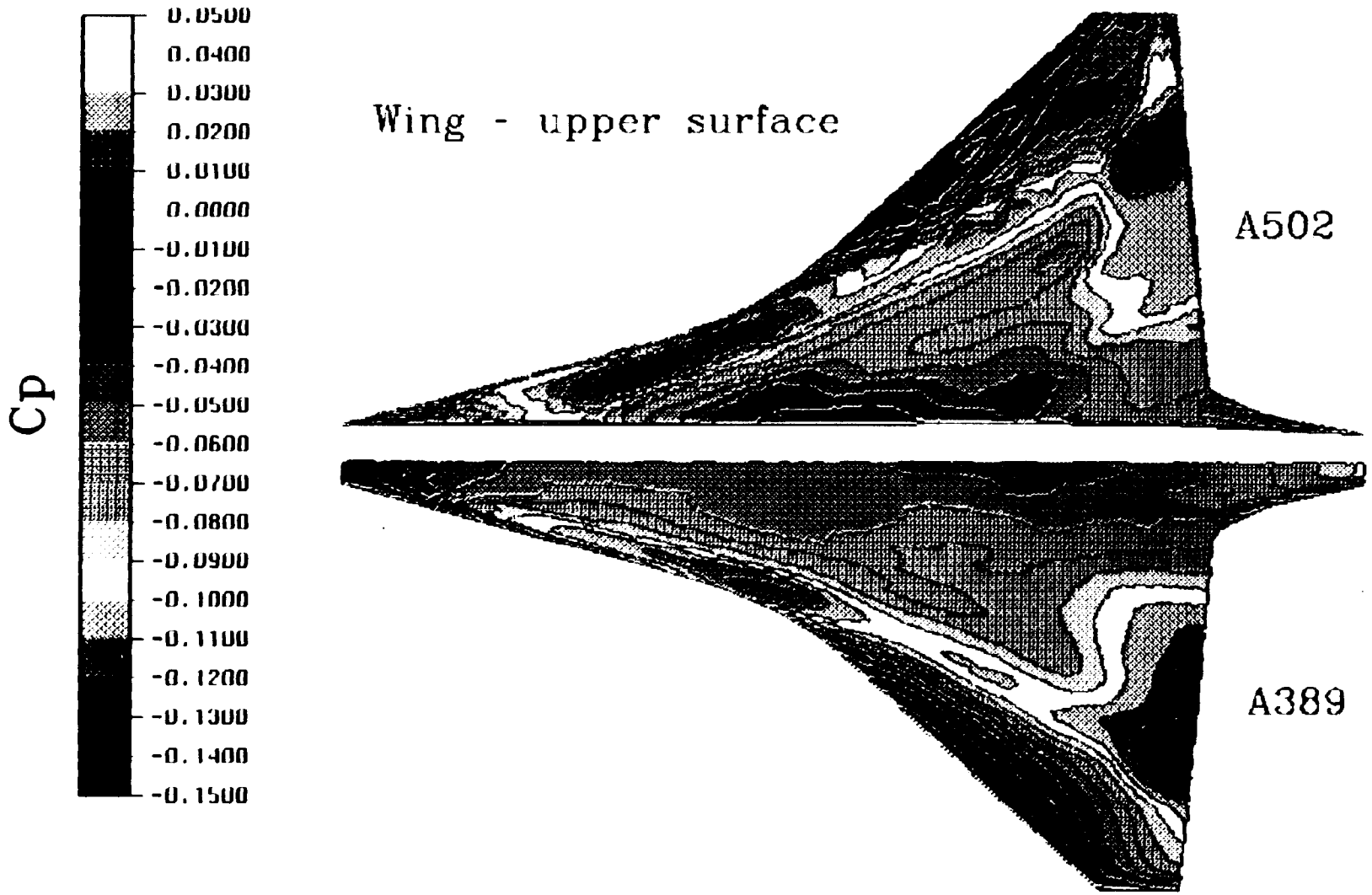

Figure 2.7.4-3 Comparison of Wing Upper Surface C_p's (A502 vs A389)

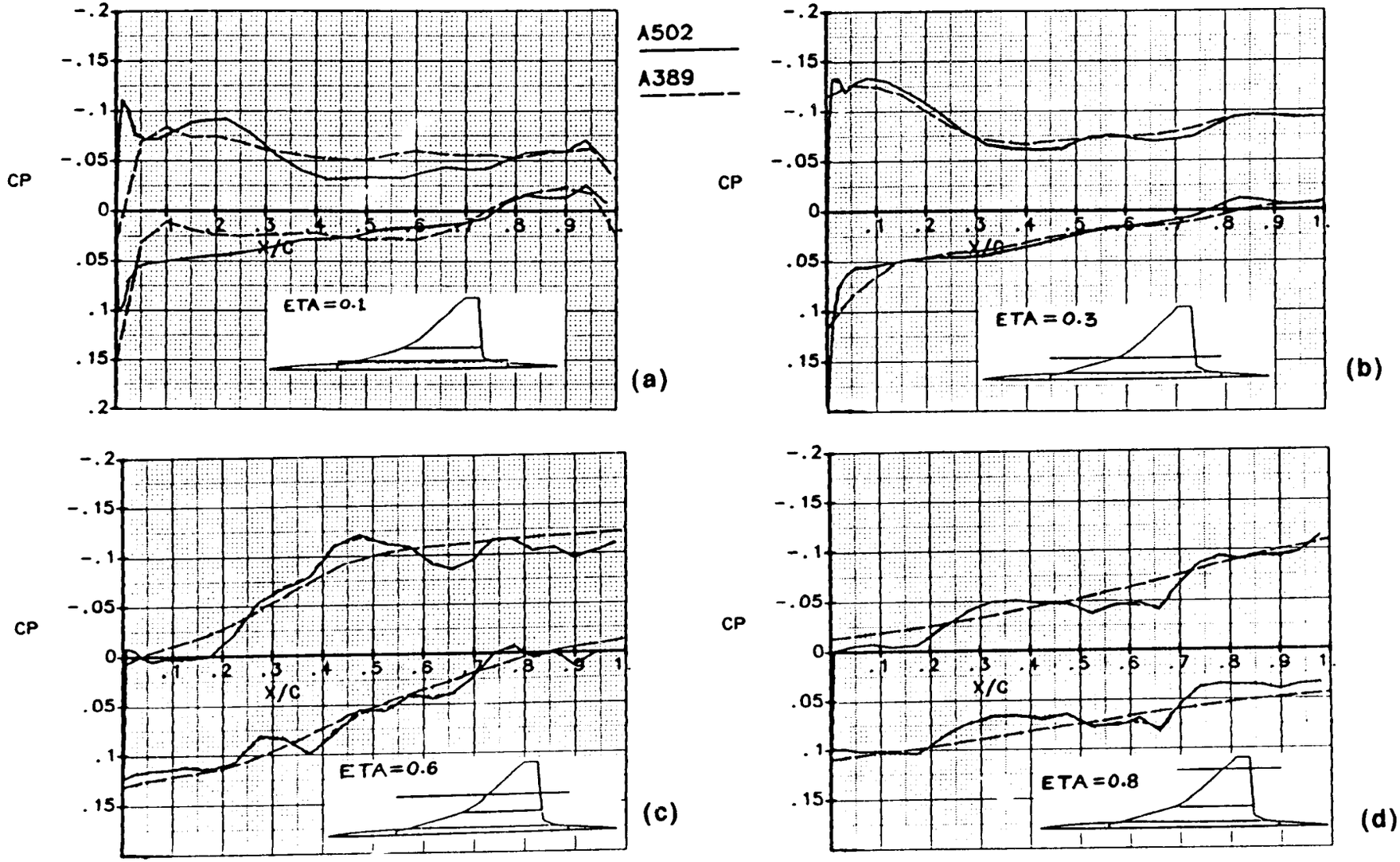

Figure 2.7.4-4 Comparison of C_p's Predicted by A502 and A389 W/B, M=2.4, $\alpha=6^o$

considerable roughness compared to the A389 predictions. This may be partly due to the fact that considerable smoothing to calculated Cp distributions is applied internally in the A389 code. If this roughness in the A502 predicted Cp's were smoothed, the resulting Cp's would be quite comparable to A389's over most of the wing semispan. In the region close to the wing/body junction (e.g. ETA = 0.1) the two solutions differ significantly due to the approximations inherent in A389 for treatment of the body.

Considerable effort was devoted to smoothing the geometry definition of the original configuration and revising the panel scheme. This did not improve the roughness of the predicted Cp distributions, however, as shown in Figures 2.7.4-5 (a) through 2.7.4-5 (d).

It was intended to couple the output, in terms of surface velocity components, of the inviscid flow code with a 3D boundary layer code [38]. An interface program to transfer the necessary data from the inviscid code to the boundary layer code was written. However, the quality of the surface velocity component data from the A502 panel code was rather poor and proved unacceptable for the boundary layer code.

The Cp prediction of the A389 code was considerably smoother. However, this code does not compute surface velocity components and therefore it was unsuitable for coupling with the 3D boundary layer code [38] used.

At this point, it was decided to employ a 3D Euler code for inviscid flow field prediction. The Boeing Euler code was developed by Dr. N.J. Yu and was based on Jameson's FL057 [39]. Figure 2.7.4-6 shows the surface fitted grid used for the Euler solution. A dense grid was used near the wing leading edge. However, as will be seen from the solution, the grid was not dense enough in this region.

Figure 2.7.4-7 shows a comparison of the upper surface wing pressure distribution between A502 and Euler code predictions. Again, there is a similarity of gross features. However, a comparison of detailed Cp distributions along streamwise cuts shows significant discrepancies between the two predictions as seen in Figures 2.7.4-8 (a) through 2.7.4-8 (f). Particularly on the inboard wing (strake) upper surface, the Euler solution shows (Figures 2.7.4-8 (a) through 2.7.4-8 (c)) low (suction) pressures persisting up to much greater values of x/c than does the A502 solution. On the lower surface of the outboard wing the Euler solution predicts (Figures 2.7.4-8 (d) through 2.7.4-8 (f)) a relatively slowly decreasing pressure away from the attachment line up to 5 percent x/c, despite the fact that the leading edge in this region is sharp. Also, the value of the attachment line Cp is much lower than what would be expected at the sweep angle (47 degrees) in this region. It is believed that this anomalous behavior is caused by a lack of adequate grid resolution in the sharp leading edge region.

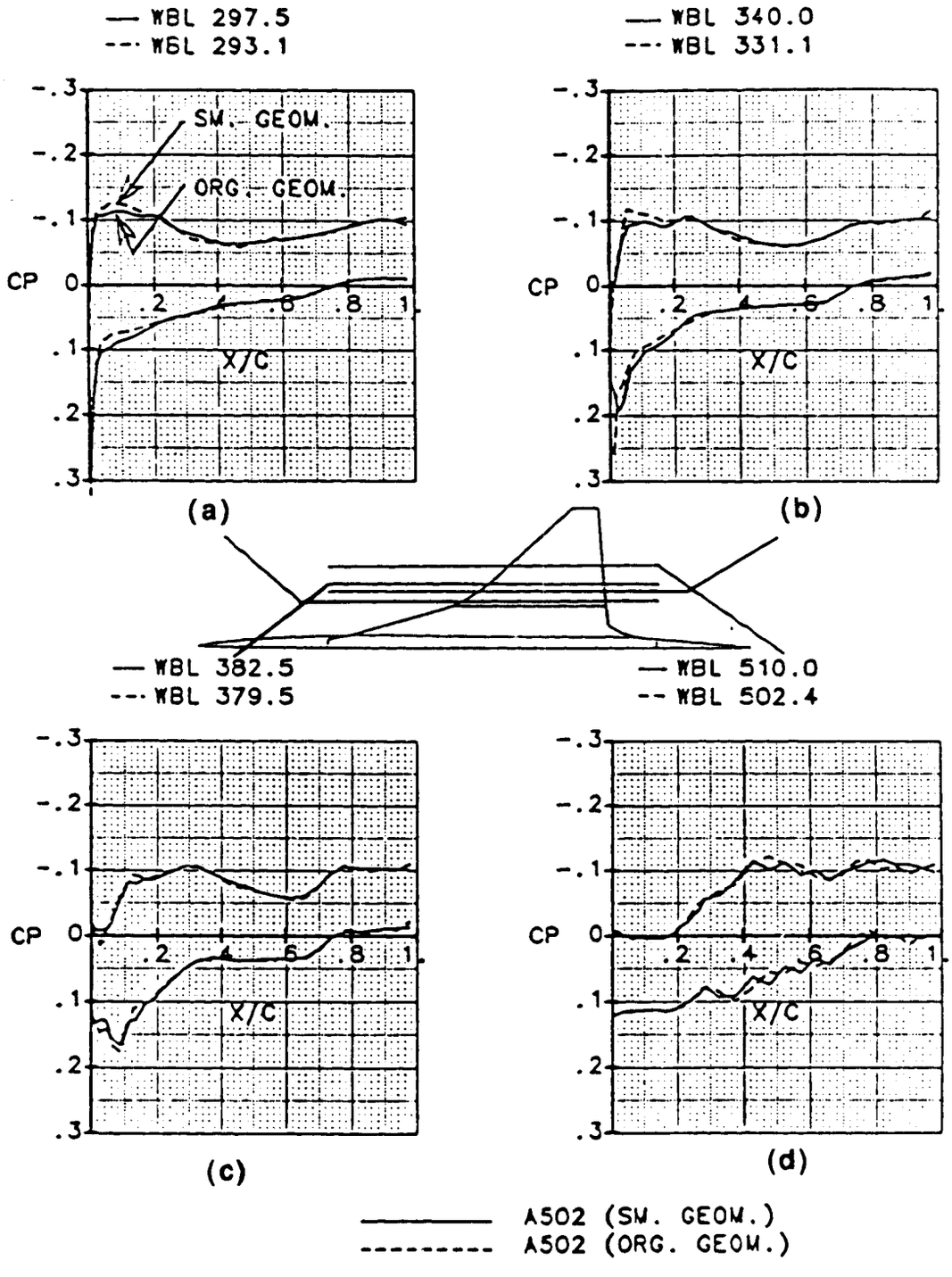

Figure 2.7.4-5 Comparison of Predicted Cp's for Original and Smoothed Geometry

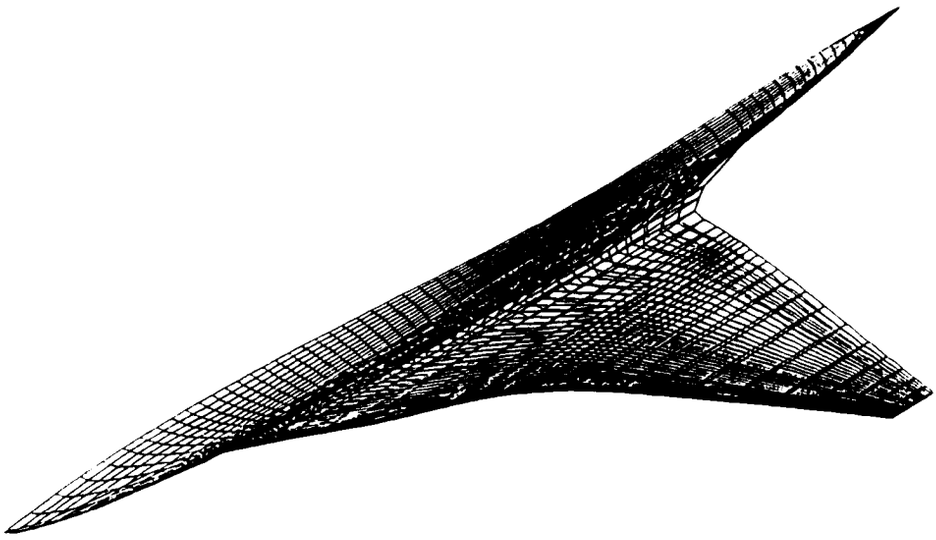

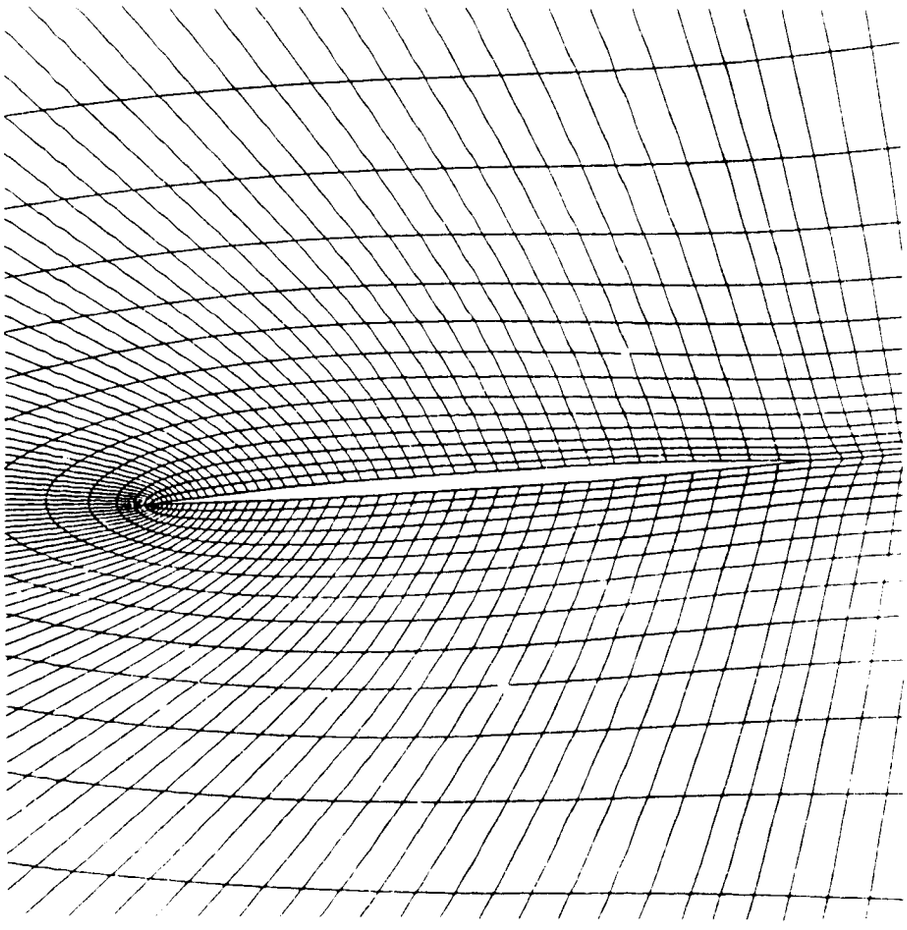

Figure 2.7.4-6 Surface Fitted Grid for Euler Solution

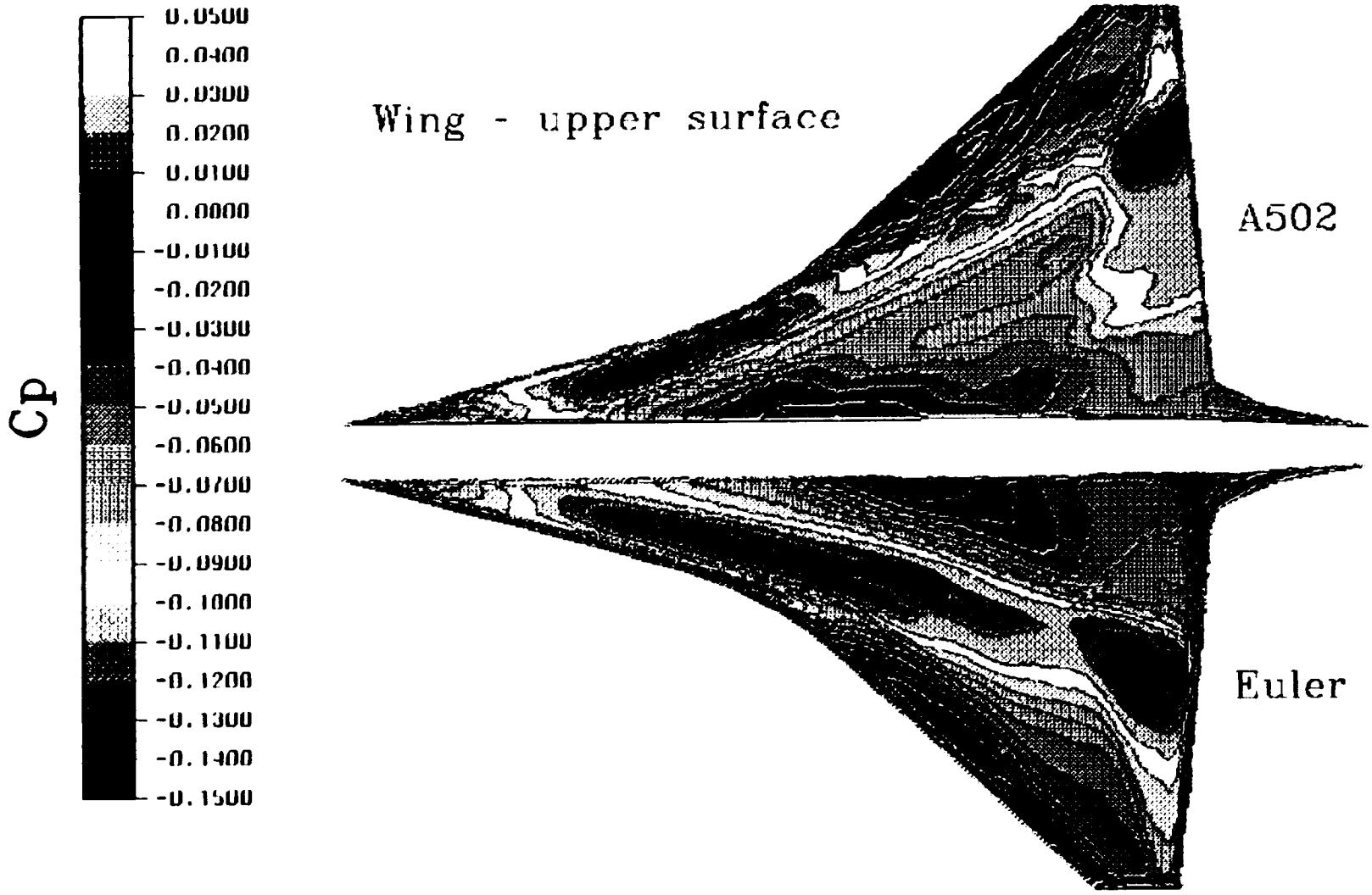

Figure 2.7.4-7 Comparison of Predicted Cp Distributions - Euler vs A502

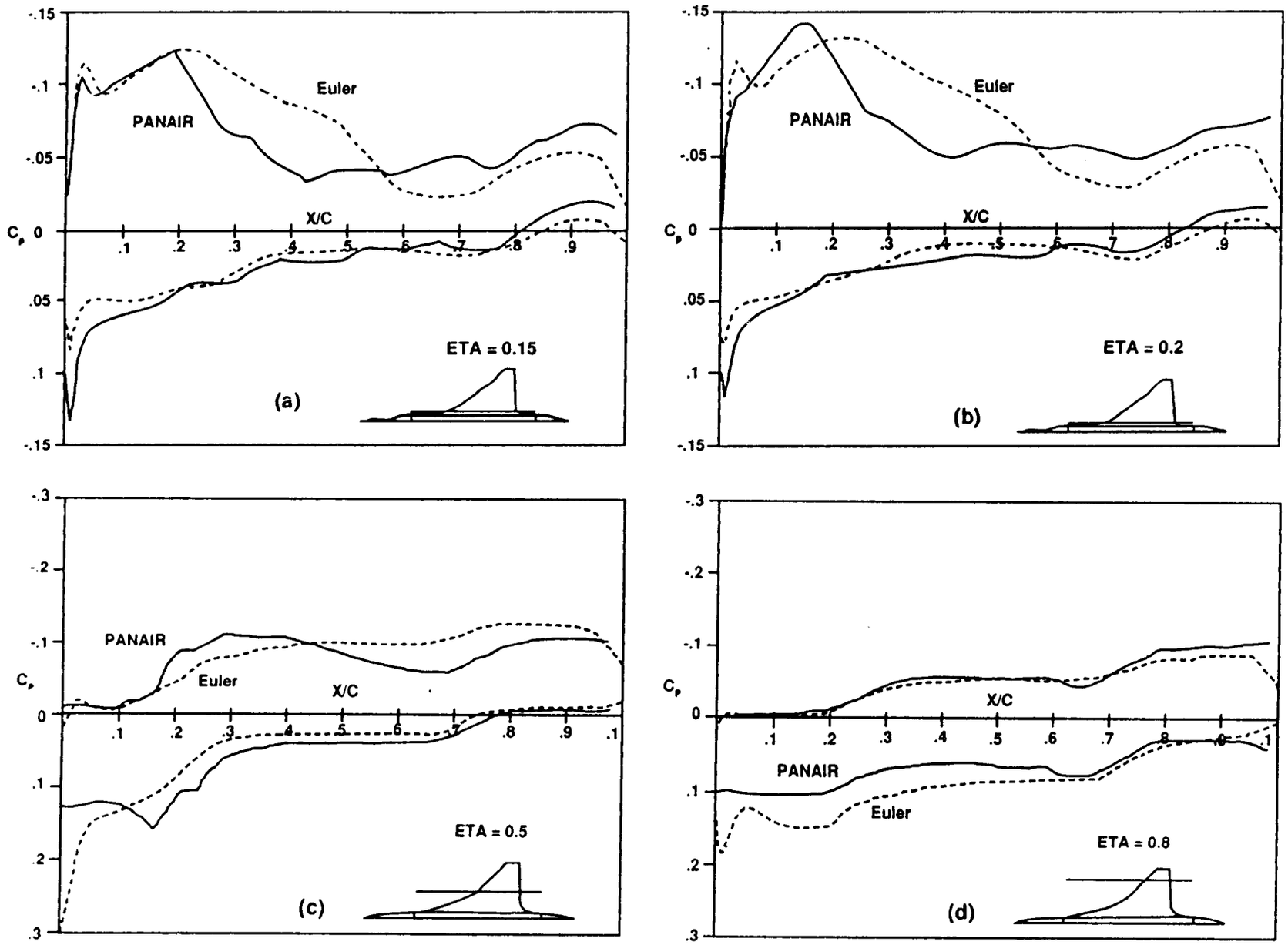

Figure 2.7.4-8 Comparison of Predicted Cp Distributions Euler vs A502

This was substantiated in a separate study using a 2D Euler code on a sharp nosed airfoil. It was found that the predicted pressure distribution downstream of the leading edge was strongly dependent on the grid density employed, and as the grid density was increased, the initial pressure variation was confined to smaller distances.

A coupling of the Euler code solution with the A411 3D boundary layer program via the interface program was successfully accomplished. However, an extensive 3D laminar boundary layer solution on the wing surface could not be obtained. This was caused by separation of the predicted laminar boundary layer shortly after the pressure peak on the upper surface at approximately 3 percent chord location (see Figures 2.7.4-8 (a) through 2.7.4-8 (c)). A turbulent solution was achieved, however, as shown in Figure 2.7.4-9 because the turbulent boundary layer was able to withstand the pressure recovery without separation.

At this point it became apparent that the pressure distribution on the baseline configuration would have to be modified if a laminar boundary layer solution for the wing were to be achieved. The adverse pressure gradient following the initial pressure peak on the inboard wing upper surface would have to be substantially milder if a laminar separation were to be avoided. Furthermore, as will be discussed in connection with crossflow instability (Section 2.7.7), a zero pressure gradient is most desirable following the adverse pressure gradient to maintain laminar flow on a swept wing. Finally, to suppress the initial buildup of crossflow instability in the nose region, the velocity gradient leading to the suction peak needs to be even steeper than that predicted for the existing configuration. Thus, a specific type of pressure distribution on the wing surface is needed to achieve an extensive run of laminar flow without using excessive amounts of suction.

Obtaining a specified (desired) pressure distribution on the wing surface requires a 3D design CFD capability which was unavailable during the course of this study. As has been discussed, even the analysis capability revealed significant discrepancies among the predictions of three different inviscid methods. The grid resolution was inadequate particularly near the leading edge of sharp nosed wing sections. The desired wing surface pressure distribution could not directly be input to the A411 [38] 3D boundary layer code because the latter code needed a full specification of the three velocity components at the surface.

In view of the above difficulties, it was decided to pursue a somewhat simplified approach to boundary layer and stability analyses on the configuration surface. In this simplified approach, pressure distributions along the (streamwise) rib cuts of the wing, typical of the inboard and outboard regions were selected from the Euler code predictions. The inboard wing has a subsonic, rounded leading edge which leads to a "peaky" Cp distribution as shown in Figure 2.7.4-8 (b). The outboard wing has a

733-633 3-D B.L. Solution

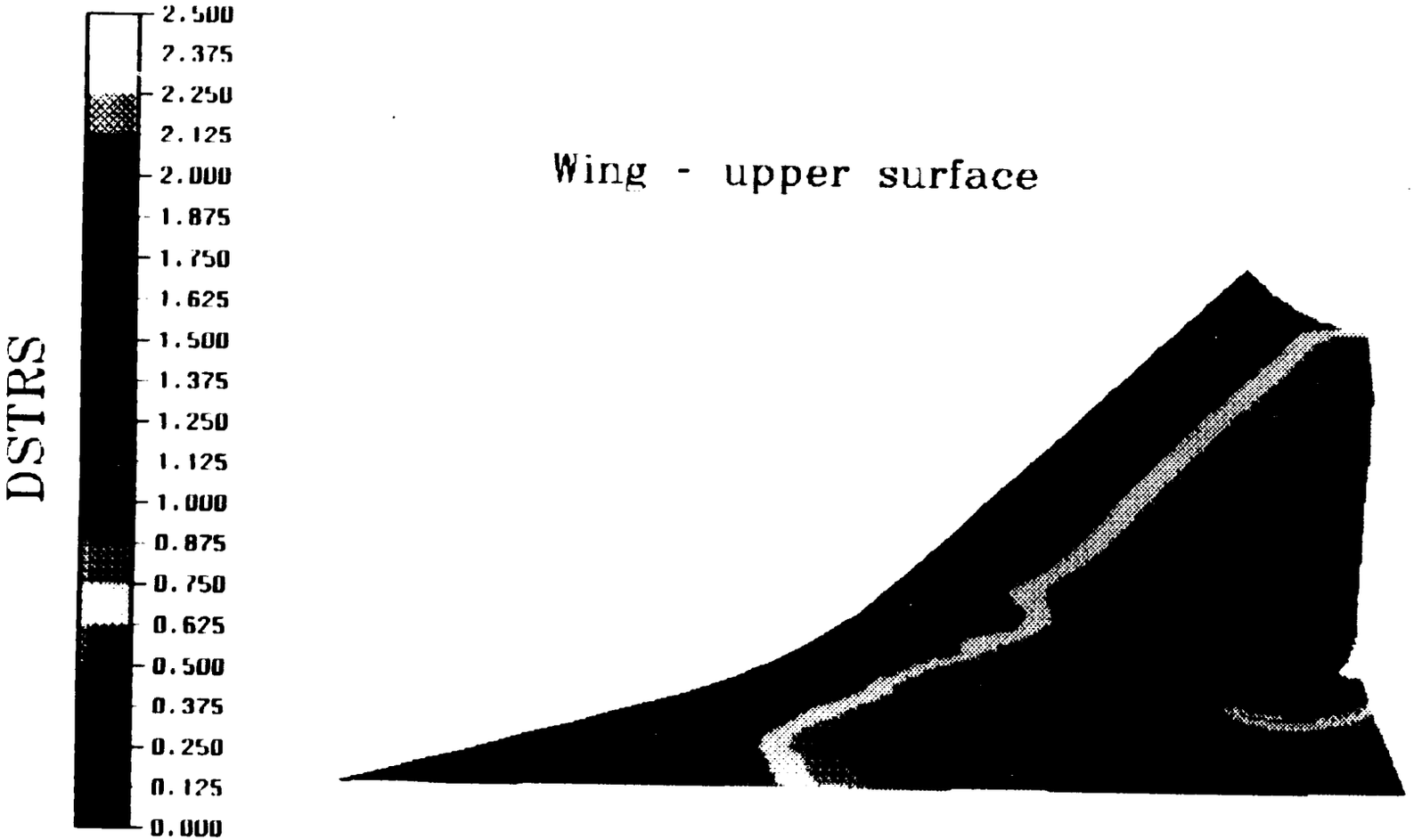

Figure 2.7.4-9 Upper Surface Turbulent Boundary Layer Solution

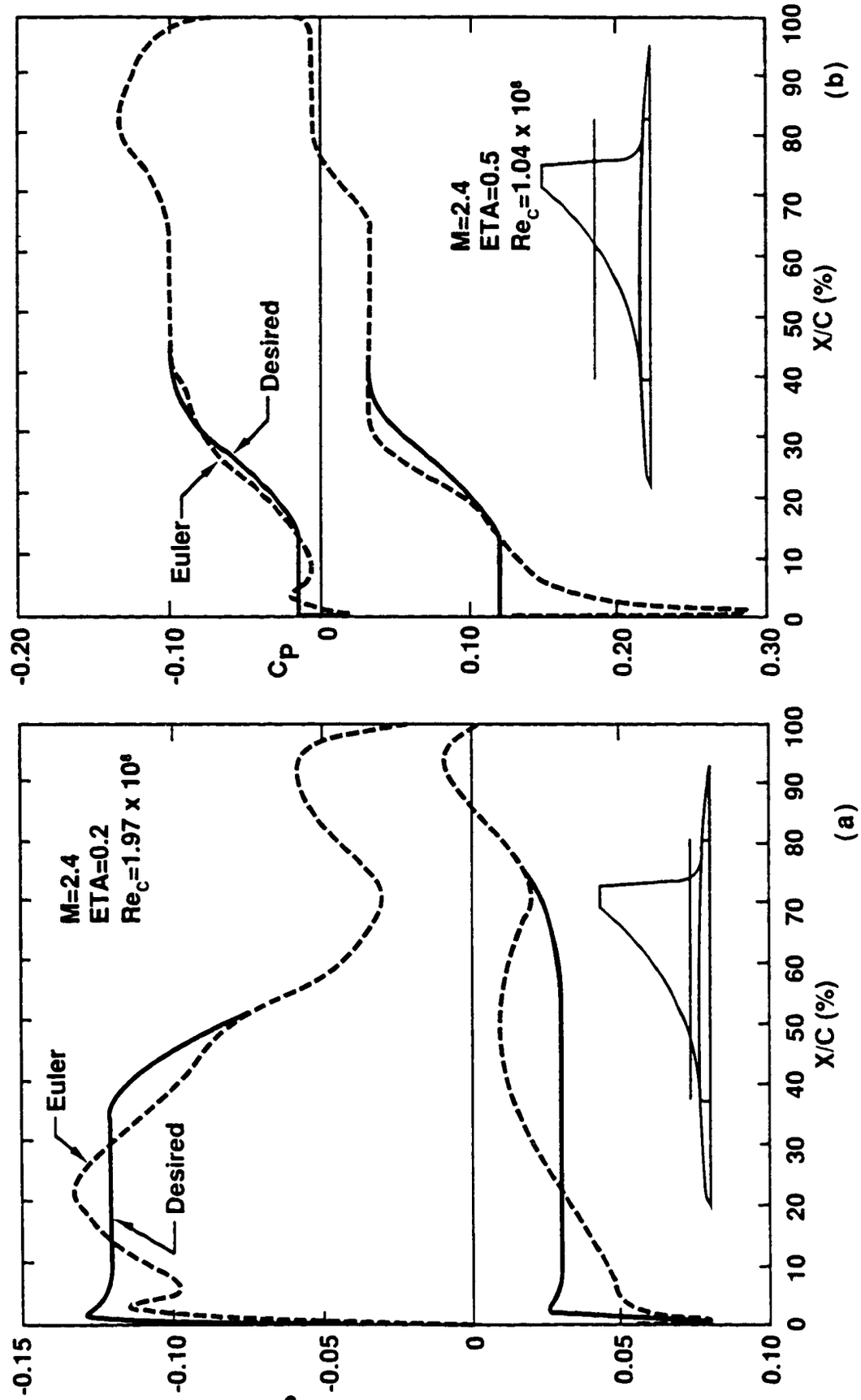

Figure 2.7.4-10 Comparison of Euler Predicted and Desired Pressure Distributions

supersonic sharp leading edge and it leads to a Cp distribution of the type shown in Figure 2.7.4-8 (d). These pressure distributions typical of the inboard and outboard portions of the wing were then modified as shown in Figures 2.7.4-10 (a) and (b) to yield "desired" pressure distributions expected to yield significant runs of laminarization based on past experience. This required more adjustments to the inboard Cp distribution than to the outboard one. As already mentioned, the predicted outboard Cp distribution is suspected of being affected by a lack of adequate grid resolution near the leading edge. Therefore, the modified Cp distribution in Figure 2.7.4-10 (b) attempted to incorporate a more physically plausible behavior in this region. Some of the earlier calculations of boundary layer stability on the outboard wing employed Cp distributions predicted by linear theory as shown in Figure 2.7.4-4 (d) because the Euler results were not yet available.

Having selected the desired pressure distributions on the inboard and outboard portions of the wing, a quasi-3D boundary layer analysis was carried out using the conical flow approximation as originally proposed by Kaups and Cebeci [40]. The calculated 3D boundary layer profiles were then analyzed for TS and CF types of instability using a Boeing modified version of the Mack code [41]. Both the boundary layer and stability computations were carried out by means of a system of programs known as Unified Stability System (USS) [42] which was developed earlier under a NASA contract.

2.7.5.1 Characteristics of the Attachment Line Boundary Layer

In the flow field of a swept wing, the attachment line is the boundary, located in the leading edge region, which separates the flows passing over the upper and lower surfaces of the wing. The flow direction at the attachment line is entirely spanwise. The chordwise component of the local inviscid flow, although zero at the attachment line, accelerates rapidly with increasing chordwise distance in the leading edge region. An "attachment line boundary layer" is established under the influence of this type of inviscid flow field in the leading edge region. Because of the rapid chordwise acceleration away from the attachment line, the attachment line boundary layer itself attains an asymptotic state within a very short distance along the leading edge

A simple criterion based on the momentum thickness Reynolds number (Re_{θ}, a.l.) of this asymptotic layer is currently used to judge the state of the attachment line boundary layer. For $Re_{\theta,a.l.}$ below 100, the attachment line boundary layer is stable against even large disturbances such as those originating in the fuselage turbulent boundary layer at the wing root. For $100 < Re_{\theta,a.l.} < 250$, the attachment line boundary layer is stable against small disturbances such as free stream turbulence. However, large

disturbances present at the wing root will propagate along the attachment line. As a result of this spanwise contamination, the entire attachment line boundary layer becomes turbulent. Chordwise propagation of turbulence from a turbulent attachment line makes the entire wing boundary layer (in most cases) turbulent as well. Several techniques which rely on relaminarization of the attachment line boundary layer by use of suction or rapid acceleration near the wing root are available to prevent the spanwise propagation of the wing root disturbances along the attachment line. If implemented, such techniques would allow for maintaining the attachment line boundary layer laminar upto $Re_{\theta,a.l.} = 250$. For $Re_{\theta,a.l.} > 250$, the attachment line boundary layer becomes unstable even to small disturbances present in the free stream or originating at the surface. For such large values of $Re_{\theta,a.l.}$, small disturbances are amplified, eventually leading to transition in the attachment line boundary layer. Increasing nose radius, sweep angle and free stream velocity, all tend to increase $Re_{\theta,a.l.}$ and therefore have a destabilizing influence on the attachment line boundary layer.

The threshold value of $Re_{\theta,a.l.} = 100$ for stability against disturbances (such as those originating at the wing root) appears to be valid for supersonic free-stream [49]. However, the threshold value of $Re_{\theta,\ a.l.} = 250$ for stability against amplification of small disturbances is derived from low speed experiments. The influence of such parameters as Mach number, surface cooling and suction on the latter threshold is not known. Based on the knowledge of the behavior of flat plate boundary layer, the latter parameters are most likely to increase the stability of the attachment line boundary layer. Therefore, the criterion of $Re_{\theta,a.l.} = 250$ for transition is probably quite conservative for supersonic attachment line boundary layers with wall suction and cooling. Further work in this area is needed.

A formula for the calculation of $Re_{\theta,a.l.}$ in adiabatic wall compressible boundary layer is given by Poll [49] as:

$$Re_{\theta,a.l.} = \left\{1 + r\left(\frac{\gamma-1}{2}\right)M_e^2\right\}^{\frac{N-1}{2}} \left\{\frac{v_e^2}{\nu_e\left(\frac{due}{dx}\right)_{x=0}}\right\}^{\frac{1}{2}} \left\{0.407 - 0.052\ ln\left[1 + \left(\frac{\gamma-1}{2}\right)M_e^2\right]\right\}$$

The calculated value of the adiabatic wall Reo,a.l. for the inboard wing was in excess of 500, which implies that the attachment line boundary layer on the (subsonic) leading edge of the inboard wing would be turbulent at M = 2.4 cruise condition if no boundary layer control were applied.

The influence of wall suction on the attachment line boundary layer was studied by W. Pfenninger [46]. The results of that study were combined with the $Re_{\theta,a.l.}$ calculated under no suction condition to generate Figure 2.7.5.1-1, which shows the effect of wall suction on $Re_{\theta,a.l.}$. Notice that moderate

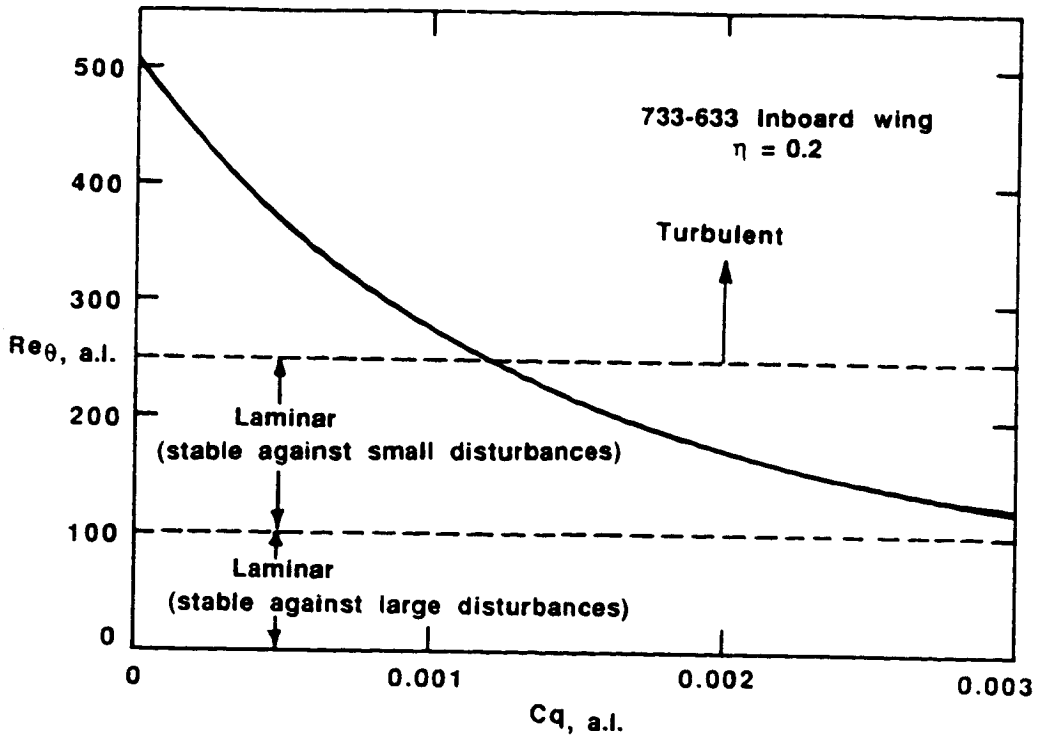

Figure 2.7.5.1-1 Effect of Suction on Re_θ, a.l.

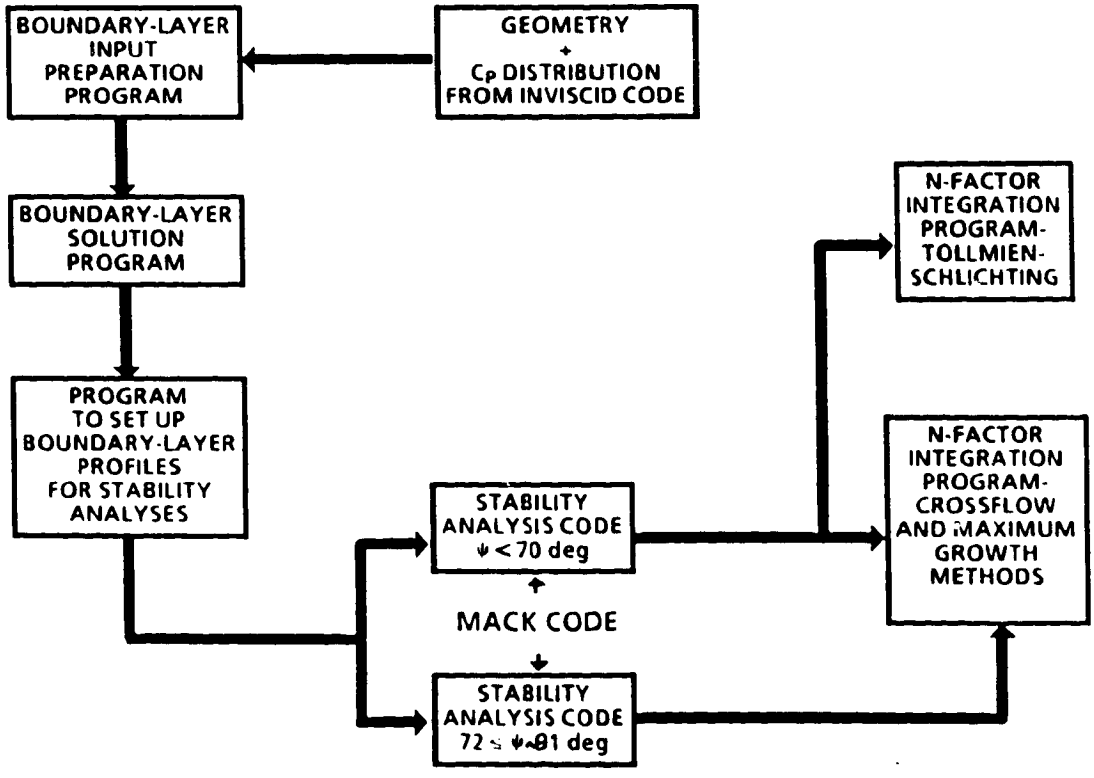

Figure 2.7.5.2-1 Structure of USS Code

amount of leading edge suction (Cq = 0.002) brings down $Re_{\theta,a.l.}$ to values which ensure the stability of the attachment line boundary layer against small disturbances. Of course, this method of stabilizing the attachment line boundary layer must be combined with an appropriate technique to prevent spanwise spreading of wing root disturbances. As will be shown later (see Sec. 2.7.7), this level of suction is also needed in the leading edge region for the control of crossflow instability. On the outboard wing where the leading edge is sharp and of lower sweep, stability of the attachment line boundary layer is not a problem.

It should be noted that at higher wing incidences, the migration of the attachment line away from the leading edge highlight effectively increases the surface radius of curvature at the attachment line location. This would tend to increase the $Re_{\theta,a.l.}$ value significantly, possibly resulting in transition in the attachment line boundary layer. This area also needs further study.

2.7.5.2 Approximate 3D Boundary Layer Analysis

As already mentioned, the A411 [38] program is capable of solving general 3D boundary layers on swept wings. For input, it requires a specification of inviscid velocity vectors at the wing surface. The latter specifications could not be generated for a desired pressure distribution over the entire wing surface. An approximate method was employed in which a specified streamwise pressure distribution along a streamwise cut was used in conjunction with a swept tapered wing assumption [40] to generate the inviscid velocity vectors along the streamwise cut. In the swept tapered wing approximation, the local isobars are assumed to be aligned with the local constant chord fraction lines. The calculation of the inviscid velocity vectors from the specified upper and lower surface Cp distribution under the swept tapered wing approximation was carried out in an input preparation program called BLGL. The latter program also locates the position of the attachment line from the specified Cp distribution and sets up a boundary layer calculation grid starting at the attachment line. The grid density is adapted to the specified pressure distribution, suction distribution, etc. with increased grid density in regions of steep variation in Cp, Cq, etc. The BLGL program thus prepares a complete input file for the A411 [38] 3D boundary layer program, starting from the specified upper and lower surface streamwise Cp distribution and employing the swept tapered wing approximation.

The A411 [36] program is a finite difference program capable of solving laminar or turbulent boundary layers with surface mass transfer (blowing or suction), heat transfer and compressibility effects. The heat transfer and compressibility effects are accounted for by simultaneous solution of the energy equation together with the momentum equation. A maximum of 100

grid points can be employed across the boundary layer. The boundary layer profiles computed by the A411 program are stored in disk files for later stability analyses.

A separate program (LAMSD) is used to pick out user specified boundary layer profiles from those calculated by the A411 program. Various characteristics of each selected profile, such as the Falkner-Skan Beta parameter, the crossflow Reynolds Number, shape factors, etc., which are necessary for the subsequent stability analyses are computed within LAMSD and the profiles are stored in a form suitable for stability analysis programs.

The three programs discussed above: BLGL, A411 and LAMSD are the first three of a system of seven programs known as the Unified Stability System (USS) which was developed recently at Boeing under NASA funding [42]. The structure of the USS system is shown in Figure 2.7.5.2-1.

2.7.6 Stability Analysis

The stability of the computed boundary layer profiles was analyzed by use of a 3D, compressible stability analysis code originally developed by L. Mack [41]. The Mack code iteratively solves for temporal or spatial stability of a 3D boundary layer profile using numerical integration from outer flow to the wall. The compressible 3D boundary layer stability equations are a system of eighth order ordinary differential equations with four unknowns characterizing the linear disturbance. These four unknowns are: wave length (λ), frequency (ω), wave angle(ψ) and spatial growth rate (dN/dS). The determination of these four unknowns by solution of the eighth order system of ordinary differential equations is an eigenvalue problem, since solution is obtained only for certain combination of the unknowns.

In the solution procedure employed within the Boeing version of Mack code, somewhat different approaches are used for wave angles below about 70 degrees and those between 72 and 91 degrees. For wave angles below 70 degrees, a program called MKM0D3 is used while for wave angles between 71 and 91 degrees a program called MKM0D5 is used. In MKMOD3, the eigenvalues representing the spatial growth rate (dN/dS) and wave length (λ) are determined iteratively for a selected pair of wave angle (ψ) and frequency (ω) values. In MKMOD5, the eigenvalues representing the spatial growth rate and frequency are determined iteratively for a selected pair of wave angle and wave length (or wave number) values. Both stability codes are part of the USS system of codes as shown in Figure 2.7.5.2-1.

The reason for calculating the boundary layer stability separately in two different wave angle ranges is the philosophy employed at Boeing for transition prediction. In this philosophy, the zero frequency (stationary) crossflow disturbance growth which occurs at wave angles close to 90

degrees is considered to be the measure of crossflow instability. An accurate determination of the zero frequency crossflow disturbance growth requires the calculation of growth rates at several closely spaced wave angles close to 90 degrees. This is what is done in program MKMOD5 of the USS system. Program MKMOD3 attempts to determine the wave angle corresponding to the maximum growth rate of TS disturbances by performing the growth rate calculations over a range of wave angles. The integrated values of TS and CF growth rates thus determined are employed in the transition criterion used at Boeing.

It may be recalled (see Section 2.3) that the most amplified TS disturbance even in a 2D supersonic boundary layer is oblique to the flow direction, i.e., the wave angle of the most amplified disturbance is greater than zero. At M = 2 to 3, this wave angle for maximum disturbance amplification is as large as 60 to 65 degrees. This is still true of the 3D supersonic boundary layers except that at such large wave angles, the 3D boundary layer velocity profile may suffer from inflectional instability in addition to the viscous one. Thus, the "TS" disturbance growth rates calculated by MKMOD3 code in the present study for 3D boundary layers at wave angles of 60 to 65 degrees could actually be some combination of the viscous TS and inflectional traveling wave crossflow instabilities. The calculated "TS" growth rates in the present study for 3D supersonic boundary layers are significantly larger than what would be expected from 2D considerations possibly due to the presence of inflectional instability. This point will be further elaborated in Section 2.7.7.

Once the "TS" and CF disturbance growth rates are calculated in the MKMOD3 and MKMOD5 codes, the N-factors for TS and CF instabilities are next calculated in the programs INTTS2 and INTCF2 of the USS system (see Figure 2.7.5.2-1) by integration of the spatial growth rate results. The N-factor for TS growth is calculated at a fixed value of the wave angle (which is chosen to yield maximum growth rates) for a number of frequencies. For each frequency, the N_{TS} initially grows and then decays as the boundary layer thickness increases. High frequencies amplify and decay in the early part of the boundary layer, while low frequencies amplify and decay after the boundary layer has experienced some growth. The envelop of the N-factor growth for all the characteristic frequencies of the boundary layer at a fixed wave angle is then used in the transition criterion.

Similarly, for the determination of the crossflow N-factors, the envelop of individual N-factor growth curves for various spanwise wave numbers at zero frequency is constructed. The envelop value of the crossflow N-factor is then used in the transition criterion.

2.7.7 Stability Results

To establish the validity of the present stability analysis method (Mack code) it was desirable to compare the present N-factor growth prediction for a well documented flow with experimental transition measurements. Due to the scarcity of well documented 3D boundary layer transition data (see Section 2.4), such a comparison could only be made for the simple cases of measured transition on a cone or a flat plate. Since in the latter cases, transition occurs due to the TS (viscous) instability, and shows extreme sensitivity to freestream noise environment, only flight data are considered meaningful for a comparison with theoretical predictions. It is difficult to perform a flight transition experiment on a flat plate and no such data were found in the literature. Most flight transition experiments are performed on a cone. Well documented supersonic transition results from flight tests of a 10 degree cone mounted on the nose of an F-15 aircraft are available [25]. Unfortunately, tools to analyze the stability of the supersonic boundary layer on cones were unavailable at Boeing during the present contract. Therefore, calculated results for flat plate supersonic boundary layer stability were converted to equivalent cone results using a correlation derived from Chen et. al. [24] and compared with transition data of [25].

Figure 2.7.7-1 shows results of the Mack code predictions for N_{TS} growth in an adiabatic wall flat plate boundary layer as a function of the x-Reynolds number for several freestream Mach numbers. For each Mach number, the N_{TS} factor is calculated by integrating the maximum growth rate disturbance which corresponds to the wave angle indicated in the figure. Thus the wave angle of the disturbance which has the maximum growth rate shifts from 0 degrees at M = 0.8 to 65 degrees at M = 2.4. Notice that with increasing Mach number in this range, the growth of N_{TS} with x-Reynolds number for this adiabatic flat plate boundary layer is considerably retarded. For example, the N_{TS} value of 10 is reached at $Re_x = 5.6 \times 10^6$ at M = 0.8 while at M = 2.4 the same N_{TS} value is reached at $Re_x = 19.2 \times 10^6$, i.e., a factor of approximately 3.5 increase in Re_x to attain $N_{TS} = 10$.

The same results are cross-plotted in Figure 2.7.7-2 where the x-Reynolds number needed to reach various values of N_{TS} is plotted as a function of the Mach number. The results of this flat plate calculation for $N_{TS} = 10$ are then converted to equivalent cone Reynolds number using the cone to flat plate transition Reynolds number ratio of 0.65 and compared with the F-15 cone flight transition data [25] as shown in Figure 2.7.7-3. This ratio was determined from the results of Chen et. al. [24] at M = 3.5 and reasonably verified in quiet tunnel tests. The e^{10} prediction shows a trend of increasing cone transition Reynolds number with Mach number, although the slope of the prediction curve is somewhat greater than that indicated by the flight data. This may be caused by a constant correction factor of 0.65 being applied at all Mach numbers to convert the flat plate prediction to

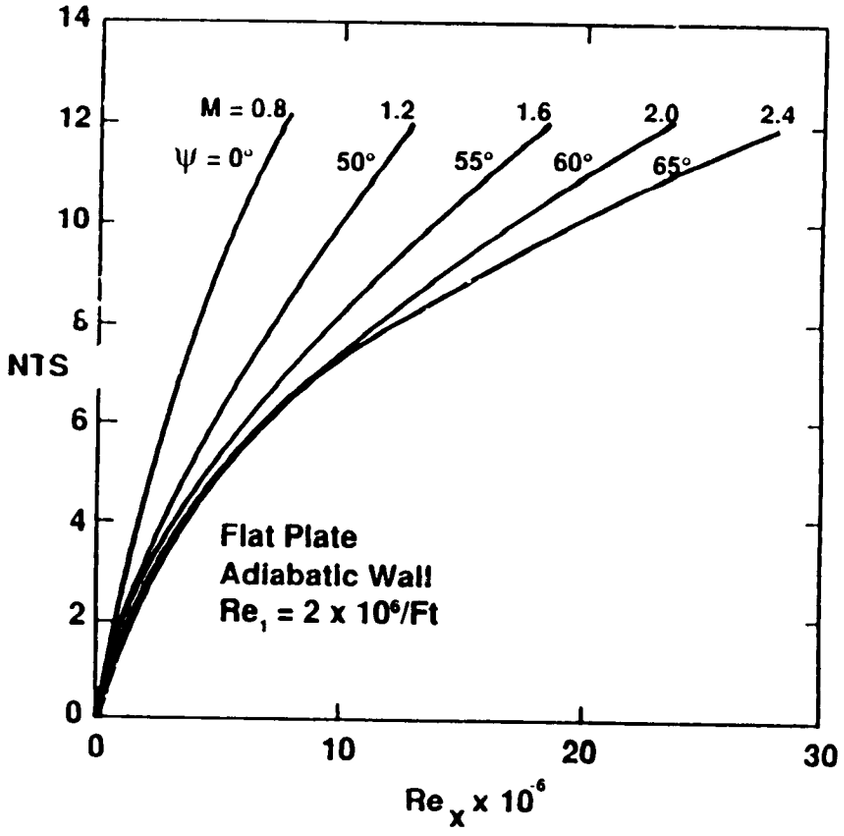

Figure 2.7.7-1 Effect of Mach Number on NTS Growth in Adiabatic Wall Flat Plate Boundary Layer

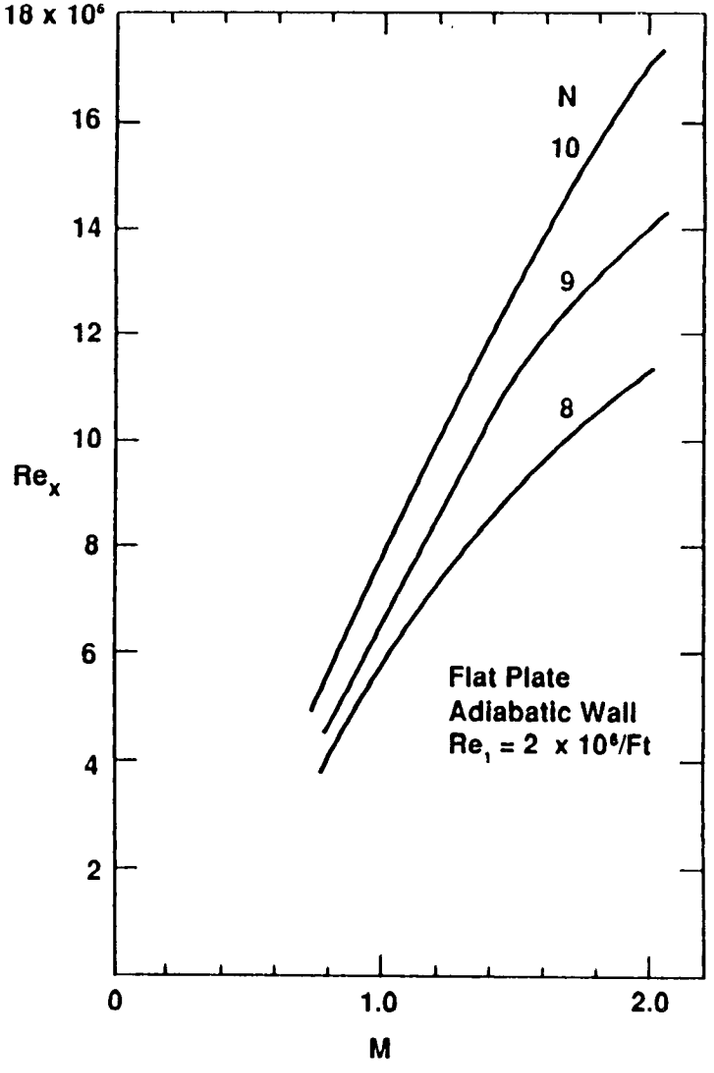

Figure 2.7.7-2 Transition Reynolds Number as a Function of Mach Number for Various Assumed N-Factors at Transition

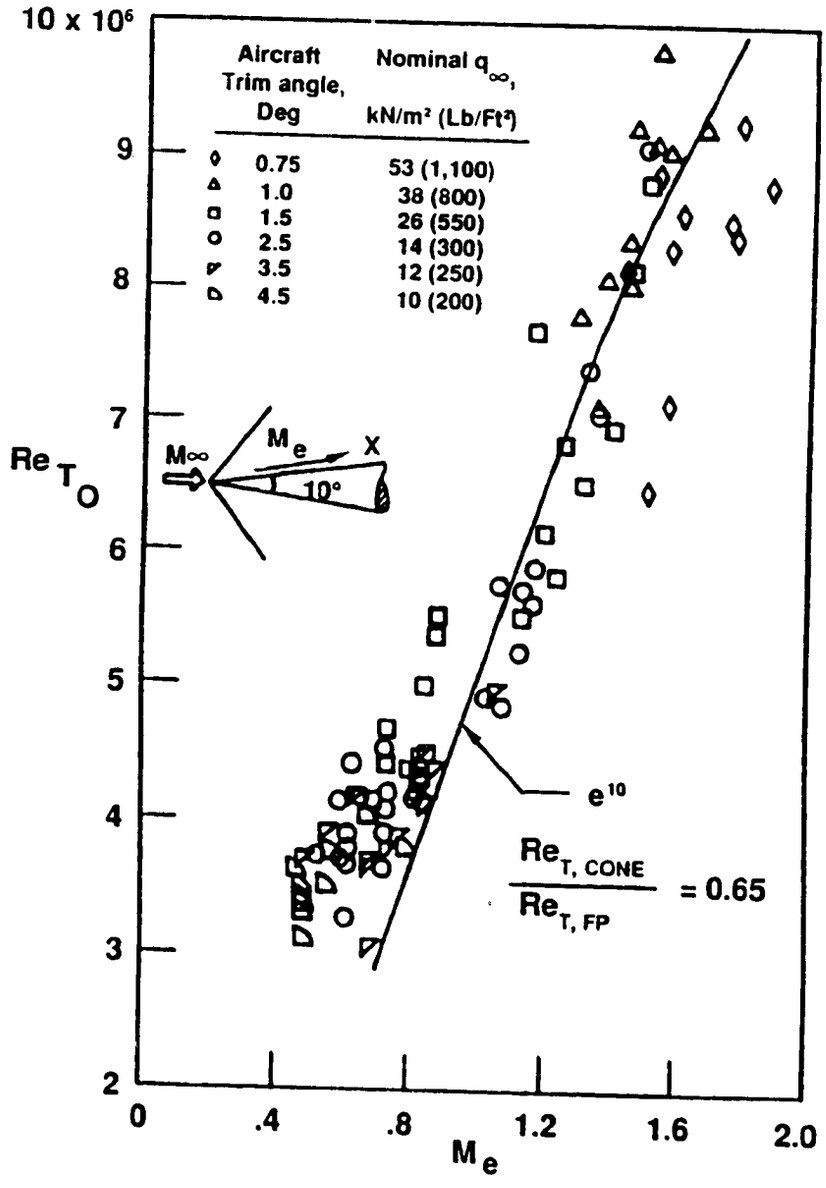

Figure 2.7.7-3 Comparison of Mack Code Prediction with NASA-Dryden Flight Transition Data on Cones

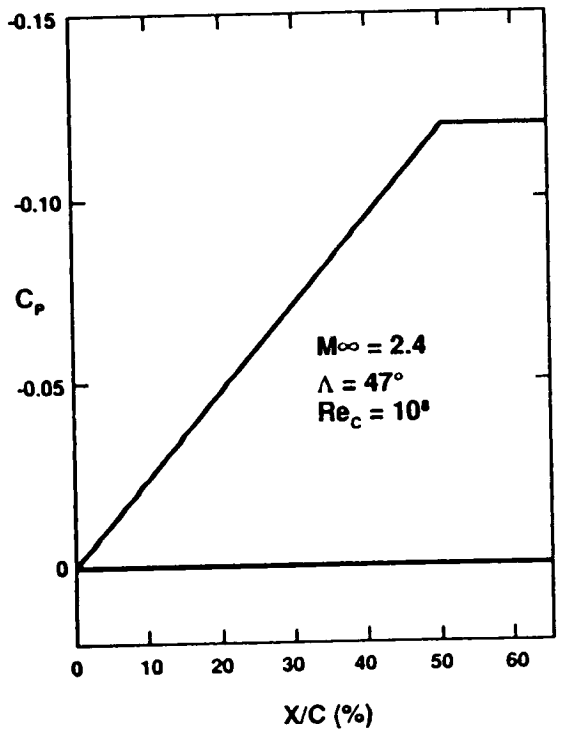

(a)

T-S Amplification Factors
(Boeing Method)

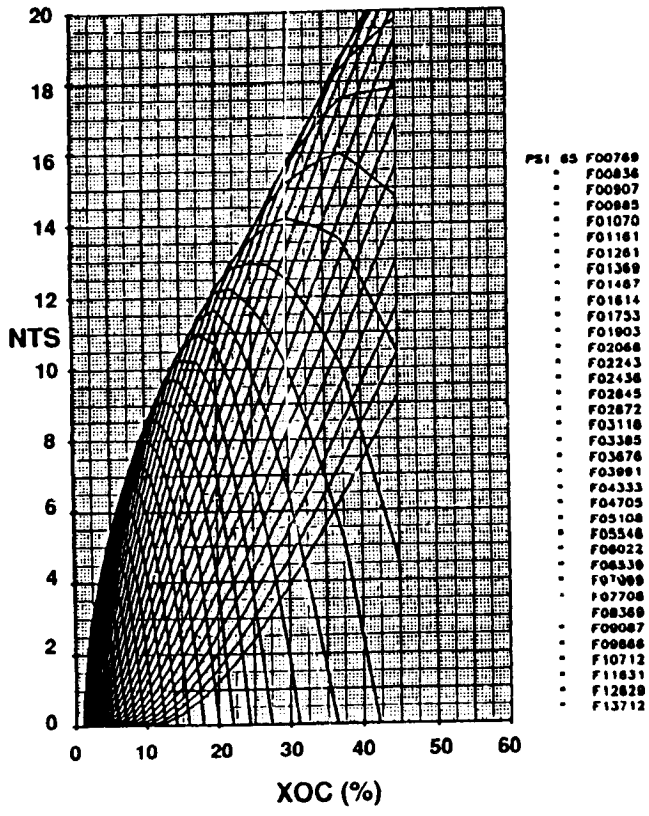

(b)

Crossflow Amplification Factors
Stationary CF Disturbance Growth (Boeing Method)

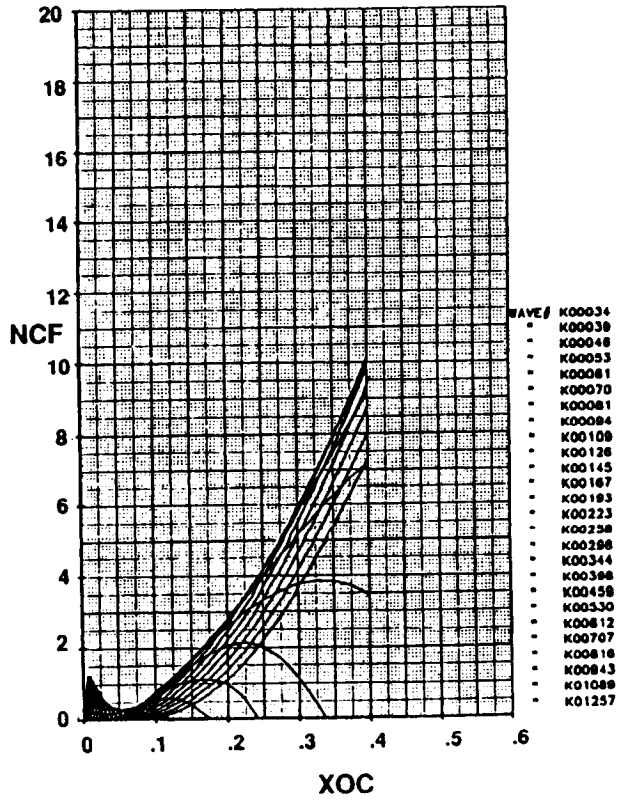

(c)

Figure 2.7.7-4 N_{TS} and N_{CF} Growths on a Swept Wing with Linearly Decreasing Cp

cone prediction. Considering the scatter in the data, the prediction still appears reasonable.

Next, we will study the nature of TS and CF instability growths on a swept wing with a hypothetical linearly decreasing Cp distribution as shown in Figure 2.7.7-4(a). The wing is assumed to be an infinite swept wing with a 47 degree sweep angle. The results of TS and CF instability growths are shown in Figure 2.7.7-4(b) and (c). The N_{TS} is determined by integration of growth rates of various frequency disturbances at a fixed wave angle of 65°. This is the wave angle value for which maximum TS amplification is attained in a 2D flat plate boundary layer having the same free stream Mach number of 2.4. As discussed earlier (Section 2.7.6), a behavior of initially increasing and then decreasing N_{TS} values for each frequency is noticeable. The N_{TS} values indicated by the envelop of all frequencies would be used for transition prediction.

The N-factor for crossflow is plotted individually for various spanwise wave numbers at zero frequency (stationary waves). The behavior for all fixed wave number disturbances is similar: initial growth of N_{CF} followed by a decay as the boundary layer grows. The N_{CF} values indicated by the envelop of all wave number curves would be used for transition prediction.

We will next examine and compare the growth of what has been termed the "TS" N-factor in 3D and 2D boundary layers. For this purpose, the same pressure distribution as shown in Figure 2.7.7-4(a) is assumed and the "N_{TS}" growth calculations are made for $\Lambda = 47°$ and 0°. The results are shown in N_{TS} envelops of Figure 2.7.7-5. All N_{TS} envelops were determined by integration of the TS spatial growth rates at a fixed wave angle of 65 degrees. It may be seen that for the same streamwise pressure distribution, the calculated N_{TS} growth for $\Lambda = 47°$ is far more rapid than the $\Lambda = 0°$ case. In fact, while the N_{TS} for the $\Lambda = 47°$ case continues to grow along the chord, that for the $\Lambda = 0°$ case reaches a peak of $N_{TS} = 7.5$ at approximately 22 percent chord and then decreases. The N_{TS} trend for the $\Lambda = 0°$ case reflects what would intuitively be expected for a favorable pressure gradient boundary layer. The results for $\Lambda = 47°$ case are, on the other hand, counter-intuitive. Not only does the N_{TS} continue to grow chordwise, it grows at a faster rate than even the flat plate boundary layer. This behavior of the calculated N_{TS} for the $\Lambda = 47°$ case could possibly arise from the contribution of inflectional instability in a 3D boundary layer. In the present study, the calculated N_{TS} values, which could have been affected by the inflectional instability in addition to the viscous one, are nevertheless used together with the stationary crossflow (N_{CF}) values for transition prediction. It is also evident from this example that a streamwise pressure gradient (even a favorable one) on a swept wing is undesirable from the point of view of achieving laminar flow: Not only a crossflow instability is generated, the TS growth is also accelerated.

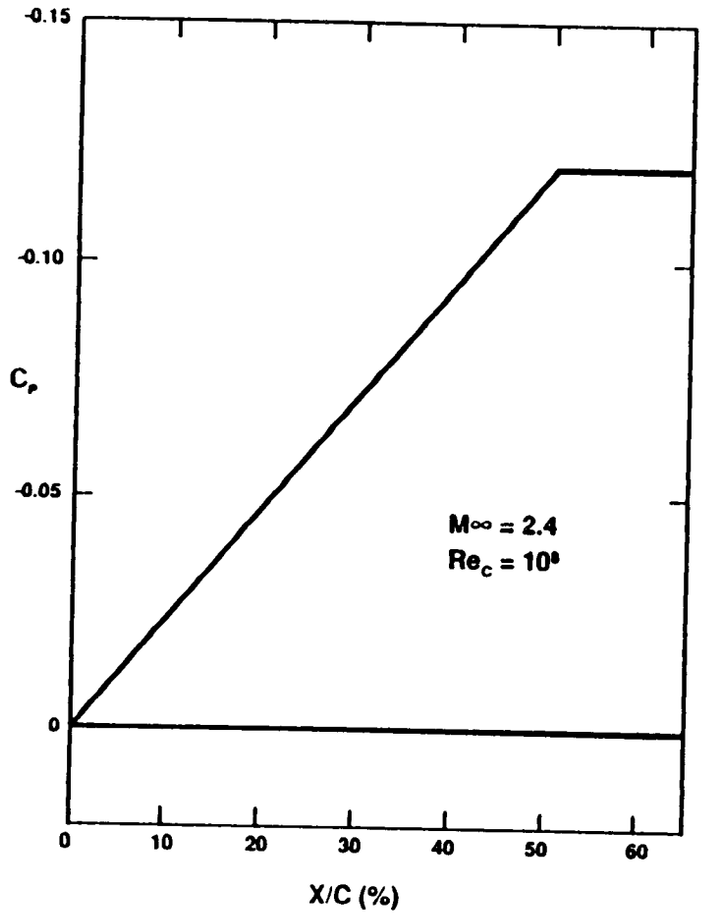

Figure 2.7.7-4(a) Hypothetical Linearly Decreasing Cp

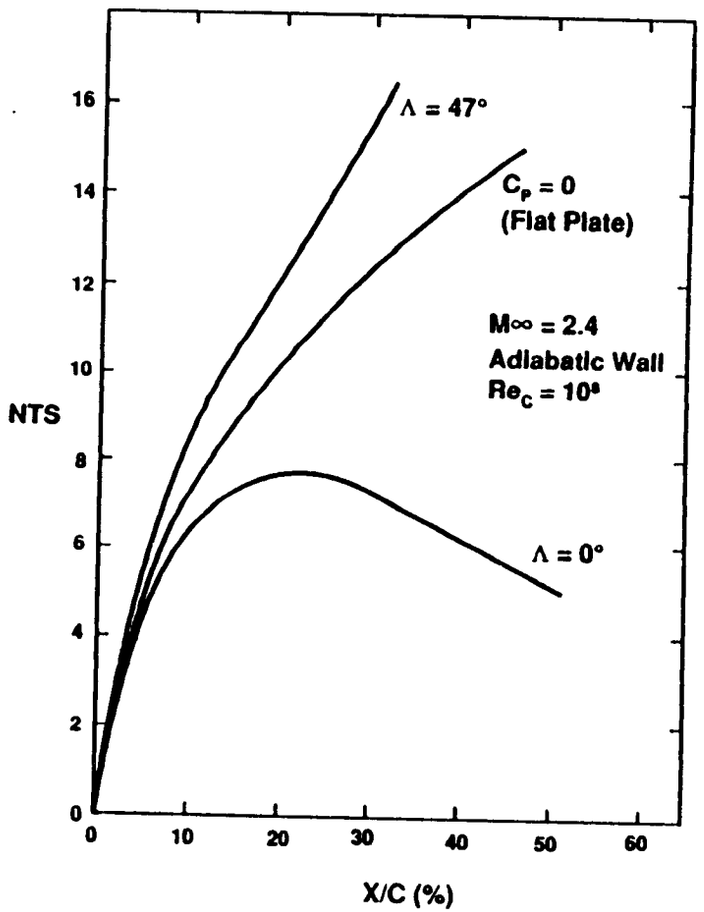

Figure 2.7.7-5 Comparison of N_{TS}-Factor Envelops for Swept and Unswept Wings with Flat Plate

Next, we turn to some of the stability results which were obtained early in the study to assess the effects of suction and cooling on the outboard (supersonic leading edge) part of the wing. The Euler solution was not available at the time for the inviscid flow field, therefore, the pressure distribution as predicted by the A389 linearized lifting surface [33] program was used (see Figure 2.7.7-6). The swept, tapered wing approximation [40] was employed for 3D boundary layer calculation. The effect of wall suction and cooling on the N_{TS} growth are shown in Figure 2.7.7-7(a) thru (c). In all three plots, curve 1 represents the baseline case of no suction and adiabatic wall. In case 2, Figure (a), suction is applied between 0 and 10 percent x/c at a level of C_Q = 0.0002. This level of suction is seen to completely damp the growth of TS instability. Following the termination of suction at x/c = 0.1, N_{TS} begins to grow in a manner similar to case 1. In case 3, Figure 2.7.7-7(a), a mild level of suction of C_Q = 0.00005 is applied and it is seen to be quite effective in damping the TS growth. The total amount of suction used in case 3 up to x/c = 0.4 is the same as that used in case 2, however, the mild suction applied over a longer distance is seen to be more effective. This may be due to more suction being applied between x/c of 0 and 10 percent in case 2 than is necessary to completely damp N_{TS}.

The effectiveness of wall cooling in damping N_{TS} is seen in Figure 2.7.7-7(b). Cooling effectively reduces the wall temperature below the level of adiabatic wall temperature which is approximately 310°F at M = 2.4. It should be noted that some amount of cooling is naturally present on the SST skin. This is due to: (1) the radiation to surroundings and (2) internal conduction to the structure and fuel. A simple surface heat balance was carried out to estimate the skin temperature for laminar or turbulent flow in the boundary layer. The results of this analysis indicated that for laminar boundary layer on the external surface, a skin temperature of about 150°F may be expected, using the skin conductance value employed in fuel heating analyses. This level of skin temperature is seen to cut the N_{TS} growth by almost half. Maintaining the skin temperature at even lower level of 60°F is seen to reduce the N_{TS} growth by a factor of about 4 compared to the adiabatic wall case.

Finally, effects of both suction and cooling are shown in Figure 2.7.7-7(c). Notice that with skin temperature maintained at 150°F, suction applied at even C_Q = 0.0001 level (x/c of 0 to 10 percent) damps out the N_{TS} growth. Thus both mild suction and cooling are very effective in damping the TS instability.

The effect of suction and cooling on the stationary crossflow waves is not so dramatic as will be discussed next with reference to Figure 2.7.7-8(a) thru (c). As before, case 1 represents the baseline case with no suction or cooling and it is the response of the stationary crossflow instability to the

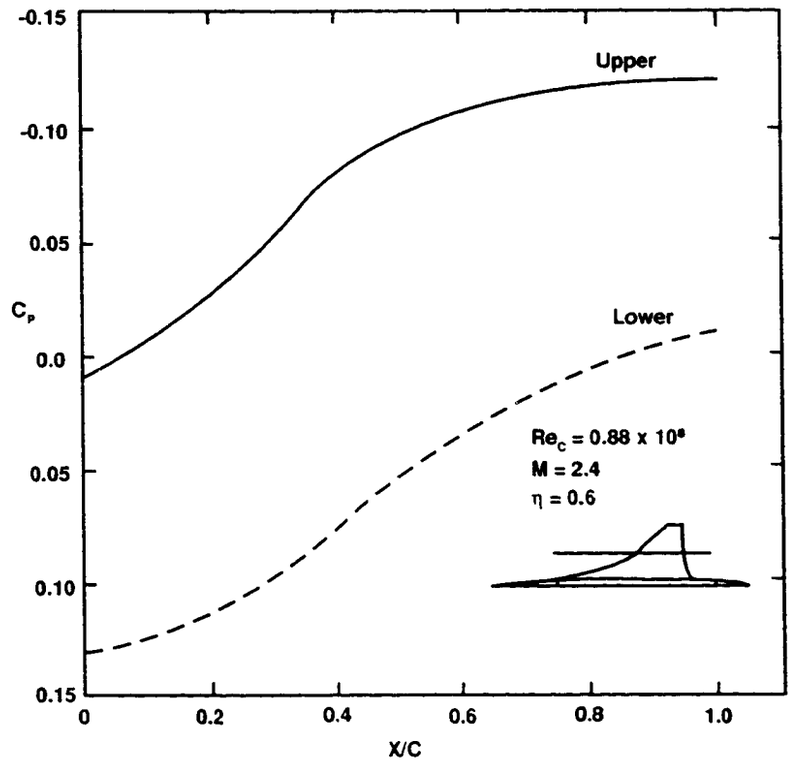

Figure2.7.7-6 **Cp Distribution Used in the Initial Swept Tapered Wing Boundary Layer Analysis**

T - S AMPLIFICATION FACTORS (BOEING METHOD)
M = 2.4, ETA = 0.6, SST WING (UPPER)

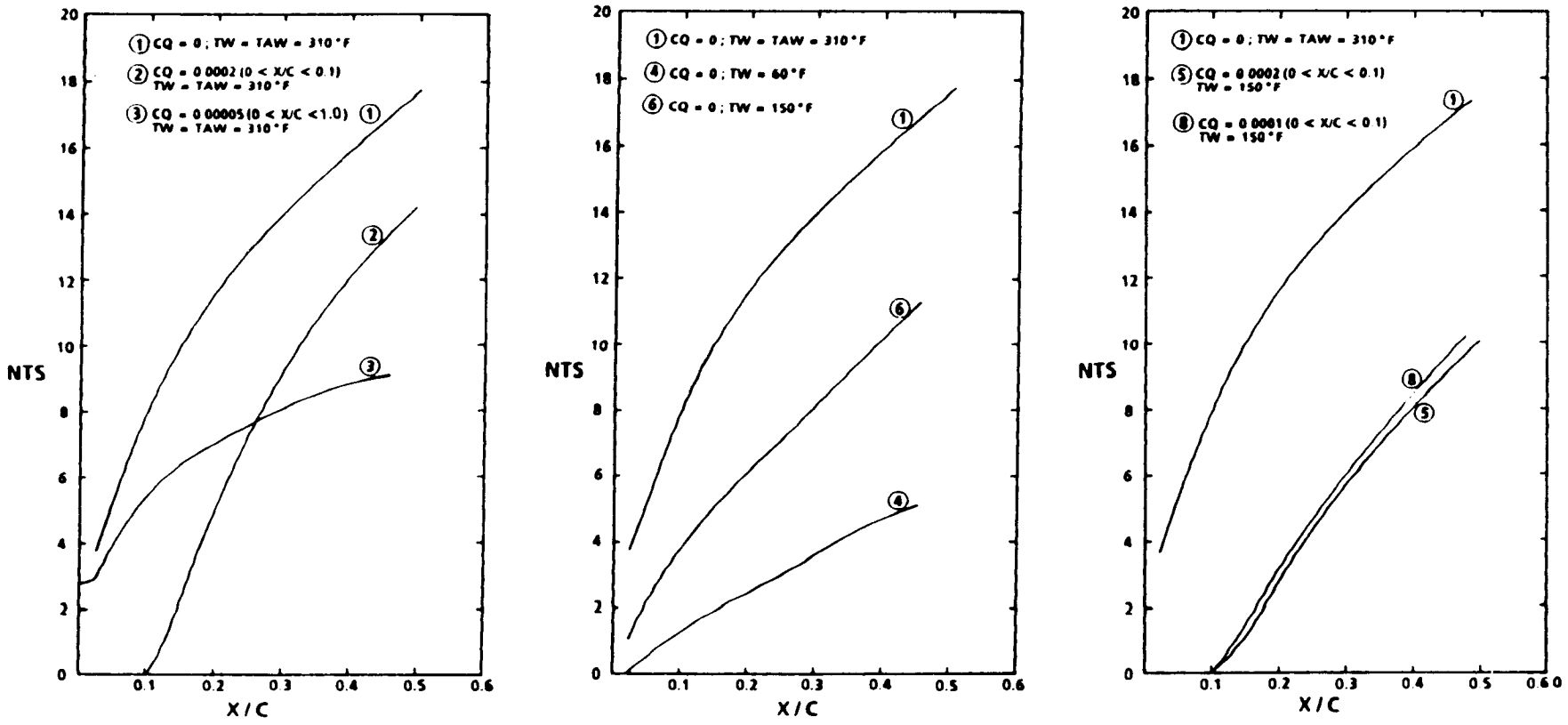

Figure 2.7.7-7 Effect of Suction and Cooling on N_{TS} Growth

CROSSFLOW AMPLIFICATION FACTORS
STATIONARY CF DISTURBANCE GROWTH (BOEING METHOD)
M = 2.4, ETA = 0.6, SST WING (UPPER)

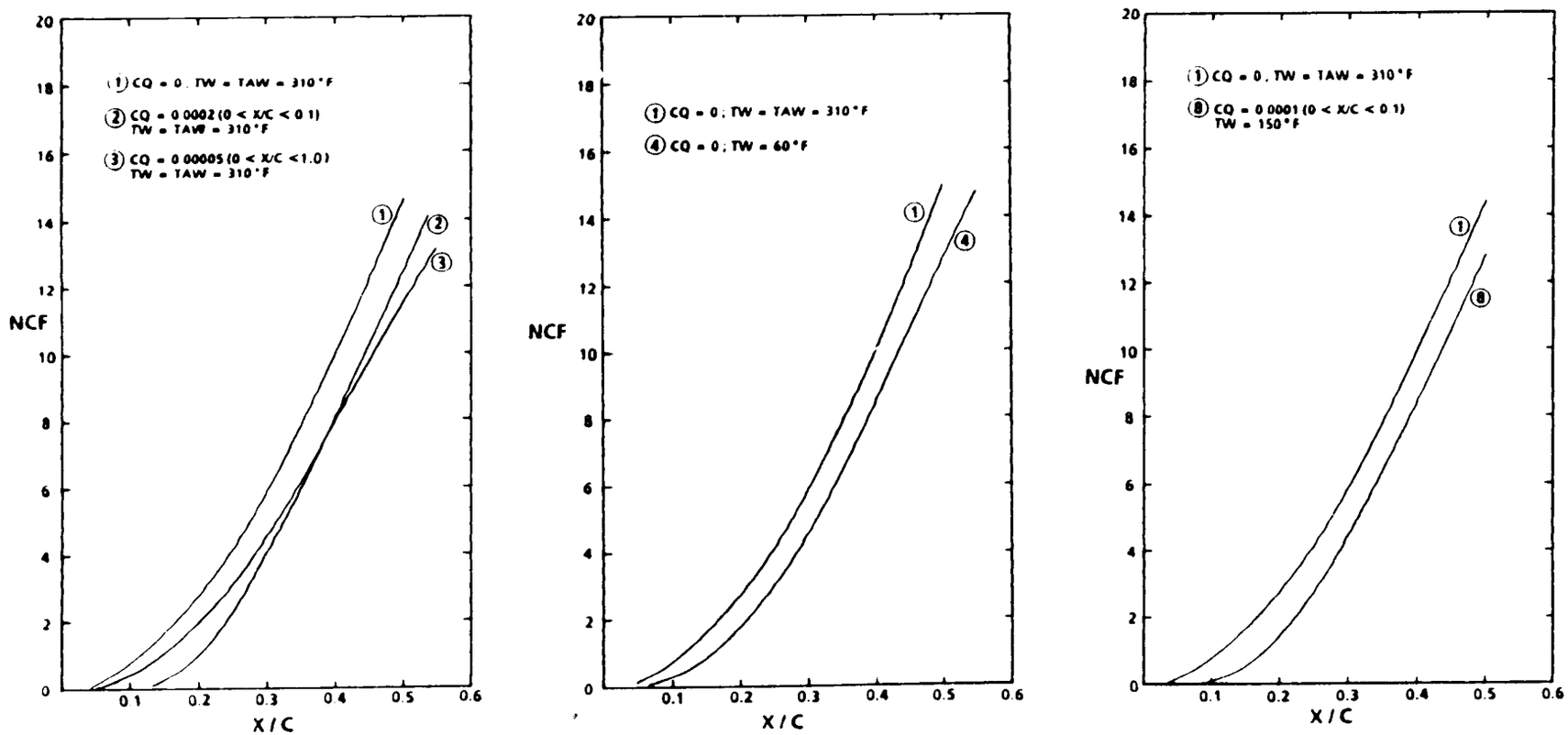

SUCTION (a)

COOLING (b)

SUCTION & COOLING (c)

Figure 2.7.7-8 Effect of Suction and Cooling of NCF Growth

streamwise pressure distribution as shown in Figure 2.7.7-6 on the sharp, 47 degrees leading edge sweep wing. The combination of a mild streamwise pressure gradient and a moderate sweep leads to a gradually developing stationary crossflow instability as shown.

Suction applied at a level of C_q = 0.0002 between x/c of 0 and 0.1 does damp the small initial N_{CF} growth as shown in case 2, Figure 2.7.7-8(a). However, following the termination of suction, the crossflow builds up rapidly, and the attainment of a given N_{CF} value is only delayed by 5 percent or so in x/c. Application of mild suction at the level of C_q = 0.00005 over full chord also has only a weak influence on N_{CF} growth when compared to its influence on N_{TS} growth as seen earlier. Cooling of the surface, even down to 60°F has only a small influence on N_{CF} growth as seen in Figure 2.7.7-8(c).

It may therefore be concluded that while mild suction and cooling are quite effective in damping the N_{TS} growth, they have only a weak influence on the growth of stationary crossflow (N_{CF}) instability. The inherently enhanced stability of the TS disturbances in a supersonic boundary layer, together with the strongly damping influences of mild suction and cooling on their stability means that the control of stationary crossflow (N_{CF}) instability by pressure gradient and strong suction will be the key to the achievement of high transition Reynolds numbers on the SST configuration.

Next, we will discuss the results of stability analyses based on pressure distributions which were modified forms of the Euler solutions. These modifications were discussed in Section 2.2.4 and presented in Figures 2.7.4-10(a) and (b) . For the outboard supersonic leading edge wing, a steep variation in the pressure from the attachment line value to the levels shown for upper and lower surfaces in Figure 2.7.4-10(b) was assumed. The attachment line Cp value was calculated as the stagnation pressure recovered from the component of the freestream normal to the leading edge and after passage through a detached normal shock. The region of steep variation in Cp was assumed to extend over 2 nose radii as shown in Figure 2.7.7-9. The nose radius itself was assumed to be 0.02 percent chord (approximately 1/8 inch).

The TS and CF N-factor growths for the outboard wing were first determined without the application of suction. The basic Cp distribution at η = 0.5 for the upper surface is replotted in Figure 2.7.7-10. The chord Reynolds number at this span station is 1.04×10^8 and the leading edge sweep is 47 degrees. The crossflow instability growth rate at a point on the wing is closely related to the value of the crossflow Reynolds number (RXFLO) of the boundary layer profile at that point. Therefore, it is instructive to observe the behavior of RXFLO. Figure 2.7.7-11 shows the crossflow

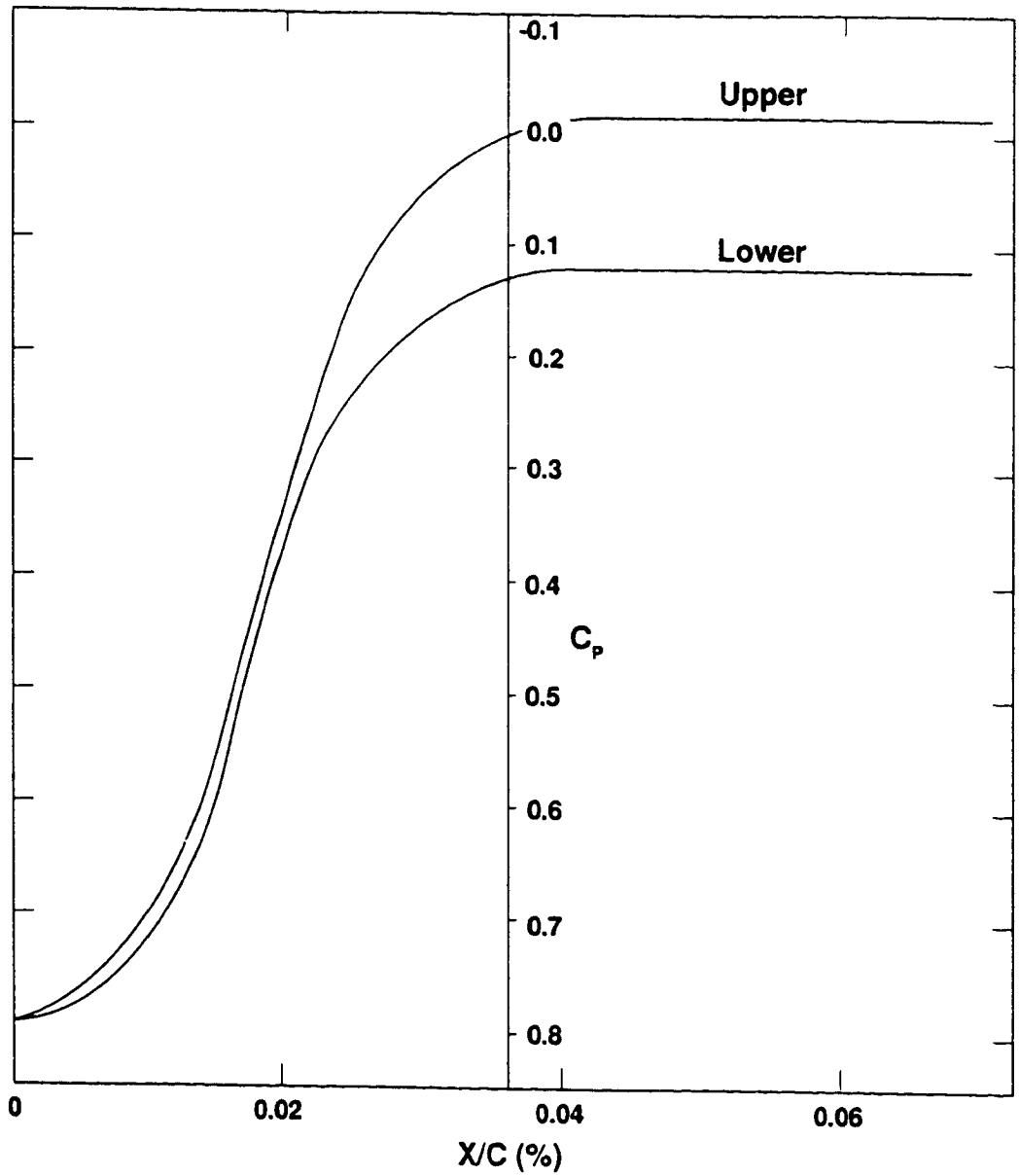

Figure 2.7.7-9 Assumed Cp Variation in the Nose Region of Outboard Wing

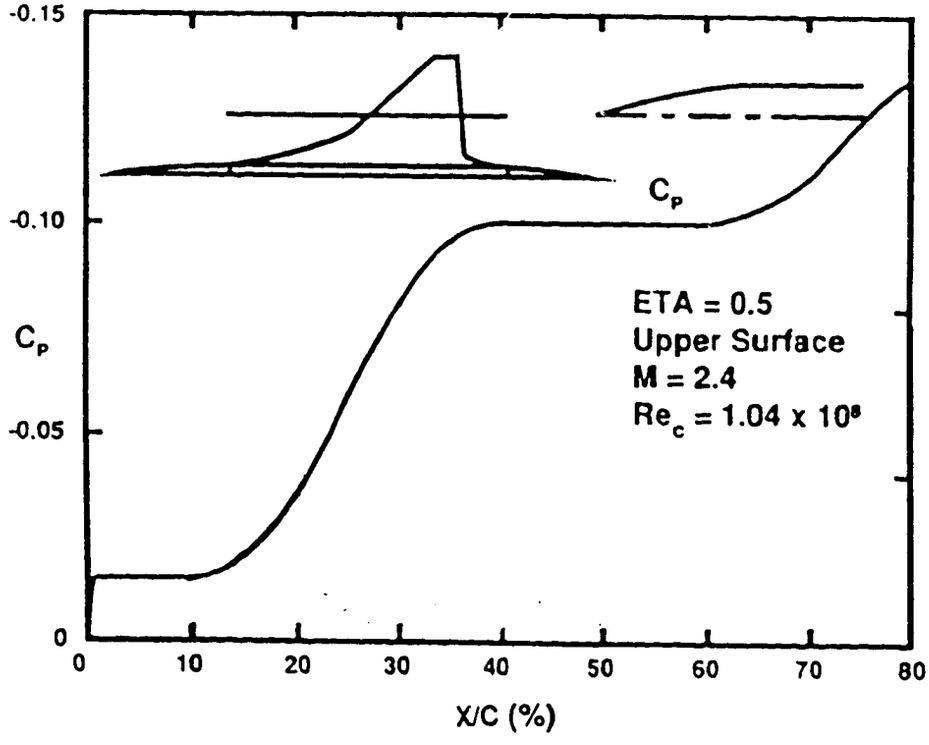

Figure 2.7.7-10 Upper Surface Cp Distribution for Outboard Wing

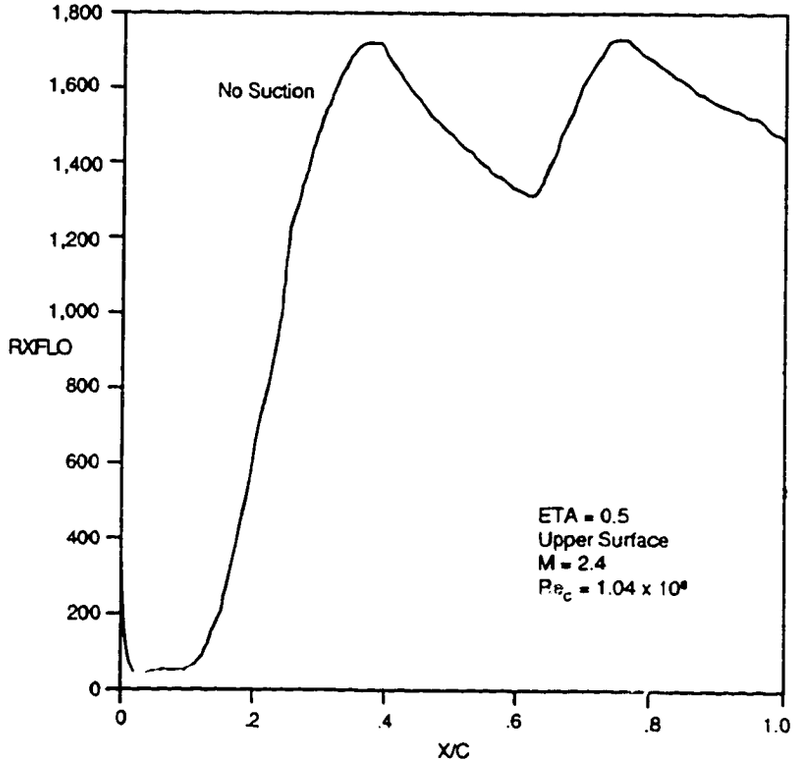

Figure 2.7.7-11 Cross Flow Reynolds Number Build Up for Upper Surface Outboard Wing - No Suction

Reynolds number versus x/c obtained from the 3D boundary layer solution. The initial steep acceleration in the leading edge region causes a build up of crossflow. However, since the boundary layer at this point is so thin and the distances involved are so small, RXFLO does not reach very high values. There is in fact a reduction of the initial crossflow buildup,and in the zero pressure gradient region up to x/c = 0.1, the crossflow Reynolds Number stays at stable values less than about 50. The region of favorable pressure gradient starting at x/c = 0.1 causes RXFLO to increase again, with some reduction when this pressure gradient is relieved. However, in the zero pressure gradient region between x/c of 0.4 and 0.6, RXFLO stays at high values that were achieved during the preceding region of pressure gradient. The effectiveness of any suction scheme in suppressing crossflow instability may be judged from an examination fo the behavior of the crossflow Reynolds number.

There is a further increase in RXFLO beyond x/c = 0.6 due to the second pressure gradient region on the wing. However, this region is not of interest because it was intended to achieve laminarization only up to x/c = 0.6.

The growths of N_{TS} and N_{CF} for the outboard wing without suction are shown in Figures 2.7.7-12(a) and (b), respectively. Notice that the favorable streamwise pressure gradient coupled with 47° sweep causes an accelerated growth of N_{TS} (calculated at a fixed wave angle of 65°) between x/c of 0.1 and 0.4. This is possibly caused by the contribution from inflectional instability as noted earlier. The N_{CF} does not start building up until about x/c = 0.15. Beyond that it grows rapidly as the crossflow Reynolds number builds up to high values as already discussed.

Knowing N_{TS} and N_{CF} at various x/c values on the wing, one can plot the trajectory of N_{TS} versus N_{CF} at various x/c values as shown in Figure 2.7.7-13. As the trajectory crosses over into the band, transition becomes imminent. For the no suction case just discussed, this would occur shortly after x/c = 0.2.

To extend the laminar run beyond x/c of 20 percent, suction control would be needed. To minimize the penalties associated with suction, it is desirable to use as little of it as possible and only in discrete regions. After some experimentation, a suction scheme was determined which would control the N_{TS} and N_{CF} growth enough to satisfy the transition criterion shown in Figure 2.7.7-13. As shown in Figure 2.7.7-14, this scheme employed two suction regions of 10 percent chord length each: one between 10 and 20 percent chord and the other between 20 and 40 percent chord. A suction level of Cq = 0.0002 was employed in each region.

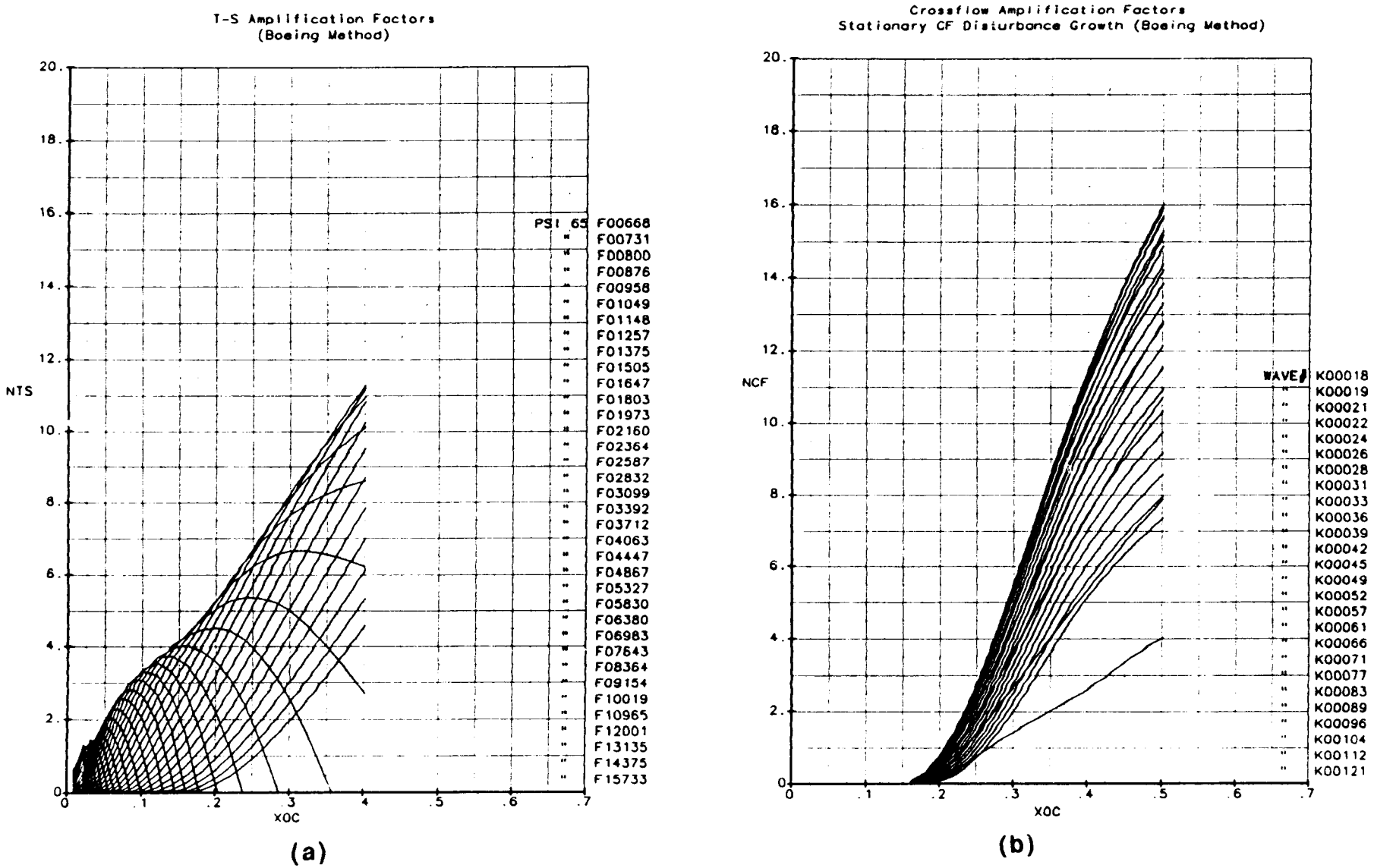

Figure 2.7.7-12 N_{TS} and N_{CF} Growth on Outboard Wing Upper Surface - No Suction

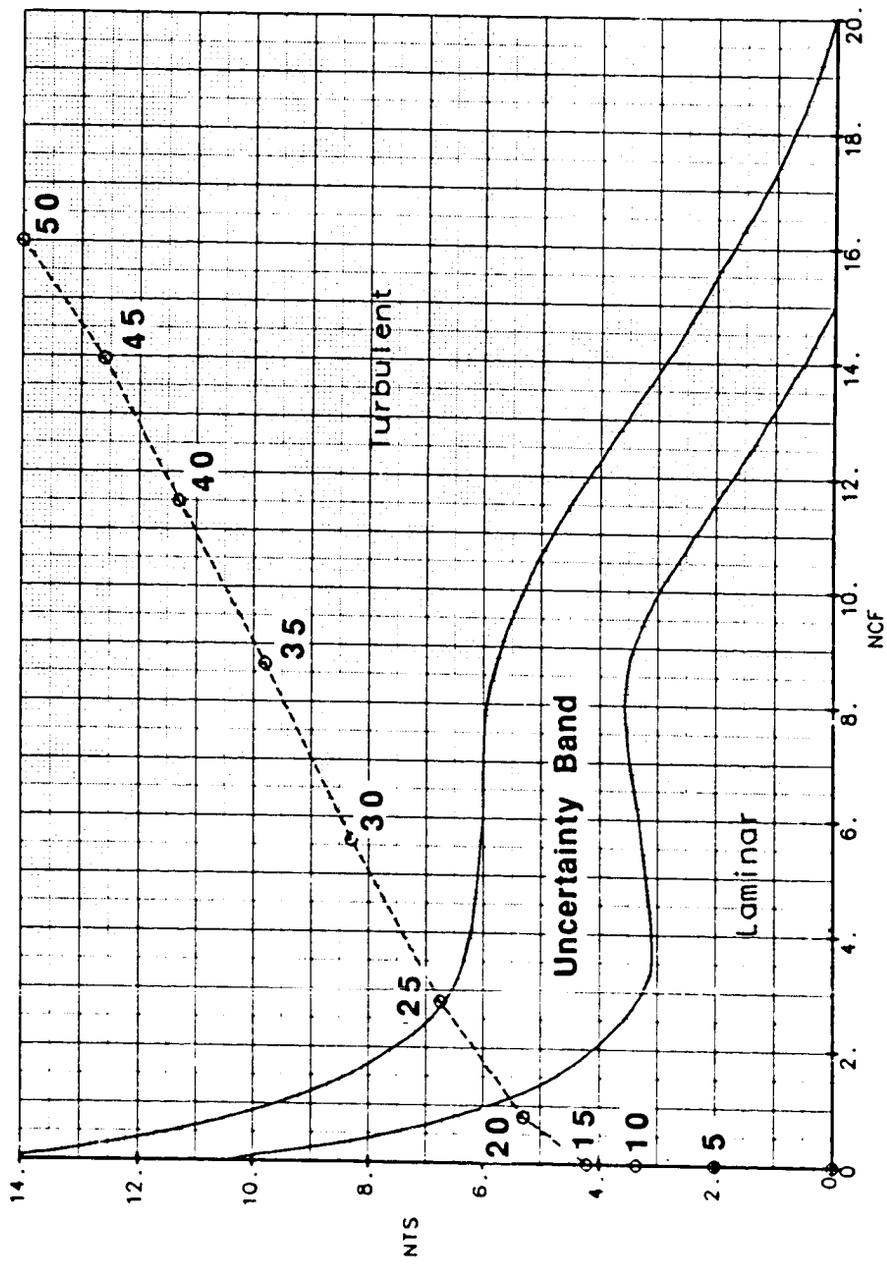

Figure 2.7.7-13 Trajectory of NTS vs NCF for Outboard Wing Upper Surface - No Suction

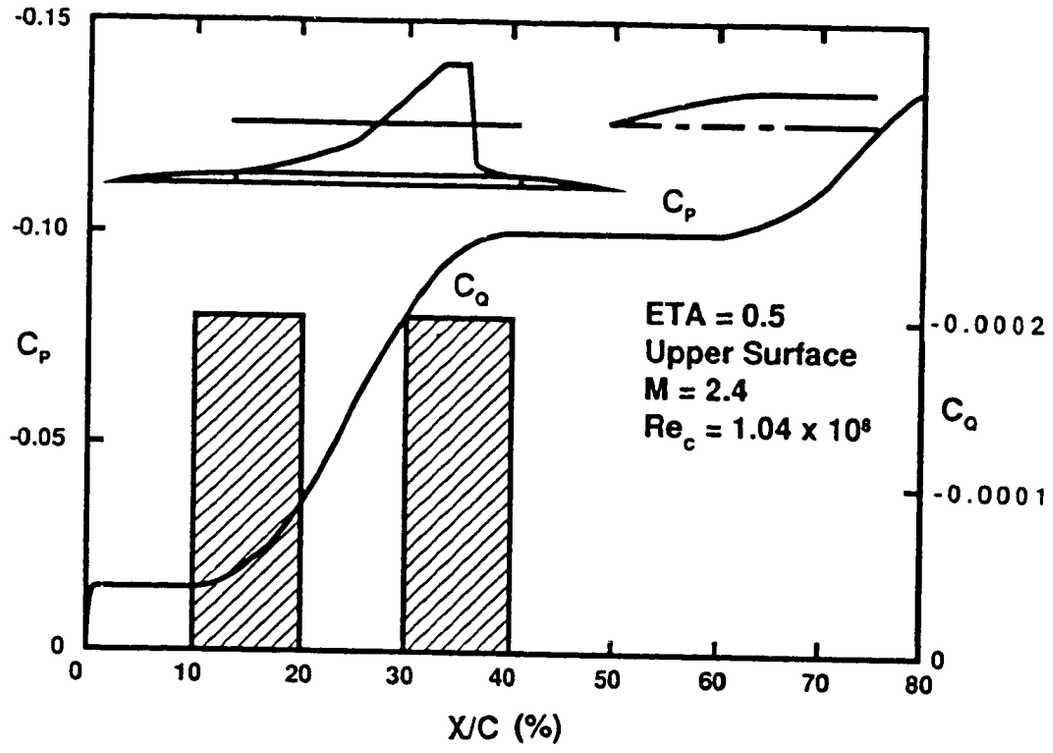

Figure 2.7.7-14 Upper Surface Cp Distribution and Suction Distribution for Outboard Wing

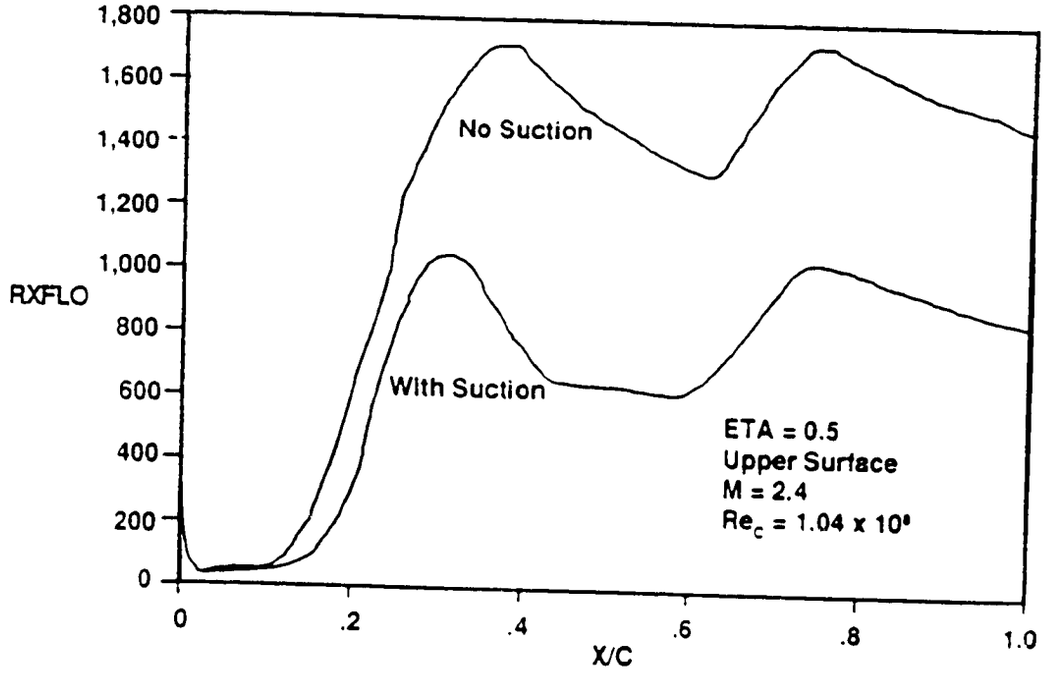

Figure 2.7.7-15 Comparison of Cross Flow Reynolds Number Buildup With and Without Suction Outboard Wing Upper Surface

We will now examine how this suction scheme modified the crossflow Reynolds number and the growths of N_{TS} and N_{CF} . Figure 2.7.7-15 shows a comparison of RXFLO with and without suction. Note that suction reduces the peak value of RXFLO at x/c = 0.3 by about a factor of 1/2. The second suction region (between 30 to 40 percent chord) also helps reduce the crossflow Reynolds number to values less than half the baseline values.

The effect of suction on N_{TS} is shown in Figure 2.7.7-16(a). The application of suction in the first region (10 to 20 percent chord) arrests the accelerated growth of N_{TS} as compared to no suction case. Suction reduces the N_{TS} values and drops the envelop value of N_{TS} to zero by about x/c = 0.15, while the suction continues to x/c = 0.2. This seems to indicate that even a lesser suction level than the one employed (C_q = 0.0002) would have been effective in controlling the N_{TS} in this region. However, the suction level employed (C_q = 0.0002) was found necessary for control of stationary crossflow instability. Following the termination of suction at x/c = 0.2, the N_{TS} values grow again, only to be damped completely by the second suction region between 30 and 40 percent chord. Following the termination of the second suction region, N_{TS} values begin to grow as shown.

The growth behavior of N_{CF} with this suction scheme is shown in Figure 2.7.7-16(b). The impact of the two region suction is to retard the growth of N_{CF} somewhat as may be seen from a comparison with the baseline no suction case.

The envelop values of N_{TS} and N_{CF} are plotted in Figure 2.7.7-17. It may be seen that the two region suction scheme employed manages to keep the trajectory of N_{TS} versus N_{CF} below the lower boundary of the transition band up to about 55 percent chord. The 60 percent chord point is near the center of the band. Therefore, if this transition criterion is valid, laminarization up to approximately 60 percent chord would be achievable by use of the proposed suction scheme.

The crossflow N-factor reaches fairly high values (10 to 14) in the laminarization scheme just described. At N_{CF} values greater than 10, the validity of the transition data band is suspect. In the F-111/B757 NLF test during which these transition data were generated, these high values of N_{CF} were reached in the rounded nose region of the wing where the possibly stabilizing effect of convex surface curvature are present. Therefore, laminar flow may have been maintained in those tests despite the high N_{CF} values because of the possibly stabilizing influence of the convex surface curvature.

An alternative Cp distribution and suction scheme may be employed on the outboard wing surface for a better control of the crossflow instability and consequently, reduced values of N_{CF}. In such a scheme, the gradual

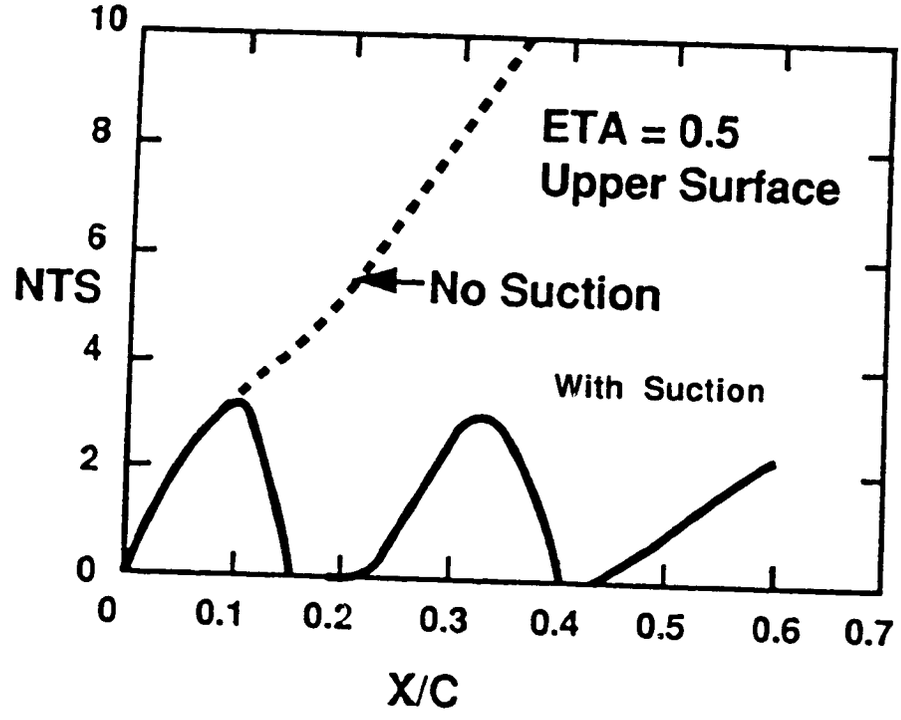

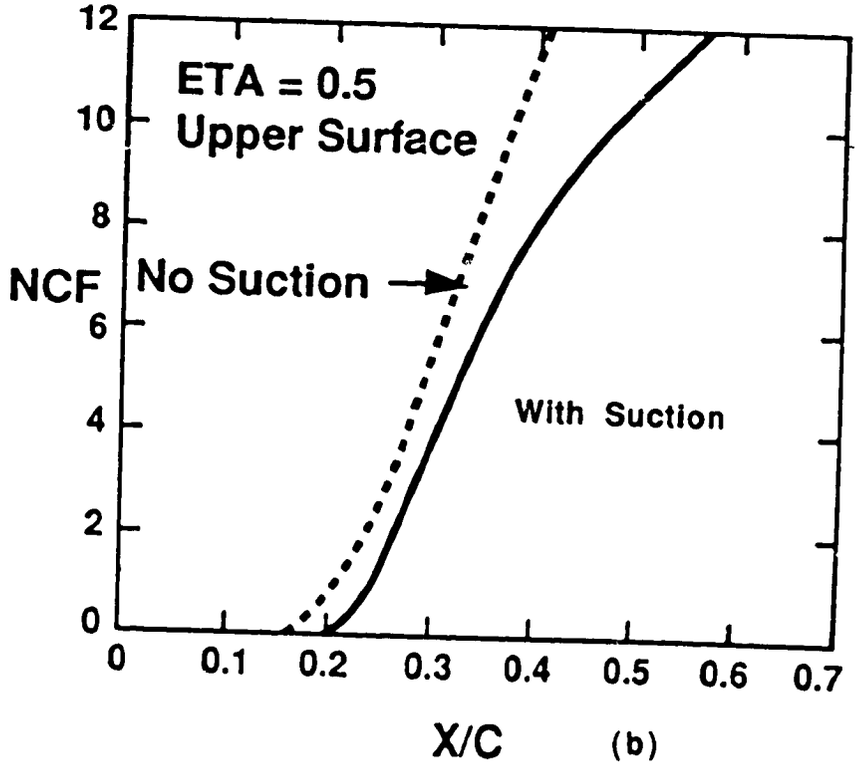

Figure 2.7.7-16 NTS and NCF Growth on Outboard Wing Upper Surface With and Without Suction

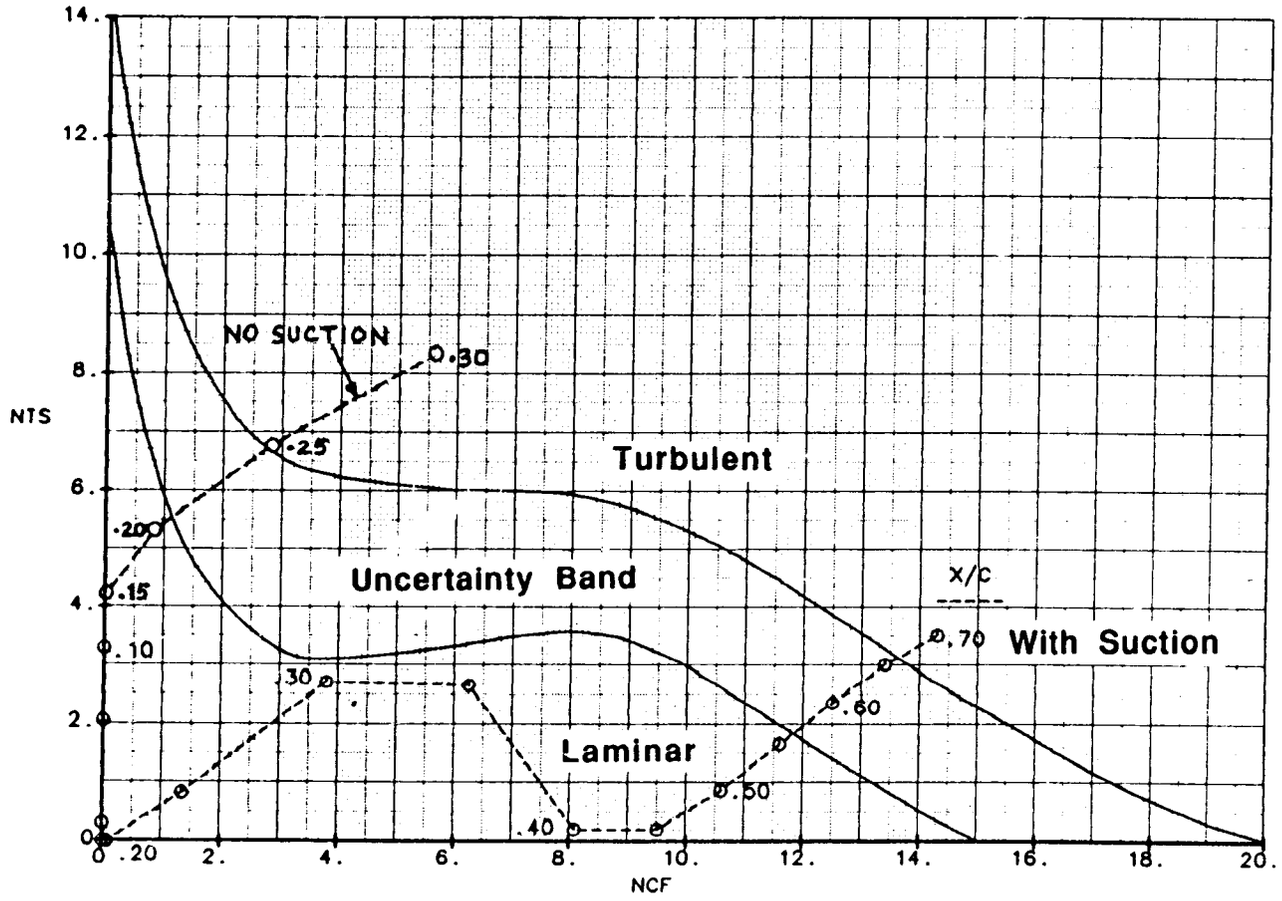

Figure 2.7.7-17 Trajectory of N_{TS} vs N_{CF} for Outboard Wing Upper Surface With and Without Suction

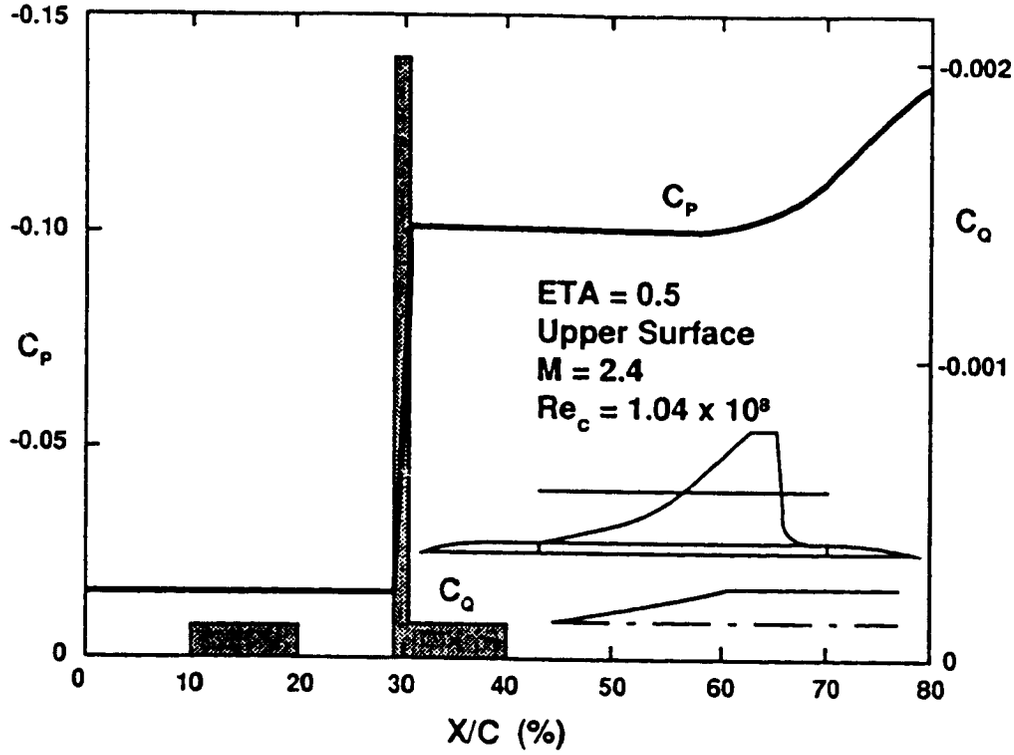

Figure 2.7.7-18 Modified Upper Surface Pressure and Suction Distribution

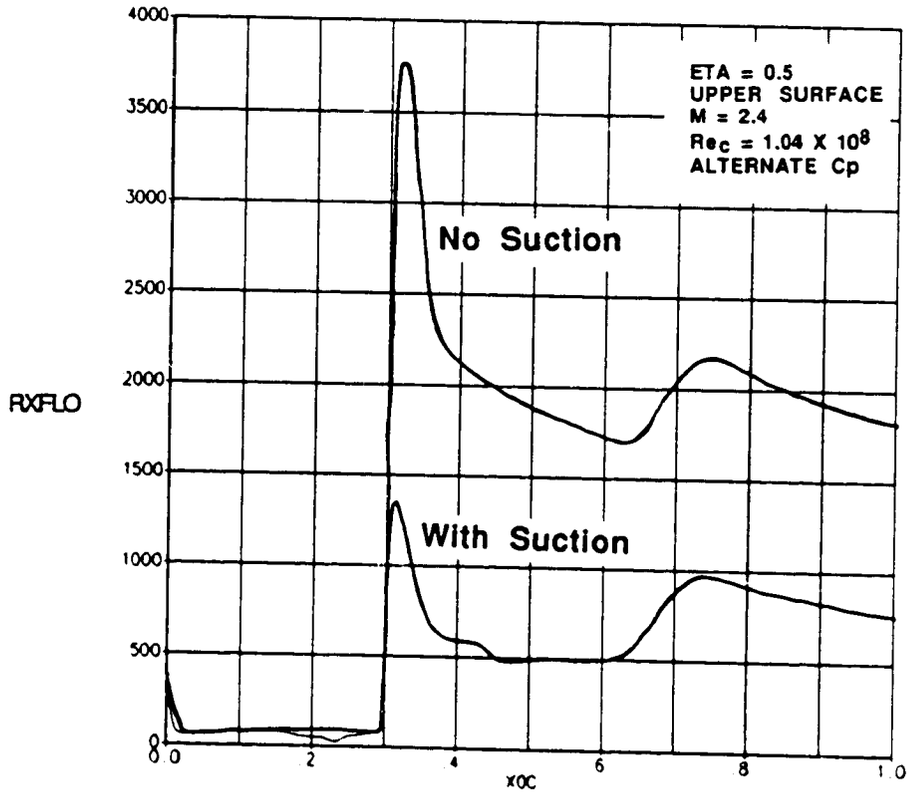

Figure 2.7.7-19 Comparison of Crossflow Reynolds Number With and Without Suction. Alternate Cp Distribution Outboard Wing Upper Surface

transition from the wedge section of the airfoil to the slab section (see Figure 2.7.7-10) would be made more abruptly, so that a steep Cp variation as shown in Figure 2.7.7-18 is achieved. Such a steep Cp variation is achievable in supersonic flow because of Prandtl-Meyer expansion at the shoulder. In the boundary layer and stability calculations,the steep Cp variation was confined to a region 1 percent in x/c, located between 29 and 30 percent chord. The suction scheme is also shown in Figure 2.7.7-18. In the first region between 10 and 20 percent x/c, suction is applied at a level of C_Q = 0.0001. In the second region a stronger suction at the level of C_Q = 0.002 is applied between x/c of 29 and 30 percent, i.e., in the same region where the steep variation in Cp occurs. Following this region of strong suction, weaker suction is applied at the level of C_Q = 0.0001 between 30 and 40 percent chord. The total suction requirement for this scheme is the same as that for the scheme shown in Figure 2.7.7-14.

The effect of this suction scheme on the crossflow Reynolds number development may be seen in Figure 2.7.7-19. The peak RXFLO value is reduced by a factor of 3 while the residual level in the 40 to 60 percent x/c region is reduced by a factor of 4 or 5.

Stability calculations were run only for the case with suction. The N_{TS} and N_{CF} growths are shown in Figures 2.7.7-20(a) and (b). The effect of the first suction region is to arrest the growth of N_{TS} and indeed reduce N_{TS} to zero at the end of the first suction region (i.e., at x/c = 0.2). This suction also thins the boundary layer somewhat, which helps reduce crossflow buildup further downstream in the region of steep Cp variation. Following the termination of suction at x/c = 0.2, N_{TS} begins building up and leads to eventual transition beyond x/c = 0.6.

The crossflow N-factor (N_{CF}) does not begin to increase until x/c = 0.3 as seen in Figure 2.7.7-20(b) because there is no pressure gradient up to this point. Beyond the region of strong suction, however, it begins to grow, presumably at a rate slower than what it would have been without suction. This may be seen from a comparison of crossflow Reynolds Number growths with and without suction in Figure 2.7.7-19.

The trajectory of N_{TS} versus N_{CF} for this alternate scheme for the outboard wing is shown in Figure 2.7.7-21. In this case, both N_{TS} and N_{CF} stay well below the lower boundary of the transition band. Also the N_{CF} values stay well below 10.

Next, we consider the suction requirements for laminarization of the inboard wing. Here the Cp distribution is as shown in Figure 2.7.4-10(a). The upper surface Cp distribution is replotted in Figure 2.7.7-22. In this case the velocity component normal to the leading edge is subsonic and the section has a large nose radius compared to the outboard wing.

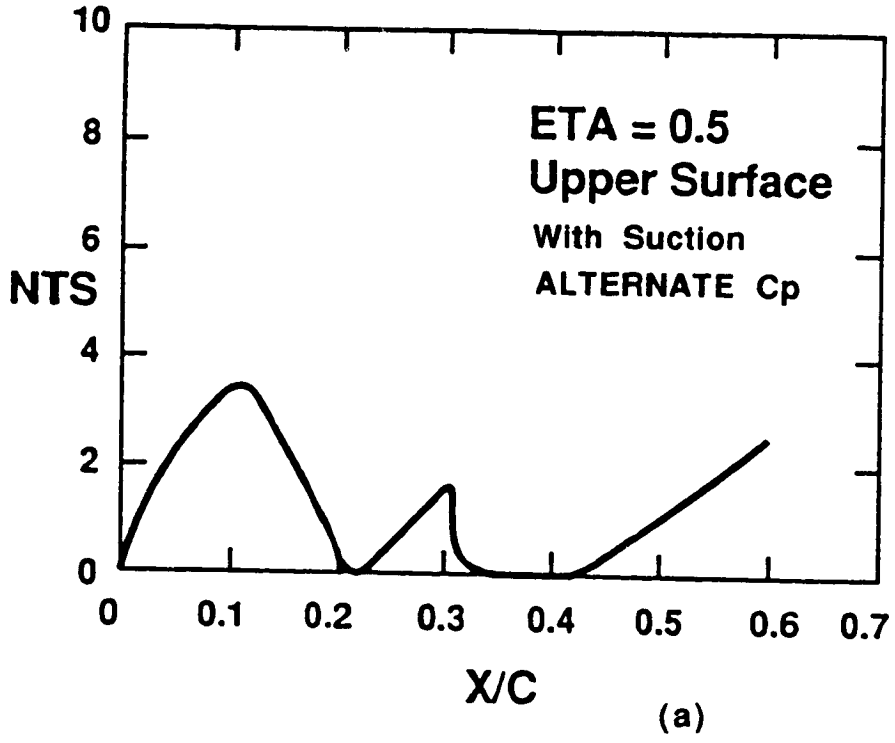

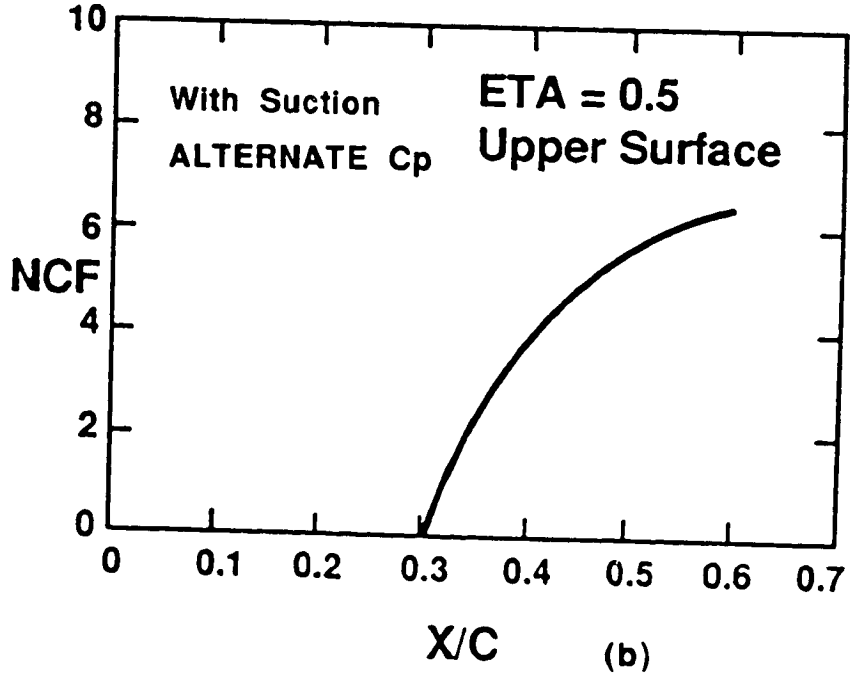

Figure 2.7.7-20 NTS and NCF Growth on Outboard Wing Upper Surface. Alternate Pressure and Suction Distributions

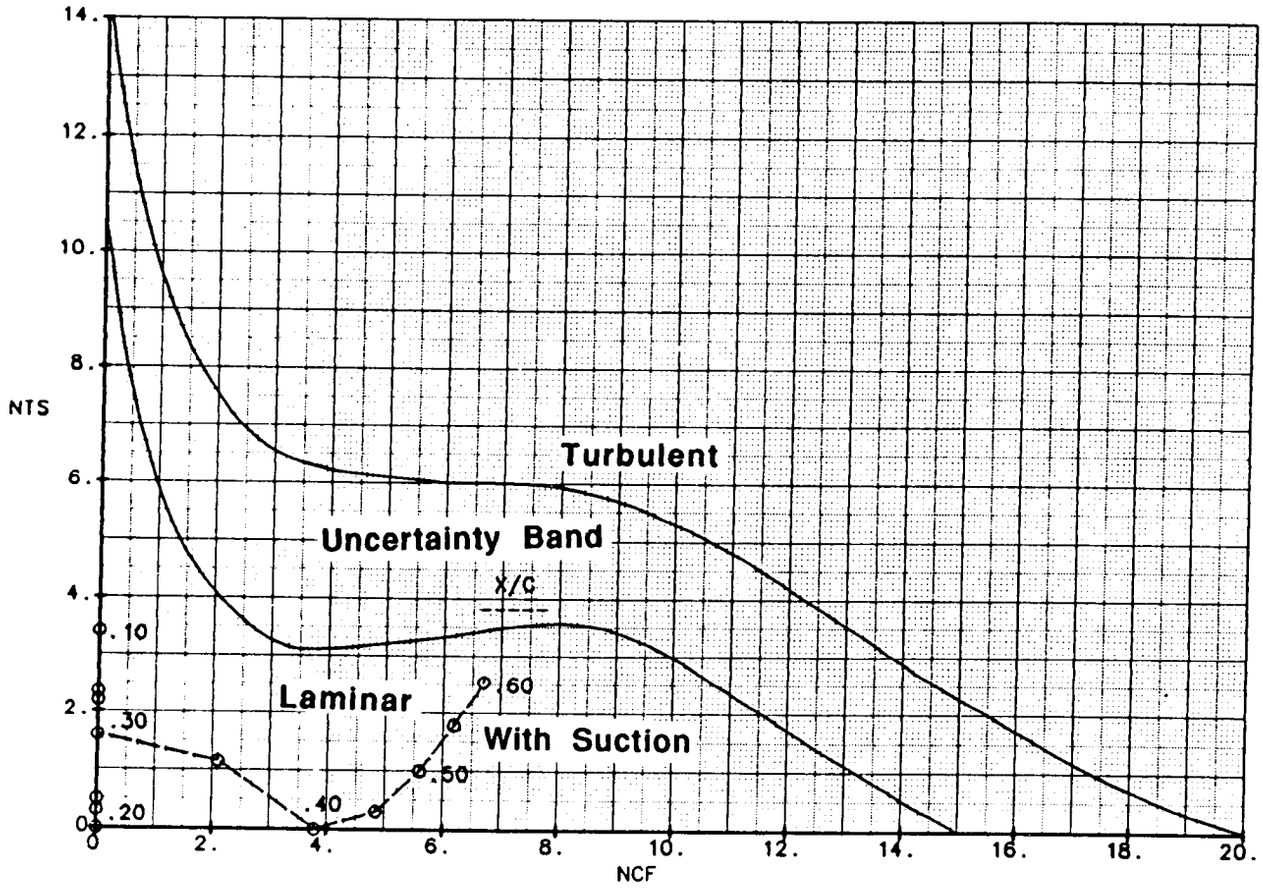

Figure 2.7.7-21 Trajectory of N_{TS} vs N_{CF} for Outboard Wing Upper Surface. Alternate Cp and Suction Distributions

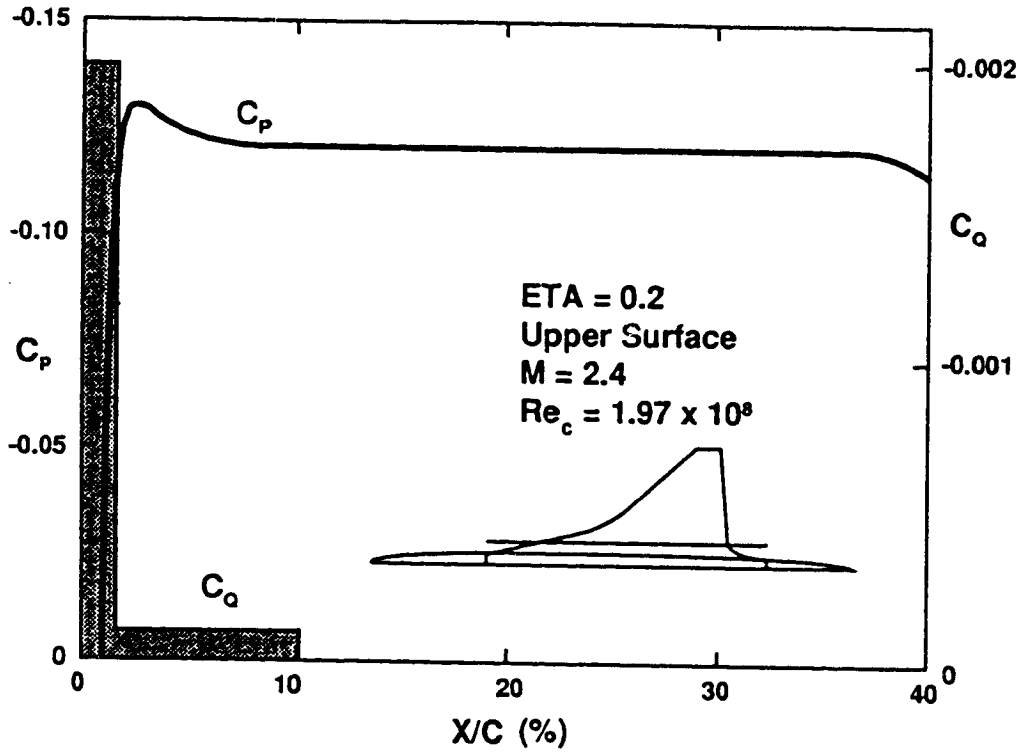

Figure 2.7.7-22 Inboard Wing Upper Surface Pressure and Suction Distributions

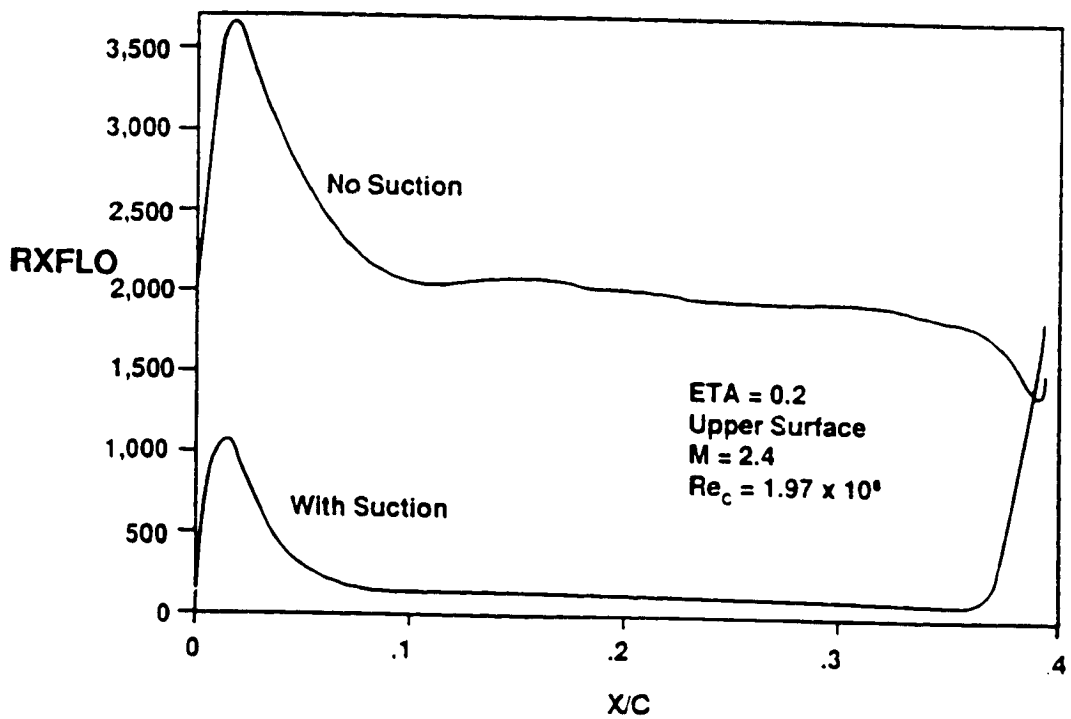

Figure 2.7.7-23 Cross Flow Reynolds Number Buildup for Inboard Wing Upper Surface With and Without Suction

The suction peak on the upper surface occurs at x/c of 1.5 percent. Also, the chord length for the inboard wing section is twice that for the outboard wing section considered. Thus the leading edge pressure gradient is steep, but significantly less steep than what is experienced at the sharp leading edge on the outboard wing. The boundary layer in the rounded leading edge region of the inboard wing gets significantly thicker than that on the sharp leading edge of the outboard wing. Consequently, large values of crossflow Reynolds numbers and crossflow N-factors are reached in the leading edge region of the inboard wing. Unlike the sharp leading edge outboard wing, strong suction is needed in the leading edge region of the inboard wing to control the crossflow instability. Suction at the level of C_Q = 0.002 was applied in the region of steep variation in Cp in the vicinity of the attachment line followed by a region of mild suction at Cq = 0.0001 up to 10 percent chord as shown in Figure 2.7.7-22. The chord Reynolds number at this span station (η = 0.2) is approximately 200 million and the leading edge sweep angle is 75 degrees. Note that strong suction is also needed in the vicinity of the attachment line to damp the TS instability of the attachment line boundary layer.

The crossflow Reynolds number development for this type of Cp distribution with and without suction is shown in Figure 2.7.7-23. Without suction, RXFLO reaches a peak value of more than 3500 but decreases significantly to about 2000 because of the small pressure recovery built into the desired Cp distribution following the suction peak (see Figure 2.7.7-22). This technique for reducing the crossflow Reynolds number was originally proposed by Dr. W. Pfenninger [43]. In the zero pressure gradient region between x/c of 10 and 35 percent, the crossflow Reynolds number stays at relatively high values of about 2000. The application of suction according to the scheme shown in Figure 2.7.7-22 dramatically reduces the peak in RXFLO to a value around 1000 and then a combination of the weak suction and a small adverse pressure gradient reduces RXFLO to values around 50 where crossflow instability is not a problem.

The growth of N_{CF} with and without suction is shown in Figure 2.7.7-24(a). Without suction, the rapid development of RXFLO causes N_{CF} to buildup to rather high values in a short distance. With suction, this growth is curtailed and after reaching a peak value, the crossflow N-factor N_{CF} actually decreases to zero. Thus a boundary layer free of stationary crossflow instability is established beyond x/c of about 0.15.

The N_{TS} results were obtained only for the case with suction and are shown in Figure 2.7.7-24(b). The presence of suction up to 10 percent chord damps the TS waves in the boundary layer. Following the termination of suction at x = 0.1, N_{TS} begins to grow much in the same manner as for a flat plate boundary layer.

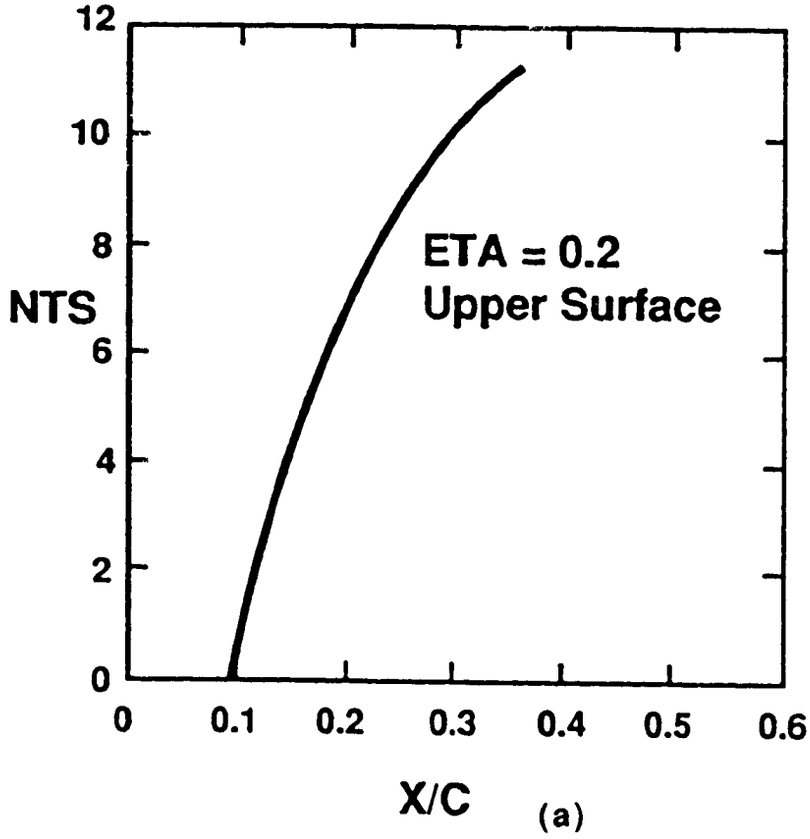

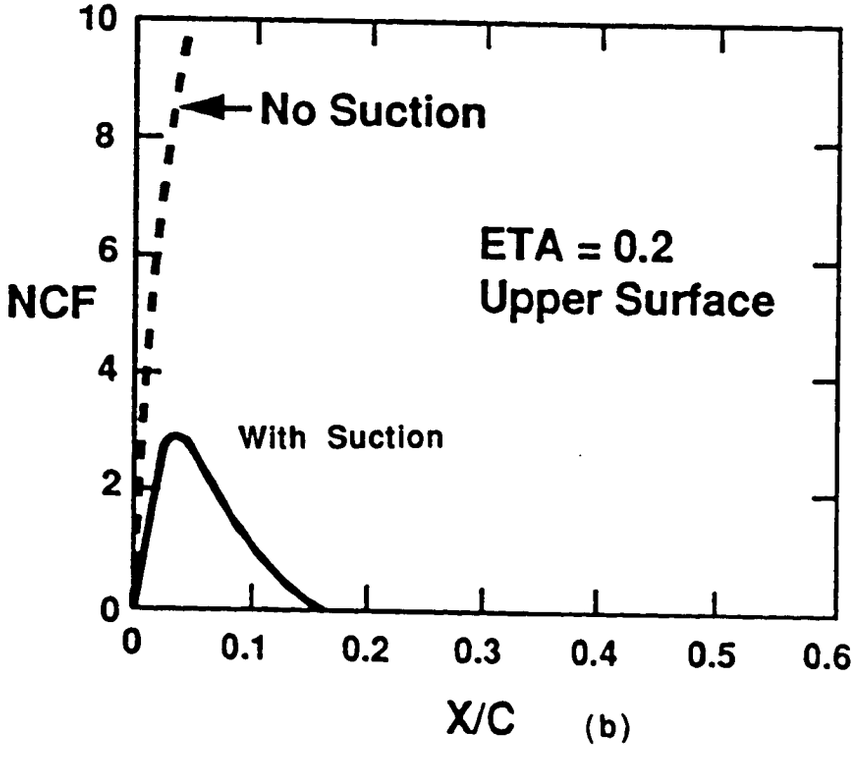

Figure 2.7.7-24 N_{TS} and N_{CF} Growths for Inboard Wing Upper Surface

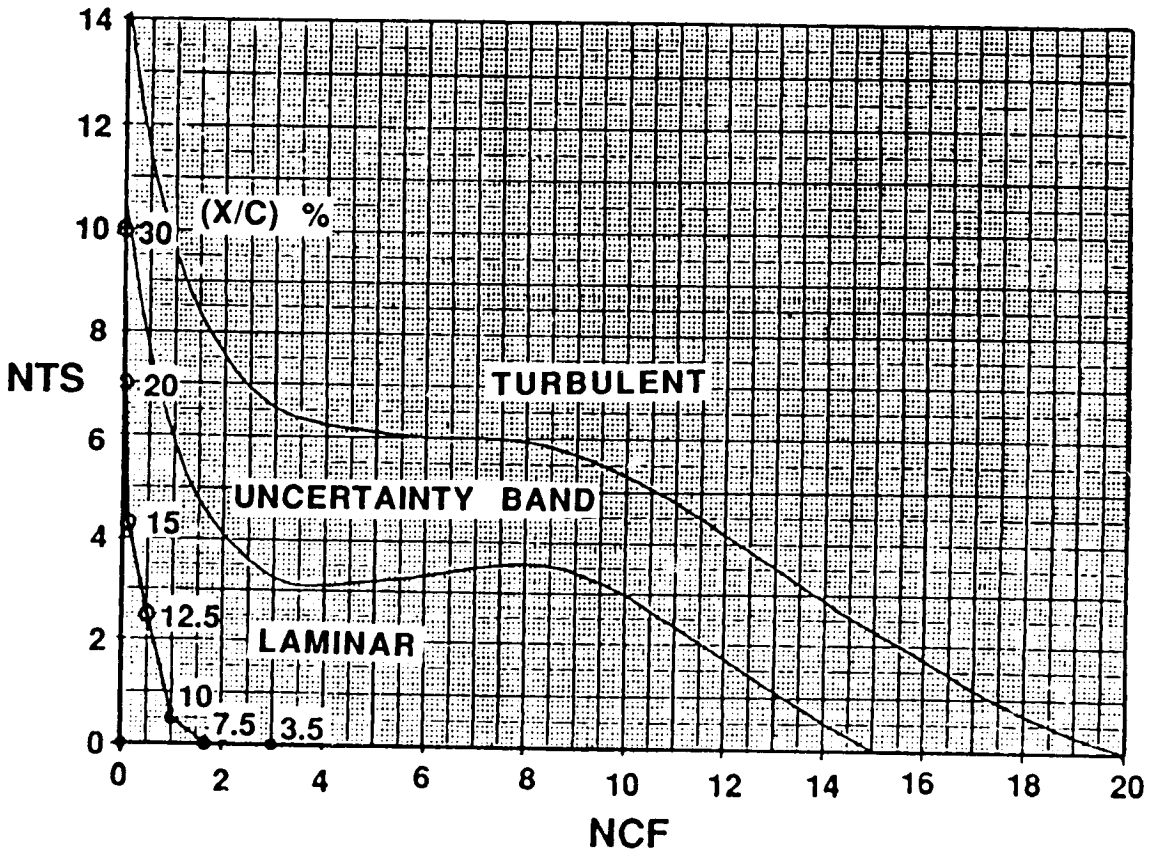

Figure 2.7.7-25 Trajectory of N_{TS} vs N_{CF} for Inboard Wing Upper Surface With Suction

The trajectory of N_{TS} versus N_{CF} for the inboard wing with suction is shown in Figure 2.7.7-25. Notice in this case, that transition is eventually caused by the TS growth at about 30 percent chord. Additional weak suction would damp this TS growth and extend the laminar run. However, for the SST configuration under study, the region beyond about 30 percent chord on the inboard wing contains the landing gear bay on the lower surface with surface mismatch problems, where a laminar run would not be feasible. Also, the Cp distribution on the upper surface begins to deviate from the constant value at approximately 35 percent chord and would lead to additional crossflow instability without strong suction.

Due to schedule constraints, detailed stability calculations for the lower surface of the wing could not be carried out. In view of the similarity of the desired upper and lower surface Cp distributions as shown in Fig. 2.7.4-10, a suction scheme identical to the one employed on the upper surface was assumed. The extent of laminarization on the lower surface was assumed to be the same as that on the upper surface with this suction scheme.

2.8 LAMINARIZATION SCHEMES

Three possible wing laminarization schemes were considered as shown in Figure 2.8-1. In all three schemes, the suction regions and laminarized regions for the wing lower surface were assumed to be identical to those on the upper surface.

In Scheme 0, laminarization of both inboard and outboard wing areas was achieved up to approximately 30 percent chord by use of suction in the areas indicated. The estimates of achievable laminarization extent were based on the stability theory considerations of Section 2.7.7. The level of suction needed in the areas indicated was as shown in Figures 2.7.-14 and 2.7.7-22. It was found that while the suction mass flow rate required for the inboard wing was nearly twice that required for the outboard wing (in Scheme 0), the area laminarized on the inboard wing was only 75 percent of the area laminarized for the outboard wing. This inferior benefit/penalty ratio for the inboard wing results from two effects:

1. A strong suction level (C_Q = 0.002) is needed near the rounded leading edge of the inboard wing for the suppression of the attachment line and crossflow instabilities. This is not a problem for the sharp leading edge outboard wing, where a significant run of natural laminar flow starting at the leading edge (attachment line) is achieved.

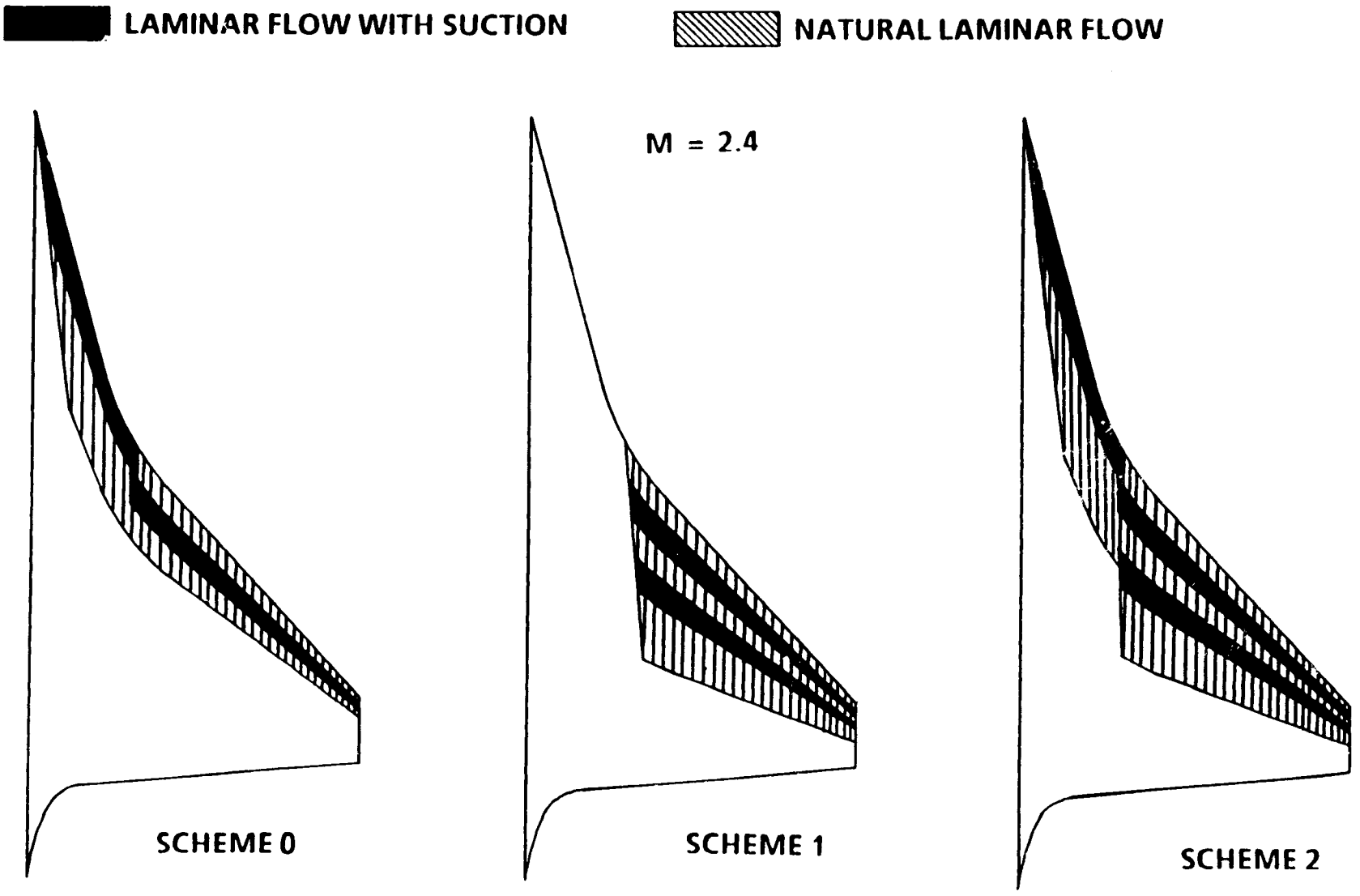

- LOWER SURFACE ASSUMED TO BE IDENTICAL TO THE UPPER SURFACE IN ALL SCHEMES.

Figure 2.8-1 Laminarization Schemes

2. Because of the high leading edge sweep angle (75°), approximately half of the inboard wing area is contaminated by the turbulent wedge which exists at the wing/fuselage junction. Much larger quantities of suction would be required to eliminate the turbulent wedge by relaminarization of the turbulent boundary layer on the fuselage and the junction region.

In light of the above considerations, it appeared more "cost effective" to extend the laminar run on the outboard wing up to 60 percent chord by the addition of a second suction region between 30 and 40 percent chord, while not attempting to laminarize the inboard wing at all as shown in Scheme 1 of Figure 2.8-1. The total suction requirement of Scheme 1 was 25 percent less than that of Scheme 0, while the laminarized area was 15 percent greater. No laminarization was attempted beyond 60 percent chord in Scheme 1 because of the presence of spoilers, trailing edge flaps, etc., in the aft portion of the wing upper surface and engine installation on the lower surface.

In Scheme 2, laminarization of the inboard wing was added to that of Scheme 1. Scheme 2 thus represented about the maximum wing area that could be laminarized for the modified pressure distribution (see Figures 2.7.4-10(a) and (b)) and reasonable suction rates, and in light of practical considerations.

In the present study, net benefits of LFC implementation were evaluated for Schemes 1 and 2 only. Scheme 0 was not evaluated any further.

2.9 INTEGRATION OF LFC WITH HIGH LIFT SYSTEM

One of the most challenging tasks in the application of laminar flow control to supersonic transport configurations will be its integration with the leading edge high lift devices. High lift requirements on the baseline airplane dictate the use of a variable geometry (droop nose) on both the inboard and outboard parts of the wing. This poses two difficulties in achieving cruise laminarization:

1. Suction surfaces may occupy some of the areas of the moveable flaps, thereby requiring accommodation of the collector ducts within the flaps and flexible connections to the ducts in the fixed part of the structure. This is difficult to accomplish in the very thin leading edge on the outboard part of the wing.

2. Very close manufacturing tolerances are required to avoid tripping of the laminar boundary layer by steps caused by surface mismatch between fixed and moveable parts of a flexible structure.

For the outboard wing a design concept was proposed for the integration of the high lift system with the laminar flow suction system, which offers potential solutions to these difficulties. In this concept, no suction is applied on the surfaces of the outboard wing flaps having a sharp leading edge. However, the flap was shortened from the existing 6 feet (approx.) streamwise width across the entire span to approximately 10 percent of the local streamwise chord. Previous stability calculations indicated that it would be possible to maintain natural laminar flow over this streamwise distance without suction. In the cruise configuration, suction is applied immediately downstream of the retracted flap which should improve the step height tolerance of the laminar boundary layer at the flap/fixed structure joint. In the high lift configuration, the sharp leading edge flap segment is drooped in the same manner as the original configuration. However, instead of seeking vortex control on the leading edge flap as in the original configuration, a fully attached flow on the flap upper surface and over the flap hingeline will be maintained by use of suction. This boundary layer control (BLC) technique should allow the use of shorter flap widths employed in this design concept and perhaps even improve the high lift L/D performance.

For the inboard part of the wing, two favorable factors exist, which may eliminate the need for a variable geometry (droop) leading edge. First, the leading edge is rounded which allows for maintaining attached flow at high angles of incidence if adequate suction is applied at the surface and second, ample suction power is already available in the leading edge region for suppression of attachment line and crossflow instabilities for cruise laminarization. The elimination of the variable geometry at the inboard wing leading edge also eliminates surface mismatch problems.

The suction requirements for BLC in terms of mass flow rates and compressor power could not be established within the resource allocation of the current contract. The high lift suction requirements and compatibility with cruise LFC suction requirements should be explored in future studies.

3.0 STRUCTURAL AND SYSTEMS CONCEPT DEVELOPMENT

3.1 SCOPE

The aerodynamic analysis of Chapter 2 established the suction regions and mass flow rate requirements to achieve partial laminarization of the inboard and outboard portions of the wing. The objective of Task 2 of the study (see Section 1.2) was to develop structural and systems concepts to achieve the desired level of suction in the specified regions and to accomodate the various components of the suction system on the SST configuration with minimal penalties. The penalties associated with the suction system installation are: system weight, fuel volume displacement and power required to drive the suction compressors. Various methods of locating and powering the suction compressors were considered with a view to minimizing these penalties. Structural concepts for possible use of the LFC suction system for low speed boundary layer control (BLC) were developed for high lift system integration.

The configuration chosen for the structural and systems concept development studies was again model 733-633 [36], i.e. the same as that used for the aerodynamic analyses. The benefits and penalties associated with the implementation of the two laminarization schemes considered in Sec. 2.8 were evaluated for this configuration. The results were later scaled on the basis of the wing reference area for the updated turbulent baseline configuration, Model 1080-834 [44]. The reasons for this approach were:

i) The geometry definition and structural and systems arrangements of Model 733-633 were reasonably well documented and available at the beginning of the present study.

ii) The updated, all composite, turbulent version, Model 1080-834 was not available at the beginning of the present study, but later become available.

3.2 REQUIREMENTS

3.2.1 Definition of Laminarized Regions

Figure 3.2.1-1 defines the LFC suction regions with reference to the Boeing Model 733-633 supersonic transport (SST) configuration. The 733-633 cruise speed is Mach 2.4, cruise altitude range 60,000 to 64,000 ft and maximum taxi weight 750,000 lbs. Fuel tanks of 8,000 cu.ft. capacity are in the wings. Propulsion is provided by 4 wing mounted turbojet engines. Wing planform is double delta, consisting of outboard supersonic leading edge wings and of inboard subsonic leading edge wings or strakes.

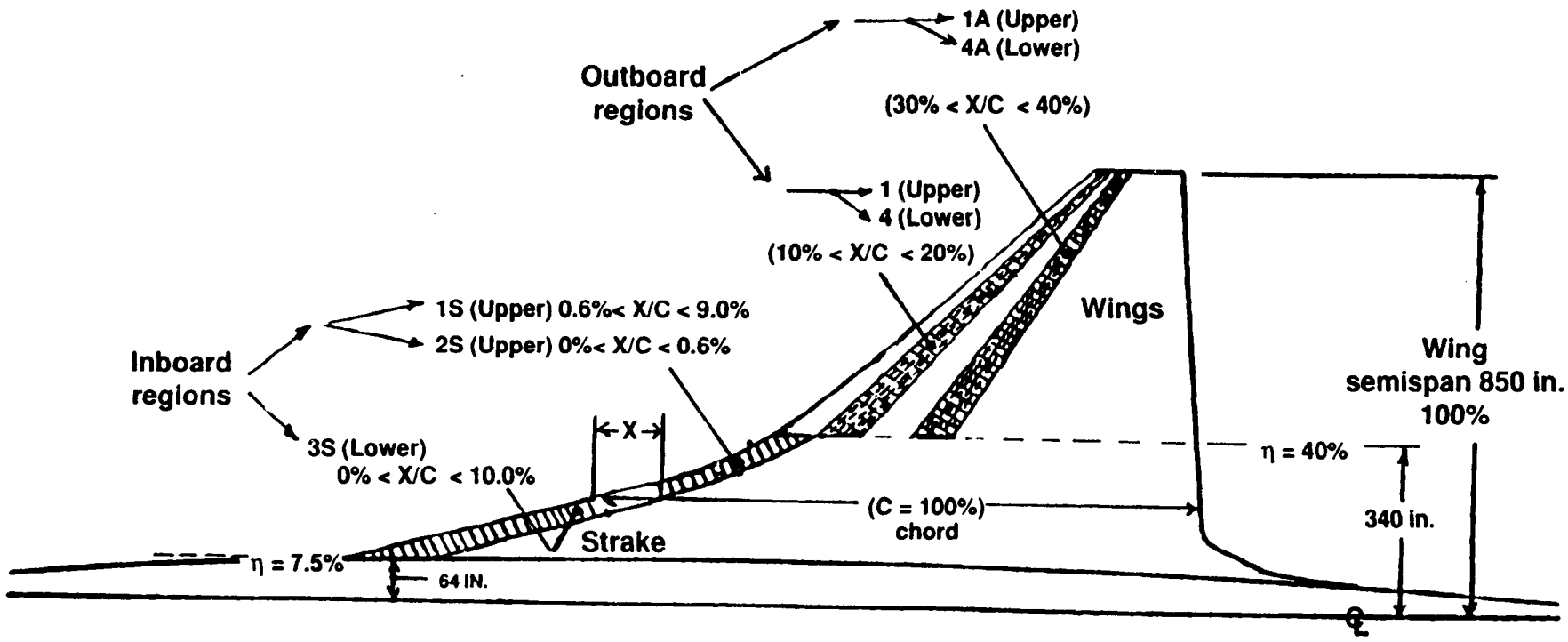

Figure 3.2.1-1 Suction Regions

In one phase of the study (laminarization Scheme 1) only the outboard, regions of the wings were to be laminarized. In the following phase of the study (laminarization Scheme 2) laminarization of the combined inboard and outboard regions of the wings was evaluated.

3.2.2 Performance Requirements

Air mass flow, pressure coefficient (Cp), air plenum pressure, compressor inlet pressure and temperature were specified for the purpose of benefit evaluation studies based on Mach 2.4 at a 60,000 ft minimum cruise altitude. The requirements for laminarizing the outboard wing regions are in the upper section of Table 3.2.2-1, the inboard wing regions in the middle section and the combination of inboard/outboard wing regions are in the lowest section.

TABLE 3.2.2-1 - SUCTION SYSTEM REQUIREMENTS

Region	Wing Location	Flow Lb/sec	Cp PSF	Plenum PSF	Compr. In PSF	Temp. Deg. F
1	Outboard, upper	0.677	-0.02	139	89	212
1A Scheme 1	Outboard,lower	0.677	-0.07	110	60	212
4	Outboard,lower	0.677	+0.10	212	162	212
4A	Outboard,lower	0.677	+0.05	180	130	212
1S	Inboard,upper	0.30	-0.13	72	30	212
2S	Inboard	0.57	-0.09	96	56	212
3S	Inboard,lower	1.52	+0.03	169	129	212
1S	Inboard	0.30			30	212
2S+1A	Combined	1.247			56	212
3S+4A	Combined	2.197			129	212
Scheme 2						
1	Outboard	0.677			89	212
4	Outboard	0.677			162	212

The compressor outlet pressure at cruise conditions was not specified but was selected as 275 PSF in a trade study, that is described in Section 4.5.2 of this report.

3.2.3 Installation Requirements

Equipment must be as tightly packaged as possible on supersonic transports to minimize wave drag. Thinness of the wings is the main challenge to the installation of a laminar flow control system. Wing thickness to chord ratio decreases from 4.1 percent inboard to 2.0 percent outboard. See Figure 3.2.3-1.

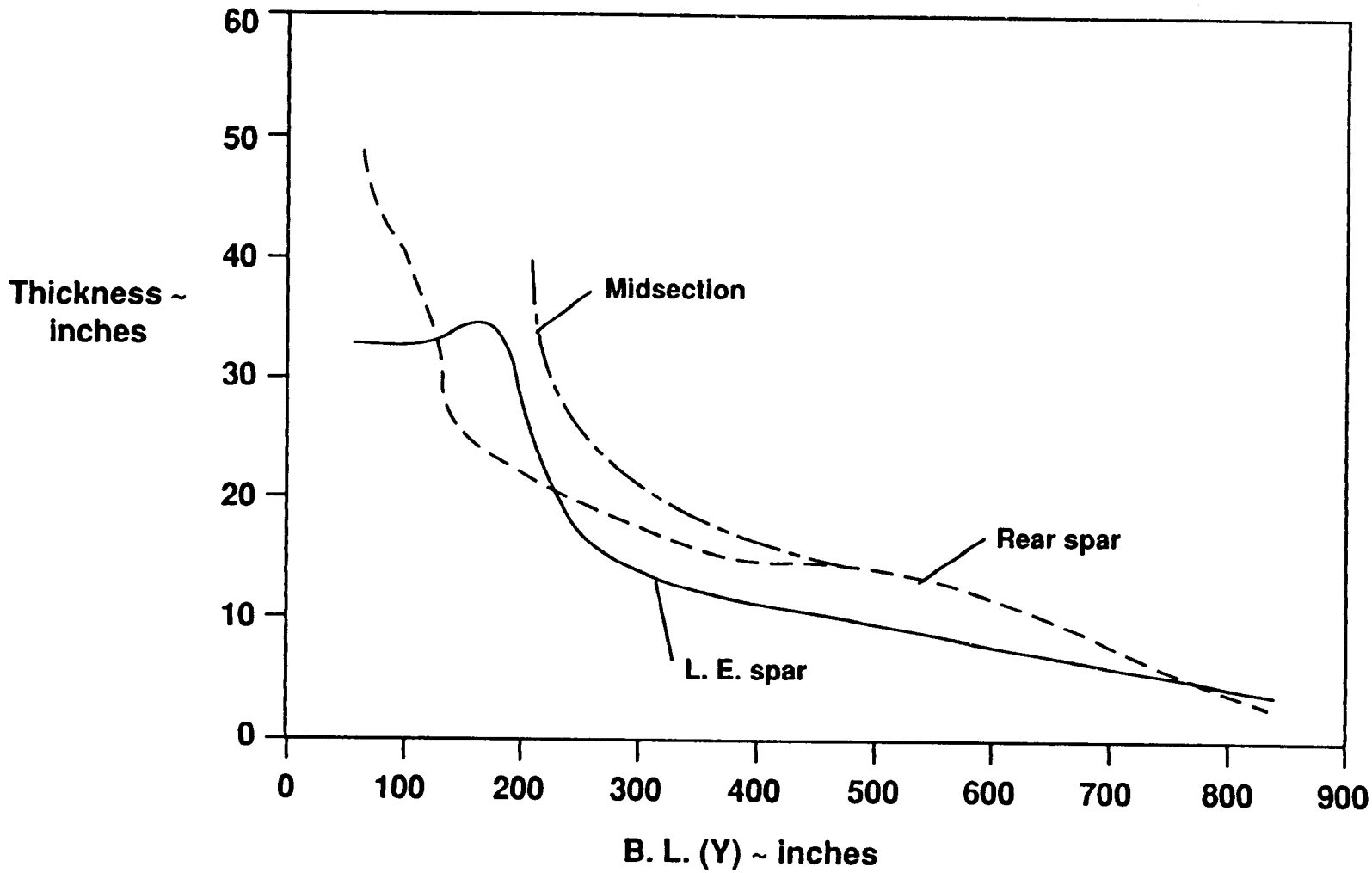

Figure 3.2.3-1 Spar Depth Vs. Spanwise Location - Model 733-633 Wing

3.2.4 Integration of Laminar Flow Control with High Lift Devices

The aerodynamic concept proposed in this study for integration of the laminar flow control system with the high lift system was described in section 2.9 of this report. However the systems concept and suction requirements for only cruise LFC were developed in the present study. The corresponding requirements for the boundry layer control (BLC) high lift system concept were not developed in the present study. Therefore, the compatibility of the two suction system requirements could not be established in the present study. System requirements for the high lift BLC concept and its compatibility with the cruise LFC suction system should be evaluated in a future study.

The BLC/high lift concept requires replacing the moveable leading edge vortex lift augmentation surfaces (slats) at the inboard wing leading edge with fixed structure. It appears possible to remove the slats, because the suction system used in a boundary control (BLC) mode could provide acceptable L/D takeoff performance for noise attenuation. The reliability requirements for takeoff would then have to be consistent with high lift devices. This issue requires further aerodynamic research. Redundant air compressors may be required for flight safety during the use of the suction system for boundary layer control near the ground.

3.3 STRUCTURAL CONCEPT DEVELOPMENT

Figure 3.3-1 illustrates the structural concept of the laminar flow wing.

3.3.1 Perforated Skins

The skins, throughout the seven suction regions, though perforated, perform the normal structural functions of wing skin; namely to carry in-plane spanwise & chordwise direct loads and shear loads in conjunction with skin stiffenening elements.

The skin is 6AL-4V titanium material. Perforation is accomplished by either the electron beam or the laser beam process.

The function of fuel containment normally performed by the wing skins is accomplished in the suction regions by the stiffenining elements and the ducting.

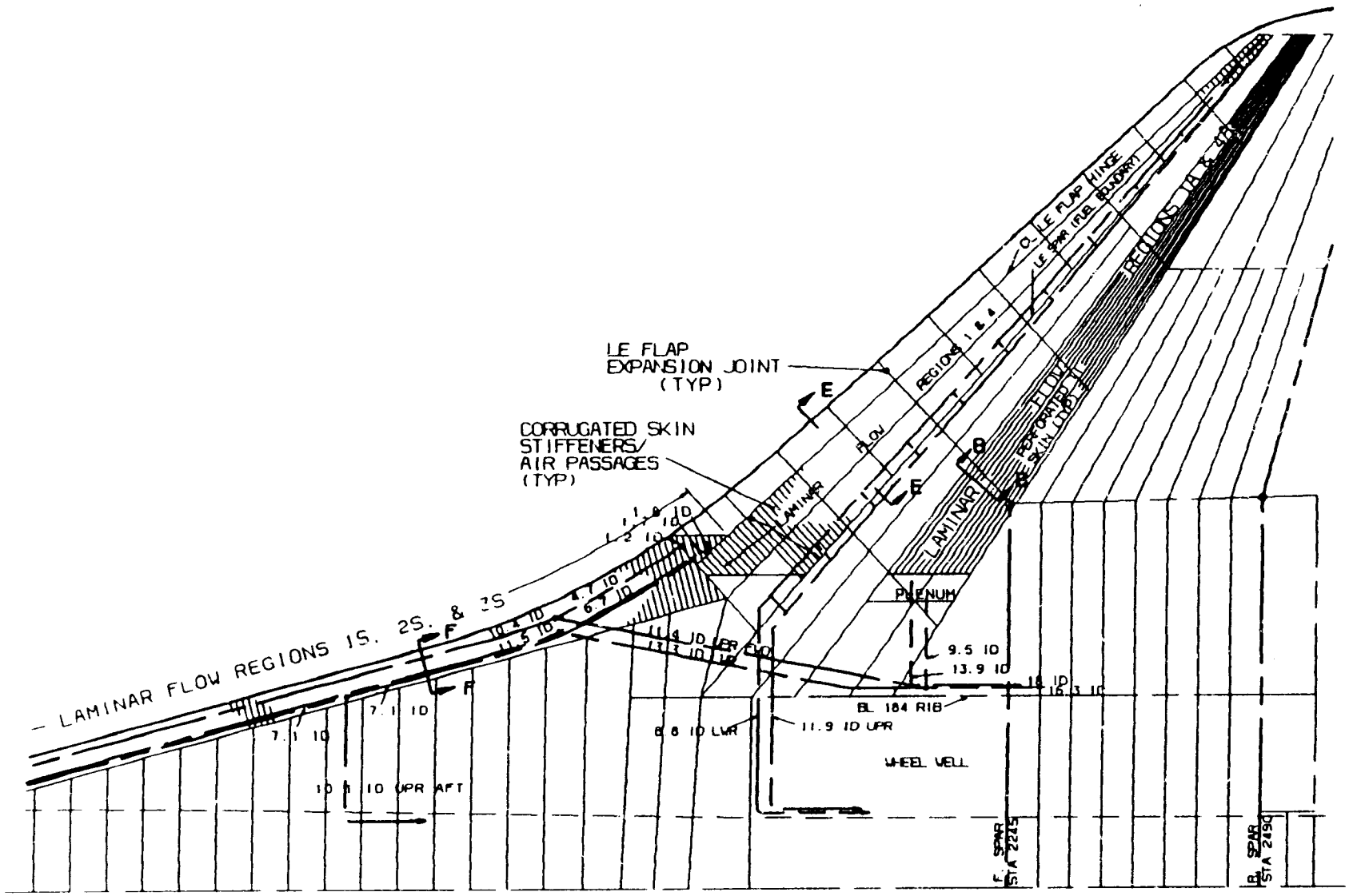

Figure 3.3-1 HLFC Structural Concept

3.3.2 Structural Arrangement

Corrugated titanium skin stiffening elements are situated to provide air movement along primary load paths: spanwise in the wing box and chordwise in the leading edge. The corrugations bonded to the skins also serve to stiffen the upper and lower skins in compression and shear.

a) Regions 1A and 4A. Suction air is carried by semicircular lobes attached to the corrugated skin stiffeners, Figure 3.3.2-1. The lobes are constructed of graphite composite with walls sized to carry external fuel pressure. The lobe diameter is the minimum practical at the outboard end and is gradually increased inboard to accommodate the increased air flow required.

   In this portion of the wing box the allowable compression and shear stresses are estimated to be lower than that aft of this region which is constructed of honeycomb sandwich. Therefore a greater than normal share of wing bending & torsion may be carried by the honeycomb sandwich portion of the wing box.

b) Regions 1 & 4. Regions 1 & 4 extend from the leading edge flap hinge line aft to the 20 percent wing chord line, Figure 3.3.2-2. Suction air is carried by corrugated skin stiffeners, plenums, feeder ducts and main ducts. One plenum approximately 66 inches long and its feeder duct supplies the main duct between each pair of ribs. Again the main duct is tapered to provide for increasing air volume inboard.

   The fuel boundary is at the spar approximately 69 inches aft of the flap hinge line at the spanwise location of section E-E, Figure 3.3.2-2.

c) Leading Edge Flap Hinge. Figure 3.3.2-3 illustrates the concept for suction at the leading edge in the vicinity of the flap hinge. A thin titanium perforated blade seal attached to the flap provides suction on the exposed upper surface during flap extension through the Region 1 upper surface ducting system. The blade seal is flexible to assure a positive seal against the upper surface of the fixed leading edge during flap extension.

d) Regions 1S, 2S, & 3S. Figure 3.3.2-4 show regions 1S, 2S, & 3S extending to 9% chord line on the upper surface and 10% chord lines on the lower surface.

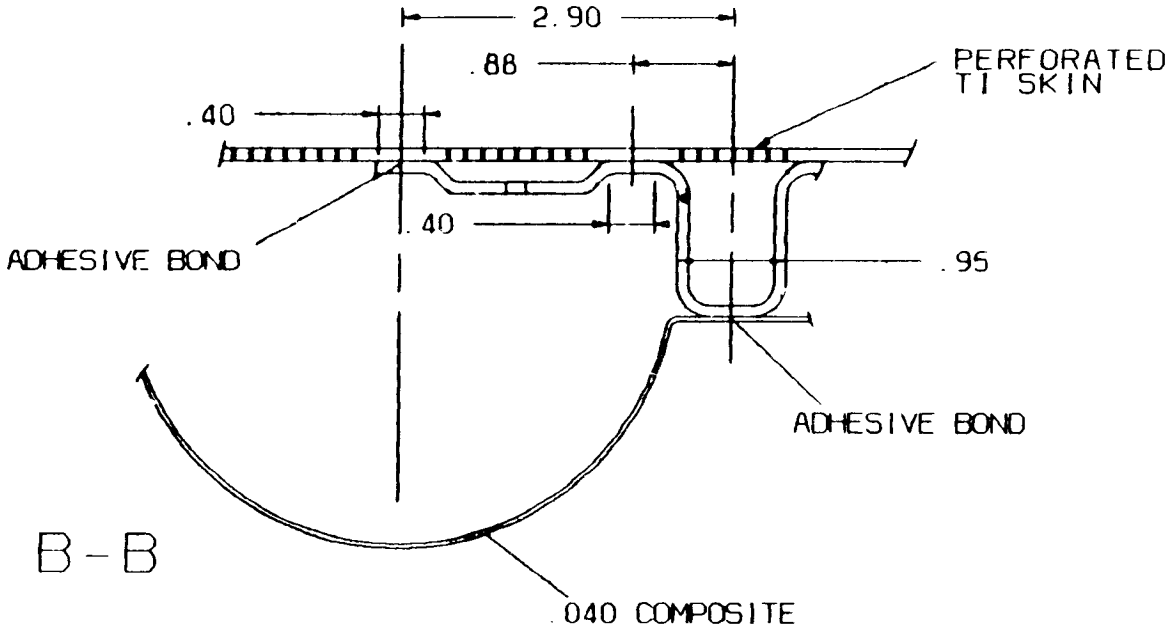

Figure 3.3.2-1 Concept for Structural Integration of Suction Ducting

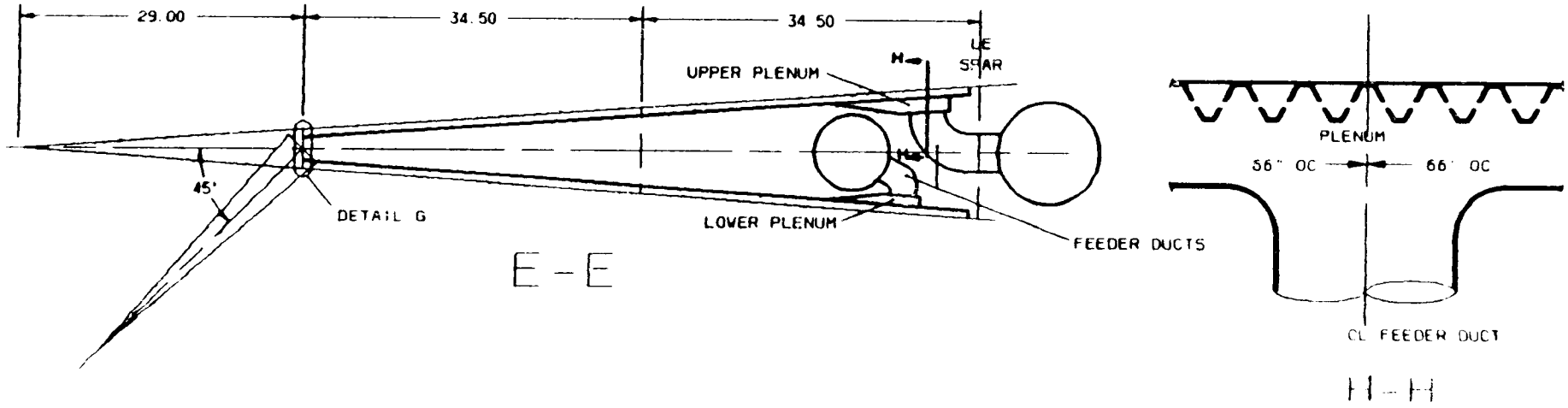

Figure 3.3.2-2 Structural Concept for Outboard Wing Region Aft of the Hingeline

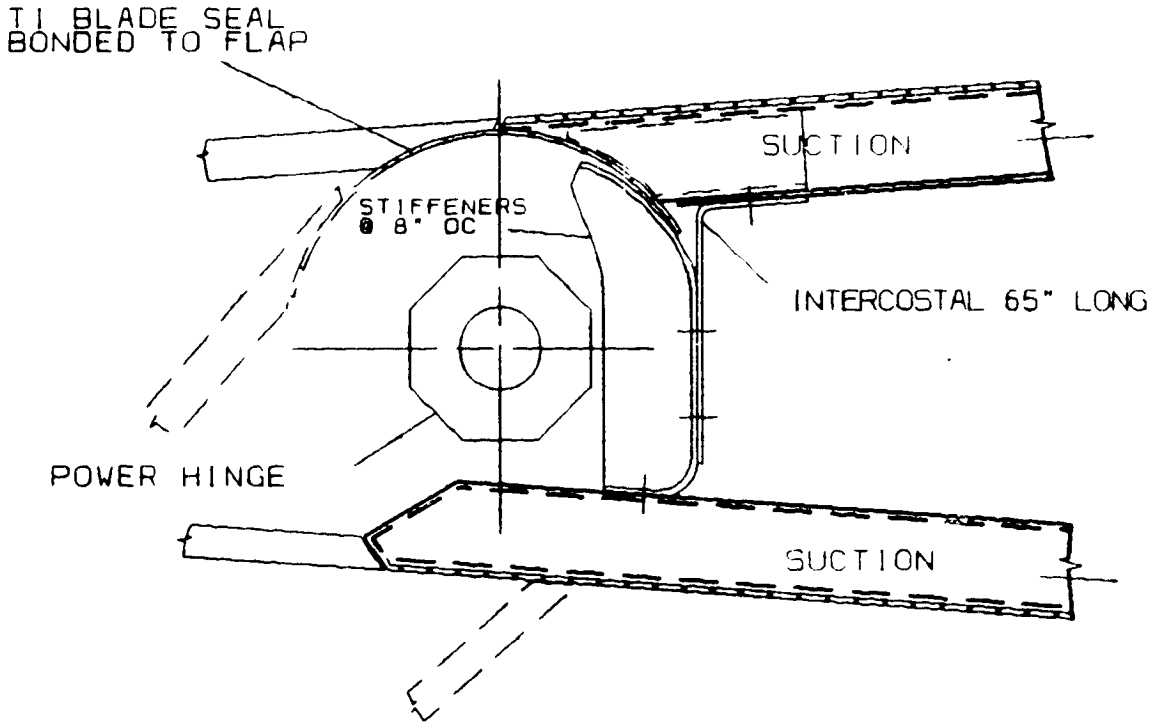

DETAIL G

Figure 3.3.2-3 Detail of Suction Region Aft of Leading Edge Flap Hingeline

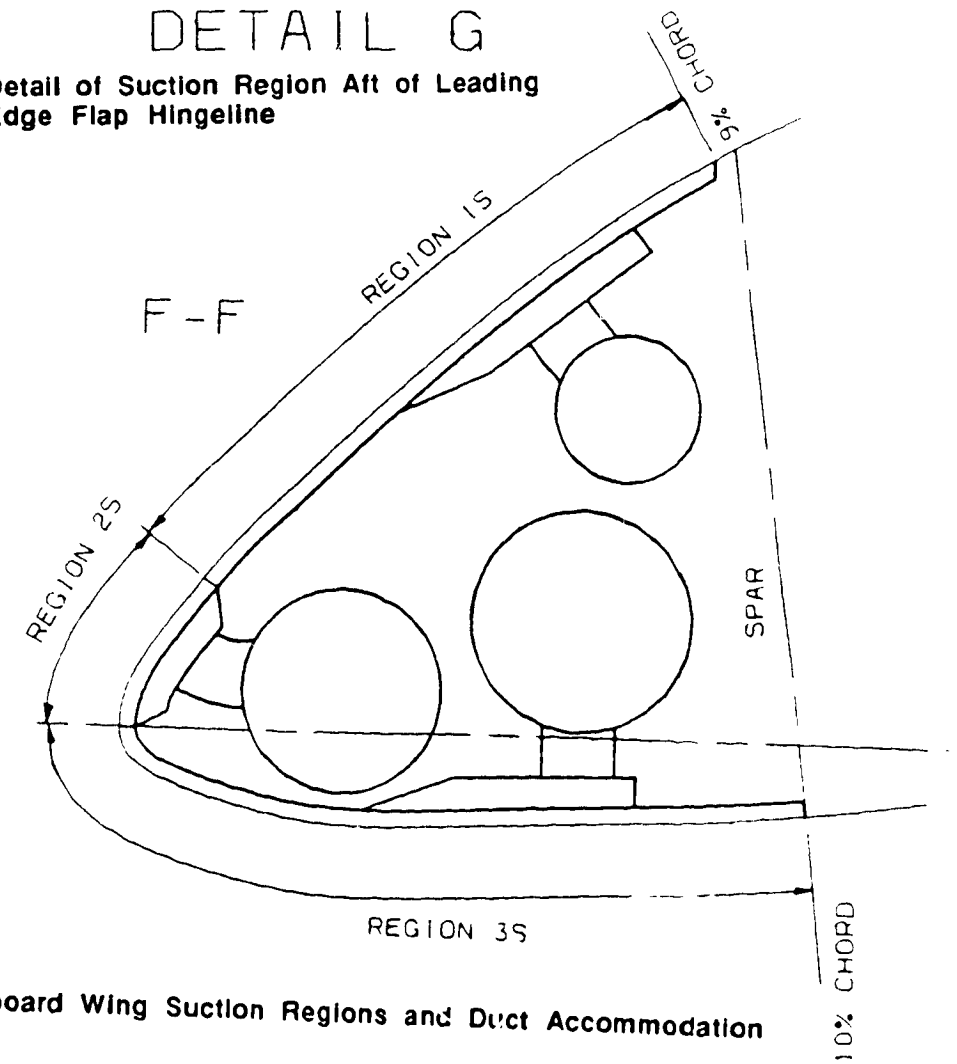

Figure 3.3.2-4 Inboard Wing Suction Regions and Duct Accommodation

The structural concept and arrangement of these regions is similar to that of Regions 1 & 4 except there are two upper surface regions which call for another set of plenums, feeder ducts & main duct. The diameters of the main ducts must be held to smaller sizes in order to accommodate them at the aft end where the airfoil is comparatively thin.

e) Duct Routing. Figure 3.3-1 illustrates a feasible routing of ducts from the suction regions to the compressors in the inboard wing. Alternate approaches must be examined to assure minimum duct weight and minimum fuel displacement.

3.4 SYSTEMS CONCEPT DEVELOPMENT

3.4.1 Suction System Arrangement

Two alternate suction system arrangements were considered:

a) local installation of air compressor/motor units
b) central air compressor plant installations

Local compressor units, complete with electric motors, were attractive because of the relatively small volume of fuel displaced by exhaust air ducts compared to the low pressure suction ducts. The wing thickness however was found to be inadequate for the compressor/drive units near the thin outboard wing leading edges.

The trailing edge of the inboard wings just aft of the rear spar was investigated as a location for a central compressor plant installations. The depth aft of the rear spar of the wing and inboard of the engines was too thin for the required large air compressors, and adequate space was not available for equipment installation. Adequate space could not be found in the narrow body either. Displacing fuel from the fuel tanks could not be avoided.

Accessibility from the ground up was required for maintainability. Three alternate compressor plant locations meeting this requirement were evaluated on the basis of equipment weight and fuel displacement:

a) Electric driven compressors next to the wheel wells Figure 3.4.1-1
b) Mechanical driven compressors ahead of the rear spar outboard of the inboard engine, Figure 3.4.1-2
c) Mechanical driven compressors ahead of the rear spar inboard of the inboard engine, Figure 3.4.1-3

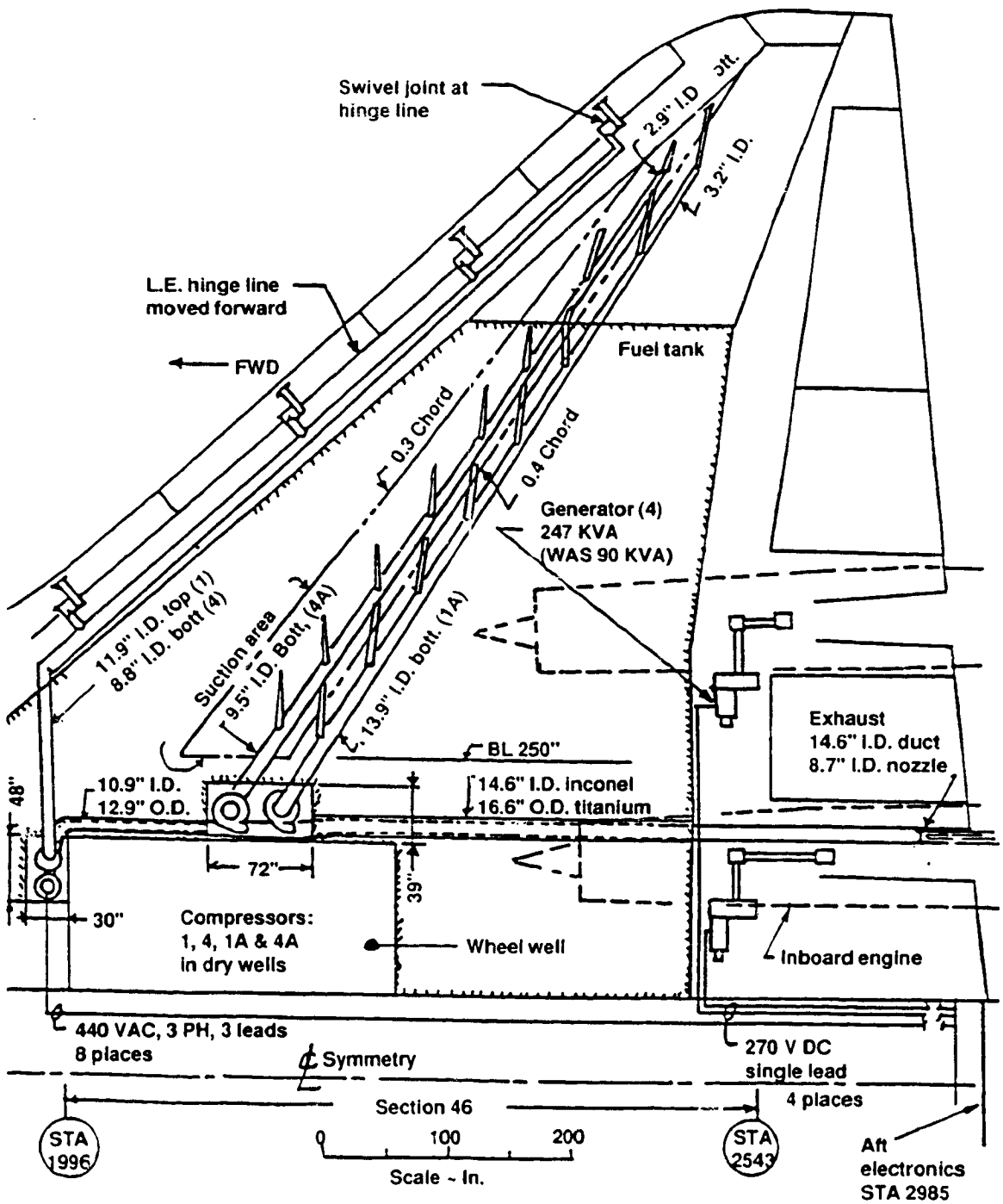

Figure 3.4.1-1 Outboard Wing HLFC (Scheme 1) Electrical Compressor Drive

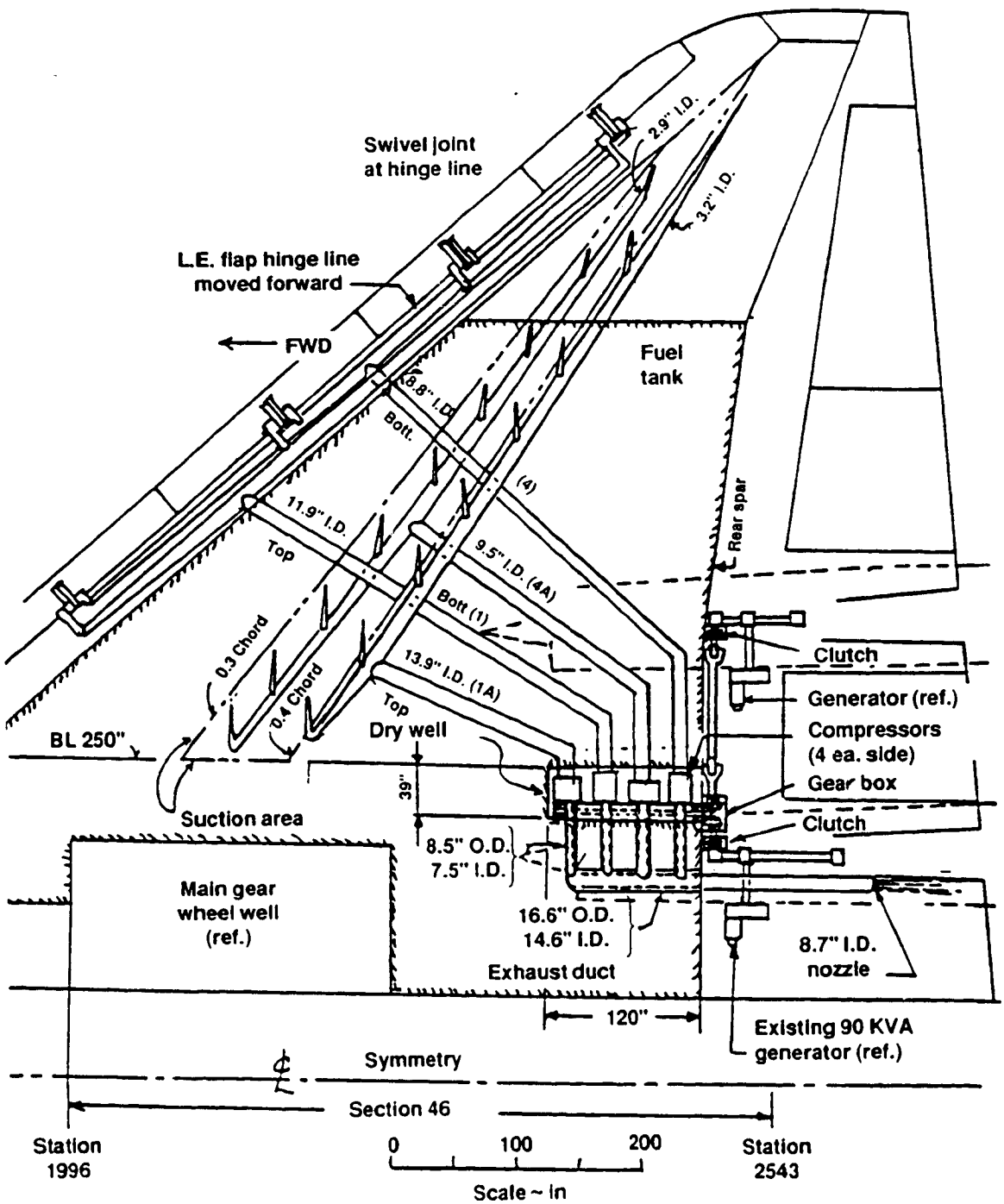

Figure 3.4.1-2 Outboard Wing HLFC (Scheme 1) Mechanical Compressor Drive

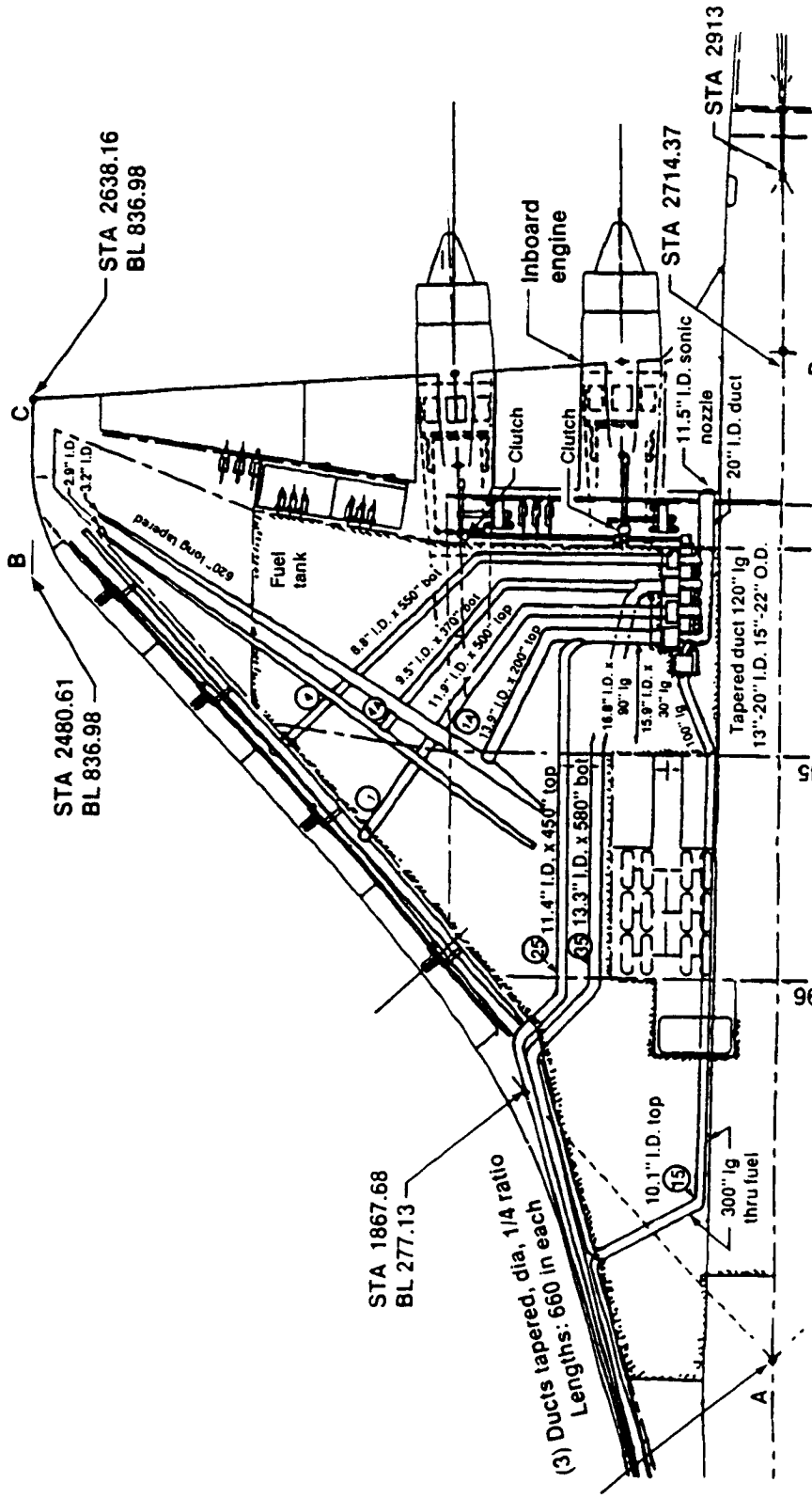

Figure 3.4.1-3 Combined Inboard and Outboard HLFC (Scheme 2) Mechanical Compressor Drive

The rear spar installation outboard of the inboard engine was preferred because of the minimum required equipment weight.

3.4.2 Compressor Drive Power Transmission

The alternatives for engine power transmission were to use:

a) Pneumatic
b) Hydraulic
c) Electric
d) Mechanical

a) The advantages of compressed air (pneumatic) power transmission were compatibility with high speed air compressors, flexibility of installation and ease of control. The disadvantage was the increased specific fuel consumption because of an estimated 45% overall power transmission efficiency. Bleed air was not pursued further in the present study. Bleed air should be reconsidered as a standby power candidate for redundant compressors, if needed.

b) Hydraulic power transmission was briefly considered because it is more efficient (61%), than pneumatic power transmission and lighter weight than electric power transmission, but was rejected because hydraulic motors were found to be too slow for direct drive of the high speed air compressors.

c) Electrical power transmission was evaluated in more detail. See Figure 3.4.1-1 showing a possible electric power driven compressor system. The advantages of electric power were flexibility of installation and speed control, plus high power transmission efficiency (73%) compared to pneumatic and hydraulic power transmission systems. The disadvantage was the weight of the electric power generators, frequency controllers, power cables, motors and electric equipment cooling provisions.

d) Mechanical power transmission was selected in the study because of high mechanical efficiency (95%) and comparatively low combined weight of the equipment. Refer back to Figures 3.4.1-2 and 3.4.1-3 for the mechanical driven compressor system arrangements envisioned.

Mechanical power was provided from either the inboard or the outboard engine, for redundancy. Clutches were provided for unloading each engine during start, and for suction system startup and shutdown. The compressors were located in a dry bay at a minimum distance from the engines.

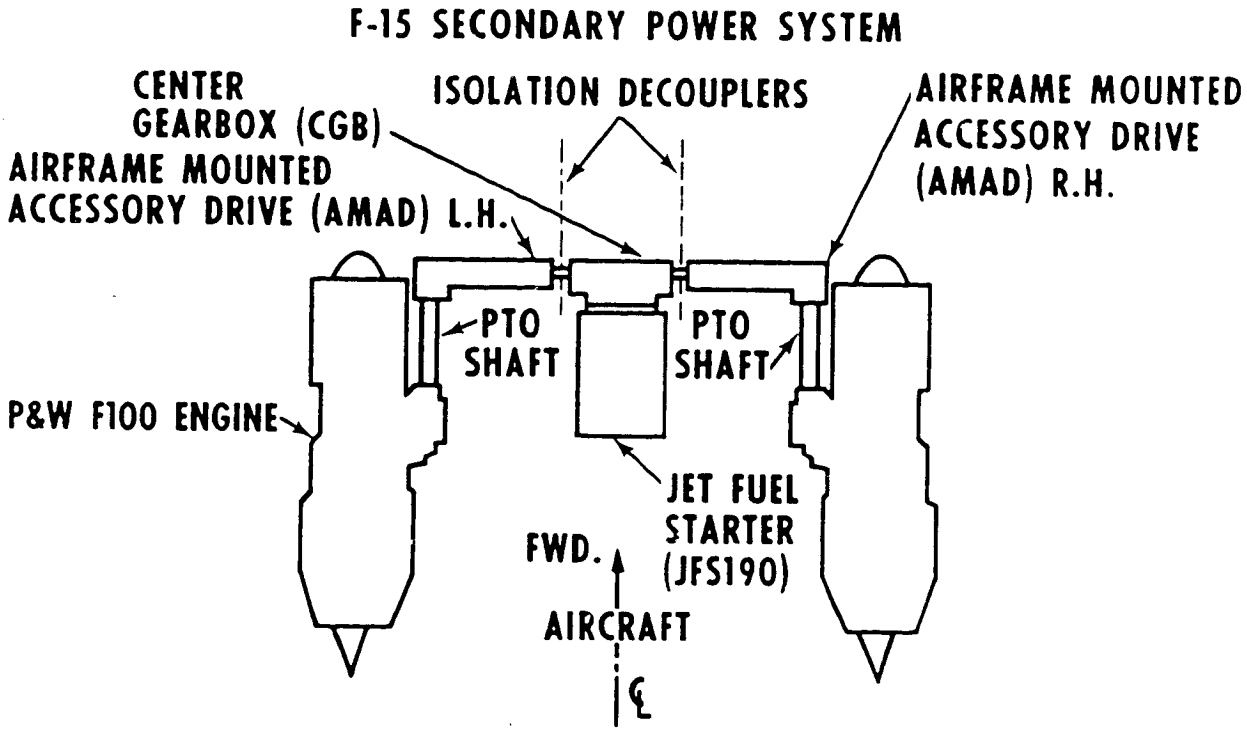

Figure 3.4.2-1 Engine Shaft Pwer Extraction Scheme for F-15

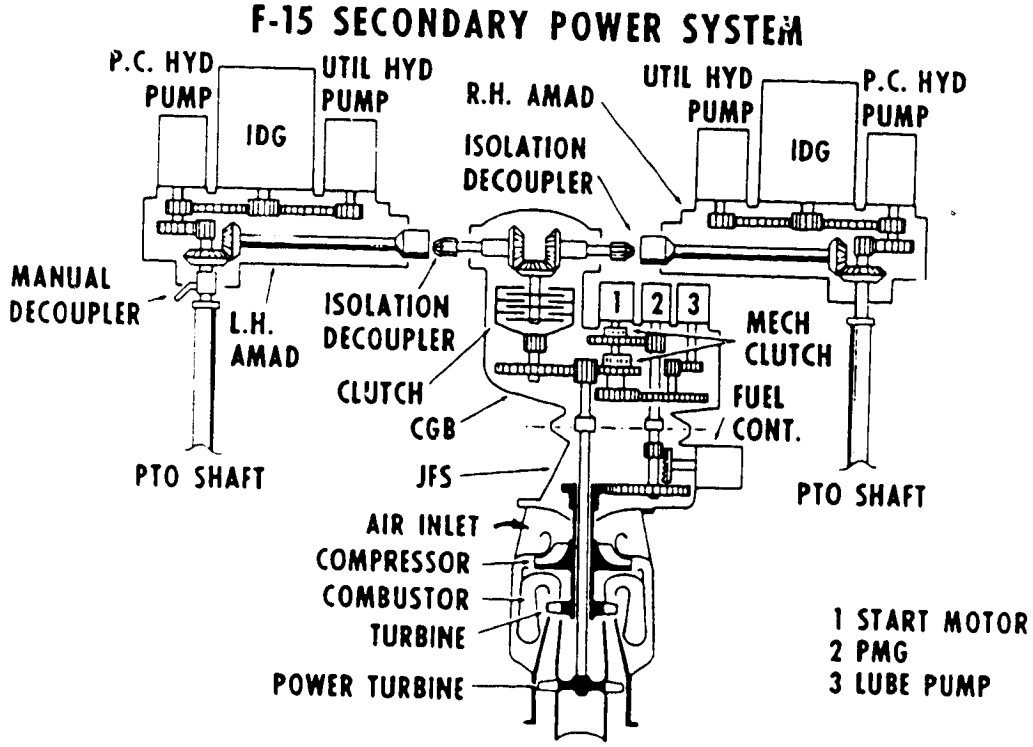

Figure 3.4.2-2 Schematic Diagram of Airframe Mounted Accessory Drive and Jet Fuel Starter for F-15

Power transmission in excess of a few feet had to include universal joints to accommodate wing deflections.

The operating speed of engine power takeoffs, right angle gearing and clutches was set approximately at 12,000 RPM. The compressors were located in a dry bay at a minimum distance from the engines depending on availability space and access. A compressor speed of 30,000 RPM was selected in the study based on inputs from manufacturers and requirement of extended service life for the gear drive. The speed increaser gear box driving the compressors was located inboard of the compressors.

The accessory gear drive arrangement required was similar to that found on military aircraft, i.e., the F-15 and the B-1. See Figures 3.4.2-1 and -2 illustrating the coupling of an AiResearch high speed jet fuel starter (JFS190) to either of two P&W F100 turbojet engine power takeoffs by an airframe mounted accessory drive (AMAD) on the F-15. The peak power of the JFS190 was 166 horsepower. The power levels required for laminar flow control suction were in the 1000 horsepower range that was above the F-15 AMAD but below those of helicopter drives.

The achievement of reliability and maintainability levels comparable to subsonic commercial aircraft at the high power levels required for laminar flow control suction is feasible, but will require a very substantial effort.

3.4.3 Compressor Characteristics

The compressors had to fit in the wings. The maximum allowable compressor envelope diameter was determined from the wing thickness in Figure 3.2.7-1 and from the 30-inch rib spacing of the Model 733-633, whichever was less. The envelope diameter was assumed to be 1.6 times larger than the impeller diameter to provide room for the debris containment shield.

An assortment of compressor data was obtained through courtesy of Garrett AiReserch, and Sundstrand Pneumatic Systems, in response to Boeing requests for suggestions during the course of the present study before the requirements were finalized, see Appendix III.

The required compressor characteristics were predicted by Boeing based on the manufacturers data and on a standard reference. The total compressor shaft power requirements were 626 horsepower (HP) for the outboard wing regions (scheme 1) and 1219 HP for the combined outboard/inboard wing regions (scheme 2). The efficiency predictions were evaluated with regard to fluid viscosity and compressibility effects. The impeller tip Reynolds numbers were all less than one million for fully developed turbulent flow.

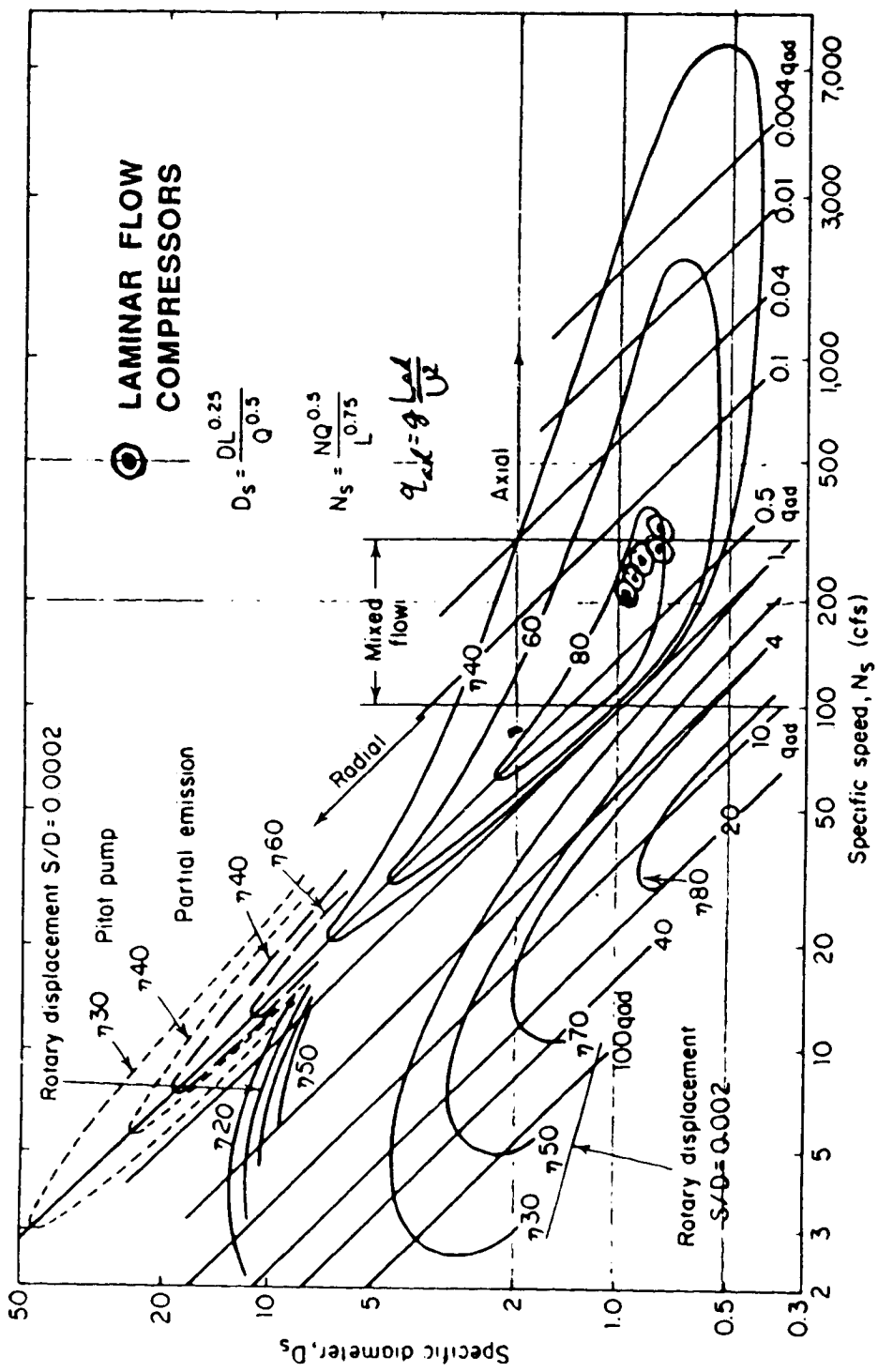

Figure 3.4.3-1 Turbocompressor Performance

because of the low inlet air densities at cruise altitude. The impeller tip speeds of the compressors meeting the installation constraints were found to be in the low supersonic range.

Figure 3.4.3-1 illustrates the fit of the predicted compressor characteristics at the high efficiency ridge of the turbocompressor performance chart.

It was concluded from the analysis of compressor requirements that:

a) Fitting the compressors in the allotted space was feasible at the selected 30,000 RPM speed using supersonic impeller tip speeds.

b) Compressor pressure ratio was the most critical design requirement. A compressor pressure ratio of 9 to 1 appeared to be feasible with acceptable efficiency. A pressure ratio of 5 to 1 was preferred for design simplicity.

c) Achieving the predicted compressor efficiencies will require time and effort because of the supersonic tip speeds and because of the relatively low Reynolds numbers at cruise altitude.

d) Achieving operational reliability comparable to commercial aircraft will require a sustained product improvement program over a period of years.

Possible use of the laminar flow compressors for low speed BLC at sea level where the air is ten times denser than at the airplane cruise altitude, presents unique design problems that need to be addressed in future studies.

3.4.4 Equipment Cooling Requirements

High powered machinery that runs continuously requires active cooling on supersonic transport airplanes. The cooling requirements for the various types of equipment were estimated as follows:

a) Air compressors were cooled by the inlet air.
b) Gear boxes were cooled by lubrication oil circulation at the rate of 5 percent of the power transmitted.
c) Electric motor bearings and starter windings were cooled by lubrication oil circulation at the rate of 10 percent of the output power.
d) Semiconductor devices were air cooled to prevent exceeding 250°F.

Laminar flow over the wings reduced aerodynamic heat to such an extent that more than sufficient fuel heat sink was available.

In future studies of LFC implementation on HSCTs many issues related to safety, reliability and maintainability as noted below will need to be addressed.

3.4.5 Safety

Asymmetry of the airplane in the event of failure of the laminar flow control suction system or of the leading edge flaps on one side must be sensed and symmetry restored within the time allowable for airplane safety in proximity of the ground.

Structural integrity of the wings must not be impaired by the suction system installation. The collapse strength of the air ducts and equipment bays must be consistent with the fuel tank design pressures.

Hot exhaust air ducts and other high temperature system components must be separated from the fuel to preclude ignition. Automatic fire extinguishing provisions are required.

High speed rotating equipment that is susceptible to overspeed damage requires a debris containment shield.

3.4.6 Reliability

Reliability of the laminar flow suction system is not considered to be flight safety critical. Loss of laminar flow would result in reduced cruise speed and range. A single thread system is deemed to be adequate, except for redundant power sources. Power must be provided from either the inboard or outboard engine of each wing to maintain low drag in case of engine failure during takeoff. It must be possible to shut down the suction compressors (a) to unload the engines during engine start, (b) to accomplish the transition from vortex lift to boundary layer control at liftoff and (c) to restore symmetry in the event of mechanical failure.

3.4.7 Maintainability

The LFC system hardware should be designed with a view to minimizing the additional maintenance required.

4.0 DESIGN/BENEFIT STUDIES

The objective of the design/benefit studies was to quantify the net impact of laminar flow control on the size and cost characteristics of a Mach 2.4 supersonic transport aircraft. This objective was achieved by designing and installing candidate LFC systems on a well-defined turbulent SST design, evaluating drag, weight, volume and power consumption impacts on the fixed-size airplane (fixed MTOW, wing area and engine size), and finally using these results to generate and compare the size characteristics of LFC aircraft with those of corresponding turbulent configurations for the same mission ground rules and range requirements.

4.1 STUDY APPROACH

The overall approach and scope of the Design/Benefits Studies are shown schematically in Figure 4.1-1. Since application of an LFC system involves many considerations affecting airplane structure, systems, operation and performance, it was felt that a comprehensive and traceable assessment of all factors could best be achieved by designing, installing and evaluating such a system on a well defined turbulent SST design. The benefits of LFC could then be evaluated by comparing the size and performance characteristics of the laminarized airplane with those of a baseline turbulent airplane sized to the same mission range and ground rules and in a consistent manner.

The turbulent "baseline" selected for the study was the Boeing Model 1080-834 "double-delta" configuration. This airplane is currently the subject of study in parallel High Speed Commercial Transport (HSCT) work being performed by NASA and Boeing [44], and is a geometrically similar but updated technology version of the Model 733-633 which was developed in the NASA/Boeing SCAR studies of the 1970's [36]. This design was selected, not only for its excellent performance characteristics, but also because of its detailed and well-validated geometric and technical data bases.

Three candidate laminarization schemes were examined in Section 2.8. The two most "cost-effective" of these schemes in terms of drag reduction versus suction requirements were selected for systems and structural concept development in Section 3.0. Preliminary design calculations of the suction system requirements for laminarization schemes 1 and 2 were carried out. The required components of the suction system (plenums, ducting, compressors, etc.) were installed within the existing physical envelop of the wing in order to properly assess the volume taken up by the suction system without encroaching on the areas of the configuration which were already allotted to existing systems. The resulting installations were evaluated by structures, systems, weights and propulsion disciplines to estimate incremental "uncycled" weight, volume and power extraction penalties.

The LFC system design and penalty evaluation studies were all performed on the Model 733-633 configuration having a wing of 7700 square feet

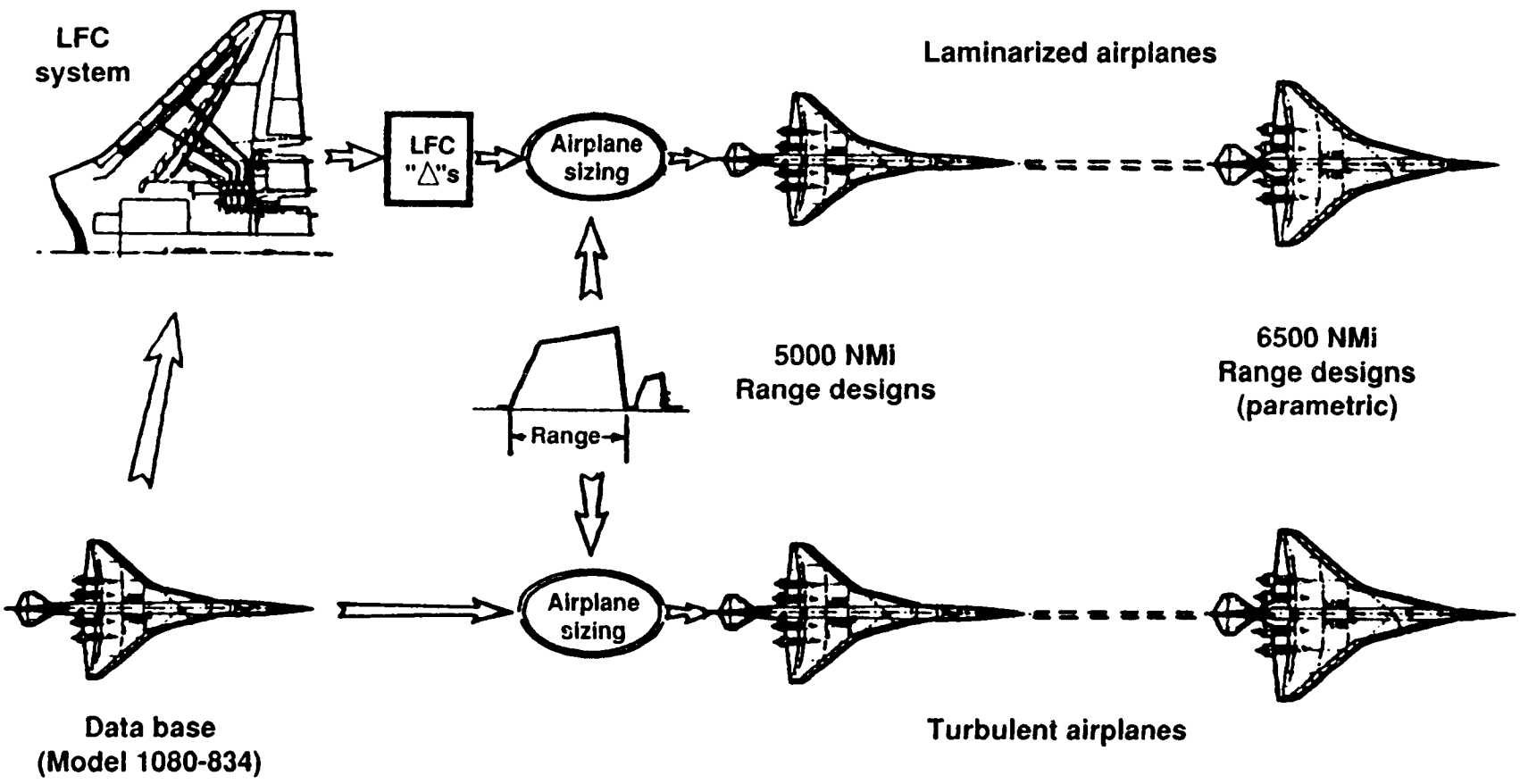

Figure 4.1-1 Design/Benefit Study Overview

reference area. Although larger than the 1080-834 wing (wing reference area of 7050 ft^2 for the point-of-departure airplane and 7466 ft^2 for the mission sized airplane), this datum was chosen because (a) final sizing of the Model 1080-834 baseline had not been completed at that point in time, and (b) a detailed geometric definition of a 7700 square feet wing already existed in the form of the Model 733-633 wing. Since the benefits of LFC can be fully assessed only by the inclusion of synergistic vehicle sizing effects, the datum wing size in any case was only a starting point. It was assumed that for wing sizes different from the datum, system weight, and power requirement penalties would vary proportionally with wing area. The volume displacement penalty was assumed to be a fixed percentage of the available fuel volume, which in turn varied as 1.5 power of the reference wing area. This was felt to be a reasonable assumption based on physical considerations and bearing in mind the relatively small anticipated variations in wing area away from the datum 7700 square feet, (at least for the 5000 nm mission) and the overall tolerance on the system penalty assessments.

Two parallel data bases were used in the airplane sizing process, (1) the unmodified turbulent airplane data base and (2) an LFC airplane data base which consisted of the turbulent data base plus incremental drag, weight, TSFC and fuel volume "scaling laws" derived from the LFC system analyses. These data bases were used to generate the size characteristics (MTOW, OEW, Block Fuel, Engine Size, Wing Area, etc.) of turbulent and LFC airplanes designed for 5000 nm range carrying 247 passengers. This mission is representative of a Los Angeles to Tokyo range requirement, with some "cushion." From previous sensitivity studies it was anticipated that for the estimated benefits and penalties of LFC implementation, the reductions in the MTOW and wing areas for the 5000 nm range would be of the order of 10 percent or less. Therefore, the geometric size characteristics of both the turbulent baseline 1080-834 and the LFC airplanes were sufficiently close to those of the "point of departure" airplane so that no balance or overall configuration problems were anticipated in the design synthesis of these airplanes.

Since the synergistic sizing benefits of LFC are a strong function of the range requirement, it was decided to examine this sensitivity by reiterating the sizing process for a design range of 6500 nm, which is representative of the U.S. East Coast to Tokyo range requirement. This time, considerably less confidence was placed in the ability to synthesize realistic airplane designs using the required size characteristics, since the predicted gross weights, wing areas and engine sizes were substantially greater (on the order of 60% to 65%) than those of the Model 1080-834 baseline. These parameters have a considerable impact on (a) the ability to balance a configuration with a body of fixed length and capacity, and (b) the validity of extrapolating weight and volume assumptions particularly for critical, gross-weight-sensitive configuration components such as the landing gear. The small-scale plan views in Figure 4.1-1 illustrate the changes in geometric shape and balanceability caused by the size differences between the 5000 nm and 6500

nm designs. The 6500 nm configurations must therefore be regarded at best as indicative of the problems of configuring a very-long-range, high gross-weight supersonic transport.

Nevertheless, in spite of these "configuration realism" concerns, it is felt that the incremental percentage differences between the 6500 nm LFC and turbulent designs are valid, at least to a first order.

4.1.1 Study Process and Data Flow

The design and evaluation of a candidate LFC system concept was divided into four major processes as shown in Figure 4.1.1-1.

The system specification process utilized the aerodynamic prediction methods and boundary layer stability analyses described in detail in Section 2.0 above to select candidate areas for laminarization and to specify distributions of suction volume flow rates and surface pressure distributions.

The system design and installation process defined the LFC suction system components required to satisfy the aerodynamic specifications within a given aerodynamic envelope. Description of systems and structural concept development is given above in Section 3.0, but briefly the process resulted in a detailed definition of porous skin and collection areas, ducting geometry, compressor power requirements, drive system, structural modifications and installation provisions.

Analysis and evaluation of the LFC system and comparison with the baseline unmodified turbulent design resulted in increments in airplane empty weight, available fuel volume, and TSFC. These increments, together with the drag savings achieved through use of the LFC system are termed "uncycled," since they apply to a given, fixed size configuration, and are not directly translatable into figures-of-merit which reflect airplane size, and ultimately, cost differences for a given design mission.

The "uncycled" increments were applied to the performance-related data bases of the baseline turbulent configuration to generate a corresponding data base for the airplane with LFC. These data bases consisted of the weight, drag and propulsion characteristics of the "as drawn" airplanes plus "scaling rules" which in essence are partial derivatives representing the variations of performance-related variables (OEW, parasite drag) with changes in configuration size characteristics (e.g. wing area, engine size) and non-geometric design variables (e.g. design MTOW). An airplane performance and sizing method was then used to generate the airplane size characteristics required to satisfy a particular mission profile and range requirement. This process also involved the variation of a number of airplane parameters to arrive at a near optimum design (minimum MTOW) subject to the set of mission constraints.

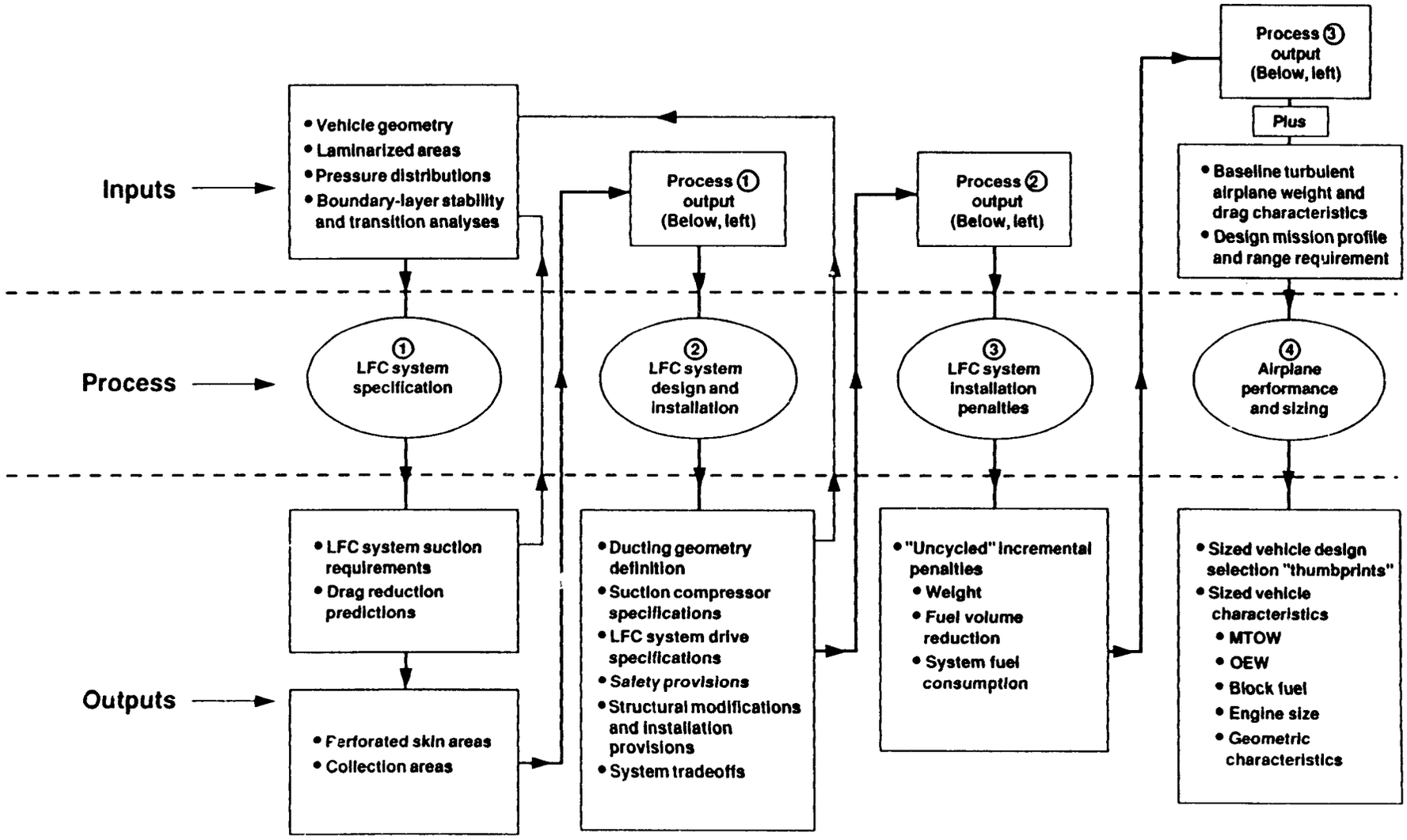

Figure 4.1.1-1 Design/Benefit Process and Data Flow

Comparison of the characteristics of the LFC aircraft with the baseline turbulent airplane sized for the same mission ground rules yielded the benefits attributable to the application of LFC.

4.1.2 Airplane Sizing Considerations

Arriving at an "optimum" sized airplane definition for a given set of mission requirements and ground rules is a process which involves the synergism of multiple design and performance-related variables. Very often, performance increments attributable to a design or technology change on a fixed-size airplane (fixed geometry and design weights) are magnified when the airplane is resized to satisfy a given set of mission requirements. Any reduction achievable in airframe weight for instance is reflected in a proportional savings in fuel and gross weight, which in turn results in a further savings in airframe weight (smaller wings, engines, empennage and lighter landing gear) and so on. A reduction in fuel consumption characteristics, either through reduced drag or improved engine efficiency, will similarly "cycle" through reduced fuel, to reduced airframe weight.

These effects get progressively more pronounced as the severity of the mission requirements (e.g. range) is increased. The relative leverage of weight and fuel efficiency improvements is also modified as design range is increased: because a long range airplane must carry proportionately more fuel than a short range airplane (increased "fuel fraction"), a given percentage reduction in fuel consumption will have a greater impact on gross weight: weight is always important but, for long ranges, drag and TSFC approach it in importance.

The airplane sizing process, which is usually carried out iteratively using a computer program, is illustrated graphically by the "X-plot" in Figure 4.1.2-1. Two lines are plotted on a graph of operating empty weight (OEW) versus maximum takeoff weight (MTOW). A fixed payload is assumed, implying a body of fixed length and volume. Aerodynamic parameters such as wing aspect ratio, taper ratio and thickness ratio are also assumed fixed. Fixed values of wing loading and thrust-to-weight ratio: are assumed in order to maintain approximately constant takeoff field length, climb and acceleration capability and aero-propulsion match. These assumptions mean that as the MTOW is increased, the wings, engines and empennage get progressively larger in relation to the body, as indicated by the airplane sketches in the figure. The strength and geometric characteristics of the landing gear are also assumed to vary to accommodate increased gross weight.

The line labelled "should-weigh" in Figure 4.1.2-1 is a function of mission requirements and fuel efficiency characteristics (e.g. range factor) and represents the maximum OEW allowable (for a given MTOW) if mission range is to be met.

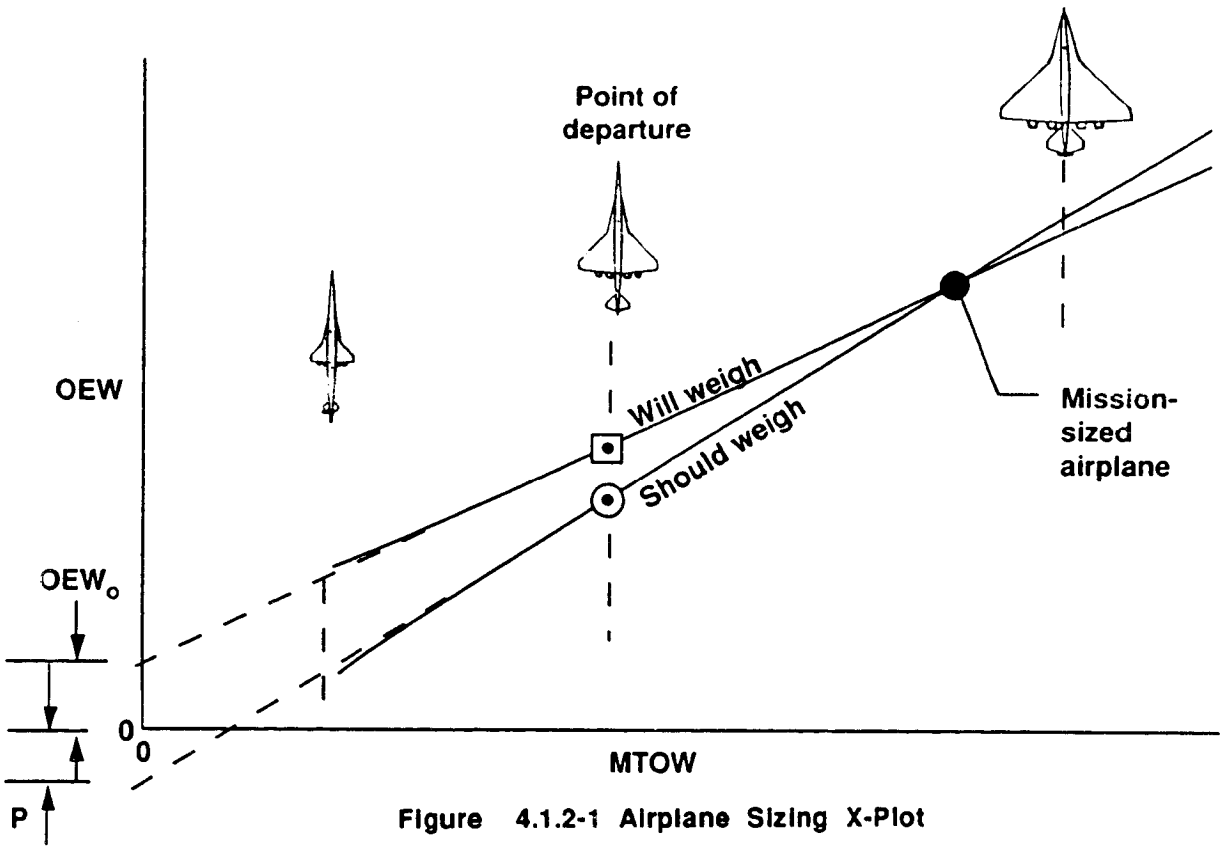

Figure 4.1.2-1 Airplane Sizing X-Plot

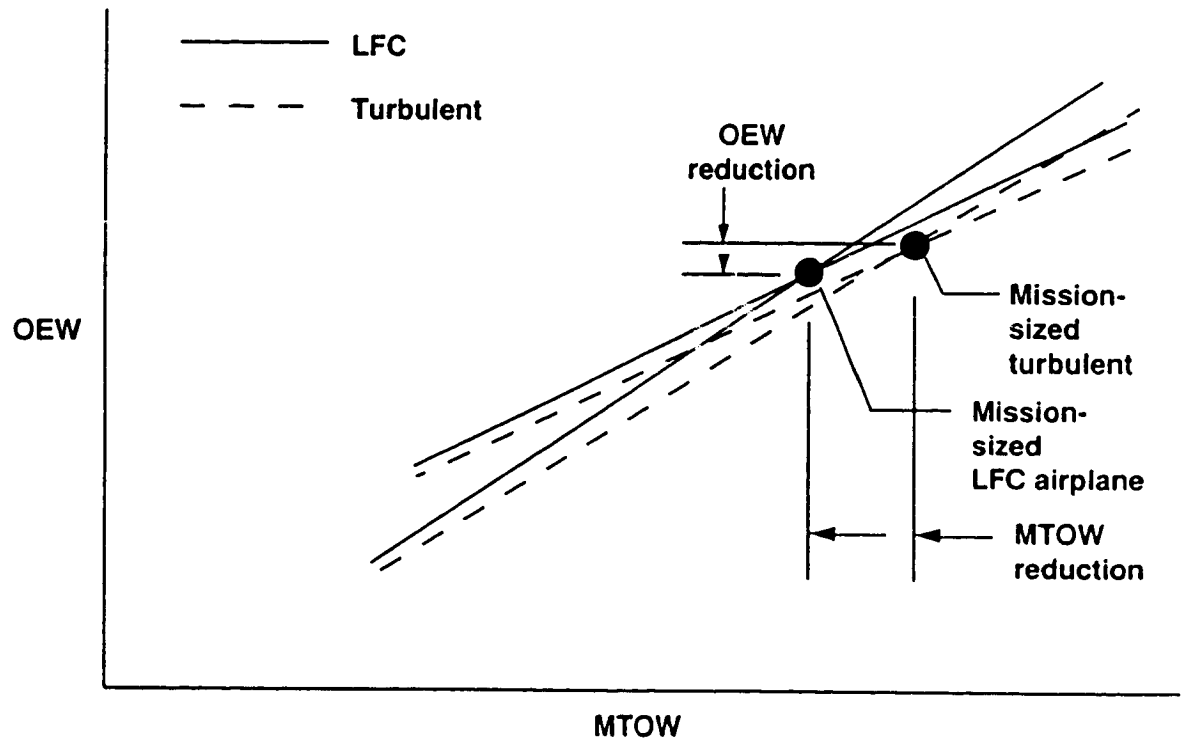

Figure 4.1.2-2 Sizing Effects of LFC

The line labelled "will-weigh" is determined from weight analysis and intersects the OEW axis at some positive value. This reflects the fact that the body, passenger accommodations, environmental control systems, etc. are held constant even as the gross weight, wing area and engine size hypothetically approach zero. The slope of the "will-weigh" line is determined by the rate of change of weight of those configuration components whose size is driven by gross weight (wing, engine, gear, etc.)

The airplane will meet or exceed the mission range requirements when the "will-weigh" OEW is equal to or less than the "should-weigh" OEW, a condition which is given by the intersection of the two lines in Figure 4.1.2-1.

Previous analyses have indicated that, although in general both lines are curved (due to slow variations in both lift-to-drag ratio and "unit weights" of wing, engines, etc.), the curvature is relatively small and little error is introduced by assuming linear variations. A simple linear analysis highlights the major variables and considerations, while capturing the essence of the sizing process. Under these assumptions, the should weigh line can be expressed as follows:

$$OEW_S + P = MTOW - \text{Fuel required}$$
$$= MTOW\,(1 - \zeta)$$

or

$$OEW_S = MTOW(1 - \zeta) - P \qquad \text{Equation 4.1.2-1}$$

where P is the payload
and ζ is the required fuel fraction derived from mission performance analysis.

The "will-weigh" line can be approximated by assuming constant unit weights for wing and propulsion installation and constants of proportionality for landing gear and gross-weight-dependent systems. (An awkward non-linear variation in empennage size is ignored-with the justification that empennage weight is small compared with wing weight-and instead empennage weight is assumed proportional to wing area):

$$OEW_W = OEW_O = \underset{\text{Wing}}{w_W S} + \underset{\text{Propulsion}}{w_T T} + \underset{\text{Landing Gear}}{k_G MTOW} + \underset{\text{Systems}}{k_S MTOW} + \underset{\text{Empennage}}{k_E S}$$

or

$$OEW_W = OEW_O + (w_W + k_E)\frac{MTOW}{W/S} + w_T \frac{T}{W} \cdot MTOW + (k_G + k_S)\,MTOW$$

$$= OEW_O + K_W\,MTOW \qquad \text{Equation 4.1.2-2}$$

where

$$K_W = \frac{w_W + k_E}{W/S} + w_T \frac{T}{W} + k_G + k_S \,. \qquad \text{Equation 4.1.2-3}$$

For transport airplanes, previous analyses indicate that the wing is the major contributor to the slope (K_W) of the will-weigh line. In this regard it is important only only to seek to minimize wing unit weight (w_W), but also to choose as high a wing loading (W/S) as mission constraints will allow. The propulsion system is usually the second most powerful contributor (low T/W desirable) with landing gear and systems following in importance. The intercept (OEW_O), although hypothetical, is strongly dependent on payload size and the weight of body and payload-related systems.

"Mission-sized" airplane characteristics are determined by equating OEW_S (equation 4.1.2-1) to OEW_W (equation 4.1.2-2) which yields:

$$MTOW = \frac{OEW_O + P}{[(1-\zeta) - K_W]} \qquad \text{Equation 4.1.2-4}$$

As expected, mission-sized gross weight is strongly influenced by payload and associated structure and systems. However, and just as importantly, it is seen to be inversely proportional to the difference in slopes between the should-weigh and will-weigh lines. The factor $1/[(1-\zeta) - K_W]$ - sometimes termed the "growth factor" - can become large at long ranges, where the required fuel fraction, ζ, is large. Under these circumstances, small percentage changes in either fuel efficiency, or the weights of wing, engines, landing gear, etc. can produced a much-magnified percentage change in the growth factor, and hence in mission-sized gross weight.

Ultimately, there exists a range requirement which results in an infinite growth factor (should-weigh and will-weight lines are parallel) and no solution to the mission requirements is possible.

Because of the leverage of these considerations, it is important that incremental technology or design changes be evaluated for mission-sized airplanes. This is particularly true for the application of concepts such as, LFC which produce a benefit in one performance-related variable (e.g. drag) at the expense of another (e.g. weight). The net benefit of such a concept is the relatively small difference between two opposing performance effects, the magnitude - and even sign - of which is strongly influenced by synergistic sizing effects. Figure 4.1.2-2 illustrates these effects for an LFC system. In the figure the dashed lines denote the baseline turbulent airplane and the full lines the LFC airplane. The drag reduction produced by LFC results in a reduction in required fuel fraction, causing an anti-clockwise rotation (increase) in the should-weigh line. At the same time the installed weight increment of the system causes a similar rotation of the will-weigh line. The net effect depends on the relative magnitude of the two rotations and also on the angle between the two original lines. In the situation show, illustrates not only a sizable reduction in MTOW (and fuel burn) but also a reduction in sized airplane OEW, despite the original

"uncycled" weight penalty. This would help defray, or even overcome, any airframe cost penalty associated with the LFC system.

The above discussion illustrated the determination of sized vehicle characteristics for fixed values of wing loading (W/S) and thrust-to-weight ratio (T/W). These were selected to maintain consistency in some of the likely performance-related mission constraints such as takeoff field length. However, the particular values chosen for these two variables may not represent the optimum combination for the mission as a whole. In addition, other constraints, such as approach speed, initial cruise altitude capability or available fuel volume, which vary with takeoff W/S and T/W in a more complicated manner, may ultimately become important in the selection of final sized airplane parameters.

A standard method of examining the interaction of the various mission constraints and of selecting a close-to-optimum set of vehicle characteristics is via a "Thumbprint" plot. A schematic of such a plot is shown in the top left of Figure 4.1.2-3 and is really the connecting medium for a set of sizing exercises each at fixed W/S and T/W. In other words, the characteristics determined in each "X-plot" (or iterative equivalent) become one point in the Thumbprint T/W versus W/S space, as illustrated in the figure. The figure-of-merit chosen to represent the "goodness" of the parameter selection (in this case MTOW) is shown as a set of constant-value contours. Mission constraints, representing minimum or maximum acceptable values of such parameters as takeoff field length, approach speed, and transonic thrust margin are superimposed as constant-value lines.

The fuel volume constraint is the locus at which fuel volume required for the mission is equal to that volumetrically available in the designated fuel tank areas of the configuration. Since the majority of the fuel load of a transport aircraft is carried in the wings, the fuel volume available is a strong function of wing area, with the result that, on the Thumbprint, the fuel volume constraint is mainly a function of W/S.

Selection of "optimum" sized vehicle characteristics involves choosing the point on one or more constraint lines which is closest to the "eye" of the MTOW contours. The situation depicted in Figure 4.1.2-3 with fuel volume and transonic thrust margin being the critical constraints, is representative of the situation pertaining to both the LFC and turbulent airplanes in this study, as discussed in Section 4.3 below. The "double delta" planform chosen as the basis of the study is deficient in available fuel volume for design ranges of 5000 nm and above. Further refinements to the configuration would logically be aimed at seeking ways to increase the available fuel volume with as little penalty in drag and weight as possible. Since both LFC and turbulent airplanes were found to be constrained in a very similar fashion, and since further refinements would involve substantial reconfiguration effort and in any case would impact LFC and turbulent designs to a similar extent, it was felt that a comparison of sized airplane characteristics at this stage was valid, at least to a first order.

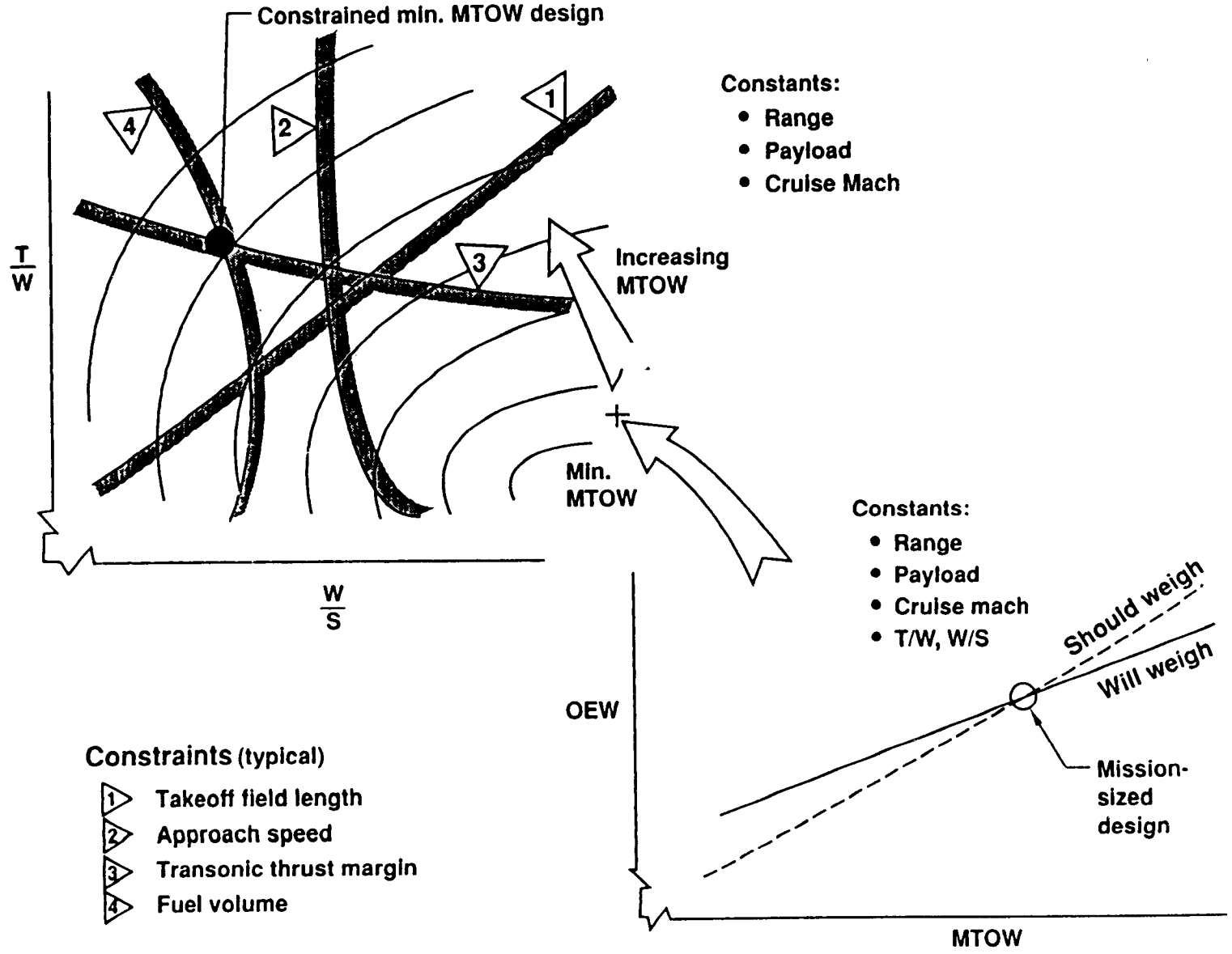

Figure 4.1.2-3 Airplane Sizing and Constraints

4.2 EVALUATION OF LFC BENEFITS AND PENALTIES

Determination of the net benefits of LFC implementation on an SST configuration requires considerations of the aerodynamic benefits of laminarization together with the penalties of suction system weight, volume and power requirements. In this section, the individual benefits and penalties of LFC implementation were evaluated for two laminarization schemes (schemes 1 and 2 of Figure 2.8-1). Only direct shaft mechanical drive for suction compressors was considered in this evaluation.

4.2.1 Aerodynamic Benefit Evaluation

The aerodynamic benefits of LFC application in terms of reduced skin friction drag for the configuration were evaluated on the basis of achievable laminarization on the inboard and outboard parts of the wing. The achievable laminarization by use of a hybrid suction scheme on the wing upper surface was determined in Section 2.8 from stability theory calculations and the Boeing transition criteria. A hybrid suction and laminarization scheme identical to the upper surface was assumed for the lower surface. Two hybrid laminarization schemes selected for detailed systems evaluation were also discussed in Section 2.8.

4.2.1.1 Estimation of Skin Friction Reduction

The skin friction drag estimate of the turbulent configuration was based on flat plate strip theory calculation within the A389 [35] program. To evaluate the skin friction drag reduction due to laminarization, a similar calculation procedure was adopted, except that the boundary layer in each streamwise "strip" was assumed to be part-laminar with a specified laminar to turbulent transition location. For the purpose of this analysis, the wing surface was divided into 37 streamwise strips of equal width (2.5 percent semispan), starting at the body side (7.5 percent semispan) and extending up to the wing tip. The transition location in each strip was then specified by superimposing the map of the laminarization areas for schemes 1 and 2 as shown in Figure 4.2.1.1-1. For each strip, the part-laminar skin friction was calculated by matching the momentum thickness of the laminar boundary layer at the transition location with that of the turbulent boundary layer at the transition location. As a consequence of the momentum integral equation, the momentum thickness θ of the flat plate boundary layer (laminar or turbulent) may be related to the average skin friction coefficient C_F by

$$\theta = \frac{X \cdot C_F}{2} \qquad \text{Equation 4.2.1.1-1}$$

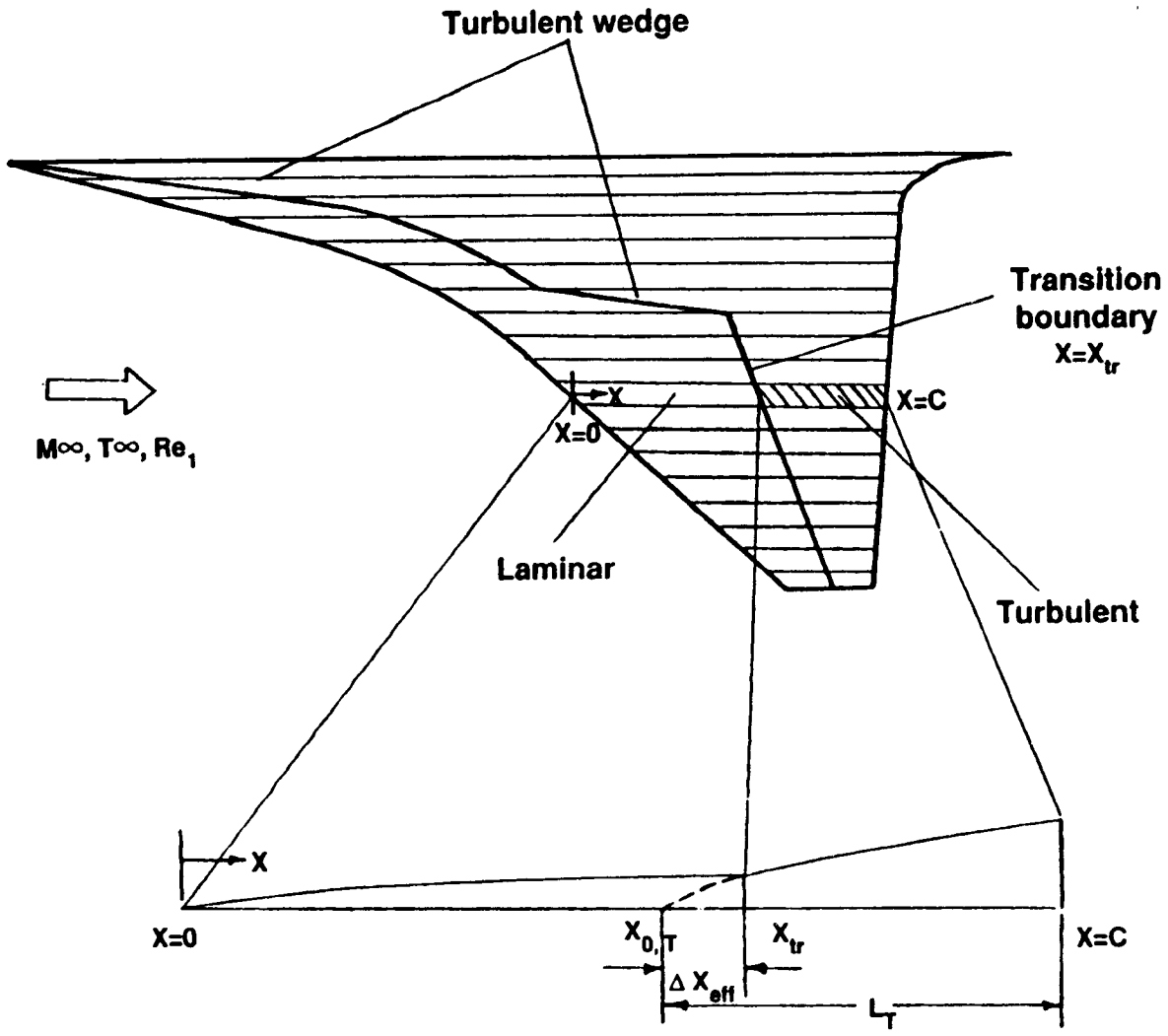

Figure 4.2.1-1 Strip Theory Calculation Method for Part-Laminar Skin Friction

where X = distance from the boundary layer origin
C_F = average skin friction coefficient over distance X
θ = momentum thickness at X

The laminar and turbulent skin friction coefficients were calculated by Blasius and Prandtl-Schlichting formulas [4] corrected for compressibility using the Sommer and Short [45] correction. These are given as

$$C_{F,L} = \frac{1.328}{Re^*_x}\left(\frac{T_\infty}{T^*}\right) \qquad \text{Equation 4.2.1.1-2}$$

$$C_{F,T} = 0.455\ [\log_{10} Re^*_x]^{-2.58}\left(\frac{T_\infty}{T^*}\right) \qquad \text{Equation 4.2.1.1-3}$$

where, the reference temperature T^* is calculated from Sommer and Short [45] correlation

$$\frac{T^*}{T_\infty} = 1 + 0.1551\ M_\infty \qquad \text{Equation 4.2.1.1-4}$$

The Reynolds number (Re^*_x) based on reference properties is related to the Reynolds number (Re_x) based on free-stream properties by the following equation derived from the Sutherland law of viscosity:

$$Re^*_x = \left(\frac{T_\infty}{T^*}\right)^{2.5}\left(\frac{T^* + 216}{T_\infty + 216}\right) \cdot Re_x \qquad \text{Equation 4.2.1.1-5}$$

The temperatures are in °R.

Then the condition of momentum matching at the transition location may be expressed as (see Figure 4.2.1.1-1):

$$[\theta_L]x_{tr} = [\theta_T]\ \Delta x_{eff} \qquad \text{Equation 4.2.1.1-6}$$

i.e. $x_{tr} \cdot C_{F,L}\ (x_{tr})\ \lambda = \Delta x_{eff} \cdot C_{F,T}\ (\Delta x_{eff})$ Equation 4.2.1.1-7

The factor λ is equation 4.7 is introduced to account for the reduced momentum thickness of the laminar profile due to wall suction. From the boundary layer calculations conducted during stability analyses, this factor was found to be approximately 0.8. Equation 4.7 was solved iteratively to determine Δx_{eff}. The average (part-laminar) skin friction coefficient for the strip was then calculated from

$$(C_F)_{PL} = \frac{L_T}{C} C_{F,T}\ (L_T) \qquad (4.8)$$

where, C = local chord for the strip

$$L_T = C - x_{tr} + \Delta x_{eff}$$

A computer program was written to perform this iterative calculation strip by strip over the entire wing planform and thereby estimate the net skin friction drag reduction for the wing. The input to the program consisted of free stream temperature, Mach number and unit Reynolds Number. A separate input file was created to supply data on chord lengths and transition locations for 38 spanwise locations on the wing. The output from the program listed fractional wing area laminarized and fractional reduction in the skin friction due to laminarization as compared to an all turbulent wing.

The skin friction drag of the wing accounts for nearly half of the total skin friction drag of the 1080-834 configuration. Other components of the total skin friction drag are:

Body	25%
Nacelles	10%
Empennage	10%
Fences & Excrescence	5%

Implementation of laminarization schemes 1 and 2 resulted in 24 percent and 34 percent reductions respectively in the wing skin friction drag. This also represented 30 percent and 41 percent respectively of the wing wetted area where laminar flow was achieved.

Because of the much smaller chord Reynolds Numbers (as compared to the wing) and sharp supersonic leading edges, a significant run of natural laminar flow was achievable for the horizontal and vertical surfaces of the empennage section. A 20 percent reduction in the all-turbulent skin friction of the empennage surfaces was assumed.

In a similar fashion, a 20 percent reduction in the skin friction drag of the nacelles was considered achievable due to natural laminar flow design. No laminar flow benefit was assumed for the body. The net reduction in the total skin friction drag of the configuration due to the implementation of LFC schemes 1 and 2 on the wing and NLF for nacelles and empennage amounted to 16 percent and 22 percent respectively.

For inputs to the performance analysis program, the above percentage reductions in skin friction drag were assumed to be applicable down to flight Mach number of 1.5. At transonic Mach number of 1.1, the LFC system was assumed to be inoperative. Therefore only the skin friction drag reduction benefits of natural laminar flow were assumed. These were: 10 percent reduction for the wing and 20 percent for nacelles and empennage.

4.2.1.2 Impact on Other Drag Components

The total drag of a supersonic transport configuration consists of skin friction drag, zero lift wave drag, drag-due-to-lift and trim drag. A typical polar with drag buildup is shown in Figure 4.2.1.2-1. Note that the drag-due-to-lift at supersonic speeds has both a vortex drag and a wave drag component. The zero lift wave drag (or drag-due-to-volume) can be calculated in the A389[35] program by two different methods: a near field method and a far field method.

The two methods usually yield answers which are within 10 percent of each other. For the baseline turbulent 1080-834 configuration at cruise Mach number of 2.4 and C_L = 0.12, the total drag consists of the following components:

Skin Friction Drag	37%
Zero Lift Wave Drag	18%
Drag-Due-To-Lift + Trim drag	45%

In view of the above breakdown of the total configuration drag, the net drag reduction due to laminarization by schemes 1 and 2 amounts to 6.0 percent and 8.2 percent respectively. This level of drag reduction due to laminarization would result in a cruise L/D improvement from 9.2 for the turbulent baseline to 9.8 for scheme 1 and 10.0 for scheme 2.

The question now is: How are other drag components affected by the implementation of these LFC schemes? There are two possible modifications necessitated by LFC implementation: a) modification of the Cp distribution on the inboard wing surface to achieve significant laminarization without use of excessive suction, and b) increased wing thickness to accommodate the suction system hardware and/or fuel displaced. The modification of the existing Cp distribution on the inboard wing and the assessment of its impact on the drag-due-to-lift requires a nonlinear wing design capability using a full potential or Euler solver (see Section 2.7.4).This capability was unavailable at the time of the current study and could not be developed within the limitations of the schedule and resources of the contract.

The second modification, namely, increased wing thickness to accommodate the fuel displaced by the suction system has an impact on the zero lift wave drag of the configuration. This impact was evaluated in conjunction with laminarization scheme 2 only. Initial net benefits analysis of scheme 2 without wing thickness increase revealed that the fuel volume displacement caused by the suction system components (ducts, compressor dry wells, etc.) was a large fraction of the net fuel savings by LFC implementation.

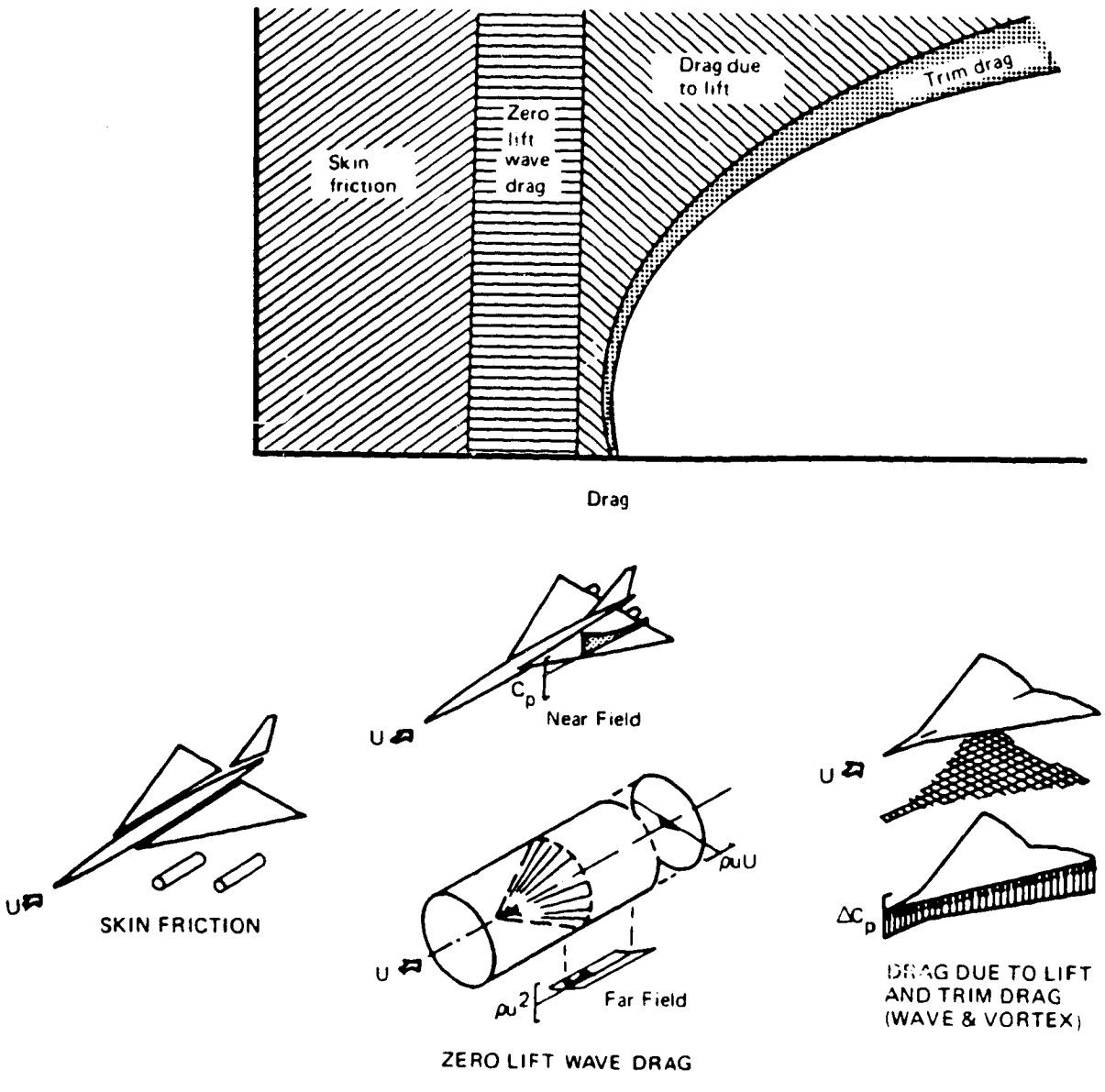

Figure 4.2.1.2-1 Supersonic Cruise Drag Buildup

Since the wing is sized by fuel volume requirements for this type of configuration rather than takeoff field length (TOFL) or approach speed (V_{app}) considerations, the wing planform area can be reduced further by increased wing thickness up to the point where either TOFL or V_{app} limit is reached. The penalty incurred in this process is the increased wave drag at supersonic speeds, while the benefits are reduced structural weight due to a) smaller wing area, and b) increased structural efficiency resulting from increased wing thickness. Only the aerodynamic penalty of increased wing thickness will be discussed in this section. The beneficial impact of wing thickening on the structural weight (OEW) will be discussed in Section 4.2.3.4. Aerodynamically, it would be expected that thickening the subsonic leading edge inboard wing (strake) would have a smaller impact on wave drag than if the outboard supersonic leading edge wing was thickened. This turns out to be structurally beneficial as well because bending moments are largest at the wing root. Therefore, in order to increase the fuel volume capacity of the configuration, the wing thickness in the inboard region was increased in several different ways and the impact on wave drag was studied by use of the Near Field Wave Drag (NFWD) module of the A389[35] program.

The different modified inboard wing maximum thickness distributions that were attempted are shown in Figure 4.2.1.2-2. The basic spanwise distribution of maximum thickness is shown as ANL633. In distribution ANL633M, the inboard wing thickness was increased by 10 percent between 7.5 percent (wing root) and 25 percent semispan stations (η). The thickness increment was dropped to zero at η = 0.3. For thickness distribution designated ANL633N, the 10 percent thickness increment was applied between wing root and η = 0.15 station, with the increment reduced to zero at η = 0.2. Finally, for thickness distribution ANL633L, the 10 percent increment in thickness was applied between wing root and η = 0.1 with the increment dropping to zero at η = 0.175 station.

The increases in volume and wave drag at M = 2.4 cruise are shown in the following table:

TABLE 4.2.1.2-1
Impact on Wave Drag and Wing Volume of Thickening the Inboard Portion of 733-633 Wing

Thickness Distribution	Volume Increment ft^3 (lb_mfuel)	Cruise $C_{D,O}$ Increment ($X10^{-4}$)	(Fuel Capacity Increment) / ($C_{D,O}$ Increment)	(lb_m) (count)
ANL633M	789(39,000)	1.08	36100	
ANL633N	591 (29,550)	0.68	43500	
ANL633L	387 (19,350)	0.43	45000	

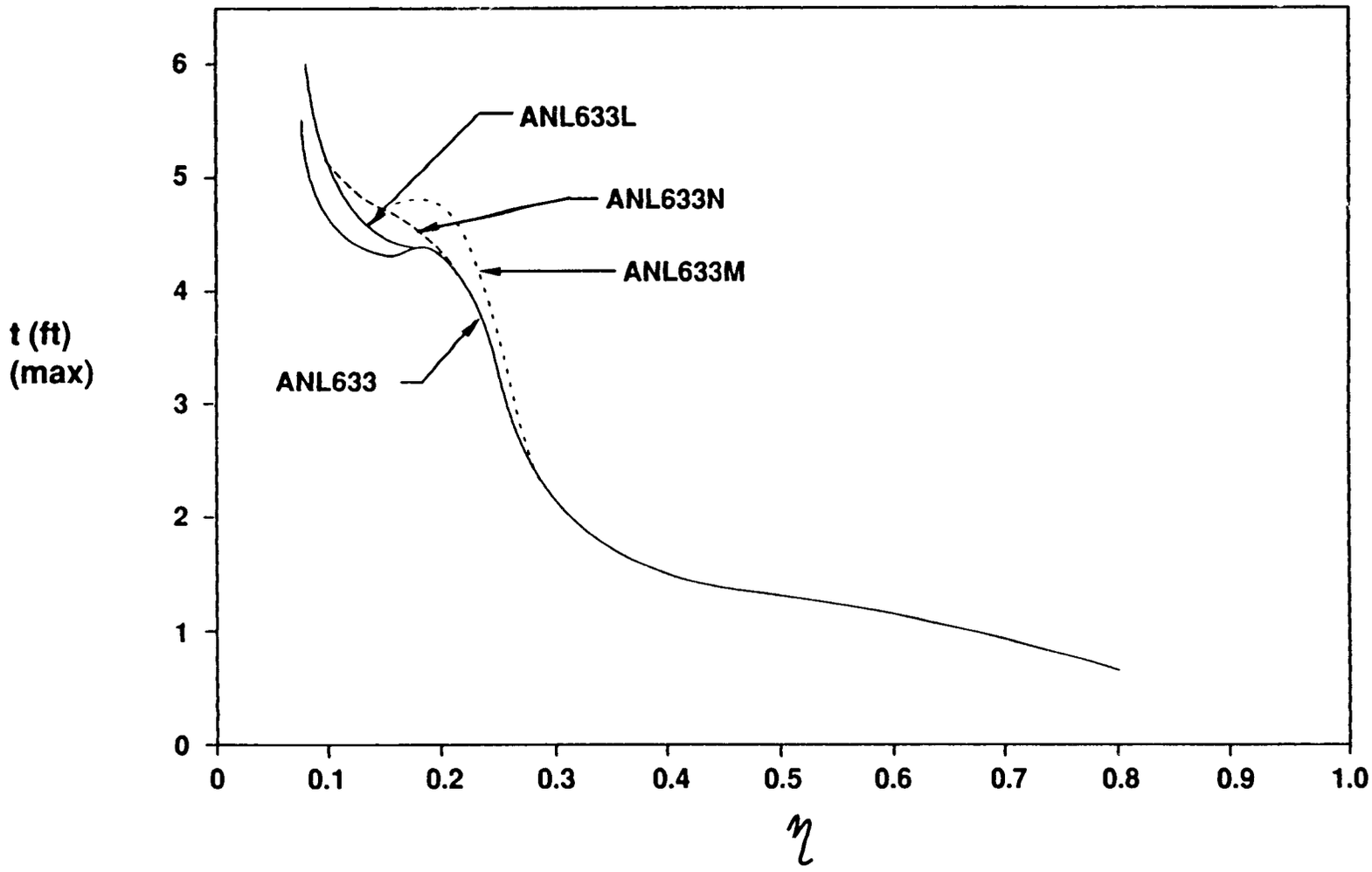

Figure 4.2.1.2-2 . Baseline and Modified Maximum Thickness Distributions

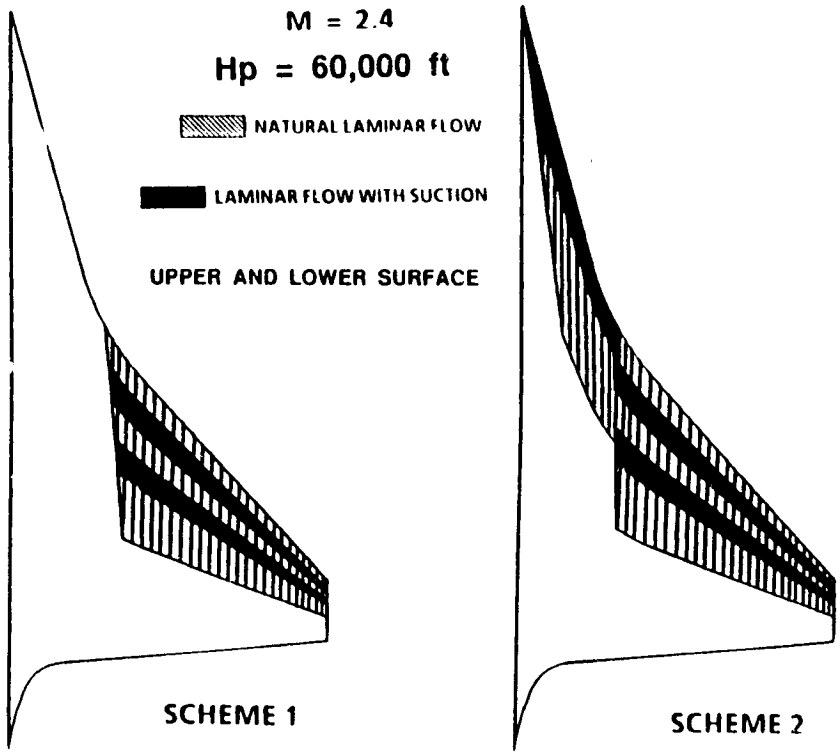

• Wing Wetted Area Laminarized	30%	41%
• Wing Skin Friction Drag Reduction	24%	34%
• Net Reduction in Configuration Skin Friction Drag (Including NLF on Nacelles and Empennage)	16%	22%
• Net Reduction in Configuration Total Cruise Drag	6.0%	8.2%
• CRUISE L/D (Baseline = 9.2)	9.8	10.0

Figure 4.2.1.2-3 Aerodynamic Benefits of Laminarization

It may be seen from the last column of Table 4.2.1.2-1 that confining the wing thickening process to region closest to the wing root (as in ANL633L) leads to minimal wave drag penalty. Also, the increase in cruise wave drag coefficient is seen to be approximately one count for accommodating a volume equivalent of about 40,000 lb_m of fuel.

The increased wave drag was accounted for in the performance and sizing program. At lower supersonic Mach numbers down to M = 1.1, the wave drag was increased by the same percent as at M = 2.4.

The aerodynamic benefits of laminarization by schemes 1 and 2 in terms of cruise drag reduction are summarized in Figure 4.2.1.2-3.

4.2.2 Suction System Requirements and Penalties

Concepts for the suction system and its installation on the SST configuration were discussed in Chapter 3 (Sec. 3.4). The conceptual designs were based on the specified suction regions and mass flow requirements which resulted from aerodynamic analysis of Chapter 2. Comparisons of system weight, volume displacement and power requirements were made in Section 3.4 between electric motor driven versus direct mechanical shaft driven compressor arrangements for laminarization scheme 1. It was concluded that the mechanical drive system has a clear advantage in terms of system weight and power requirement penalties. The electrical drive system showed only a small volume displacement advantage. For this reason, only the mechanical drive system was considered for design/benefit studies leading to evaluation of net benefits of LFC implementation for laminarization schemes 1 and 2.

Another trade evaluated was the suction air discharge velocity. The suction air coming in from various regions at different inlet pressures is compressed by individual compressors to a common exit pressure in the discharge duct. As the compressor exit pressure is raised, the suction air discharge velocity approaches the free stream velocity, and to the first order, the net suction air momentum drag drops to zero. However, the power required to compress the suction air to the required pressure to achieve this condition increases significantly.

Increased compressor power requirement in turn increases the thrust specific fuel consumption (TSFC) and equipment weight penalties. A trade study was conducted to establish the optimal compressor exit pressure.

4.2.2.1 Compressor Power Trade Study

The compressor discharge pressure that was used in Section 3.4.3 of this report for compressor drive power calculations was 275 PSF selected by considering tradeoffs between suction drag and exhaust thrust. Suction drag

resulted from the ram drag of the air at the inlet to the suction system. Exhaust thrust was obtained from the momentum of the air discharged overboard. The net suction air momentum drag was the difference of the ram drag minus the exhaust thrust. Drag horsepower was calculated from the net drag and from the aircraft cruise velocity (M=2.4).

The considerations were as follows:

a) An exhaust pressure exceeding the ambient static pressure at the flight altitude is needed to maintain continuous flow.
b) The suction system should have the ability to operate at altitudes lower than the cruise altitude. (An average cruise altitude of 62,000 ft was used.)
c) Compression of the air reduces the flow area of the exhaust ducts.
d) The exhaust air flow can produce useful propulsive thrust if it is accelerated through a nozzle and the resulting jet is directed aft.
e) An exhaust jet velocity equal to the flight velocity would cancel the suction drag.

Figures 4.2.2.1-1 relates the exhaust velocity to the air compressor power. Figure 4.2.2.1-2 illustrates the effect of compressor power on the net suction drag. Figures 4.2.2.1-3 shows the effect of air compressor outlet pressure selection on the compressor drive power. Figure 4.2.2.1-4 illustrates the trades between compressor drive power and the resulting net suction drag power. The effects of compressor horsepower selection on system weight and displaced fuel volume were determined with the mechanical compressor drive. See Figures 4.2.2.1-5 & -6. The scope of the data was limited to the outboard wing regions only, but the following observations apply to the combined inboard outboard wing regions as well:

a) The lowest possible compressor power results in the least systems penalties.
b) Increasing compressor drive power to reduce the net drag horsepower yields diminishing returns.
c) The point of diminishing returns is at the transition from subsonic to choked flow at the exhaust nozzle.
d) The flow transition occurs when the exhaust pressure reaches two times the ambient static pressure at the flight altitude.

4.2.2.2 Mechanical/Electrical Equipment Weights

The weight of the suction system equipment was estimated on the basis of the state of the art in 1988, with projections to the year 2000. The bare equipment weights were estimated first and were then increased by appropriate factors to include fasteners, fittings, foundations, doublers and other structural provisions based on past commercial airplane experience. The scope of this discussion is limited to the bare hardware.

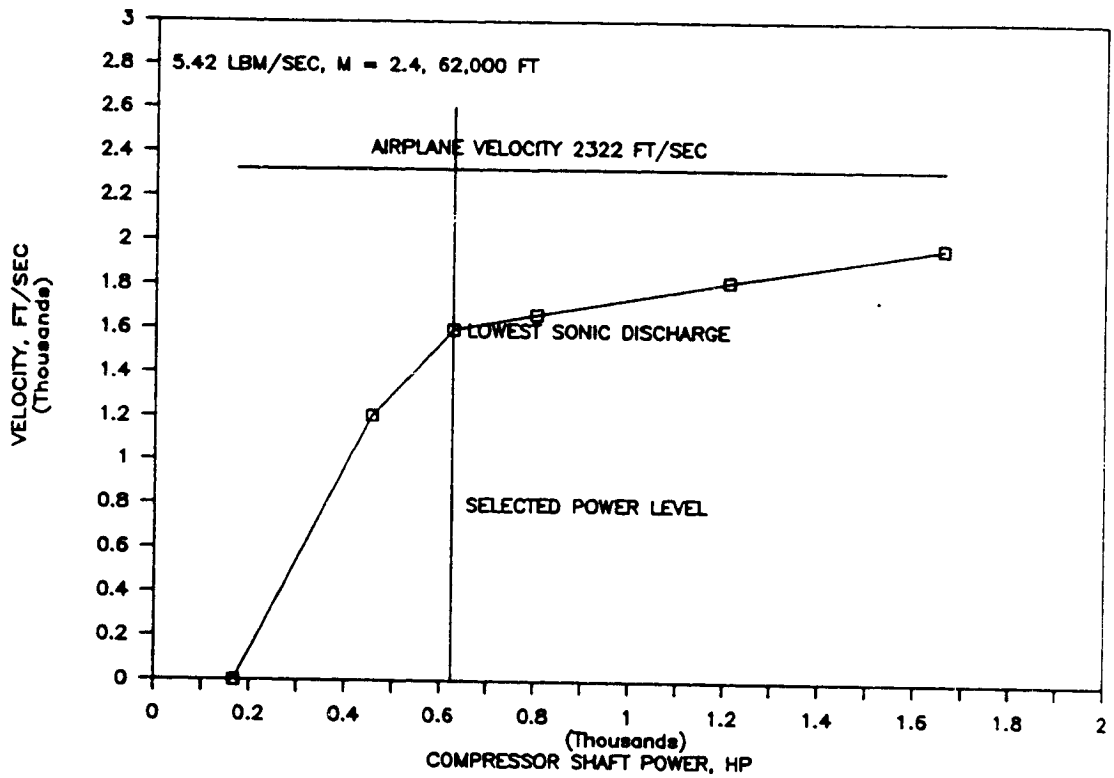

Figure 4.2.2.1-1 Variation of Compressor Power Requirement with Suction Air Exit Velocity

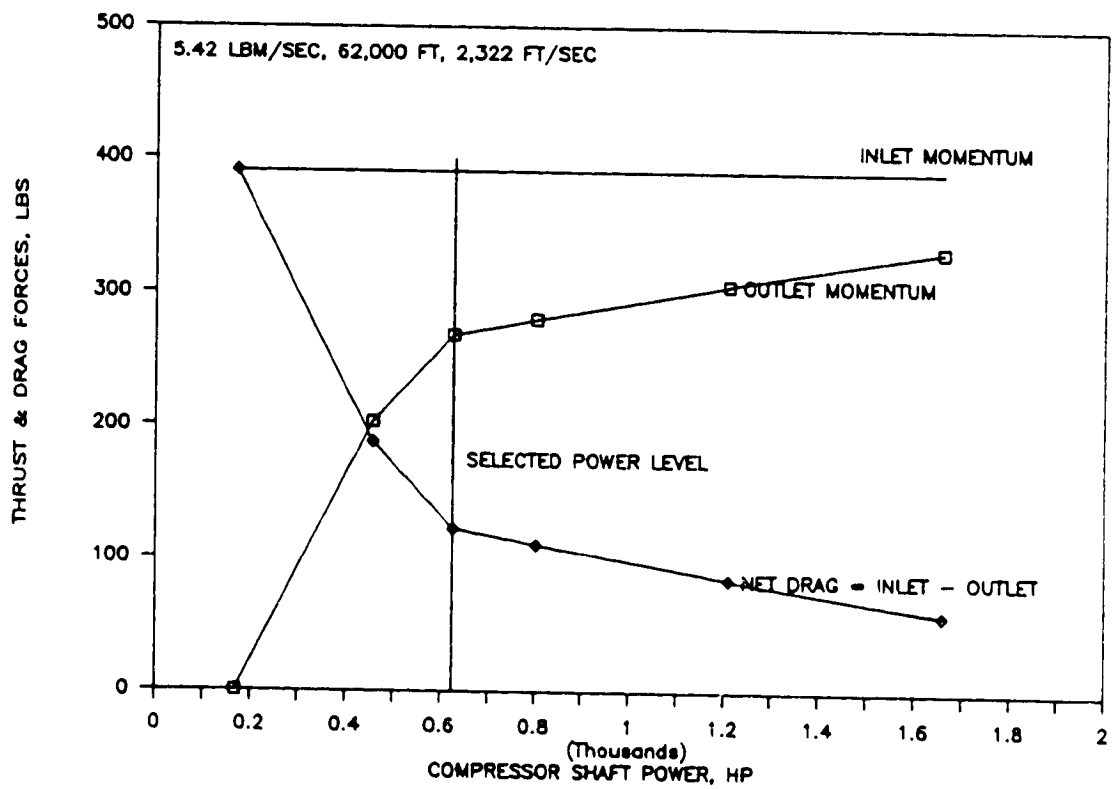

Figure 4.2.2.1-2 Variation of Suction Air Momentum Drag with Compressor Power

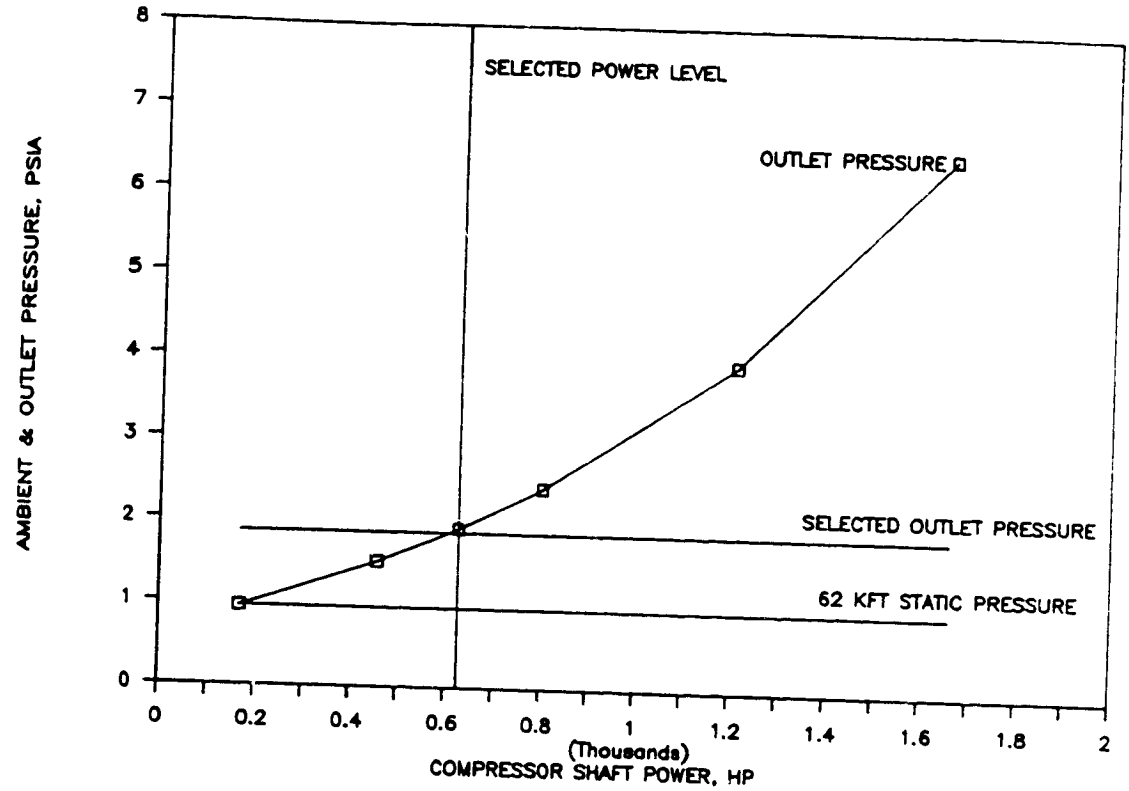

Figure 4.2.2.1-3 Variation of Compressor Power Requirement with Exit Total Pressure

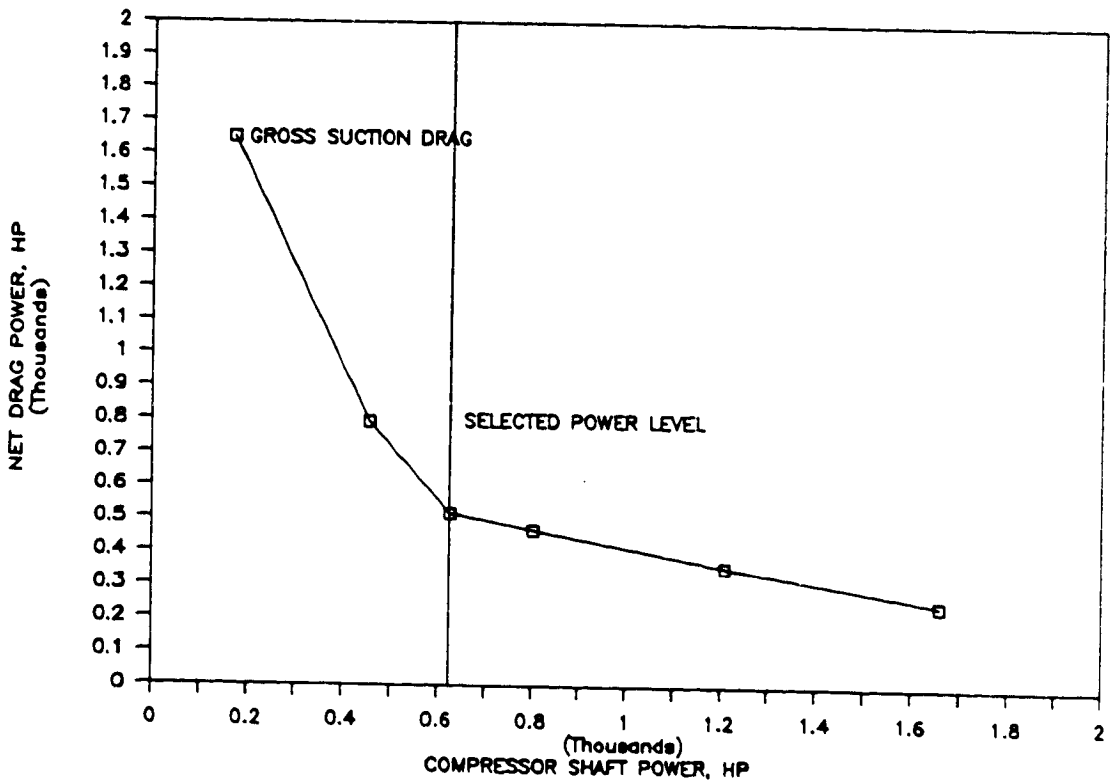

Figure 4.2.2.1-4 Variation of Suction Air Momentum Drag Power with Compressor Power

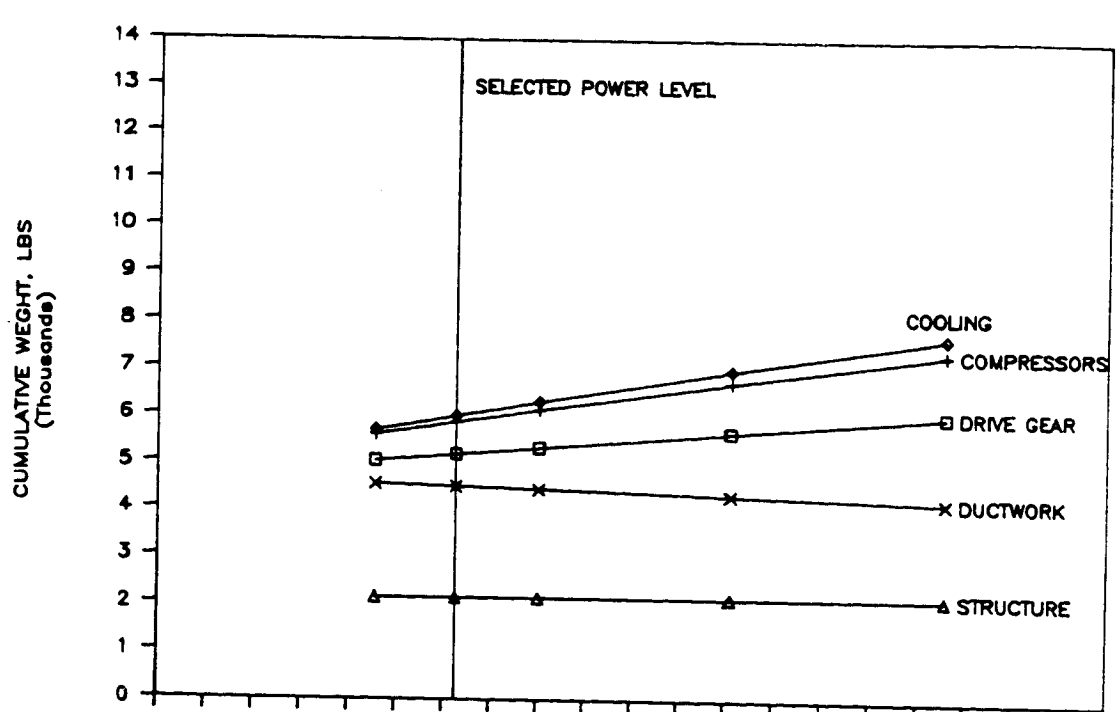

Figure 4.2.2.1-5 Laminar Flow System Weight Increment

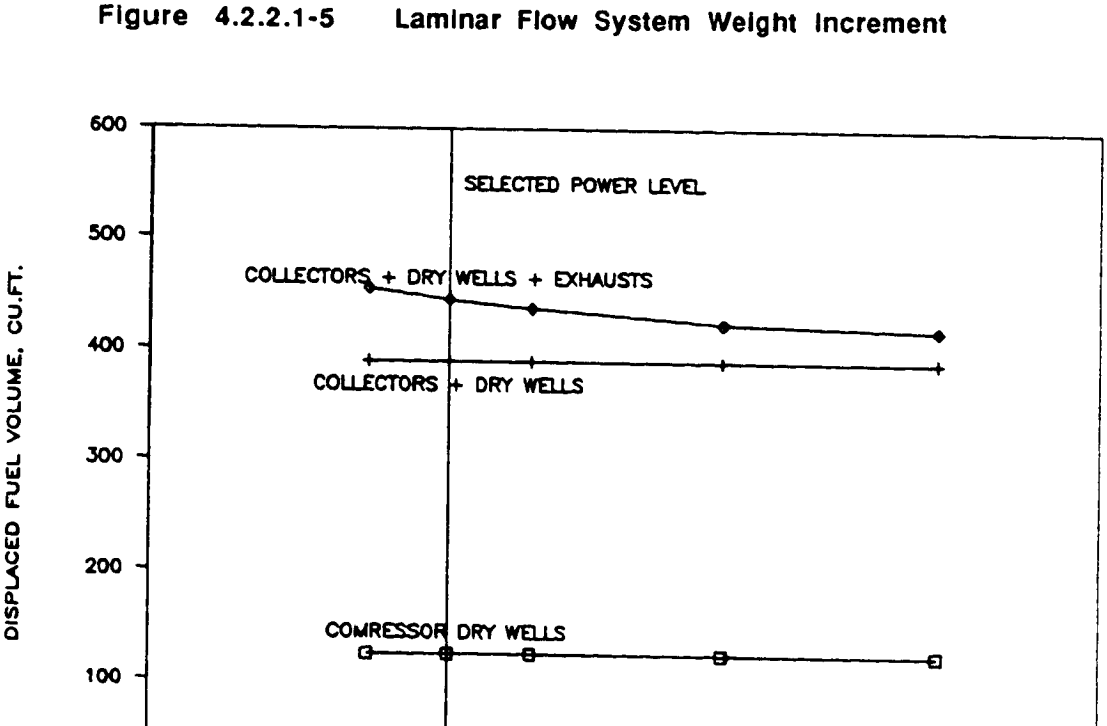

Figure 4.2.2.1-6 Laminar Flow System Fuel Volume Displacement

Suction compressor weights were derived from data which were supplied by the equipment manufacturers Garrett and Sundsrtrand in response to various Boeing requests during the exploratory phases of this study. The specific weights of compressors in pounds per shaft horsepower were correlated with the horsepower level and with the pressure ratio for shaft driven compressors, Figure 4.2.2.2-1.

The specific weight of the compressor drive gear was 1.11 lb/HP, that was obtained from the the F-15 airframe mounted accessory drive. See Figure 4.2.2.2-3.

The combined weight of the cooling coils and circulating pumps required was estimated at 10 lbs per ton of air conditioning, where one ton of air conditioning equals 12,000 BTU/hour (3.5 KW).

The effects of compressor drive efficiency and of the required compressor horsepower level were evaluated. See Figure 4.2.2.2-3.

These estimates of equipment weights were conveyed to the weights staff as an input to the weights analysis of the entire suction system and are included in section 4.2.3 estimates.

4.2.2.3 Volume of Displaced Fuel

The volume of fuel displaced by air plenums, air ducts and by equipment bays was estimated with reference to the suction system arrangements shown in Figures 3.4.1,-2 and -3.

The volume of air ducts was calculated from the duct cross sectional area and the length was scaled from the Figures 3.4.1, -2 and -3, as applicable. The walls of collector ducts were 0.050 inch thick, which was relatively thin in comparison to the duct diameter. The hot exhaust duct walls were surrounded by an outer jacket with a 1-inch air space between the duct wall and the jacket for separating the hot exhaust air from the flammable fuel. The outer wall diameter was used for the displaced fuel volume calculation.

The volumetric air flow was calculated from the mass flow specified in Table 3.2.2-1 and the air density. The air density was determined from (a) the air pressure and (b) the air temperature.

a) The air pressure for the collector duct of each outboard wing region was assumed to be equal to the applicable compressor inlet pressure in Table 3.2.6-1. This assumption was on the conservative side. The air pressure for the collector duct a reasonable pressure drop was assumed of each inboard wing region was set equal to the mean of the plenum pressure and of the compressor inlet pressure to obtain a closer approximation. The air pressure in the exhaust duct was 275 PSF, as described in Section 4.2.2.1.

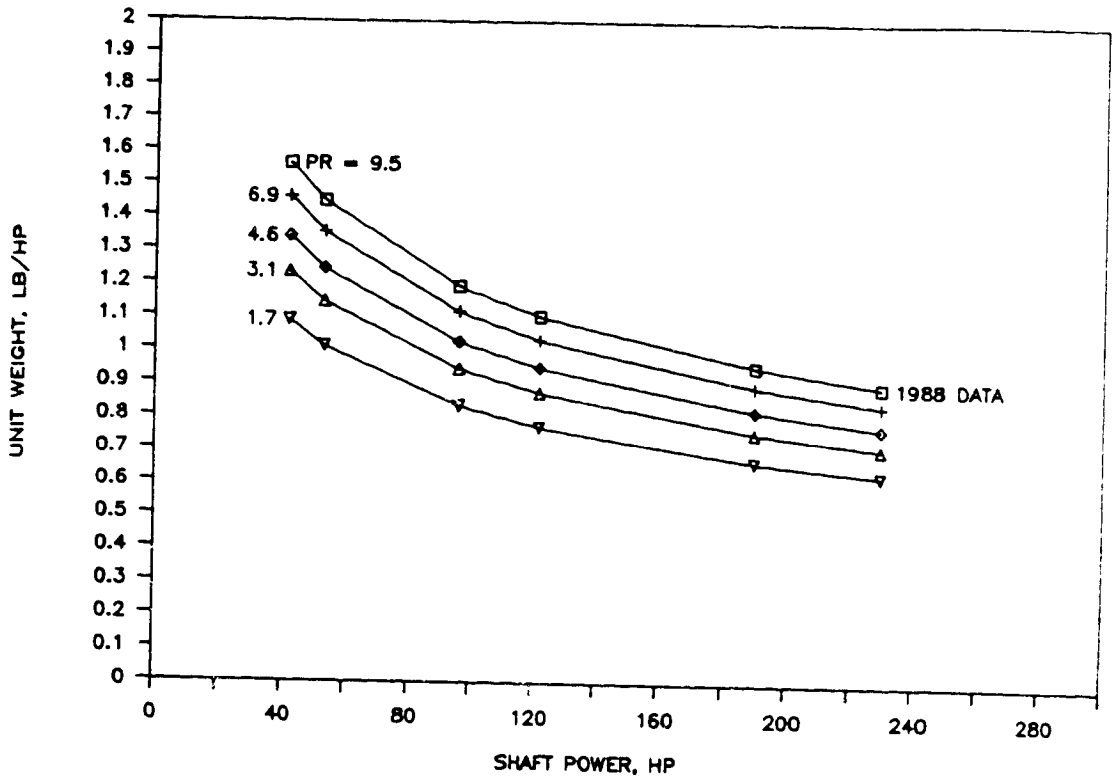

Figure 4.2.2.2-1 Air Compressor Weight Data

PERFORMANCE SUMMARY

JET FUEL STARTER (MODEL JFS 190-1/CGB)

PERFORMANCE

166 SHP PEAK DURING MAIN ENGINE START, INSTALLED NO BLEED AIRFLOW PROVISIONS
54 SHP DURING LIMITED DUTY OPERATION (GROUND CHECKOUT)

WEIGHT SUMMARY

ESTIMATED WEIGHT (DRY)

JET FUEL STARTER	99 LB	N. A.
CENTRAL GEARBOX	70 LB	70
LEFT-HAND AMAD	59 LB	59
RIGHT-HAND AMAD	56 LB	56
TOTAL JFS/AMAD SYSTEM	284 LB	185 lbs/166 HP = 1.11 LB/HP

Figure 4.2.2.2-2 F-15 Secondary Power System Performance and Weight Data

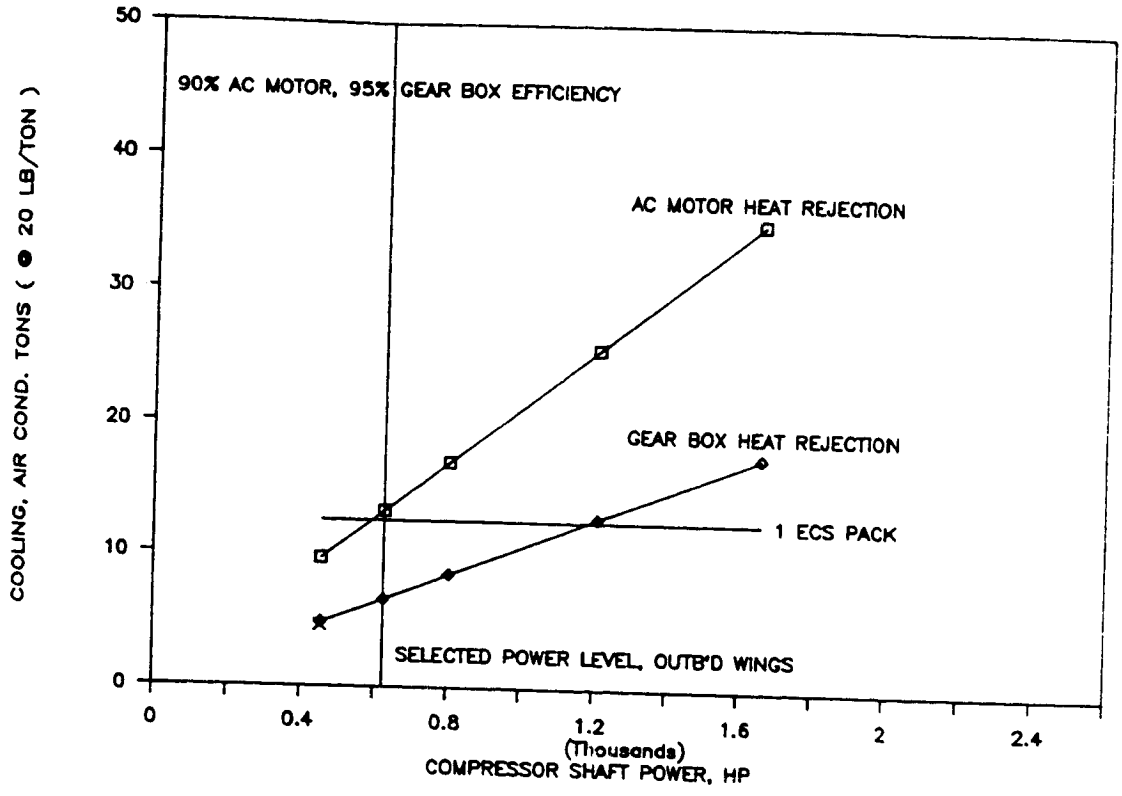

Figure 4.2.2.2-3 Laminar Flow System Cooling Requirements

TABLE 4.2.2.1

System Trades Summary

Laminarized Regions Comressor Drive	Outb'd Wing (Scheme 1) Mechanical	Inb'd/Outb'd (Scheme 2) Mechanical
Figure	3.4.1.-2	3.4.1-3
Air flow, lbs/sec	5.4 2	10.20
Exhaust Pressure, PSF	275	275
Compressor Shaft Horsepower	626	1219
Fuel Volume Displaced, cu. ft.	445	825
Suction Air Momentum Drag (lb f)	121	228

b) The air temperatures for the collector ducts were as specified in Table 3.2.2-1. The air temperatures for the exhaust ducts were the compressor discharge temperatures listed in Figures 3.4.3-4 and -5 of Appendix V. The temperature of the combined exhaust stream was the weighted average of the several compressor discharges.

The air duct flow area was calculated in a first approximation from the volumetric flow and the air velocity at an assumed Mach number of 0.3. The velocity of sound in each air duct was determined by the absolute air temperature. The assumed Mach Number of 0.3 was the highest that was felt to be allowable considering pressure drop and duct vibrations induced by turbulence at fittings.

The axial inlet velocity of compressors is usually at a Mach number of 0.2 and rarely exceeds 0.4. Several iterations of pressure drop calculations will be required during the process of integrating the ductwork with the wing structure to finalize the duct sizes.

The compressor power and volume displacement penalties of the suction system for laminarization Sheme 2 were nearly double those for scheme 1. The results of systems requirements and penalties are summarized in Table 4.2.2.1.

4.2.3 Weights Analysis

The 7700 Ft^2 wing reference area 733-633 SST configuration was the basic geometry airplane used to configure the suction system for hybrid laminar flow control (HLFC). This configuration was modified to install suction systems for laminarization schemes 1 and 2 as shown in Fig. 4.2.1.2-3. For laminarization scheme 1, two approaches to locating and powering the suction compressors, one mechanical and the other electrical, were explored as discussed in Section 3.4.2. The mechanical shaft drive approach was found to be superior from the power requirement and equipment weight points of view. On the basis of this finding, only the mechanical shaft drive approach was considered for laminarization scheme 2. The systems layouts for laminarization scheme 1 are shown in Fig. 3.4.1-1 and Fig. 3.4.1-2 for electrical and mechanical drive systems respectively. Fig. 3.4.1-3 shows the systems layout of mechanical drive system for laminarization scheme 2. Weight estimates were made for all three suction systems including structural ducting, equipment and installation weight penalties.

4.2.3.1 Methodology/Assumptions

The conceptual design of suction systems discussed in Section 3.4. provided a description, count, location and layout of the required components for the three configurations. These components were grouped

into suction system components, suction system drive components and structural weight penalties. In general weight estimates were made on the basis of vendor inputs, Boeing engineering inputs and calculations of the system ducting layouts. Appropriate factors were included for routing and installations of components and ducting. The total fuel volume displaced by the suction and exhaust ducting routed through the fuel tanks as well as the equipment bays was also calculated. Description, weight basis and appropriate installation factors are shown for the individual components.
At the time the present weights analysis was performed, the development of the structural concept described in Chapter 3 was not completed. Therefore, reasonable estimates of weight penalties associated with installation of titanium suction surfaces imbedded in the composite structure were applied. A perforated titanium outer skin of 0.040 in thickness, a titanium honeycomb core and an epoxy composite inner skin were assumed for the sandwich construction as shown in Fig. 4.2.3.1. The weight penalty of this sandwich panel was determined by comparison with an all composite sandwich of equal strength. Suction plenums, made of epoxy composite material, were assumed to be attached to the inner skin to collect the flow from the suction regions and route it to the tapered spanwise collector ducts via a series of feeder ducts. The outflow from the taper ducts was routed to the compressor inlet via suction ducts. All ducts were assumed to be made of epoxy composite material.

The importance of minimizing the fuel volume penalty became clear after the net performance benefits were evaluated for the suction system layouts as shown in Figs. 3.4.1-1, 3.4.1-2, and 3.4.1-3. Improved structural concept development work was initiated for efficient integration of suction ducts with the load bearing structure as described in Section 3.3.2. However, the impact of this improved design concepts on the weight and volume displacement penalties as well as on the net performance benefits was not evaluated.

4.2.3.2 Component Definitions/Descriptions/Assumptions

Suction system components

a. compressors - modified vendor supplied data+10% installation, see section 3.4.6 and figure 3.4.3-2 for more details.

b. compressor/motor cooling - allowance for heat rejection of dry bay mounted motors/compressors, see section 3.4.5.

c. suction ducting - .05 single wall composite, 10% duct routing factor, 50% of duct wt for installation.

d. suction plenums - same projected area as suction regions.

e. exhaust ducting - .05 inconel inner wall/.05 titanium outer wall, 25% of exhaust duct wt. for installation

f. slat modification - allowance to section leading edge slat in order to separate suction regions.

Suction system drive components

a. auxiliary drive mechanism - shafts,clutches and gearboxes between engine and compressors, see section 3.4.6.

b. generator/converters - added electrical generation and conversion equipment to drive the compressors, based on lb/HP factor.

c. power wiring - 270VDC generator to aft E/E bay converters, 400 VAC to converter motors, estimate based on power carrying capacity and measured length of the feeders.
d compressor motors - vender data, 10% installation, see section 3.4.6.

Structural penalties

a. equipment dry bays - measured volume x 2.5 lb/ft3.

b. holes for ducts through spars/ribs - allowance based on 2x removed weight of penetrated area.

c. suction skin allowance - .04 thick titanium sheet for suctioned areas.

4.2.3.3 Results of Weights Analysis

Table 4.4.2.3-1 shows major configuration differences such as compressor drive, count, total horsepower and suctioned regions. Table 4.2.3.3-2 shows the delta weight to the 733-633 SST geometry for the three configurations.

In general, comparing delta weights for the electrically driven compressors(+7675 lbs) vs the mechanically driven system(+6000 lbs) for the same regions, the mechanical system is lighter and displaces approximately the same fuel volume. The added weight for the conversion equipment of the electrical system is not offset by the flexibility of the compressor location. Locating the compressors closer to suctioned areas reduces the suction ducting weight but not enough to compensate for the added weight of the extended exhaust ducting.

Configuration 3, (scheme 2) which added suction to the inboard strake region, almost doubles the required compressor horsepower and displaced fuel volume and increases airplane suction regions to fourteen. But, by combining regions of nearly the same inlet pressures, only 10 compressors

TABLE 4.2.3.3-1

CONFIGURATION COMPARISION

	CONFIGURATION 1 scheme 1	CONFIGURATION 2 scheme 1	CONFIGURATION 3 scheme 2
Laminarization scheme			
Compressor drive	shaft	electric motor	shaft
Suction regions/airplane	8	8	14
Suction regions see figure 3.2.1-1	upper/lower outbd slat upper/lower outbd wing 30>40 % chord	same as config 1	same as config 1 plus upper/lower strake
Number of compressors/airplane	8	8	10
Total compressor horsepower	625	625	1220
Maximum suction duct diameter(in)	13.9	13.9	16.8
Leading edge slat	moveable	moveable	fixed strake moveable outbd
Total configuration delta weight (lbs)	6000	7675	8600

TABLE 4.2.3.3-2

WEIGHT SUMMARY

	CONFIGURATION 1 Scheme 1 MECHANICAL DRIVE	CONFIGURATION 2 scheme 1 ELECTRICAL DRIVE	CONFIGURATION 3 scheme 2 MECHANICAL DRIVE
SUCTION SYSTEM	**LBS/AIRPLANE**	**LBS/AIRPLANE**	**LBS/AIRPLANE**
COMPRESSORS/INSTALLATION	680	680	1030
COMPRESSOR COOLING	130	130	260
SUCTION DUCTING(single wall .05 composite)	1330	1085	2375
EXHAUST DUCTING(double wall inconel/titanium)	810	1540	765
L E SLAT MODIFICATION	210	210	290
(upper/lower suction region seperation)			
TOTAL SUCTION SYSTEM WEIGHT	3160	3645	4720
SUCTION SYSTEM DRIVE			
AUXILARY DRIVE MECHANISM	700	100	1630
GENERATORS/CONVERTERS (Delta 640 KVA)		840	
POWER WIRING(generator to compressor/motors)		650	
COMPRESSOR MOTORS/INSTL		255	
COMPRESSOR MOTOR COOLING		130	
TOTAL SUCTION SYSTEM DRIVE DELTA WEIGHT	700	1975	1630
STRUCTURE PENALTY			
COMPRESSOR DRY BAY	310	325	570
HOLES FOR DUCTS THRU SPARS/RIBS	310	210	770
REVISE L E SLAT(Apply porous ti skin)	720	720	1010
REVISE WING(porous ti wing skin sections)	800	800	800
TOTAL STRUCTURAL WEIGHT	2140	2055	3150
CONFIGURATION DELTA WEIGHT	**6000**	**7675**	**9500**
CHANGE STRAKE MOVEABLE LEADING EDGE SLATS TO FIXED	0	0	-900
TOTAL CONFIGURATION DELTA WEIGHT	**6000**	**7675**	**8600**
TOTAL FUEL VOLUME DISPLACED(FT3)	**445**	**440**	**825**

were needed and the system weight increased by 60%(+9500 lbs prior to any weight credit for a fixed leading edge on the strake).

These system delta weights were developed for a point design airplane of 7700 ft2 wing reference area and were scaled by wing area ratios during the sizing process.

4.2.3.4 Estimate of Weight Savings Due to Wing Root Thickening

The accomodation of the fuel displaced by the suction system by thickening the wing root region was discussed in Section 4.2.1.2 together with the associated wave drag penalty. The weight savings due to increased structural efficiency are discussed here. Of the total wing weight of 90000 lb, 30 percent is between the body side and 20 percent span stations. Thus the baseline structural weight of the wing inboard of the 20 percent semispan station is approximately 27000 lb. An average thickening of 7 percent in this region would be expected to decrease the weight by the same percentage amount. This results in a 2000 lb reduction in the OEW. This OEW reduction benefit was included in the net performance benefit analysis.

4.2.3.5 Weight Risk Areas

The weight estimate of the auxiliary drive mechanisms are a risk area because of the lack of detailed definition, estimation methodology, complication of installation and magnitude of the weight involved. Other areas,which are cause for concern, are the design definition of the fuel tank ducting installations, leading edge detail design and outboard wing fuel tank area suction system. In future HLFC studies each of these areas must be addressed at a more detailed level.

4.2.4 Propulsion System Performance Penalty

The power requirement to drive the suction compressors for schemes 1 and 2 was established in Section 4.2.2 after considerations of trades between suction air momentum drag on the one hand and equipment power and weight requirement on the other. The power required to drive the suction pumps could either be provided by an auxiliary power unit (APU), or it could be extracted from the main engines. The existing systems arrangement on the baseline configuration relied on power extraction from the main engines for auxiliary power and did not employ an APU. It was decided to pursue the same approach for powering the suction compressors in the interest of minimizing the weight penalty and complexity. After considerations of weight and power requirement penalties, a direct shaft drive approach was adopted. This approach was more efficient in terms of power transmission from main engines to the suction compressors than any other approach considered.

In comparison with the cruise power generated by the main engines, the power extracted to drive the suction system is indeed quite small. For example, the total cruise thrust required is approximately 70,000 lbf at M = 2.4, which translates into 300,000 HP thrust power. The actual power generated by the engines in terms of the jet kinetic energy is even higher because of the propulsive efficiency being less than unity. The 1200 Hp required at cruise to drive the suction compressors in l .ninarization scheme 2 is thus less than 0.4 percent of the total power generated by the engines at cruise condition. T. engines are usually sized for transonic thrust requirements and are oversized for takeoff and cruise conditions. Since the suction system was inoperative at transonic acceleration, no increase in engine size was necessitated.

The actual impact on the engine performance was evaluated by means of the Boeing GSA program, assuming the GE STJ858 (M = 2.4) turbine bypass turbojet as the power plant. The net penalties of shaft power extraction were as follows:

Table 4.2.4-1

Propulsion System Performance Penalty

Laminarization Scheme	Scheme 1	Scheme 2
Shaft Power Extracted	626 HP	1226 HP
Cruise TSFC penalty	0.1 %	0.2 %
Cruise Thrust Penalty	0.1 %	0.2 %

These penalties were incorporated in the performance and sizing program by applying the same percent loss in engine performance at lower Mach numbers in the supersonic climb and descent segments of the mission.

4.3 COMPARISON OF SIZED AIRPLANES

In this section, the net benefits of LFC implementation on SST performance and size characteristics are presented. These results were obtained by incorporating the "uncycled" benefits and penalties of LFC, as determined in Section 4.2, into the Boeing Mission Performance and Sizing Program

(A226) data base, generating mission-sized airplane characteristics for both LFC and turbulent designs and comparing the two.

Section 4.3.1 presents summary percentage changes in required airplane size characteristics due to the implementation of LFC and discusses the various factors impacting the results. Section 4.3.2 describes the mission profile and constraints assumed in the performance and sizing computations.

4.3.1 Summary Results and Discussion

Ten sets of sized airplane characteristics were generated in the Design/Benefits studies. These represent the baseline turbulent airplane and four laminarized configurations, each sized for two design ranges: 5000 and 6500 n.mi. The results are summarized in Table 4.3.1. The four LFC configurations represent two basic laminarization schemes, namely outboard wing only (LFC Scheme 1) and outboard wing plus strake (LFC Scheme 2). Scheme 2 is further divided into three cases in order to evaluate (a) the effects of increasing available fuel volume. (L2.1 in the table) and, (b) the sensitivity of the results to system weight assumptions (L2.2).

Table 4.3-1 is also divided into three sets of columns. The left-most set of columns shows the "uncycled" percentage increments (in drag, weight, sfc and available fuel volume) obtained by installing each LFC system variation on a reference airplane with an MTOW of 750,000 lb and a wing area of 7700 square feet. Since this configuration is only a starting point and is not used directly in the sizing process, these increments should be used as a comparison reference only.

The middle set of columns shows the incremental effects of applying LFC for a design range of 5000 N. MI.: the top row shows the summary characteristics of the mission-sized turbulent airplane (Model 1080-834) while the rows pertaining to the LFC schemes show the percentage changes in these characteristics for mission-sized airplanes employing each of the several LFC variations. For example, the mission-sized airplane characteristics obtained using LFC configuration L2.1 were an MTOW of 682,000 lb; an OEW of 303,000 lb; block fuel of 286,000 lb; wing area of 6770 sq. ft. and an engine airflow of 525 lbm/sec. When compared with the corresponding turbulent airplane characteristics, percentage changes of -8.5, -6.2, -12.0, -9.3 and -9.8 are obtained. The right hand set of columns shows similar comparisons for a design range of 6500 n.mi.

The results show that from fuel burn and airplane size points of view, LFC is beneficial in all the cases examined. As discussed above in Section 4.1.2, the magnitude of the benefit is partly a function of the relative magnitude of the incremental drag and weight changes, and it can be seen that in all cases except L2.2, the uncycled net percentage change in total drag is of the order of three times the uncycled net percentage change in OEW.

TURBULENT	Model 1080-834	UNCYCLED (FIXED AIRPLANE SIZE) (S=7700 FT2; Wa=630 lb/sec; MTOW=750 klb) INCREMENTS						5000 NMI DESIGN RANGE SIZED AIRPLANES					6500 NMI DESIGN RANGE SIZED AIRPLANES				
		CRUISE FRICTION DRAG	OTHER DRAG COM-PONENTS	SYSTEM RELATED OEW	OTHER OEW COM-PONENTS	CRUISE SFC	VOLUME-TRICALLY AVAILABLE FUEL CAPACITY	MTOW ~1000LB	OEW ~1000LB	BLOCK FUEL ~1000LB	WING AREA FT2	ENGINE AIRFLOW LBM/SEC	MTOW ~1000LB	OEW ~1000LB	BLOCK FUEL ~1000LB	WING AREA FT2	ENGINE AIRFLOW LBM/SEC
		BASE	BASE	BASE	BASE	BASE	BASE	745	323	325	7466	582	1170	471	578	11,350	863
		PERCENTAGE CHANGES WITH LFC						PERCENTAGE CHANGES WITH LFC					PERCENTAGE CHANGES WITH LFC				
LFC SCHEME 1	L1.0 • DATUM WING THICK-NESS	-6.0 (OF TOTAL AIRPLANE DRAG)	+0.2 MOMEN-TUM	+1.8	0	+0.1	-5.2	-6.6	-4.1	-9.9	-4.2	-8.9	-10.7	-7.8	-13.9	-6.9	-12.9
LFC SCHEME 2	L2.0 • DATUM WING THICK-NESS	-8.2	+0.3 MOMEN-TUM	+2.7	0	+0.2	-8.2	-7.2	-3.4	-12.0	-3.5	-9.5	-12.6				
	L2.1 • THICKENED WING ROOT	-8.2	+0.3 MOMEN-TUM +0.8 WAVE	+2.7	-0.7	+0.2	0	-8.5	-6.2	-12.0	-9.3	-9.6	-12.6	-9.8	-15.9	-11.7	-13.6
	L2.2 • L2.1 WEIGHT SENSI-TIVITY	SAME AS L2.1	SAME AS L2.1	+5.4	-0.7	SAME AS L2.1	SAME AS L2.1	-4.4	-0.7	-8.6	-6.5	-6.4	-7.5	-2.9	-11.8	-7.6	-8.8

TABLE 4.3.1 DESIGN/BENEFITS STUDY SUMMARY RESULTS

In case L2.2, where the calculated LFC system weight penalty was arbitrarily doubled, the relative leverage of drag over weight is obviously much reduced. However appreciable benefits in sized airplane fuel burned and gross weight were still obtained, and even OEW showed a slight reduction.

As expected, and again as discussed in Section 4.1.2 above, LFC benefits increase as the design range requirement is increased.

Although the relative leverage of drag over weight is an indication of LFC system efficiency, the magnitudes of the changes are obviously also important in determining the sized airplane benefits, as a comparison of L1.0 with L2.0 reveals. Laminarization of the outboard, supersonic-leading-edge portion of the wing, as represented by L1.0, can be achieved relatively efficiently because of relatively modest suction requirements, as discussed above in Sections 2.8 and 4.2.2. However, the magnitude of the skin friction drag reduction achievable is obviously limited. The additional system required to laminarize the strake call for substantially more powerful, heavier, compressors and larger ducts, for an additional 2% total airplane drag reduction. The drag/weight "leverage" achieved with L2.0 is reduced from that of L1.0 (5.8%/1.8% as compared to 7.9%/2.7%) but because the magnitude of the drag reduction benefit is larger, the sized L2.0 airplanes still show an additional benefit when compared with the L1.0 airplanes.

Early on in the airplane sizing studies it became apparent that the limited fuel volume available in the double delta wing was constraining the wing loadings of all designs to values lower than those required to meet takeoff field length and approach speed constraints (12,000 feet and 160 knots respectively). As discussed in Section 4.1.2 above, wing loading has an important impact on empty weight and should be maximized within the bounds imposed by the performance constraints. The turbulent airplane "Thumbprint" chart (see section 4.3.3 below) for 5000 n.mi. design range revealed, for instance, that the required gross weight was 5% higher when the fuel volume constraint was satisfied than it would have been if the constraint were hypothetically removed. Since the wing fuel capacity of the laminarized airplanes was being further eroded by LFC system volume requirements, this became a matter of concern for the LFC designs, particularly Scheme 2 which was found to displace 8% of the wing fuel volume for the 7700 sq. ft. reference wing size.

It was argued that what could be done to the LFC airplanes to increase fuel capacity could also be done to the turbulent design, and that any comparison between LFC and turbulent designs should be done on as consistent a basis as possible. However, it was also argued that, (a) strict consistency could not be achieved anyway within the limited time and budget available, (b) the fuel volume constraint was probably more of a penalty to LFC Scheme 2 than to the turbulent airplane, and (c) the magnitude of the potential penalty was large enough to warrant further exploration. It was therefore decided to study a variation of Scheme 2, designated L2.1 featuring a wing root section

which was thickened just enough to replace the fuel volume displaced by the LFC system.

Comparison of L2.1 with L2.0 in Table 4.3.1 shows that thickening the wing root appears to be a favorable trade for the 5000 n.mi. design. Most of the benefit probably derives from the fact that, although still constrained by fuel volume (as discussed in the comparison of thumbprints below in Section 4.3.3), the impact of the constraint has been reduced. Thickening the wing results in a wave drag penalty of roughly 0.8% of airplane drag, but this is largely compensated for by a more efficient wing structure which results in a 0.7% reduction in uncycled O.E.W. (relative to L2.1).

Comparison of L2.1 with L2.0 for the 6500 n.mi. design range case, however, leads to a different conclusion. Since the fuel volume available in the wing varies roughly as the 1.5 power of wing area and outpaces the variation of fuel volume required, the impact of the fuel volume constraint is much reduced: in fact, in both cases, the fuel volume constraint lies very close to the 12,000 ft. takeoff field length line. In this case, no gross weight benefit is obtained by increasing the available fuel volume, and in fact a small block fuel penalty (relative to L2.0) is incurred due to the wave drag increment.

It is apparent that it is not possible to ascribe an unqualified set of values for the benefits of laminar flow control: the benefits are dependent on many factors, the primary ones being the details of the system implementation, design range, the airplane configuration, its available fuel volume, and the manner in which the required airplane size is constrained by mission performance requirements.

The net performance benefits in terms of MTOW, OEW and block fuel reductions calculated for the LFC configuration L2.1 (see Table 4.3.1) as compared to the turbulent baseline configuration Model 1080-834 are shown in Figure 2 of the Executive Summary section of this report.

4.3.2 Mission Profile and Constraints

The mission profile used in the performance and sizing calculations is shown in Figure 4.3-2. A total of ten "segments" is used to describe the mission, with the reserve segments being treated as part of the mission for fuel computation purposes. Total range is computed from the end of takeoff (end of segment 2) to the approach pattern outer marker (end of segment 5). Block fuel is computed from the beginning of departure taxi (beginning of segment 1) to the end of arrival taxi (end of segment 10) with the reserve fuel (segments 7, 8 and 9) excluded. The 6% trip fuel allowance is assumed to be "burned" as the first reserve segment: in other words it is carried (as a weight penalty) in segments 1 through 6, but not in reserve segments 8 and 9.

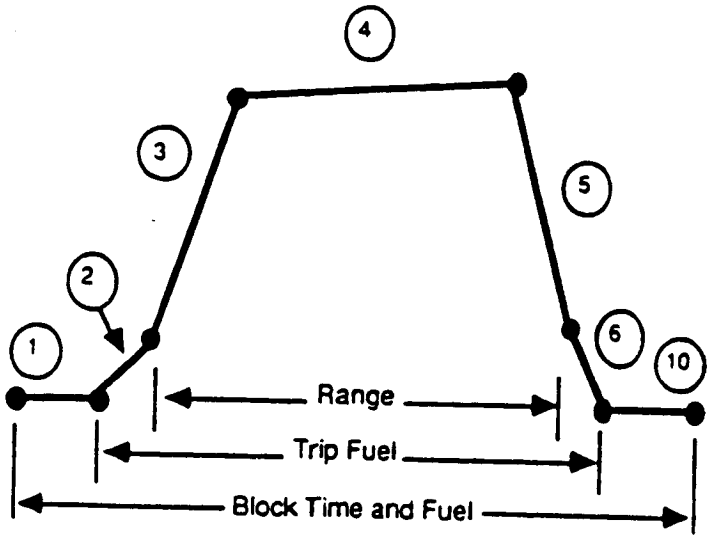

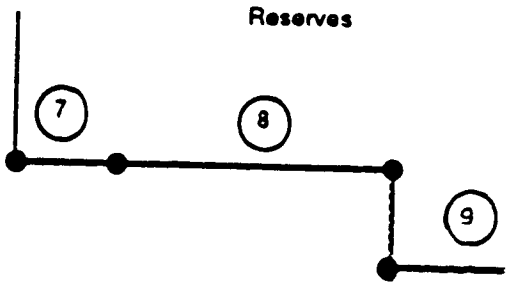

1	Taxi	10 min, h = 0, ground idle fuel flow
2	Takeoff	To h = 35 ft
3	Accelerate and climb to best cruise altitude	To M = cruise
4	Supersonic cruise	Climb cruise
5	Descend and decelerate	Flight idle fuel flow
6	ILS appraoch	To touchdown
7	Allowance	6% trip fuel
8	Subsonic cruise to alternate	M = 0.9, h = 37,800 ft, R = 260 nm
9	Hold	30 min, h = 15,000 ft, M = optional
10	Taxi	5 min, h = 0, ground idle fuel flow

Figure 4.3-2 Flight Profile and Reserves

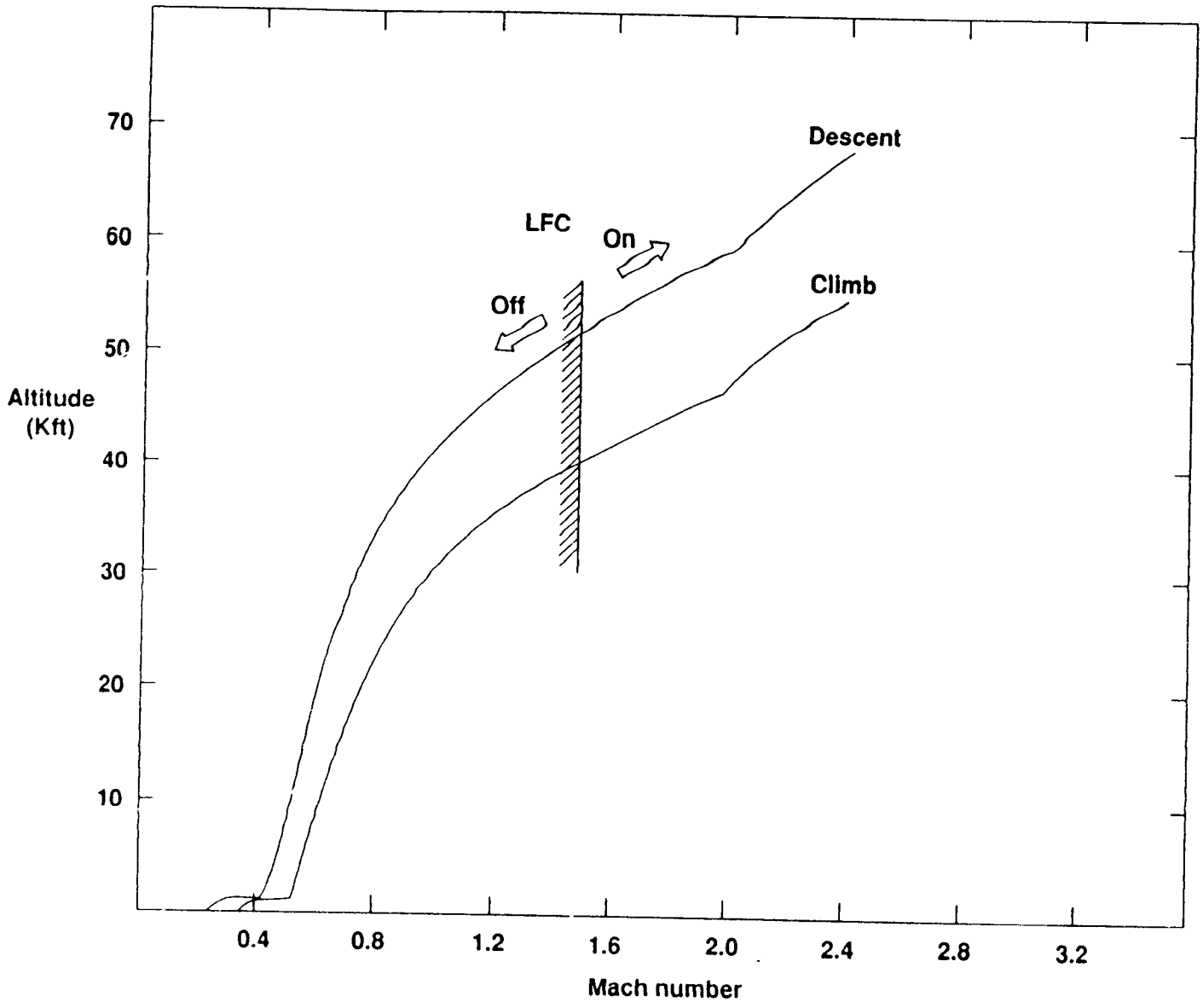

Figure 4.3-3 Climb and Descent Speed/Altitude Schedules

Nominal altitude versus Mach number trajectories for climb and descent are shown in Figure 4.3-3. These are based on trajectory optimization studies performed during the U.S. SST program and strike a compromise between the conflicting requirements of minimum fuel consumption, transonic acceleration margin requirements, sonic boom intensity and structural and flutter "placards". Since structural placard considerations predominate during climb, no attempt was made to re-optimize the trajectories for different thrust-to-weight ratios or wing loadings. Climbing cruise is assumed along an optimum-fuel-mileage altitude versus weight schedule (subject to available thrust constraints). Small "disconnects" between the nominal trajectory end-of-climb and start-of-descent altitudes, and the corresponding altitudes for optimum cruise fuel flows are accounted for by inserting additional segments representing constant-Mach climb or descent, or constant-altitude cruise.

A design payload of 51,900 lb was assumed in all sizing studies. this represents 247 passengers plus baggage at 210 lb per passenger. The fuselage and passenger accommodations were configured and weighed assuming a "tri-class" layout with a first class, business class and tourist "mix" of 8%, 19% and 73% respectively.

Mission performance requirements, which were applied as constraints in the Thumbprint selection process, are as follows:

- Takeoff Field Length: FAR field length not to exceed 12,000 ft at sea level, 86^{o}F at Maximum Takeoff Weight (MTOW).

- Approach Speed: Not to exceed 160 knots at Maximum Landing Weight (MLW).

- Climb Thrust Margin: 30% transonic (acceleration through M1.1); 10% supersonic (top-of-climb)

  Climb Time: Time to climb to initial cruise altitude not to exceed 45 minutes.

5.0 CONCLUSIONS

The following are the principal conclusions resulting from this initial study on the application of laminar flow control to a supersonic transport configuration:

1. The present study revealed the aerodynamic feasibility of achieving significant laminarization on the wing surface of a supersonic transport configuration. Preliminary assessment of systems and structural requirements to achieve this laminarization showed that the aerodynamic benefits of drag reduction outweigh the system weight, volume and power requirement penalties. The net benefits in terms of reductions in MTOW, OEW, and fuel consumption are impressive and improve with increasing mission range.

2. For the Mach 2.4 cruise, 5000 NMI mission, LFC implementation resulted in 8.5, 6.2, and 12.0 percent reductions respectively in MTOW, OEW, and fuel consumption when compared with a baseline turbulent configuration. For a 6500 NMI mission, these benefits increased to 12.6, 9.8, and 16.0 percent, respectively. A preliminary calculation showed a 25 percent reduction in fuel heating rate resulting from the implementation of laminarization scheme 2.

3. Linear stability analysis showed stabilizing influence of increasing Mach number on the 2D boundary layer TS disturbances. Mild suction and cooling further enhanced this stability even in 3D boundary layers. However, the influence of the latter parameters on the crossflow instability was rather weak. Therefore, careful tailoring of wing pressure distributions, together with strong suction will be needed to control the crossflow instability and achieve high transition Reynolds numbers on the wing surface.

4. While a significant run of natural laminar flow is achievable on a sharp supersonic leading edge wing, attachment line instability and rapid crossflow development in the vicinity of a rounded, highly swept subsonic leading edge would lead to an early transition. Strong suction at the level of C_q = 0.002 would be needed in the attachment line region to suppress the attachment line and crossflow instabilities.

5. The preliminary structural and systems concept development work performed during this study showed the feasibility of installing a LFC suction system in an existing SST configuration at acceptable weight, volume, and power requirement penalties. Further reductions in installation penalties appear feasible with refinements of these concepts.

6. Of the various methods for powering the suction compressors, direct shaft power extraction from the engines was found to be the best from the standpoint of transmission efficiency and system weight. The

penalties for extraction of shaft power from the main engines to drive the suction compressors were rather small: a 0.2 percent loss in engine thrust and the same percent increase in TSFC.

7. Compressor power and weight penalties dictate that the suction air be discharged at a velocity much less than the freestream velocity, even at the expense of a suction air momentum drag penalty. The condition of sonic discharge was found to be the best compromise.

8. The present study pointed to a need for a significant research and development effort in aerodynamics, structures, and systems technologies in order to realize the potential benefits of LFC implementation in a practical system.

   - The need for a supersonic 3D nonlinear wing design capability to achieve pressure distributions desirable for laminar flow design. A general 3D boundary layer and stability analysis capability is also needed.

   - A flight transition database on 3D supersonic boundary layers is needed to formulate reliable supersonic transition criteria.

   - Supersonic LFC concepts utilizing suction through a perforated surface need to be validated for rounded subsonic leading edge and sharp supersonic leading edge wings in wind tunnel and flight tests.

   - A host of issues related to suction system design, structural integration, flow control, safety, reliability, and maintainability need to be addressed. Additionally, concepts for leading edge protection and cleaning, anti-icing, deicing, erosion control, and highlift system compatibility need to be developed.

6.0 RECOMMENDATIONS

Several research needs were identified during the course of the present study for improvements in existing prediction capability, validation of laminarization concepts, assessment of the impact of laminar flow on the overall aerodynamic performance of the configuration as well as enhancement of the net benefits of LFC implementation.

I. Improved Transition Prediction and Wing Design Capability
II. Conceptual Design Studies
III. Wind Tunnel and Flight Experiments

An identification and brief description of tasks under the above three areas follows.

6.1 IMPROVED TRANSITION PREDICTION AND WING DESIGN CAPABILITY

Tasks in this area relate to improvements in prediction methodology for transition on SST Configurations, nonlinear wing design capability, as well as for boundary layer control on highly swept wings.

6.1.1 Invisid Flow Field Prediction

Several discrepancies were observed in the configuration Cp predictions by three inviscid techniques. Also, the resolution of the predictions was inadequate in the sharp leading edge region. An improved resolution of Cp prediction in the leading edge region is needed using solution adaptive or zonal grid structure. Experimental validation (in wind tunnel or flight) of Cp predictions is needed to resolve the differences observed between linear and nonlinear methods.

6.1.2 Coupled 3D Boundary Layer Solution

A 3D boundary layer solution coupled with the calculated inviscid flow field is needed for subsequent stability analyses. The influence of boundary layer development on the calculated inviscid Cp distribution also needs to be evaluated.

6.1.3 Full 3D Stability Analysis Capability

Current approach employs stability analysis and integration of growth rates

performed on boundary layers calculated under swept, tapered wing (conical flow) approximation. Procedures for stability calculation and growth rate integration on full 3D boundary layers need to be developed.

6.1.4 Wing Design Capability to Obtain a Desired Cp Distribution for Laminar Flow

Achievement of a significant run of laminar flow on the wing surface requires a specific type of Cp distribution. Methods need to be developed to design wing sections of a 3D configuration to yield this type of Cp distribution. Existing linear wing design methods could be modified to accomplish this. However, a nonlinear, inviscid (full potential or Euler) design capability would be desirable. The impact of a laminar flow wing design on the configuration drag components also needs to be evaluated.

6.1.5 Curvature Effects on Supersonic Boundary Layer Stability

Recent work [47] has shown that convex streamline curvature has beneficial influence on subsonic boundary layer stability. Curvature effects are important in the subsonic, rounded leading edge region of SST configurations and their influence on the 3D supersonic boundary layer stability should be evaluated.

6.1.6 TS and CF Wave Interactions in Supersonic Boundary Layers

Current theoretical treatment of TS and CF wave interactions and its effects on 3D boundary layer stability should be extended to supersonic boundary layers.

6.1.7 Entropy Layer Effects Near Sharp Nosed Supersonic Leading Edges

The presence of a finite nose radius on a "sharp" leading edge airfoil causes a local supersonic blunt body flow with a detached curved shock. The shock curvature causes an "entropy layer" effect in which the initial boundary layer development is under an edge velocity which is lower than the far field stream velocity. This has a beneficial effect on the boundary layer stability. The extent of this benefit needs to be evaluated analytically and weighed against the wave drag penalty caused by the blunt nose.

6.1.8 Stability of Attachment Line Boundary Layer

The momentum thickness criterion for transition in the attachment line boundary layer is based on low speed test data. Transition criterion for the attachment line boundary layer based on stability theory calculations is needed. The effect of supersonic Mach numbers radius of curvature, sweep angle and of suction and cooling on the attachment line boundary layer stability needs to be evaluated.

6.1.9 LFC Effectiveness at Transonic and "Off Design" Supersonic Mach Numbers

The effectiveness of any laminar flow control scheme designed for supersonic cruise conditions must also be evaluated during transonic acceleration and supersonic climb.

6.1.10 Suction Air Slot Injection Effectiveness for Turbulent Skin Friction Reduction

The discharge of LFC suction air through a slot in a region of the configuration surface where the boundary layer is turbulent offers a possibility of some reduction in turbulent skin friction coefficient. The required flow rates, however, should be matched with the flow rates available from the LFC suction system and the impact on wave drag and wake momentum drag should be considered.

6.1.11 Establish Suction Requirements for Low Speed Boundary Layer Control on Highly Swept Wings at High Lift Conditions

Availability of suction in the leading edge region offers the possibility of boundary layer control to prevent separation and vortex formation and thereby improve the L/D ratio at low speed, high angle of attack conditions. The 3D boundary layer separation behavior on highly swept rounded leading edge wings as well as at the hingline of sharp leading edge drooped nose wings at high angles of attack conditions needs to be studied. Suction requirements to prevent boundary layer separation for both types of situations need to be determined.

6.2 CONCEPTUAL DESIGN STUDIES

Tasks in this area relate to practical aspects of LFC application to supersonic transport configurations and systems approach to determining the net performance benefits.

6.2.1 HLFC System Design and Net Benefits for Highly Swept Leading Edge Configurations

The configuration selected for the present study has a double delta planform with an outboard wing having a supersonic leading edge. It would be worthwhile looking at configurations having an all subsonic leading edge such as the arrow wing planform. The suction requirements at the leading edge are likely to be higher, but the crossflow instability will be less of a problem downstream of the leading edge region provided a streamwise zero pressure gradient is achieved in this region. Furthermore, for this type of configuration, wave drag is lower and skin friction drag higher due to the increased wetted area. Therefore, viscous drag reduction by LFC implementation will have greater impact on the total drag.

6.2.2 Suction Surface Flow Control and Integration with Composite Structure

Structural design concepts for assemblies of perforated suction surface and internal flow passages which allow the desired suction distribution for a specified external pressure distribution need continued development. The pressure drop through the internal flow passages will have to be carefully controlled to achieve the desired suction distribution without excessive internal pressure losses. Concepts for metering and regulating the internal flow through the duct system will also need to be developed. Concepts for structural integration of suction surface assemblies with the composite wing structure within the acceptable tolerances for surface mismatch need to be developed. Work on development of manufacturing and fabrication techniques for suction surface assemblies and its integration with composite structure should be initiated early.

6.2.3 Structural Concepts for Integrated Suction Ducts

Drag reduction due to implementation of LFC on a SST results in significantly less of fuel required for a mission. Since the type of configuration considered in the present study is fuel volume limited, a reduction in the wing area is possible with associated structural weight reduction. However, since the laminar flow control suction system displaces

a significant fraction of the fuel saved, full benefits of reduction in the wing area and the associated structural weight are not realized. Innovative structural concepts which integrate suction ducts with the load bearing structure would minimize the fuel volume displacement penalty and allow greater net benefits to be realized by LFC implementation.

6.2.4 Wing Planform Area Reduction by Fuel Volume Redistribution

The volume of fuel displaced by suction ducts could be accommodated near the wing root if the root thickness is increased together with the necessary adjustments of the fuselage cross sections. This will lead to increased wave drag, however, improved structural efficiency will allow some structural weight reduction. The availability of the extra fuel volume will allow accommodation of the displaced fuel and therefore a reduction in the wing area up to the point where the wing size is constrained by the takeoff field length (TOFL) or approach speed limitations.

6.2.5 LFC Using Passive Suction - Particularly for Nacelles and Empennage

The nature of pressure distribution particularly on a supersonic leading edge wing section offers decreasing surface pressures from leading to trailing edge on both upper and lower surfaces. If laminarization is attempted only on the forward portion of the wing, the decreasing surface pressures present a possibility of using passive suction on the forward part and venting the suction air to the lower pressure aft region (where no laminarization is attempted) via an internal duct system. Provided the duct pressure losses can be kept to a minimum, passive suction without mechanical compressors may be possible.

6.2.6 Suction Requirements for Laminarization of Fuselage and Wing/Body Junction

Suction laminarization of the fuselage offers a potential for further drag reduction, although at the expense of additional hardware. An important benefit of fuselage laminarization may be the elimination of the turbulent wedge at the body side, which propagates on the wing surface and significantly reduces that portion of the wetted area of a highly swept wing which could potentially be laminarized.

6.2.7 Systems for Protection from Insect Contamination, De-icing and Anti-icing

Systems concepts for protection of the leading edges from contamination due to insect impacts, deicing and anti-icing need to be developed for compatibility with LFC and high lift BLC requirements. Insect contamination characteristics of highly swept round leading edge wings as well as moderately swept sharp leading edge wings in high lift configuration need to be determined. Several leading edge protection concepts available from subsonic LFC applications need to be explored for applicability to highly swept rounded or moderately swept sharp leading edge wings. Behavior of residues from insect impact under high shear, aerodynamic heating conditions typical of supersonic cruise need to be studied.

6.3 WIND TUNNEL AND FLIGHT EXPERIMENTS

Tasks in this area relate to i) acquisition of a database for development of supersonic transition criteria, ii) validation of laminarization concepts developed in the present study iii) assessment of laminar flow design on other drag components of an SST configuration and iv) determination of the effectiveness of the LFC suction system when used as a boundary layer control system to improve the low speed performance.

6.3.1 Baseline Cp Data on Supersonic Cruise Configurations for Validation of 3D Codes

Wind tunnel and flight test data on wing pressure distributions are needed for validation of 3D boundary layer coupled inviscid codes.

6.3.2 Impact of Laminar Flow Design on Other Drag Components

Wind tunnel tests on a high speed model having a laminar flow wing design will be needed to assess the impact on zero lift wave drag and the drag-due-to-lift, as well as to validate linear and nonlinear code predictions.

6.3.3 Wind Tunnel Experiments to Test the Effectiveness of Suction in Suppressing CF Instability

Since even a small amount of suction is very effective in suppressing the TS instability and wind tunnel noise primarily affects the TS growth, suction laminarization experiments on unswept wings have been very successful in maintaining laminar flow up to high Reynolds numbers even in noisy tunnels.

Therefore if the TS growth is effectively suppressed with mild suction, the stronger suction requirements for suppression of CF growth may be studied even in noisy tunnels. Mild suction does not have an appreciable influence on CF growth.

By use of techniques similar to those developed for testing large size LFC models in low speed wind tunnels, relatively high Reynolds numbers may be achieved in the existing supersonic wind tunnels (e.g. AEDC-16S, NASA Ames 9' x 7' supersonic etc.).

On highly swept, rounded, subsonic leading edge wings, crossflow instability grows rapidly in the leading edge region, while on moderately swept, sharp, supersonic leading edge wings with a mild streamwise favorable pressure gradient, the CF instability grows slowly. Suction requirements to control the CF instability in both of these situations may be studied in conventional supersonic wind tunnels provided the growth of TS instability is suppressed by use of continuous mild suction on the wing surface.

6.3.4 Supersonic Transition Database Development

To establish a supersonic transition database for 3D boundary layers having both TS and CF types of instability, natural laminar flow flight tests on supersonic aircraft are needed. On rounded, subsonic .leading edge wings, attachment line instability and rapid initial growth of CF instability causes transition to occur at or very close to the attachment line. Therefore, a good spatial resolution is not available for transition measurements. Baseline natural laminar flow flight experiments should therefore be conducted on swept wings with a sharp, supersonic leading edge with a controlled streamwise pressure gradient. Such flight experiments could be performed on a supersonic fighter aircraft such as the F-104 with a sharp leading edge glove having a larger sweep than the baseline wing. Alternatively, this type of experiements could also be performed on the outboard wing panel of the F-16XL. The attachment line boundary layer at a sharp leading edge is inherently stable and initial cross flow instability growth in the leading edge region is small. A significant run of laminar flow may be obtained on the wing surface with a gradual buildup of TS and CF instabilities (N-Factors). The longer laminar run provides adequate spatial resolution for transition measurements. The TS and CF growths may be controlled by adjustments of streamwise pressure gradient or sweep angle by modifications of the glove design. Effects of surface cooling may also be investigated in such a flight experiment. The effects of leading edge nose radius of supersonic leading edge wings on transition may also be investigated. Increasing nose radius gives rise to entropy layer effect, which has a favorable influence on TS instability. However, increasing nose radius on a swept wing has a detrimental effect on attachment line and CF instabilities. Therefore, an

optimal nose radius for laminar flow design may be determined from such a flight experiment.

6.3.5 Supersonic HLFC Flight Tests

Supersonic HLFC flight tests will be needed to validate the laminarization concepts developed in the present study for both supersonic and subsonic leading edges. These tests will require design of suction gloves to yield specific (desired) pressure and suction distributions. Supersonic wing design capability and wind tunnel validation of glove Cp distributions will be needed in preparation for the flight test program. Stability calculations on the glove boundary layer will have to be performed and (previously developed) supersonic transition criteria applied to estimate transition location. For tests on subsonic leading edge, spanwise contamination of the attachment line boundary layer will have to be prevented. The HLFC flight experiments with a suction glove installed on a subsonic leading edge wing could be performed on the F-16XL aircraft recently acquired by NASA.

6.3.6 Low Speed Wind Tunnel Tests to Establish BLC Suction Requirements and Effectiveness

Low speed wind tunnel tests on highly swept, rounded leading edge wings as well as sharp leading edge drooped nose wings at high angles of attack need to be conducted to test the effectiveness of suction boundary layer control in preventing flow separation and vortex formation. For highly swept, rounded leading edge wings at high incidence angles, separation occurs near the leading edge in the adverse pressure region following the suction peak. The separation which begins at the outboard portion of the wing, results in vortex formation and moves progressively inboard as the angle of attack is increased. Because of the leading edge vortex formation, the pitching moment characteristics of highly swept wings become adverse at high angles of attack and result in the so-called "pitchup" problem. Since the separation pheonmena are viscous dominated, the pitchup problem is strongly Reynolds number (model scale) dependent. Suction requirements to preserve attached flow may be estimated from 3D boundary layer analyses, and wind tunnel tests at adequate model scale need to be conducted to verify the theoretical predictions of suction requirements.

On sharp leading edge drooped nose wings, fully attached flow could be maintained on the leading edge flap as well as past the hinge line if the flap is aligned with the approaching flow and suction boundary layer control applied in the hinge region. The possible benefits in terms of improved L/D of operating in this mode rather than in the trapped leading edge vortex flap mode need to be experimentally evaluated.

REFERENCES

1. Driver, Cornelius: How Different a Modern SST Would Be.. Aerospace America, November 1986.

2. Morkovin, M. V.: Instability, Transition to Turbulence and Predictability. AGARDograph No: 236. Presented at AGARD Fluid Dynamics Panel Symposium on Laminar-Turbulent Transition, Lyngby, Denmark, May 1977.

3. Kerschen, E. J.; Boundary Layer Receptivity and Laminar Flow Airfoil Design. Presented at Symposium on Natural Laminar Flow and Laminar Flow Control Research. NASA Langley Research Center, March 1987.

4. Schlichting, H.: Boundary Layer Theory. Sixth Edition McGraw-Hill Book Co. (1968).

5. Smith, A. M. O.: Transition, Pressure Gradient and Stability Theory. Proceedings of 9th International Congress of Applied Mechanics, Brussels. Vol. 4 (1956). Also Rept.-ES 26388 Douglas Aircraft Co. (1956).

6. Collier, F. S. and M. R. Malik: Stationary Disturbances in Three Dimensional Boundary Layers Over Concave Surfaces. AIAA paper No. 87-1412 (1987).

7. Reed, H.: Wave Interactions in Swept-Wing Flows AIAA paper No. 84-1678 (1984).

8. Preliminary Design Dept., Boeing Commercial Airplane Co.: F-111 Natural Laminary Flow Glove Flight Test Data Analysis and Boundary Layer Stability Analysis. NASA CR-166051, January 1984.

9. Anderson, B. T. and R. M. Meyer: Effects of Wing Sweep on Boundary Layer Transition for a Smooth F-14A Wing at Mach Numbers from 0.7 to 0.825 (Glove I). NASA TM 101712, May (1990).

10. Boeing Commercial Airplanes: Flight Survey of the 757 Wing Noise Field and Its Effects on Laminar Boundary Layer Transition. Vol. 1-3. NASA CR 178216 (1987).

11. Wagner, R. D., D. V. Maddalon and D. F. Fisher: Laminar Flow Control Leading Edge Systems in Simulated Airline Service. Presented at the 16th Congress of International Congress of

the International Council of Aerospace Sciences (ICAS), Jerusalem, Israel. Paper No. ICAS-88-3.7.4 Sept. (1988).

12. Bushnell, D. M. and M. R. Malik: Transition Prediction in External Flows via Linear Stability Theory. IUTAM Symposium Transonicum III. Göttingen, W. Germany May 1988.

13. Mack, L. M.: Stability of the Compressible Laminar Boundary Layer According to a Direct Numerical Solution. in AGARDograph 97 part I pp. 329-362 (1965).

14. Mack. L. M.: Linear Stability Theory and the Problem of Supersonic Boundary Layer Transition. AIAA Journal Vol. 13, No. 3. pp. 278-289, March (1975).

15. Reshotko, Eli: Boundary Layer Stability and Transition. Annual Reviews of Fluid Mechanics (1976).

16. van Driest, E. R. and J. C. Boison: Experiments on Boundary Layer Transition at Supersonic Speeds. Journal of Aeronautical Sciences Vol. 24, No. 12, December (1957).

17. van Driest, E. R. and C. B. Blumer: Boundary Layer Transition at Supersonic Speeds: Roughness Effects with Heat Transfer. AIAA Journal, Vol. 6, No.4. April (1968).

18. Rumsey, C. B. and C. F. Merlet: Supersonic Free-Flight Measurement of Heat Transfer and Transition on a 10 Degree Cone Having a Low Temperature Ratio. NASA TN-D951 August (1961).

19. Sternberg, J.: A Free-Flight Investigation of the Possibility of High Reynolds Number Supersonic Laminar Boundary Layers. Journal of Aeronautical Sciences, November (1952).

20. Beckwith, I. E.: Development of High Reynolds Number Quiet Tunnel for Transition Research. AIAA Journal, March (1975).

21. Pate, S. R. and C. J. Schueler: Radiated Aerodynamic Noise Effects on Boundary Layer Transition in Supersonic and Hypersonic Wind Tunnels, AIAA Journal, Vol. 7, No. 3, March (1969).

22. Wagner, R. D., Maddalon, D. V., and Weinstein, L. M.: Influence of Measured Free Stream Disturbances on Hypersonic Boundary Layer Transition. AIAA Journal Vol. 8, No. 9, September (1970).

23. Coles, D: Measurements of Turbulent Skin Friction on a Smooth Flat Plate in Supersonic Flow. Journal of Aeronautical Sciences, Vol. 21, No. 7, July (1954).

24. Reshotko, Eli: Recent Developments in Boundary Layer Transition Research. AIAA Journal, Vol. 13, No. 3, March (1975).

25. Beckwith, I. E. et al.: Design and Fabrication Requirements for Low Noise Supersonic/Hypersonic Wind Tunnels. Presented at Symposium on Natural Laminar Flow and Laminar Flow Control Research, NASA LaRC. NASA CP2487 March (1987).

26. Chen, F. J. et al.: Comparison of Boundary Layer Transition on a Cone and Flat Plate at Mach 3.5. AIAA paper No. 88-0411 (1988).

27. Fisher, D. F. and N. S. Daugherty: Inflight Transition Measurement on a 10 Degree Cone at Mach Numbers from 0.5 to 2.0. NASA TP-1971 (1982).

28. Malik, M. R.: COSAL - A Black Box Compressible Stability Analysis Code for Transition Prediction in Three Dimensional Boundary Layers. NASA CR-165925, May 1982.

29. Bonner, R. D., J. G. McTigue, and G. Petty: Boundary Layer Transition Measurements in Full-Scale Flight. NACA RM H58E28 (1958).

30. Collier, F.S. , et. al: Supersonic Boundary Layer Transition on the LaRC F-106 and DFRF F-15 Aircraft. Presented at NLF and LFC Research Symposium. NASA LaRC. NASA CP2487, March 1987.

31. Pate, S. R.: Measurements and Correlations of Transition Reynolds Numbers on Sharp Slender Cones at High Speeds. AIAA Journal, June (1971), pp. 1082-1090.

32. Pfenninger, W.: Supersonic LFC Experiments in Workshop on Laminar Flow control, held at NASA LaRC, April (1976).

33. Pate, S. R.: Investigation of Drag Reduction by Boundary Layer Suction on a 50 Degree Swept Tapered Wing at M = 2.5 TO 4.0. Report No. AEDC-TDR-64-221, October (1964).

34. Goldsmith, J.: Low Drag Boundary Layer Suction Experiments on a 72° Swept Wing Model at M = 2.0 and 2.25. Summary of Laminar Boundary Layer Control Research Vol. II, ASD-TDR-63-554, U.S. Air Force, Mar. 1964, pp. 487-508

35. Middleton, W.D. and J. L. Lundry: A System for Aerodynamic Design and Analysis of Supersonic Aircraft. NASA contractor Report No: CF-3351. December (1980)

36. Boeing Commercial Airplane Co.: Advanced Supersonic Configuration Studies Using Multicycle Engines for Civil Aircraft. NASA CR 145089, November 1976.

37. Magnus, A. E. and M. E. Epton: PANAIR - A Computer Program for Predicting Subsonic or Supersonic Linear Potential Flows About Arbitrary Configurations Using a Higher Order Panel Method. NASA CR 3251 April 1980.

38. McLean, J. D. and J. L. Randall: Computer Programs to Calculate 3D Boundary Layer Flow Over Wings with Mass Transfer. NASA CR (1978)

39. Jameson, A. and Baker, T. J.: Solution of Euler Equations for Complex Configurations, AIAA Paper No. 83-1929., (1983).

40. Kaups, K. and T. Cebeci: Compressible Laminar Boundary Layers with Suction on Swept and Tapered Wings. Journal of Aircraft, Vol. 14 No. 78, July 1977.

41. Mack, L. M.: Boundary Layer Linear Stability Theory. AGARD Report No. 709, (1984).

42. Rozendaal, R. A. and R. Behbehani: Variable Sweep Transition Flight Experiment (VSTFE) - Unified Stability System (USS) Description and Users' Manual. NASA CR 181918 (1990).

43. Pfenninger, W. and C. Vemuru: High Subsonic Speed LFC Airplanes: Boundary Layer Cross Flow Stabilization Wing Analysis and Design. AIAA Paper No. 88-0275, (1988).

44. Boeing Commercial Airplanes: High Speed Civil Transport Study, Airframe Technology (Vol. 3). Submitted to NASA Langley Research Center, November 1988.

45. Sommer, S. C. and B. J. Short: NACA Technical Note 3391 (1955).

46. Pfenninger, W.: Laminar Flow Control Laminarization in Special Course on Concepts for Drag Reduction. AGARD Report R-654, March (1977).

47. Collier, F. S., D. W. Bartlett and R. D. Wagner: Curveture Effects on Swept Wing Boundary Layer Stability-Theory and Experiment. Presented at the SAE Aerotech '88 Meeting, Anaheim, Ca., Oct. 3-6 (1988).

48. Reshotko, E.: Drag Reduction by Cooling in Hydrogen Fueled Aircraft. J. Aircraft, Vol. 16, Sept. 1979, pp. 584-590.

49. Poll, D.I.A.: Leading Edge Transition on Swept Wings in Laminar-Turbulent Transition. AGARD-CP-224, pp. 21-1 to 11, (1977).

50. Snepp, D. and R. Pomeroy: A Geometry System for Aerodynamic Design. AIAA paper No. 87-2902, (1987).

APPENDIX I

WING GEOMETRY DEFINITION

HSCT CONFIGURATION 733-633

WING PLANFORM DEFINITION

WING REFERENCE PLANE AT WL245

(2Y/B)	ZLE(FT)	XLE(FT)	C(FT)
0.000	-4.40	88.98	155.22
0.025	-4.40	88.98	155.22
0.050	-4.40	88.98	155.22
0.075	-4.40	88.98	155.22
0.100	-4.61	94.23	140.77
0.125	-4.87	100.84	130.20
0.150	-5.19	107.44	119.64
0.175	-5.48	114.04	111.74
0.200	-5.65	120.64	104.98
0.225	-5.67	127.24	98.21
0.250	-5.56	133.83	91.47
0.275	-5.41	140.43	84.72
0.300	-5.30	145.80	79.18
0.325	-5.11	150.05	74.77
0.350	-4.94	153.63	71.03
0.375	-4.78	156.58	67.92
0.400	-4.58	159.53	64.81
0.425	-4.41	162.03	62.14
0.450	-4.22	164.22	59.79
0.475	-4.05	166.41	57.44
0.500	-3.89	168.35	55.34
0.525	-3.75	170.29	53.24
0.550	-3.63	172.24	51.13
0.575	-3.51	174.18	49.03
0.600	-3.39	176.12	46.93
0.625	-3.28	178.06	44.83
0.650	-3.18	180.00	42.73
0.675	-3.08	181.93	40.64
0.700	-3.01	183.87	38.53
0.725	-2.92	185.81	36.43
0.750	-2.85	187.75	34.33
0.775	-2.78	189.69	32.23
0.800	-2.73	191.63	30.13
0.825	-2.66	193.56	28.04
0.850	-2.60	195.50	25.93
0.875	-2.56	197.44	23.83
0.900	-2.50	199.38	21.73
0.925	-2.46	201.32	19.63
0.950	-2.42	203.25	17.54
0.975	-2.38	205.19	15.43
1.000	-2.33	207.13	13.33

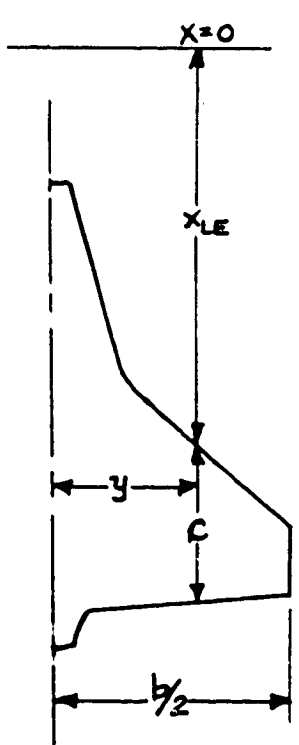

WING CAMBER SURFACE COORDINATES Z(FT)

	XPCT	0.00	5.00	10.00	15.00	20.00	25.00	30.00	40.00	50.00	60.00
		70.00	80.00	90.00	100.00						
0	Y/B/2										
0	0.000	0.00000	.20109	.39286	.58153	.76865	.95266	1.13202	1.50470	1.94878	2.42546
		2.91456	3.41297	3.89741	4.36323	-5.14000					
0	.025	0.00000	.20109	.39286	.58153	.76865	.95266	1.13202	1.50470	1.94878	2.42546
		2.91456	3.41297	3.89741	4.36323	-5.14000					
0	.050	0.00000	.20109	.39286	.58153	.76865	.95266	1.13202	1.50470	1.94878	2.42546
		2.91456	3.41297	3.89741	4.36323	-5.14000					
0	.075	0.00000	.17160	.35716	.59395	.81056	.99612	1.06062	1.37276	1.82150	2.33854
		2.74382	3.13823	3.56835	3.96742	-5.14000					
0	.100	0.00000	.32595	.54632	.70616	.84489	.91323	.99847	1.22665	1.53367	2.00820
		2.39263	2.71936	3.07142	3.44178	-5.14000					
0	.125	0.00000	.41933	.70213	.88288	1.01718	1.12226	1.22383	1.49172	1.81698	2.24991
		2.64378	3.02076	3.40443	3.80921	-5.14000					
0	.150	0.00000	.51272	.85794	1.05959	1.18946	1.33130	1.44920	1.75680	2.10028	2.49163
		2.89493	3.32217	3.73744	4.17664	-5.14000					
0	.175	0.00000	.55362	.93650	1.18630	1.39587	1.59091	1.78260	2.17381	2.56725	2.96404
		3.37424	3.77327	4.18347	4.60484	-5.14000					
0	.200	0.00000	.56223	.99953	1.29720	1.54869	1.78757	2.01701	2.45489	2.88227	3.30965
		3.73702	4.19590	4.62328	5.06116	-5.14000					
0	.225	0.00000	.56821	1.02740	1.36186	1.65507	1.92177	2.16194	2.61087	3.07944	3.51855
		3.95765	4.41640	4.85551	5.28479	-5.14000					
0	.250	0.00000	.55341	.97716	1.31110	1.60069	1.86897	2.11934	2.60097	3.07124	3.52254
		3.99079	4.44344	4.88628	5.30725	-5.14000					
0	.275	0.00000	.49862	.92692	1.26033	1.54630	1.81618	2.07673	2.59107	3.06304	3.52654
		4.02393	4.47049	4.91705	5.32972	-5.14000					
0	.300	0.00000	.48359	.87740	1.15805	1.44884	1.71461	1.96818	2.47557	2.95778	3.43951
		3.92330	4.43275	4.87212	5.26810	-5.14000					
0	.325	0.00000	.36230	.72385	1.03643	1.31776	1.57874	1.83188	2.34563	2.85190	3.36565
		3.84949	4.31090	4.75736	5.15147	-5.14000					
0	.350	0.00000	.36620	.64077	.93303	1.21399	1.48188	1.73884	2.25644	2.75678	3.25066
		3.71932	4.16653	4.59946	4.99930	-5.14000					
0	.375	0.00000	.29864	.55671	.82878	1.09725	1.35979	1.61408	2.12385	2.61482	3.09401
		3.55174	3.99087	4.41634	4.81876	-5.14000					
0	.400	0.00000	.23108	.47266	.72454	.98051	1.23770	1.48933	1.99128	2.47288	2.93737
		3.38417	3.81522	4.23324	4.63823	-5.14000					
0	.425	0.00000	.19360	.40832	.64355	.88686	1.13266	1.37410	1.85450	2.32124	2.77430
		3.21245	3.63941	4.05395	4.45605	-5.14000					
0	.450	0.00000	.17634	.37416	.58935	.81731	1.04692	1.27731	1.73831	2.18093	2.61655
		3.04358	3.45598	3.85826	4.24858	-5.14000					
0	.475	0.00000	.15908	.33999	.53514	.74776	.96118	1.18052	1.62212	2.04063	2.45879
		2.87472	3.27255	3.66257	4.04110	-5.14000					
0	.500	0.00000	.14308	.30829	.48457	.68299	.88140	1.09088	1.51538	1.91222	2.31458
		2.72248	3.10824	3.48847	3.85763	-5.14000					
0	.525	0.00000	.13647	.29541	.46264	.65118	.83150	1.02716	1.41911	1.79617	2.17856
		2.56627	2.93386	3.29613	3.64540	-5.14000					
0	.550	0.00000	.12986	.28252	.44072	.61937	.78159	.96343	1.32283	1.68012	2.04253
		2.41006	2.75948	3.10378	3.43317	-5.14000					
0	.575	0.00000	.12325	.26964	.41879	.58756	.73168	.89970	1.22655	1.56408	1.90651
		2.25385	2.58509	2.91144	3.22093	-5.14000					
0	.600	0.00000	.11665	.25676	.39687	.55575	.68178	.83597	1.13027	1.44803	1.77049
		2.09764	2.41071	2.71909	3.00870	-5.14000					
0	.625	0.00000	.11335	.24623	.38007	.52799	.64934	.79182	1.06717	1.36108	1.65948
		1.96332	2.25757	2.54733	2.82109	-5.14000					
0	.650	0.00000	.11006	.23570	.36327	.50023	.61691	.74767	1.00407	1.27413	1.54847
		1.82900	2.10442	2.37557	2.63348	-5.14000					
0	.675	0.00000	.10677	.22518	.34648	.47247	.58448	.70352	.94097	1.18718	1.43745
		1.69468	1.95128	2.20381	2.44587	-5.14000					
0	.700	0.00000	.10347	.21465	.32968	.44472	.55204	.65937	.87787	1.10023	1.32644
		1.56036	1.79813	2.03205	2.25826	-5.14000					
0	.725	0.00000	.09934	.20371	.31021	.41747	.51744	.61816	.82023	1.02595	1.23456
		1.44820	1.66472	1.87836	2.08546	-5.14000					
0	.750	0.00000	.09521	.19276	.29073	.39021	.48283	.57695	.76260	.95168	1.14268
		1.33604	1.53132	1.72467	1.91267	-5.14000					
0	.775	0.00000	.09107	.18181	.27126	.36296	.44822	.53574	.70496	.87740	1.05081
		1.22388	1.39791	1.57099	1.73987	-5.14000					
0	.800	0.00000	.08694	.17087	.25178	.33571	.41361	.49453	.64732	.80312	.95893
		1.11172	1.26451	1.41730	1.56708	-5.14000					
0	.825	0.00000	.08034	.15733	.23261	.30960	.38207	.45680	.59840	.74117	.88394
		1.02391	1.16334	1.30331	1.43993	-5.14000					
0	.850	0.00000	.07374	.14379	.21343	.28348	.35053	.41908	.54948	.67922	.80896
		.93611	1.06217	1.18931	1.31278	-5.14000					
0	.875	0.00000	.06713	.13025	.19425	.25737	.31898	.38135	.50056	.61727	.73398
		.84830	.96100	1.07532	1.18563	-5.14000					
0	.900	0.00000	.06053	.11671	.17507	.23125	.28744	.34362	.45164	.55532	.65899
		.76050	.85983	.96133	1.05848	-5.14000					
0	.925	0.00000	.05335	.10443	.15648	.20757	.25799	.30841	.40600	.49865	.59197
		.68233	.77173	.86276	.95119	-5.14000					
0	.950	0.00000	.04616	.09216	.13790	.18389	.22855	.27321	.36035	.44198	.52495
		.60417	.68364	.76419	.84390	-5.14000					
0	.975	0.00000	.03898	.07988	.11931	.16021	.19910	.23800	.31470	.38532	.45794
		.52601	.59554	.66562	.73660	-5.14000					
0	1.000	0.00000	.03180	.06760	.10073	.13653	.16966	.20279	.26905	.32865	.39092
		.44785	.50745	.56704	.62931	-5.14000					

WING THICKNESS DISTRIBUTION(T/2C),PERCENT

	XPCT	0.00	.20	.60	2.00	5.00	10.00	16.00	22.00	30.00	40.00	50.00	61.00
		65.00	72.50	75.00	80.00	85.00	90.00	95.00	100.00				
0	Y/B/2												
0	0.000	0.000000	.227000	.399000	.676000	.866000	1.058000	1.232000	1.380000	1.536000	1.646000	1.711000	1.749000
		1.743000	1.712000	1.686000	1.449000	1.118000	.742000	.383000	0.000000				
0	.025	0.000000	.227000	.399000	.676000	.866000	1.058000	1.232000	1.380000	1.536000	1.646000	1.711000	1.749000
		1.743000	1.712000	1.686000	1.449000	1.118000	.742000	.383000	0.000000				
0	.050	0.000000	.227000	.399000	.676000	.866000	1.058000	1.232000	1.380000	1.536000	1.646000	1.711000	1.749000
		1.743000	1.712000	1.686000	1.449000	1.118000	.742000	.383000	0.000000				
0	.075	0.000000	.227000	.399000	.676000	.866000	1.058000	1.232000	1.380000	1.536000	1.646000	1.711000	1.749000
		1.743000	1.712000	1.686000	1.449000	1.118000	.742000	.383000	0.000000				
0	.100	0.000000	.209001	.367002	.615005	.822008	1.059010	1.234013	1.362013	1.469015	1.568015	1.612014	1.643005
		1.616001	1.561990	1.517988	1.327989	1.042993	.718996	.381998	0.000000				
0	.125	0.000000	.217730	.382162	.644406	.873001	1.123784	1.314866	1.447460	1.565947	1.665406	1.702974	1.677000
		1.622433	1.500432	1.441729	1.260918	.997513	.692811	.370513	0.000000				
0	.150	0.000000	.228000	.399999	.678999	.932998	1.199998	1.409997	1.547997	1.679996	1.779996	1.809997	1.716999
		1.630000	1.428002	1.352003	1.182002	.944002	.662001	.357000	0.000000				
0	.175	0.000000	.251997	.449993	.719994	1.019988	1.311985	1.541982	1.693980	1.839978	1.941978	1.959980	1.809987
		1.709989	1.464995	1.374997	1.185000	.935001	.640003	.360000	0.000000				
0	.200	0.000000	.262997	.463997	.785584	1.080985	1.389981	1.629979	1.791976	1.939976	2.049974	2.067974	1.849990
		1.719998	1.458002	1.367002	1.167004	.899009	.608008	.324009	0.000000				
0	.225	0.000000	.259001	.456003	.774004	1.064006	1.369007	1.600010	1.761011	1.909011	2.018011	1.988028	1.736040
		1.628032	1.418014	1.339010	1.145008	.869010	.582009	.302008	0.000000				
0	.250	0.000000	.227975	.400896	.680462	.935270	1.203225	1.406442	1.547995	1.677934	1.801289	1.799999	1.614216
		1.527516	1.355024	1.287138	1.096842	.835197	.561625	.293202	0.000000				
0	.275	0.000000	.191998	.336997	.571996	.785995	1.010992	1.181993	1.300992	1.409991	1.549992	1.581993	1.472997
		1.410998	1.281997	1.226997	1.040997	.795998	.537999	.283000	0.000000				
0	.300	0.000000	.152002	.270004	.467006	.653008	.819012	1.002011	1.094013	1.179014	1.339013	1.409010	1.389005
		1.355003	1.198005	1.157004	.976004	.750003	.511002	.272001	0.000000				
0	.325	0.000000	.126004	.214009	.354019	.495026	.660026	.341026	.997016	1.119010	1.246015	1.299018	1.290016
		1.267014	1.184002	1.131004	.962002	.750000	.514000	.274000	0.000000				
0	.350	0.000000	.100007	.160014	.260025	.400025	.585020	.800011	.980005	1.139994	1.230004	1.264009	1.267006
		1.257003	1.169004	1.103007	.946004	.751000	.517999	.275999	0.000000				
0	.375	0.000000	.076146	.131376	.226605	.361834	.560192	.788073	1.001468	1.154312	1.220459	1.250642	1.254596
		1.250321	1.167092	1.092504	.928825	.739550	.515615	.281248	0.000000				
0	.400	0.000000	.049996	.099993	.189992	.319998	.532998	.774999	1.024999	1.170003	1.210000	1.235997	1.240997
		1.242998	1.164999	1.080999	.909995	.726996	.512996	.236999	0.000000				
0	.425	0.000000	.015000	.039000	.120000	.300000	.510000	.765000	1.020000	1.195000	1.210000	1.210000	1.215000
		1.220000	1.160000	1.075000	.865000	.690000	.480000	.280000	0.000000				
0	.450	0.000000	.012598	.032756	.106551	.266379	.486465	.752992	1.010394	1.173386	1.186465	1.188386	1.193386
		1.196945	1.165283	1.074039	.866441	.677032	.469433	.267032	0.000000				
0	.475	0.000000	.010000	.026001	.092003	.230007	.461005	.740002	1.000002	1.150004	1.161005	1.165004	1.170004
		1.172005	1.170999	1.073000	.868000	.663003	.458002	.253003	0.000000				
0	.500	0.000000	.010000	.026678	.093696	.233392	.469140	.750175	1.016958	1.166958	1.176262	1.180432	1.185602
		1.187602	1.185415	1.080801	.875970	.667579	.462409	.256052	0.000000				
0	.525	0.000000	.010000	.027410	.095526	.237052	.477924	.761155	1.035259	1.185259	1.192733	1.197086	1.202438
		1.204438	1.200970	1.089219	.884572	.672520	.467167	.259347	0.000000				
0	.550	0.000000	.010000	.028203	.097506	.241013	.487431	.773039	1.055064	1.205064	1.210558	1.215108	1.220659
		1.222659	1.217805	1.098330	.893880	.677867	.472317	.262912	0.000000				
0	.575	0.000000	.010000	.029063	.099657	.245314	.497752	.785941	1.076568	1.226568	1.229911	1.234676	1.240442
		1.242442	1.236082	1.108221	.903987	.683673	.477908	.266782	0.000000				
0	.600	0.000000	.010000	.030000	.102000	.249999	.508999	.799998	1.099997	1.249997	1.250998	1.255997	1.261997
		1.263997	1.255998	1.118999	.914999	.689999	.483999	.271000	0.000000				
0	.625	0.000000	.009943	.029798	.101354	.248586	.505809	.796769	1.095153	1.243134	1.244901	1.250103	1.256426
		1.258548	1.249174	1.112417	.909790	.686607	.481698	.269869	0.000000				
0	.650	0.000000	.009881	.029576	.100644	.247034	.502305	.793220	1.089830	1.235592	1.238203	1.243626	1.250304
		1.252559	1.241677	1.105186	.904067	.682881	.479169	.268627	0.000000				
0	.675	0.000000	.009813	.029331	.099861	.245320	.498438	.789304	1.083956	1.227271	1.230811	1.236480	1.243549
		1.245950	1.233405	1.097207	.897753	.678769	.476379	.267255	0.000000				
0	.700	0.000000	.009737	.029060	.098992	.243421	.494149	.784961	1.077442	1.218043	1.222614	1.228554	1.236058
		1.238622	1.224231	1.088359	.890750	.674209	.473285	.265736	0.000000				
0	.725	0.000000	.009652	.028757	.098024	.241302	.489366	.780118	1.070177	1.207750	1.213472	1.219715	1.227703
		1.230449	1.213999	1.078490	.882940	.669124	.469834	.264041	0.000000				
0	.750	0.000000	.009557	.028418	.096936	.238923	.483998	.774682	1.062023	1.196199	1.203212	1.209794	1.218326
		1.221276	1.202515	1.067414	.874174	.663416	.465961	.262139	0.000000				
0	.775	0.000000	.009449	.028034	.095708	.236235	.477931	.768538	1.052806	1.183142	1.191615	1.198581	1.207727
		1.210907	1.189536	1.056895	.864267	.656964	.461583	.259988	0.000000				
0	.800	0.000000	.009327	.027596	.094307	.233172	.471017	.761537	1.042305	1.168265	1.178401	1.185804	1.195651
		1.199093	1.174746	1.040631	.852978	.649614	.456595	.257538	0.000000				
0	.825	0.000000	.009186	.027093	.092697	.229651	.463068	.753487	1.030230	1.151160	1.163207	1.171114	1.181765
		1.185509	1.157741	1.024230	.839998	.641161	.450859	.254720	0.000000				
0	.850	0.000000	.009022	.026508	.090827	.225558	.453832	.744133	1.016200	1.131283	1.145552	1.154043	1.165630
		1.169725	1.137981	1.005172	.824915	.631340	.444195	.251447	0.000000				
0	.875	0.000000	.008830	.025821	.088626	.220745	.442967	.733131	.999697	1.107904	1.124785	1.133964	1.146651
		1.151159	1.114739	.982755	.807174	.619788	.436356	.247596	0.000000				
0	.900	0.000000	.008600	.025000	.086000	.215001	.430002	.720002	.980004	1.080005	1.100005	1.110004	1.124004
		1.129004	1.087005	.956005	.786004	.606003	.427002	.243001	0.000000				
0	.925	0.000000	.008091	.023812	.080908	.202439	.405048	.675867	.920590	1.020590	1.039572	1.050590	1.066118
		1.071627	1.039303	.921373	.761727	.593779	.426661	.255391	0.000000				
0	.950	0.000000	.007459	.022339	.074594	.186866	.374113	.621152	.846935	.946935	.964654	.976935	.994357
		1.000497	.980168	.878442	.731633	.578627	.426240	.270754	0.000000				
0	.975	0.000000	.006656	.020465	.066563	.167054	.334757	.551543	.753230	.853230	.869343	.883230	.903062
		.910005	.904936	.823826	.693348	.559350	.425704	.290298	0.000000				
0	1.000	0.000000	.005600	.018000	.056000	.141000	.283000	.460000	.630000	.730000	.744000	.760000	.783000
		.791000	.806000	.752000	.643000	.534000	.425000	.316000	0.000000				

APPENDIX II

ELECTRIC POWER FOR COMPRESSOR DRIVE

Electric power for laminar flow suction was supplied in the study by increasing the capacity of the airplane's engine driven generators. One additional KVA was required per compressor shaft horsepower considering efficiency and power factor. The Model 733-633 had four 90 KVA generators, that were to be increased in capacity to 250 KVA for laminarizing the outboard wing regions. The largest generator flying in 1988 was used on a military airplane and had a capacity of 150 KVA. Space for the generator diameter to fit within airplane contour is the limiting factor. Eight 120 KVA units may be considered for laminar flow control over the outboard wings of the supersonic transport. The combined inboard/outboard wings would require twice that number.

The type of electric power generator of the Model 733-633 baseline SST was variable speed constant frequency (VSCF). VSCF was found to be suitable also for laminar flow control compressor drive. Propulsion turbine shaft power was transmitted to each generator by an airframe mounted accessory drive (AMAD). Power was transmitted at 270 Volt DC from the generators to frequency controllers located at the Aft Electronics Bay in the air conditioned airplane body. Return was through the metallic structure of the 1979 Model 733-633, and through the copper wire mesh that was installed for lightning protection in the composite structure of the 1988 High Speed Civil Transport (HSCT). Power was distributed from the frequency controllers to the users at 400 Hertz AC, except for the compressor drive motors with special requirements.

Two types of electric motors were considered for compressor drives: brushless DC motors and AC induction motors. Comparative data were obtained from Sundstrand Pneumatic Systems, and from Parker Bertea. The gracious contribution of the suppliers is acknowledged.

The brushless DC motors using permanent magnets, such as samarium cobalt or other rare earth elements were lighter than comparable induction motors. See Figure A2-1. Each brushless DC motor required phase commutation by angular position feedback through a dedicated controller. The brushless motor controllers in existence in 1988 were found to be heavy weight, especially so at the low power levels. Significant DC motor controller weight reductions were predicted for the year 2000, as shown in Figure A2-2 but the reductions were insufficient to provide DC drives the weight advantage. The controllers also required substantial local cooling because of a 250°F maximum operating temperature.

The AC induction motors required no position feedback, only a special setting on the airplane electric power generating system frequency controller to match the compressor speed. The specific weight of the airplane frequency controllers benefited from the effects of the high power level and the mature state of development. A 530 Hertz frequency was estimated for two-pole motors to match a 30,000 compressor RPM. The AC induction motors were selected on the basis of total system weight for compressor drive.

FIG. A2–1 ELECTRIC MOTOR WEIGHTS

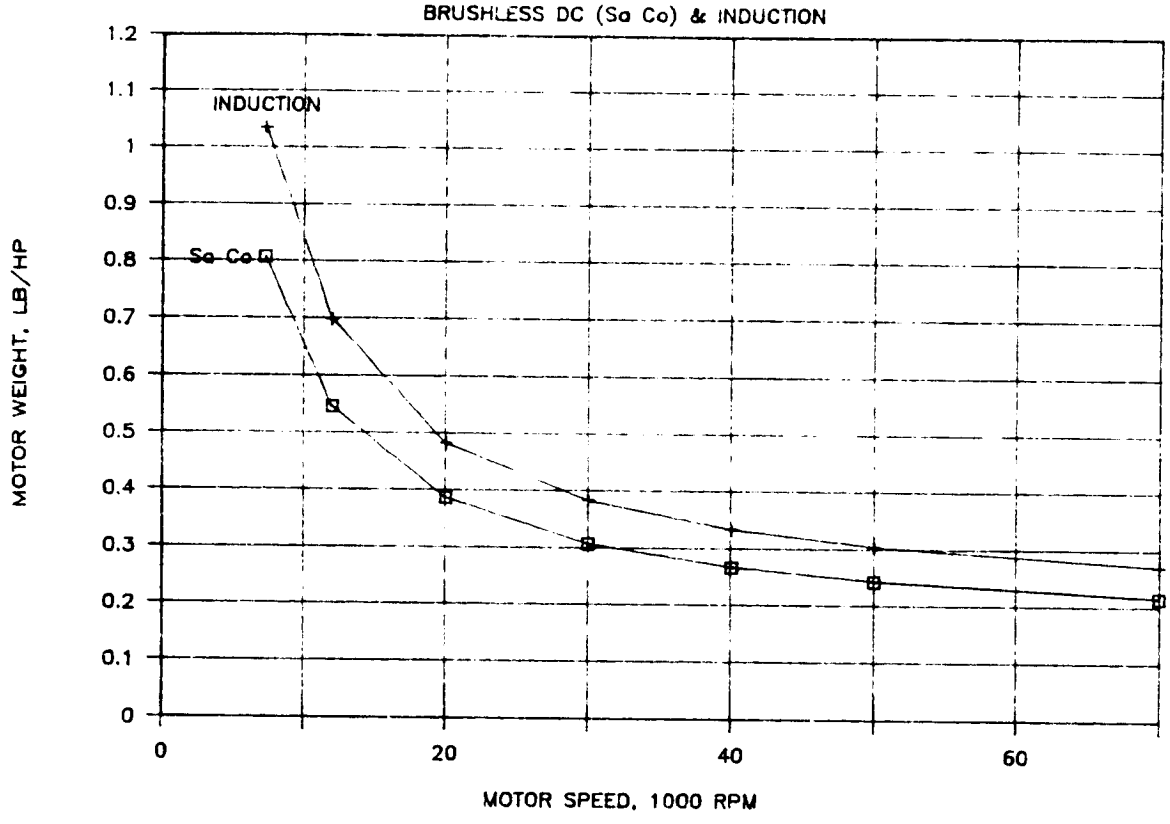

FIG. A2–2 DC MOTOR CONTROLLER WEIGHTS

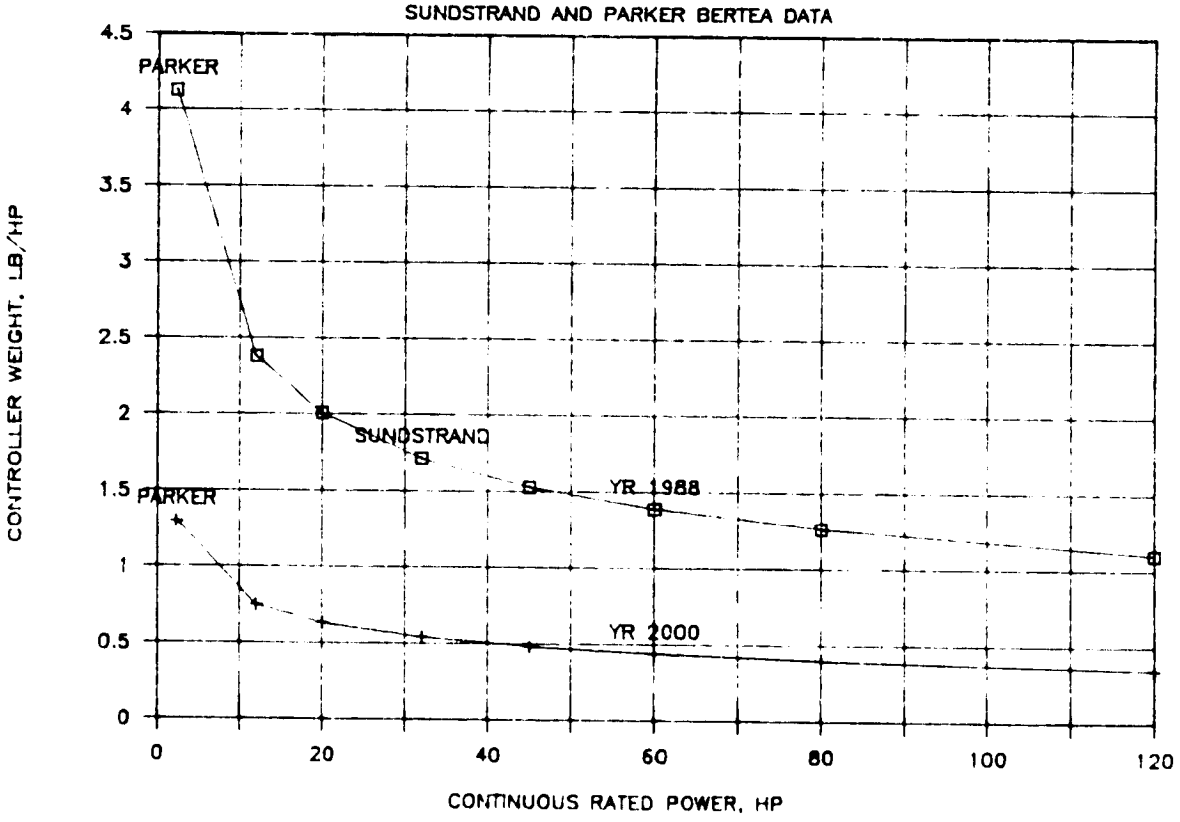

APPENDIX III

AIR COMPRESSOR SELECTION

Garrett Airesearch proposed electric motor driven compressor units for local installation along the outboard wing leading edge flap hinge line. They suggested two compressors in series: an axial and mixed flow multistage unit followed by a centrifugal unit to develop a pressure ratio of 18.5 to 1.

The axial flow and mixed flow compressors with multiple stages were smaller in diameter but longer than the single stage centrifugal compressors. See the Garrett AiResearch axial and centrifugal compressor data in Tables A3-1 and Figure A3-1.

The pressure rise obtainable by a turbocompressor of given type increases with the square of the impeller tip speed which depends on the allowable impeller diameter and on the selected speed of rotation. The speeds of rotations suggested by Airesearch for electric motor driven air compressors ranged from 30,000 RPM to 70,700 RPM. A reliability growth from 4,000 to 40,000 hours mean time between failures (MTBF) with cumulative operating time increase from 10,000 to 10,000,000 hours was reported by T.P. Emerson from Garrett in ASME Paper 78-ENAs-18. The data referred to foil air bearings used on bleed air driven air conditioner compressors on the DC-10 commercial transport, where the operating speed was 50,000 RPM.
Sundstrand Pneumatic Systems suggested 40,000 to 50,000 RPM speeds for shaft driven compressors of larger diameter for installation at the rear spar. See Table A3-2.

The compressor characteristics suggested by the manufacturers were analyzed using a standard handbook as reference. Tip speed is generally less than 1100 ft/s for industrial compressors and ranges from 1400 to 1600 ft/s for aerospace machinery. Analysis of the Sundstrand data indicated supersonic impeller tip speeds, and Garrett data subsonic tip speeds. There was agreement between the suppliers that the job was feasible but technically challenging.

Compressor characteristics meeting the performance requirements of Section 3.4.3 of this report were then predicted by Boeing using the manufacturer's data and the standard method of analysis.

Compressor drive power was calculated in two steps. First the power required at 100 percent mechanical efficiency was determined. The adiabatic temperature rise, head rise and power were calculated from the required inlet pressure, inlet temperature and mass flow, and the selected discharge pressure. The compressor speed of rotation and

outside diameter were selected on a trial basis to calculate the compressor specific speed (Ns) and specific diameter (Ds). Then, estimates of compressor mechanical efficiency
and pressure rise were obtained from the ASME 60-WA-231 turbocompressor performance chart, and the temperature rise and power were corrected for mechanical efficiency.

The procedure was iterated with increasing number of stages until the efficiency and the resulting pressure ratio were both acceptable. The Reynolds number and Mach number of the resulting design were recorded.

This analysis was was applied to a range compressor characteristics suggested at various times during the study by the compressor manufacturers Garrett and Sundstrand as well as to Boeing's own estimates for the finally selected conditions. See Figures A3-3 and -4 showing the Boeing estimates of compressor characteristics for the outboard wing regions and for the combination of inboard/outboard wing regions. The estimates were used for benefit evaluation in Section 4.2.2 of this report.

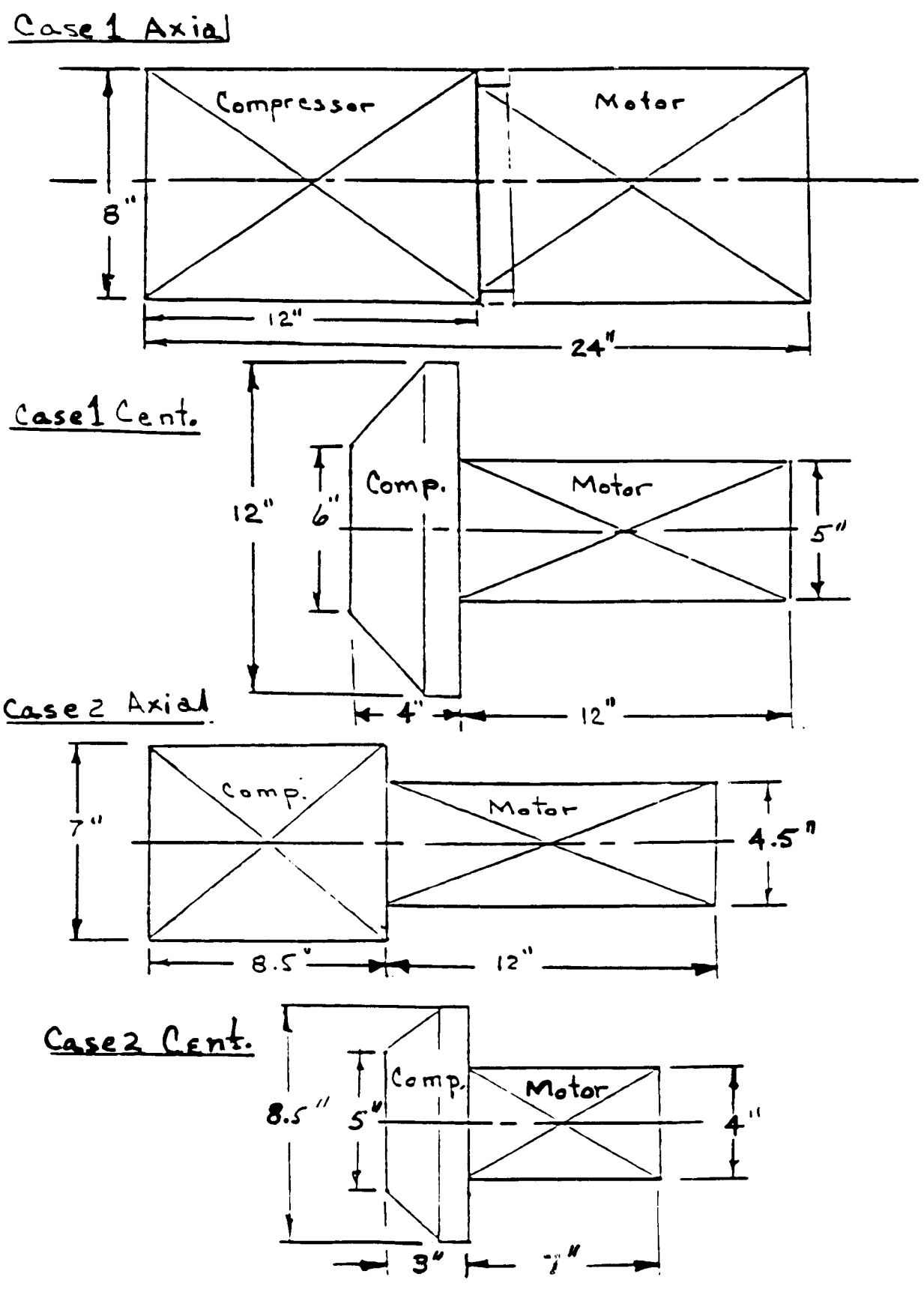

Figure A3-1 Garrett Motor-Compressor Envelope Sketches

TABLE A3-1 ESTIMATED CHARACTERISTICS
OF ELECTRIC MOTOR DRIVEN AIR COMPRESSORS
FOR LAMINARIZING THE INB'D & OUTBOARD WING REGIONS

CRITICAL SPECIFICATION REQUIREMENTS:
P2/P1 RATIO 18.5

MAX O.D. IN. 32 IN. INB'D. TAPERED TO 4 IN. OUTB'D.

MASS FLOW LB/SEC 0.150
PRES.IN PSFA 30
TEMP IN DEG F 100

FLIGHT REGIME: MACH 2.4, 60,000 FT ALTITUDE
REGION SERVED: REGION 2, LEADING EDGE, LOWER SURFACE, INB'D & OUTB'D

AIRESEARCH PROPOSED TO MEET THE PRESSURE RATIO OF 18.5 BY:
6 STAGES OF AXIAL FLOW STAGES
+1 CENTRIFUGAL STAGE AT OUTLET OF AXIAL UNIT
AIREASERCH PROPOSED TO MEET THE MAX DIAMETER RANGE BY:
(A) INB'D SET AT FULL FLOW, (B) OUTB'D SET AT ONE HALF FLOW.

LOCATION		INB'D SET		OUTB'D SET		
STAGES		6	1	6	1	
TYPE		AXIAL	CENTRIFUG	AXIAL	CENTRIFUG	
MASS FLOW	LB/SEC	0.150	0.150	0.075	0.075	ALTERNATE OPTIONS
P2/P1	RATIO	7.79	2.38	7.79	2.38	7.79*2.38 = 18.5
PRES.IN	PSFA	30	234	30	234	AXIAL OUTLET
	PSIA	0.21	1.62	0.21	1.62	
TEMP IN	DEG F	100	662	100	673	AXIAL OUTLET
	DEG R	560	1122	560	1133	
SHAFT	HP	28.6	20.8	14.7	10.5	
SHAFT	KW	21.3	15.5	10.9	7.9	(@100% EFFICIENCY)
SPEED	1000 RPM	30.0	50.0	42.4	70.7	
EFFICIENCY	PERCENT	80	77	78	76	
WEIGHT	LBS	110	60	70	40	
COMPRESSOR						
MAX O.D	IN.	8.0	12.0	7.0	8.5	
MIN O.D.	IN.		6.0		5.0	CONICAL SHAPE
LENGTH	IN.	12.0	4.0	8.5	3.0	
MOTOR						
O.D. MOT.	IN.	8.0	5.0	4.5	4.0	
LGTH.MOT.	IN.	12.0	12.0	12.0	7.0	
COMPRESSOR UNIT						
MAX O.D.	IN.	8.0	12.0	7.0	8.5	
LENGTH	IN.	24.0	16.0	20.5	10.0	

COURTESY GARRETT AIRESEARCH, LOS ANGELES, MR. E.N. HARRIS, 5/5/88

TABLE A3-2 ESTIMATED CHARACTERISTICS
FOR SHAFT DRIVEN AIR COMPRESSORS
COURTESY OF SUNDSTRAND PNEUMATIC SYSTEMS
SAN DIEGO, MR. GUIDO BIAGINI, 5-16-88

REGION		1	1A	4	4A
COMPRESSOR TYPE		AXIAL/ MIXED FLOW	CENTRIF.	AXIAL/ MIXED FLOW	CENTRIF.
NUMBER OF STAGES		2	1	2	1
MASS FLOW	LBS/SEC	0.677	0.677	0.677	0.677
INLET PRESSURE	PSIA	0.618	0.417	1.125	0.903
INLET TEMPERATURE	DEG R	722	672	722	672
PRESSURE RATIO		9.5	12.0	6.9	8.0
OUTLET PRESSURE	PSIA	5.872	5.000	7.763	7.222
SHAFT SPEED	RPM	50,000	40,000	50,000	40,000
SHAFT POWER	HP	230	230	190	180
OUTLET TEMP.	DEG R	1772.7	1672.7	1598.7	1455.1
MAX. COMP. DIA.	IN.	16	27	14	20
MAX. COMP. LNGTH	IN.	24	10	22	9
COMP. WEIGHT	LBS	220	170	170	110

TABLE A3-3 ESTIMATED CHARACTERISTICS OF AIR COMPRESSORS AND OF ELECRIC MOTOR DRIVEN COMPRESSOR UNITS FOR LAMINARIZING THE OUTBOARD WING REGIONS

REGION OF SUCTION UP/DOWN SURFACE CHORDWISE LOCATION		1A TOP 0.35	1 TOP L.E.	4A BOTTOM 0.35	4 BOTTOM L.E.
MASS FLOW OF AIR	LBM/SEC	0.677	0.677	0.677	0.677
INLET PRESSURE	PSF ABS.	60	89	130	162
	PSI ABS.	0.42	0.62	0.90	1.13
INLET TEMPERATURE	DEG R	672	772	672	772
	DEG F	212	312	212	312
PRESSURE RATIO	RATIO	4.38	3.09	2.12	1.70
OUTLET PRESSURE	PSI ABS.	1.91	1.91	1.91	1.91
ADIABATIC DISCHARGE,	DEG R	1038	1066	833	898
ESTIMATED DISCHARGE,	DEG R	1202	1191	902	955
ADIABATIC POWER	HP	84	67	37	29
ESTIMATED POWER	HP	122	96	53	42
INLET I.D.	IN.	13.9	11.9	9.5	8.8
OUTLET I.D.	IN.	7.5	7.5	7.0	7.1
SPEED, ESTIMATED	1000 RPM	30	30	30	30
DUTY	TYPE	CONT.	CONT.	CONT.	CONT.
CONTAINMENT RING	% SPEED	135	135	135	135
SHAFT DRIVEN UNIT					
COMPRESSOR TYPE	ENVELOPE DIAMETER AND WEIGHT TO BE MINIMUM				
MAX DIAMETER	IN.	27	24	20	18
MAX LENGTH	IN.	24	24	24	24
WEIGHT, ESTIMATED	LBS	116	91	56	46
ELECTRIC MOTOR DRIVEN COMPRESSOR UNIT					
COMPRESSOR TYPE	UNIT LENGTH AND WEIGHT TO BE MINIMUM				
POWER	400 V AC, 3 PH, 500 HZ, NEUTRAL TO GROUND				
COOLING	INCLUDE SHAFT MOUNTED FREON COMPRESSOR				
LUBRICATION	INCLUDE ACTIVE BEARING LUBE PUMP ON SHAFT				
MAX UNIT LENGTH	IN.	32	30	30	30
MAX DIAMETER	IN.	30	30	27	27
WEIGHT, ESTIMATED	LBS	153	123	81	68

TABLE A3-4 ESTIMATED CHARACTERISTICS
OF SHAFT DRIVEN AIR COMPRESSORS
FOR LAMINAR FLOW CONTROL ON HSCT, 7-29-88

REGION STRAKE/WING		1S	1A&S2	4A&S3	1W	4W	COMBINED
UPPER/LOWER		UPPER	UPPER	LOWER	UPPER	LOWER	
CHORDWISE %		0.6-9	0-0.6	0-10	1-10	1-10	
QUANTITY/AIRPLANE		2	2	2	2	2	10
REQUIRED PERFORMANCE							
MASS FLOW	LB/SEC	0.300	1.247	2.197	0.677	0.677	10.20
COMPR. IN	PSF	30	56	129	89	162	
P2/P1	RATIO	9.15	4.90	2.13	3.09	1.70	
TEMP. IN	DEG F	212	212	212	312	312	
DUTY		CONT.	CONT.	CONT.	CONT.	CONT.	
CONTAINMENT RING		REQ'D	REQ'D	REQ'D	REQ'D	REQ'D	
ESTIMATED CHARACTERISTICS							
STAGES		5	2	1	2	1	
SPEED	K RPM	30	30	30	30	30	
TIP DIA	IN.	12.4	16.5	16.5	14.7	11.8	
TIP SPEED	FT/SEC	1617	2156	2156	1925	1540	
NS/STAGE	RPM	240	278	301	250	208	
SP.DIA	FT	0.86	0.78	0.79	0.89	0.93	
EFF'Y %	PER STAGE	90	82	82	90	85	
EFF'Y % OVERALL		59	67	82	81	85	72
TEMP. OUT	DEG F	1216	787	409	674	460	
POWER, SHAFT	HP	102	243	147	83	34	1219
ESTIMATED INSTALLATION DATA							
I.D. COMPR IN	IN.	10.1	16.8	15.9	11.9	8.8	
I.D. COMP OUT	IN.	5.5	10.3	12.5	7.4	7.1	
O.D.	IN.	21	28	28	25	20	
LENGTH	IN.	25	18	12	14	9	
BULK, CU.FT		6	8	5	5	2	54
WEIGHT OF COMPRESSORS							
ESTIMATED	LBS	85	162	112	71	40	
COMBINED LBS/AP							938

Report Documentation Page

1. Report No.	2. Government Accession No.	3. Recipient's Catalog No.
NASA CR-181917		

4. Title and Subtitle	5. Report Date
APPLICATION OF LAMINAR FLOW CONTROL TO SUPERSONIC TRANSPORT CONFIGURATIONS	JULY 1990
	6. Performing Organization Code

7. Author(s)	8. Performing Organization Report No.
P. G. Parikh and A. L. Nagel	

9. Performing Organization Name and Address	10. Work Unit No.
Boeing Commercial Airplane Company P.O. Box 3707 Seattle, Wa 98124-2207	505-60-41-01
	11. Contract or Grant No. NAS1-15325

12. Sponsoring Agency Name and Address	13. Type of Report and Period Covered
National Aeronautics and Space Admin. Langley Research Center Hampton, VA. 23665-5225	Contractor Report Oct. '87 - Dec. '88
	14. Sponsoring Agency Code

15. Supplementary Notes

Langley Technical Monitors: D. W. Bartlett and D. Maddalon.
Laminar Flow Control Projects Office (LFCPO)
Final Report

16. Abstract

The feasibility and impact of implementing a laminar flow control system on a supersonic transport configuration were investigated. A hybrid laminar flow control scheme consisting of suction controlled and natural laminar flow was developed for a double-delta type wing planform. The required suction flow rates were determined from boundary layer stability analyses using representative wing pressure distributions. A preliminary design of structural modifications needed to accommodate suction through a perforated titanium skin was carried out together with the ducting and systems needed to collect, compress and discharge the suction air. The benefits of reduced aerodynamic drag were weighed against the weight, volume and power requirement penalties of suction system installation in a mission performance and sizing program to assess the net benefits.

The study showed a feasibility of achieving significant laminarization of the wing surface by use of a hybrid scheme, leading to an 8.2 percent reduction in the cruise drag. This resulted in an 8.5 percent reduction in the maximum takeoff weight and a 12 percent reduction in the fuel burn after the inclusion of the LFC system installation penalties. Several research needs were identified for a resolution of aerodynamic, structural and systems issues before these potential benefits could be realized in a practical system.

17. Key Words (Suggested by Author(s))	18. Distribution Statement
Laminar Flow Control Supersonic Transport High Speed Civil Transport Viscous Drag Reduction	Unclassified - Unlimited Subject Category 02

19. Security Classif. (of this report)	20. Security Classif. (of this page)	21. No. of pages	22. Price
Unclassified	Unclassified	180	